The Molecular Consequences of Hypertension on the Human Prefrontal Cortex

Hope Han

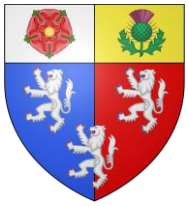

Pembroke College

University of Oxford

A dissertation submitted for the degree of

Doctor of Philosophy in Clinical Neurosciences

Apr 2025

Word Count: 36,800

Table of Contents

Abstract

Vascular disorders are important risk factors for cognitive decline and dementia, yet their molecular and cellular impact of these disorders on the human brain and its vasculature remains poorly understood. In this study, a large-scale single-nucleus atlas of the human prefrontal cortex vasculature was generated, comprising 671,162 high-quality nuclei from 43 donors—including both control and hypertensive or diabetic individuals—following strict quality control from an initial cohort of 48 donors. This atlas comprises both parenchymal and vascular compartments, including vascular, glial, neuronal, and immune cell populations, providing a comprehensive architecture of human cortical tissue. Strikingly, hypertension induced substantial transcriptional changes, particularly in vascular cell types (endothelial cells, mural cells, and endothelial-mesenchymal transition cells) and astrocytes. In contrast, no significant transcriptomic changes were observed in diabetes, suggesting that the prefrontal cortex is preferentially vulnerable to hypertension. Among hypertension-affected cell types, endothelial cells, which are key components of the blood-brain barrier (BBB), were the most affected, highlighting their high vulnerability to hypertensive stress. Notably, genes related to cell adhesion, synaptic function, and neuronal guidance were significantly downregulated, suggesting a novel role for traditional ‘neuronal’ genes in maintaining vascular integrity. Their dysregulation in endothelial cells and astrocytes may thus impair the neurovascular unit by affecting BBB integrity and angiogenesis. Many of the downregulated genes have previously been implicated in angiogenesis, and the findings position angiogenesis inhibition as a central mechanism of hypertension-induced neurovascular dysfunction. Cognitive decline associated with hypertension may therefore be a consequence of loss of BBB integrity and perfusion. Whilst hypertension-associated GWAS genes were significantly enriched in vascular cell types, there was minimal overlap between GWAS genes and differentially expressed genes. This suggests that observed transcriptomic changes may reflect

secondary consequences of disease or long-term epigenetic changes. This study provides valuable insights into the molecular consequences of hypertension on the human prefrontal cortex.

Acknowledgements

I would like to express my deepest gratitude to my supervisor, Prof. Zameel Cader, for his invaluable guidance and support throughout my DPhil journey, without which this work would not have been possible. Special thanks to the Cader Lab, the Nevado-Holgado Lab, and Novo Nordisk for their expertise, collaboration, and insightful feedback.

I am deeply thankful to my family—my parents, siblings, and two lovely nephews—and to my friends for their unwavering support and love, especially during the most challenging moments of this journey.

List of Tables

List of Figures

Abbreviations

Abbreviation	Explanation
aaSMC	Arteriolar Smooth Muscle Cells
Aβ	Amyloid β
ACE-I	Angiotensin-Converting Enzyme Inhibitors
AD	Alzheimer's Disease
aEC	Arterial Endothelial Cells
ALS	Amyotrophic Lateral Sclerosis
Ang II	Angiotensin II
APP	Amyloid Precursor Protein
ARB	Angiotensin Receptor Blockers
aSMC	Arterial Smooth Muscle Cells
Astro	Astrocytes
AVM	Arteriovenous Malformations
BBB	Blood-Brain Barrier
BH	Benjamini and Hochberg
BP	Biological Process
Bulk RNA-seq	Bulk RNA Sequencing
CAA	Cerebral Amyloid Angiopathy
CCC	Cell-Cell Communication
cEC	Capillary Endothelial Cells
CNS	Central Nervous System
COD	Cause of Death
CTRL	Control
DBP	Diastolic Blood Pressure
DEG	Differential Gene Expression
DEGs	Differentially Expressed Genes
DIAB	Diabetes
DLB	Dementia with Lewy Bodies
EC	Endothelial Cells
ECM	Extracellular Matrix
EndoMT	Endothelial-Mesenchymal Transition Cells
ExNeuron	Excitatory Neurons
FC	Fold Change
FDR	False Discovery Rate
Fibro	Fibroblasts
FTD	Frontotemporal Dementia
GABA	γ-Aminobutyric Acid
GCN	Gene Co-Expression Network
GO	Gene Ontology
GRCh	Genome Reference Consortium Human Build
GSEA	Gene-Set Enrichment Analysis
GWAS	Genome-Wide Association Study
HD	Huntington's Disease
HTN	Hypertension
InNeuron	Inhibitory Neurons
iPSC	Induced Pluripotent Stem Cell
LD	Linkage Disequilibrium
LFC	Log_2 Fold Change
MC	Mural Cells
ME	Module Eigengene

Micro	Microglia
M-PC	Matrix Pericytes
NFT	Neurofibrillary Tangles
NGF	Nerve Growth Factor
NO	Nitric Oxide
NVC	Neurovascular Coupling
NVU	Neurovascular Unit
Oligo	Oligodendrocytes
OPC	Oligodendrocyte Progenitor Cells
padj	Adjusted p-values
PC	Principal Component
PCA	Principal Component Analysis
PD	Parkinson's Disease
PFC	Prefrontal Cortex
PNS	Peripheral Nervous System
PP	Pulse Pressure
PPI	Protein-Protein Interaction
PVM	Perivascular Macrophages
QC	Quality Control
RAAS	Renin-Angiotensin-Aldosterone System
ROS	Reaction Oxygen Species
SBP	Systolic Blood Pressure
scRNA-seq	Single-Cell RNA Sequencing
SCZ	Schizophrenia
SMC	Smooth Muscle Cells
SNP	Single Nucleotide Polymorphism
snRNA-seq	Single-Nucleus RNA Sequencing
SVD	Small Vessel Disease
T2DM	Type 2 Diabetes Mellitus
TF	Transcription Factors
TOM	Topological Overlap Matrix
T-PC	Transport Pericytes
VaD	Vascular Dementia
vEC	Venous Endothelial Cells
VEGF	Vascular Endothelial Growth Factor
VNC	Vasculo-Neuronal Coupling
WGCNA	Weighted Gene Co-expression Network Analysis
WMH	White Matter Hyperintensities

Introduction

Vascular Risk Factors and Dementia

The National Health Service (NHS) defines dementia as a syndrome associated with an ongoing decline in brain functioning which interferes with daily life. Alzheimer's disease (AD) is the most common type of dementia, accounting for an estimated 50% to 75% of dementia cases and is one of the most common neurodegenerative diseases. Vascular dementia accounts for up to 20%, followed by dementia with Lewy bodies (DLB) contributing to 10-15%, and frontotemporal dementia (FTD) representing about 2% of dementia cases (National Institute for Health and Care Excellence, 2024). It has been estimated that there will be approximately 152.8 million people worldwide living with AD or a related form of dementia by 2050 (Collaborators, 2022). All types of dementia are associated with an increased mortality compared to people without dementia, and non-AD dementias are associated with higher mortality rates and shorter life expectancy than AD (C. S. Liang et al., 2021).

Memory loss is a hallmark symptom of dementia and reflects early degeneration of specific brain regions crucial for memory processing. Among the brain regions, the hippocampus plays a central role in the formation of declarative and spatial memory. The entorhinal cortex, an early site of pathology, provides key input to the hippocampus and its degeneration disrupts memory encoding. As the disease progresses, the retrosplenial and prefrontal cortices—important for object recognition and remote memory—are also affected, contributing to the spread of cognitive impairment (Rao et al., 2022).

Dementia will typically affect multiple brain functions beyond memory, including thinking, language, emotion, or behaviour. Among these, executive functions—encompassing a wide range of active cognitive processes such as reasoning, planning, problem-solving, sustained attention, and inhibitory control—are particularly vulnerable in dementia, with

evidence indicating impairments occurring even in the early stages of AD (Guarino et al., 2018). It is primarily due to the degeneration of the prefrontal cortex, which mainly serves executive function.

Currently available treatments for dementia, particularly AD, offer modest and temporary symptomatic relief but are not curative. Approved medications such as cholinesterase inhibitors and memantine may temporarily improve or stabilise cognitive and functional abilities. Long-term data suggest that cholinesterase inhibitors are associated with small but persistent cognitive benefits and even reduced mortality risk (Xu et al., 2021). Moreover, the combined use of donepezil, a cholinesterase inhibitor, and memantine, an NMDA receptor antagonist, has been shown to significantly increase five-year survival compared to monotherapies or no treatment (Yaghmaei et al., 2024). Newer anti-amyloid immunotherapies, such as lecanemab, show promise in slowing early disease progression, with clinical trials demonstrating a modest reduction in cognitive decline and amyloid burden (Heneka et al., 2024). However, all these therapies are limited by their modest clinical benefit, high costs, and potential side effects—such as amyloid-related imaging abnormalities observed with anti-amyloid therapies. As a result, prevention remains a key strategy in addressing the growing global burden of dementia (Reuben et al., 2024). A growing body of evidence highlights that nearly half of dementia cases could potentially be prevented by addressing modifiable risk factors across the life course (Livingston et al., 2024).

Pathobiology of Dementia

Alzheimer's Disease (AD)

Alzheimer’s disease (AD) is a multifactorial neurodegenerative disease characterised by complex and interconnected pathophysiological mechanisms. AD exhibits two core hallmarks histopathologically: extracellular amyloid-β (Aβ) plaques and intracellular neurofibrillary tangles (NFT) composed of hyperphosphorylated tau protein aggregation in the brain.

Under normal physiological conditions, Aβ monomers contribute to neuroprotective functions, but in AD, imbalances in production and clearance lead to misfolding, aggregation, and accumulation of Aβ in the form of oligomers, protofibrils, fibrils, and extracellular amyloid plaques. In particular, soluble oligomers and protofibrils are considered the most synaptotoxic species, and their accumulation is associated with impaired synaptic plasticity, altered calcium homeostasis, and loss of dendritic spines (Hampel et al., 2021). Aβ plays a key upstream role in the pathophysiology of AD, with evidence indicating that Aβ accumulation occurs decades before the onset of clinical symptoms and it also precedes tau pathology, synaptic dysfunction, and neurodegeneration (Hampel et al., 2021).

Meanwhile, tau proteins, which normally stabilise microtubules in neurons, undergo hyperphosphorylation and aggregation, forming NFT that correlates strongly with cognitive impairment (Vogel et al., 2020). Emerging evidence suggests that amyloid and tau affect each other in a complicated way and proposes a synergistic interaction where both pathologies amplify each other’s neurotoxic effects (Busche & Hyman, 2020). This suggests the necessity of therapeutic strategies targeting both Aβ and tau, as amyloid-based monotherapies appear to be ineffective in halting AD progression.

From a very early preclinical stage of AD, brain vasculature has already altered structure and function including blood-brain barrier (BBB) breakdown, hypoperfusion, and basement membrane thickening (Wardlaw et al., 2019). The vascular hypothesis of AD, which is one of the proposed AD pathogenic mechanisms, posits that cerebrovascular dysfunction plays a causative role in the initiation and progression of neurodegeneration (Scheffer et al., 2021). Instead of being a downstream effect of Aβ and tau pathology, vascular injury may precede and amplify these classical features of AD. Vascular risk factors are often associated with BBB breakdown, cerebral hypoperfusion and neurovascular unit (NVU) impairment, which can reduce Aβ clearance and increase its production. Notably, Aβ deposits are not only found in the hippocampus and neocortex but also in the cerebrovasculature (Chen et al., 2017). Overproduction of Aβ can in turn accelerate NFT formation and neuronal dysfunction, ultimately leading to cognitive decline (Fisher et al., 2022).

In support of the vascular hypothesis, individuals with early cognitive impairment already exhibit brain capillary damage and BBB disruption, particularly in the hippocampus, even in the absence of classical AD biomarkers—Aβ and tau accumulation. These findings suggest that BBB dysfunction may serve as an early and independent biomarker of cognitive decline, highlighting its potential role in the pathogenesis of AD (Nation et al., 2019). BBB breakdown allows the entry of blood-derived neurotoxic proteins, such as fibrinogen and thrombin, and facilitates peripheral immune cell infiltration, which in turn promotes neuroinflammation, oxidative stress, and synaptic dysfunction (Chen et al., 2023). Emerging evidence also suggests that *APOE4*, the strongest genetic risk factor for late-onset AD, contributes to neurodegeneration via a vascular pathway independent of Aβ and tau pathology. *APOE4* carriers exhibit early BBB breakdown in the hippocampus and parahippocampal gyrus, even when cognitively normal (Montagne et al., 2020). Further supporting the vascular hypothesis, several brain imaging studies have suggested that reductions in regional cerebral blood flow can predict cognitive decline and AD

progression, even before Aβ accumulation is detectable (de la Torre, 2018). Chronic cerebral hypoperfusion has therefore been proposed as a primary initiating event in AD, rather than a secondary consequence of neurodegeneration.

This shift in perspective highlights the need to investigate vascular dysfunction in AD and suggests that improving vascular health may represent a promising therapeutic strategy for preventing or delaying brain dysfunction.

Vascular Dementia (VaD)

Vascular dementia (VaD) is the second most common cause of dementia after Alzheimer's disease, accounting for up to 20% of dementia cases, and arises from a range of cerebrovascular pathologies that impair cerebral blood flow and lead to cognitive decline. VaD includes post-stroke dementia as well as forms caused by chronic cerebral small vessel disease (SVD) in the absence of overt stroke, through white matter damage, micro-infarcts, and disruption of the neurovascular unit.

The two most common subtypes of SVD are sporadic non-amyloid SVD (arteriosclerosis) and cerebral amyloid angiopathy (CAA). CAA is characterised by the deposition of Aβ proteins in the walls of small- to medium-sized arteries in the cerebral cortex and leptomeninges, and in more severe cases, cerebral capillaries are also involved (Magaki et al., 2018). The deposition of Aβ leads to the degeneration of smooth muscle cells, fibrinoid necrosis, and the formation of microaneurysms, which can damage vessel integrity and increase the risk of haemorrhagic and ischemic events (Cozza et al., 2023).

The pathobiology of VaD is mainly through vascular injury to the brain, including ischemic lesions, white matter damage, and cerebral microbleeds. SVD can lead to progressive neurodegeneration through impaired perfusion, inflammation, and oxidative stress. Notably, cerebrovascular disease often coexists with AD pathology, and may even

promote Aβ and tau accumulation by compromising the neurovascular unit and glymphatic clearance pathways, highlighting the complex interplay between vascular damage and neurodegenerative processes (Mok et al., 2024). Unfortunately, there is no cure for vascular dementia; thus, current treatment strategies focus primarily on prevention, management of vascular risk factors, and supportive care.

Dementia with Lewy Bodies (DLB)

Dementia with Lewy bodies (DLB) is the second most common neurodegenerative dementia in the elderly, clinically characterised by fluctuating cognition, recurrent visual hallucinations, and Parkinsonian motor features. Pathologically, DLB is primarily characterised by the abnormal accumulation of α-synuclein proteins, which form Lewy bodies and Lewy neurites in neurons. These aggregates are distributed across the brainstem, limbic system, and neocortex which disrupt normal neuronal function and contribute to cognitive and motor dysfunction (Garcia-Esparcia et al., 2017). α-synuclein is a presynaptic protein encoded by *SNCA* gene, and normally exists in a soluble form but can misfold into oligomers and fibrils, especially under pathological conditions. In DLB, neuronal loss impacts dopaminergic and cholinergic systems, contributing to hallmark symptoms such as memory loss, hallucinations, motor impairment, and sleep disturbances (Prasad et al., 2023). However, not all individuals with widespread α-synuclein pathology exhibit clinical symptoms, and the exact role of Lewy bodies and Lewy neurites remains unclear; some data suggest they might be neurotoxic, and others suggest a neuroprotective role (Walker et al., 2015). Also, vascular pathology does not seem to play a significant role in DLB, unlike VaD (Prasad et al., 2023). Despite growing insights into its pathology, the patho-mechanisms underlying DLB remain incompletely understood. Vascular mechanisms are not the primary focus of the current DLB research.

Frontotemporal Dementia (FTD)

Frontotemporal dementia (FTD) is a group of neurodegenerative diseases characterised by selective degeneration of the frontal or/and temporal lobes of the brain, leading to changes in behaviour, language, personality, and executive function. It is the most common cause of early-onset dementia under the age of 65 and presents with a spectrum of clinical phenotypes, including behavioural variant FTD (bvFTD), semantic and non-fluent variants of primary progressive aphasia (svPPA and nfvPPA), right temporal variant (rtvFTD), and forms associated with motor neuron disease (FTD-MND) (Antonioni et al., 2023).

FTD shows high heritability, with mutations in *MAPT, GRN, C9orf72* accounting for the majority of familial cases. The pathobiology of FTD is characterised by the abnormal accumulation of specific proteins—most notably tau, TDP-43, and FUS—within neurons and glial cells. Based on the molecular composition of these inclusions, FTD can be classified into three major neuropathological groups: TDP-43 proteinopathies (approximately 50% of cases), tauopathies (about 40%), and FET proteinopathies account for the remaining 10%, which include FUS, EWSR1, and TAF15 (Antonioni et al., 2023).

Pharmacological interventions focus on alleviating behavioural and neuropsychiatric symptoms. Non-pharmacological approaches focus on behavioural interventions, caregiver support, and targeted therapies including physical, occupational, and speech and swallowing therapy (Mollah et al., 2024). As with DLB, there has been limited investigation of vascular mechanisms in FTD.

Risk Factors for Dementia

Figure 1. 14 modifiable dementia risk factors identified by the 2024 Lancet Commission (Livingston et al., 2024).

The Lancet 2024 Commission highlighted 14 risk factors which can be potentially modified to prevent or slow the progression of dementia: less education, hearing impairment, untreated vision loss, smoking, obesity, high LDL cholesterol, depression, physical inactivity, excessive alcohol consumption, head injury, air pollution, infrequent social contact, diabetes, and hypertension (Livingston et al., 2024) (Figure 1). These risk factors can be conceptually grouped into five categories: cardiovascular and metabolic factors (hypertension, diabetes, obesity, high LDL cholesterol), lifestyle factors (smoking, excessive alcohol, physical inactivity), neurological factors (untreated vision loss, hearing loss, head injury), psychosocial factors (less education, depression, social isolation), and environmental factors (air pollution). This reflects the complex, multifactorial nature of

dementia risk and highlights how biological, behavioural, social, and environmental factors interact across the lifespan to influence brain health.

Table 1. Summary of modifiable dementia risk factors and their associated vascular dysfunction.

Risk Factor	**Key Vascular Dysfunction**	**Reference**
Hypertension	endothelial dysfunction, arterial stiffness, small vessel disease	(Maruhashi & Higashi, 2024)
Diabetes	atherosclerosis, endothelial dysfunction, basement membrane thickening, microthrombosis	(Li et al., 2023)
Obesity	endothelial dysfunction, arterial stiffness, vascular inflammation, perivascular adipose tissue dysfunction	(Koenen et al., 2021)
High LDL Cholesterol	atherosclerosis	(Mortensen et al., 2023)
Physical Inactivity	endothelial dysfunction, arterial stiffness, cerebral hypoperfusion, vascular inflammation	(Daniele et al., 2022)
Smoking	endothelial dysfunction, arterial stiffness, vascular remodelling, vascular inflammation	(Whitehead et al., 2021)
Air Pollution	endothelial dysfunction, vascular calcification, atherosclerosis, vascular inflammation	(Ding et al., 2024)
Head Injury	endothelial dysfunction, BBB breakdown, cerebral hypoperfusion, ischemia, oedema	(Z. A. Zhao et al., 2023)
Excessive Alcohol Consumption	oxidative stress, endothelial dysfunction, vascular inflammation, vascular remodelling	(Piano, 2017)
Depression	endothelial dysfunction, vascular inflammation, platelet dysfunction, autonomic dysfunction	(S. Zhao et al., 2023)

10 out of 14 factors are directly or indirectly linked to vascular pathology, underscoring the critical role of vascular health in dementia pathogenesis. Hypertension, diabetes, obesity and high LDL cholesterol have all been shown to directly affect vascular biology as the main mechanism by which they cause disease. Physical inactivity, smoking, air pollution, and head injury are associated with changes in vascular health. These factors have been

described to contribute to vascular dysfunction through a range of mechanisms such as endothelial damage, impaired cerebral perfusion, atherosclerosis, and inflammation (Table 1). Additionally, excessive alcohol consumption and depression may indirectly influence vascular health (Piano, 2017; S. Zhao et al., 2023). Risk factors show complex inter-relationships. For example, excessive drinking can contribute to obesity, which in turn increases the risk of diabetes, dyslipidemia, and hypertension (Choi et al., 2019). Obesity is also frequently observed in individuals with depression, with evidence of a bidirectional relationship; thus, these conditions compound cardiovascular risk (Zhang, 2021). Collectively, this suggests that maintaining vascular health is a key strategy for preventing dementia.

Among the vascular risk factors, hypertension and diabetes are the most strongly associated with impaired executive function. A cross-sectional study of 22,059 participants in the UK Biobank investigated how cerebrovascular risk factors affect executive function and brain structure in healthy individuals aged 44-73 years. The strongest predictor of executive function was age, followed by antihypertensive medication use (which can be considered as a robust index of established hypertension), diabetic status, and *APOE* ε4 status (Veldsman et al., 2020). Importantly, the study demonstrated that cerebrovascular risk burden was associated with reduced grey and white matter integrity within the frontoparietal network which underlies executive function.

Diabetes

Diabetes, particularly type 2 diabetes mellitus (T2DM) which accounts for approximately 90% to 95% of diabetes cases, is characterised by elevated blood glucose concentrations and is the most common metabolic disorder. Its prevalence is growing at an alarming rate

with 1.31 billion people worldwide expected to be living with the condition by 2050 (Collaborators, 2023). T2DM is a complex metabolic disorder characterised by both insulin resistance and pancreatic β-cell dysfunction, which together impair glucose homeostasis. The development of T2DM is driven by a multifactorial interplay of genetic, metabolic, and environmental factors (Galicia-Garcia et al., 2020).

Diabetes can affect multiple organs through injury to nerves and blood vessels. Several hypotheses have been proposed for pathological mechanisms, principally centred on the deleterious effects of hyperglycaemia. *In vitro* experiments and mouse models have shown that hyperglycaemia can induce excessive production of reactive oxygen species (ROS) by mitochondria of the endothelial cells, leading to microvascular damage characterised by endothelial dysfunction and basement membrane thickening, which in turn impairs the supply of oxygen and nutrients to surrounding tissues (Binjawhar et al., 2023; Busik et al., 2008; Casalena et al., 2020). In the brain, these changes may contribute to NVU disruption, BBB breakdown, pericyte loss, and astrocyte dysfunction, all of which can impair metabolic support and cerebral perfusion. Over time, this results in white matter damage, brain atrophy, and small vessel disease (Mauricio et al., 2023).

T2DM patients have up to a 2-fold increased risk of developing AD and this is believed to be driven in part by insulin resistance and deficiency, which disrupt normal insulin signalling in the brain and interfere with Aβ clearance, enhance tau phosphorylation, and promote oxidative stress and inflammation (Li et al., 2015). Based on their similar physiological and pathological mechanisms, it has even been suggested that AD should also be classified as ‘type 3 diabetes mellitus’ (de la Monte et al., 2018). Brain imaging studies have shown that T2DM patients exhibit a higher incidence of cerebral infarcts and significantly reduced volumes of total grey matter, white matter, and the hippocampus. These structural changes closely mirror patterns seen in preclinical AD, suggesting a potential overlap in underlying neurodegenerative processes (Moran et al., 2013; Motaghi et al., 2024).

First-line treatment typically includes metformin, a biguanide that enhances insulin sensitivity, particularly in the liver. Other oral agents—such as sulfonylureas, DPP-4 inhibitors, SGLT-2 inhibitors, thiazolidinediones, and α-glucosidase inhibitors—are commonly used alone or in combination depending on patient response and comorbidities. GLP-1 receptor agonists and the dual GLP-1/GIP agonist tirzepatide have shown particular benefits in improving glycaemic control and promoting weight loss (Tegegne et al., 2024). In the United States, prescribing of GLP-1 receptor agonists has increased substantially since the 2022 American Diabetes Association (ADA) guidelines recommended their use in patients with cardiovascular disease, obesity, or chronic kidney disease, with first-line use rising from around 6% to 18% by 2023 (Do et al., 2025). In the United Kingdom, prescribing trends also increased following the adoption of the ADA recommendations, but remain more tightly regulated within the NHS. A 2023 NHS safety alert highlighted global shortages and imposed restrictions to ensure prescribing aligns with licensed indications, reflecting a more controlled approach to managing demand and supply (Ibrahim & Orayj, 2024). Insulin therapy is reserved for severe cases or where oral agents are insufficient. Despite the wide range of available therapies, current treatments for T2DM remain noncurative and are often limited by suboptimal efficacy, side effects, and the need for continuous monitoring (Tegegne et al., 2024). Most interventions focus primarily on lowering blood glucose and managing symptoms, rather than addressing the underlying pathophysiology.

Growing evidence suggests that antidiabetic medications may have protective effects against cognitive decline and dementia. Among antidiabetic drugs, thiazolidinediones, particularly pioglitazone, consistently show the most robust and dose-dependent reduction in dementia risk, likely due to their ability to cross the blood-brain barrier (Slouha et al., 2023). Metformin, the most widely prescribed first-line oral antidiabetic drug, has shown inconsistent associations with dementia risk (Foretz et al., 2023). While some studies report protective effects, others indicate no benefit or even a potential

increase in dementia incidence. In contrast, sulfonylureas, especially glyburide, are generally associated with increased dementia risk, possibly due to hypoglycaemia-induced neuronal stress (Michailidis et al., 2022; Slouha et al., 2023).

Hypertension

The prevalence of hypertension has doubled from 1990 to 2019, with 626 million women and 652 million men worldwide living with hypertension in 2019 (Collaboration, 2021). Persistent high blood pressure increases the risk of dementia as well as cerebrovascular disease, chronic kidney disease, and heart failure (Canavan & O'Donnell, 2022).

Hypertension has a strong heritable component, with genetic studies estimating blood pressure heritability at approximately 50% (Mani, 2024). While early research identified rare monogenic forms of hypertension, most hypertension cases are attributed to the cumulative effect of numerous common genetic variants. A 2024 genomic study involving over one million European individuals identified 2,103 independent genetic signals associated with hypertension, including 113 novel loci. These variants collectively explain over 60% of SNP-based heritability (Keaton et al., 2024).

Hypertension is a multifactorial disease arising from the complex interplay between genetic, environmental, neural, renal, vascular, and immune mechanisms (Harrison et al., 2021). These include: 1) the kidneys, which regulate sodium balance and blood volume through mechanisms such as renin release and pressure natriuresis; 2) the vasculature, which can undergo structural remodelling and endothelial dysfunction, leading to increased resistance and impaired nitric oxide (NO) signalling; 3) the central nervous system, which contributes through sympathetic activity to promote vasoconstriction and sodium retention; 4) the immune system, which exacerbates vascular injury and sodium retention through inflammation and immune cell activation.

A proposed shared mechanism across multiple systems is oxidative stress, primarily driven by mitochondrial dysfunction and NADPH oxidase activation. ROS is upregulated in vascular, renal, and neural tissues in hypertension, often in response to stimuli such as angiotensin II, high salt intake, and shear stress (Dikalov & Ungvari, 2013; Harrison et al., 2021). Additionally, the reduced activity of mitochondrial antioxidant regulators such as *SIRT3* further amplifies ROS production. Oxidative stress then impairs vasodilation, enhances inflammation and thus exacerbates hypertension (Harrison et al., 2021).

Hypertension impairs endothelial cell (EC) function through hemodynamic stress, oxidative stress, and chronic inflammation, leading to reduced NO, increased ROS, and upregulation of inflammatory pathways such as NF-κB. These changes shift the endothelium toward a vasoconstrictive, pro-inflammatory, and pro-thrombotic phenotype, contributing to vascular remodelling and elevated peripheral resistance (Gallo et al., 2021). While oxidative stress and inflammation are primary drivers of EC dysfunction in hypertension, evidence suggests that endothelial dysfunction can both result from and precede elevated blood pressure, indicating a bidirectional relationship. Young individuals with a family history of hypertension exhibited impaired endothelial responses, likely due to disruptions in NO signalling (Higashi et al., 2012).

In the mouse brain, these changes disrupt the NVU, leading to BBB breakdown, capillary rarefaction, and white matter damage. The resulting cerebral small vessel disease, characterised by microbleeds, lacunes, and demyelination, contributes to impaired cerebral perfusion and ultimately to cognitive decline (Baggeroer et al., 2024; Guy et al., 2022; Kaiser et al., 2014).

Hypertension affects human brain health. As described above, blood pressure is a key predictor of executive function (Veldsman et al., 2020). A brain MRI study assessing BBB integrity in 22 hypertensive patients and 19 normotensive controls reported that higher systolic, diastolic, and mean arterial pressures were associated with increased BBB leakage, particularly in the cortex and grey matter (Gal et al., 2024). Also, a study has

shown that increased neuropathological features, such as neurofibrillary tangles and senile plaques, were detected in the postmortem brain tissues of hypertensive patients (Shah et al., 2012).

Current antihypertensive therapies include several drug classes targeting key pathophysiological mechanisms, such as the renin-angiotensin-aldosterone system (RAAS), sympathetic nervous system, vascular smooth muscle tone, and renal sodium handling (Redon & Carmena, 2024). Widely used antihypertensives include RAAS inhibitors (ACE inhibitors, ARBs, and direct renin inhibitors), calcium channel blockers, diuretics (thiazides, loop, and potassium-sparing), beta-blockers, and alpha-blockers. Combining antihypertensive drugs from different pharmacological classes enhances blood pressure reduction through additive effects, as each drug targets distinct but complementary pathways. This strategy not only improves efficacy but can also help minimise drug-induced side effects (Paczkowska-Walendowska et al., 2022; Redon & Carmena, 2024).

Randomised controlled trials show a 7% to 11% relative risk reduction in the incidence of dementia with antihypertensive treatment (Hughes et al., 2020). Interestingly, calcium channel blockers and RAAS blockers (ACE inhibitors and ARBs) appear to offer neuroprotective effects beyond blood pressure control (Rouch et al., 2015). Notably, antihypertensive drugs that cross the BBB are more likely to exert beneficial effects on memory and reduce the risk of AD compared to non-BBB-penetrating drugs (Glodzik & Santisteban, 2021).

Emerging evidence strongly suggests that mid-life is a critical window for vascular risk management to reduce late-life dementia risk. In mid-life individuals (aged 44-69 years), higher systolic blood pressure (SBP) was negatively correlated with executive function (Veldsman et al., 2020). However, this relationship was not observed in late-life

individuals (aged >70 years), highlighting that untreated mid-life hypertension is a significant risk factor for late-life dementia. In another study, individuals with mid-life hypertension were at increased dementia risk regardless of their late-life blood pressure status (Walker et al., 2019). Notably, individuals with mid-life hypertension followed by late-life hypotension exhibited the highest risk, suggesting that prolonged vascular stress followed by a decline in blood pressure may exacerbate underlying vascular or neurodegenerative damage. A recent cohort study demonstrated that individuals diagnosed with type 2 diabetes before the age of 50 had a significantly higher risk of dementia compared to those diagnosed at older ages, and the risk was even increased in those who were obese at the time of diagnosis (Qi et al., 2024). Collectively, these findings underscore mid-life as a critical window for intervention to prevent long-term cognitive decline.

The Neurovascular Unit (NVU)

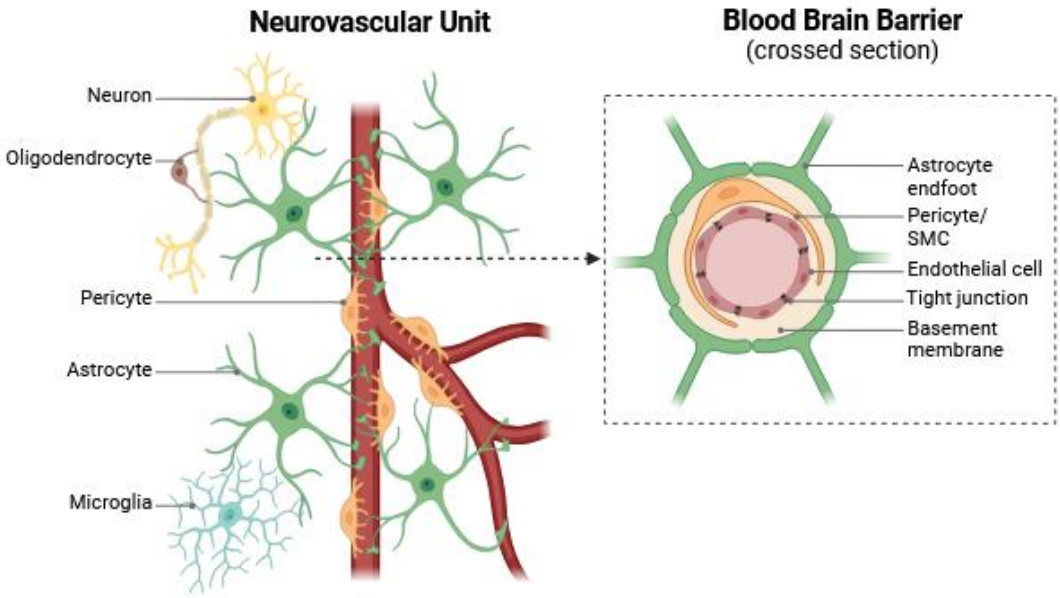

Figure 2. Structures of the neurovascular unit (NVU) and blood-brain barrier.

Reprinted from "Neurovascular Unit and Blood Brain Barrier", by BioRender.com (2024). Retrieved from https://app.biorender.com/biorender-templates

SMC, Smooth Muscle Cell.

The brain only takes up 2% of the body mass but uses 20% of the body energy at rest. The brain has a limited capacity to store energy; therefore, the normal functioning of neural circuits relies on oxygen and glucose supply from the bloodstream (Andreone et al., 2015). Neural and vascular activity are therefore tightly coupled to meet the brain's high energy demands. This is achieved through the organisation of brain tissue into the NVU consisting of vascular cells, glial cells, and neurons (Figure 2). The NVU is no longer viewed as a static structural unit but rather as a regionally specialised, dynamic, and systemically regulated network (Alkayed & Cipolla, 2023). The NVU maintains brain homeostasis by regulating cerebral blood flow and removing metabolic waste. The components of NVU establish dynamic crosstalk between the vascular and nervous systems via neurovascular coupling (NVC) and vasculo-neuronal coupling (VNC) to ensure normal neuronal function and cerebral blood flow. Neurovascular coupling refers

to the communication process in which neuronal activity alters local blood flow in the brain to meet the metabolic demands of active neurons, and communication in the opposite direction has also been proposed—referred to as vasculo-neuronal coupling. Signals from vasculature can alter glial and neuronal function to maintain brain and cerebral homeostasis (Presa et al., 2020).

Neurons and blood vessels share growth factor signals and guidance cues: vascular endothelial growth factor (VEGF) as a key angiogenetic factor has a direct impact on axon growth; nerve growth factor (NGF) as a neurotropic molecule shows angiogenic properties; neurexins, which mainly involved in the formation and maintenance of synapses between neurons, have effects on vascular remodelling and angiogenesis; axon guidance molecules semaphorins, ephrins, silts, and netrins can also act as angiogenesis driving factors (Ribatti & Guidolin, 2022).

Endothelial Cells

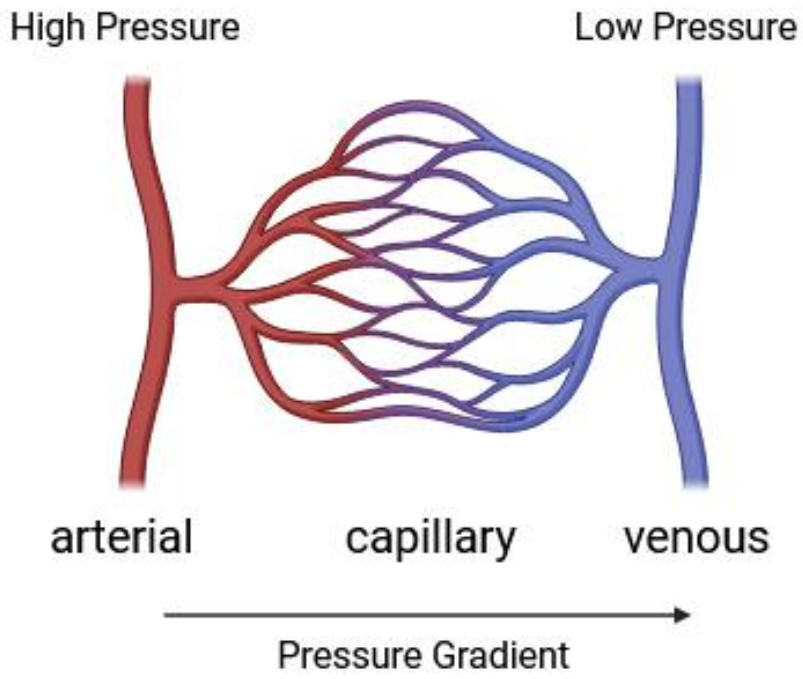

Figure 3. The hierarchy of the vascular network.

Created with BioRender.com.

The blood vessels in the brain are lined by a continuous monolayer of highly specialised endothelial cells. Unlike the peripheral vasculature endothelial cells, brain endothelial cells form a tightly connected, uninterrupted barrier through circumferential tight junction proteins, restricting the passive movement of cells and molecules from the bloodstream into the brain parenchyma, with selectivity based on molecular size, surface electrical charge, and lipid solubility (McConnell & Mishra, 2022).

Besides as a physical barrier, brain endothelial cells actively regulate the bidirectional exchange of substances between the blood and the brain. Unlike peripheral endothelial cells, brain endothelial cells suppress nonspecific transcytosis, thereby limiting transcellular transport (McConnell & Mishra, 2022). Consequently, molecular movement across the BBB is tightly regulated and highly selective.

Brain endothelial cells have been proposed to contribute to neurovascular coupling by modulating local vascular responses and facilitating signal propagation along the vascular tree. They show an increased mitochondrial load reflecting their metabolically active role in regulating NVU function. This also makes them more vulnerable to oxidative stress (Davidson & Duchen, 2007).

The NVU is distributed along a three-dimensional vascular network composed of pial and penetrating arterioles, capillaries, venules, and veins, which together support cerebral perfusion under a dynamic pressure gradient from high-pressure arterioles to low-pressure venous compartments (Figure 3). Arterial, capillary, and venous endothelial cells exhibit a gradual phenotypic change and a gene expression change along the arteriovenous axis of the human brain vasculature, referred to as zonation (Vanlandewijck et al., 2018).

Venous endothelial cells (vEC) are a functionally unique population characterised by angiogenic plasticity and high proliferative capacity. vEC can migrate against the direction of blood flow and can acquire capillary and even arterial identity (Lee et al., 2021). In contrast, arterial endothelial cells (aEC) are adapted to withstand high shear stress and pulsatile blood flow and elongated in the direction of flow, with tightly organised junctions that contribute to a low permeability barrier (dela Paz & D'Amore, 2009). Capillary endothelial cells (cEC) comprise the majority of the cerebral vasculature and are the principal site of oxygen, nutrient, and metabolite exchange between the blood and brain parenchyma (Trimm & Red-Horse, 2023).

A mouse brain single-cell study has shown that capillary EC exhibited the most substantial transcriptional changes with ageing among all endothelial subtypes classified within the arteriovenous zonation. These changes involve pathways related to BBB dysfunction, glucose and energy metabolism, and immune signalling. Notably, cEC

exhibited downregulation of genes critical for BBB integrity and molecular transport, which suppresses transcytosis. Additionally, many of these dysregulated genes overlapped with AD risk genes (Zhao et al., 2020). This suggests capillary EC is a key endothelial cell subtype with increased vulnerability to neurovascular ageing and neurodegeneration.

Mural Cells

Mural cells are perivascular cells located along the vessel wall, comprising two main subtypes: pericytes and vascular smooth muscle cells. These cells are essential structural and regulatory components of the cerebral vasculature.

Pericytes enwrap capillaries across all vascular beds, with the central nervous system (CNS) exhibiting the highest pericyte coverage in the body. In the CNS, the pericyte-to-endothelial cell ratio is approximately 1:4, in contrast to ratios of 1:10 or more in skeletal muscle. (McConnell & Mishra, 2022). This enriched distribution underscores the key role of pericytes in cerebral vascular development, BBB maintenance, and microvascular regulation. Pericytes can be contractile, and functional heterogeneity along the vascular tree reflects positional differences—such as precapillary pericytes that may act as flow regulators or sphincters and mid-capillary pericytes that maintain basal cerebral blood flow and BBB stability (Grubb et al., 2020; Hartmann et al., 2021; Nelson et al., 2020). Functionally, pericytes also modulate angiogenesis by influencing endothelial sprouting, vascular patterning, and regression after the angiogenic phase via regulation of local VEGFA levels and through paracrine signalling including PDGFB pathways (Siekmann, 2023).

Vascular smooth muscle cells (vSMCs) are key regulators of vascular tone, cerebral autoregulation, and rapid vasomotor responses (Attwell et al., 2010; Iadecola & Nedergaard, 2007). vSMCs are embedded within the walls of arteries, where they form

multiple concentric layers surrounding larger vessels (McConnell & Mishra, 2022). During neurovascular coupling, NO primarily mediates arteriolar dilation via vSMC relaxation. NO is synthesised by two main sources within the NVU: neurons and endothelial cells. In neurons, NO is generated by neuronal nitric oxide synthase (nNOS) in response to glutamate-induced calcium influx following synaptic activation. In endothelial cells, NO is produced by endothelial nitric oxide synthase (eNOS), which is activated by both intracellular calcium and blood flow-induced wall shear stress (Dormanns et al., 2016). In contrast, capillary diameter has been proposed to be determined by astrocyte-derived arachidonic acid products such as prostaglandins, which act on pericytes to induce their relaxation (Mishra et al., 2016; Siekmann, 2023).

Astrocytes

Astrocytes are the most abundant glial cells in the CNS, characterised by their polarised morphology and extensive interactions with both neurons and the cerebral vasculature. Their endfeet almost completely ensheath the brain vasculature, including the endothelial and surrounding mural cells, forming a key structural and functional interface known as the glio-vascular unit (McConnell & Mishra, 2022).

While arterioles were associated with the thickest astrocytic sheaths, capillaries showed the highest density of astrocyte process contacts per surface area. Despite differences in sheath thickness and vessel diameter, the number of astrocytic processes contacting a given length of vessel was similar across arterioles, capillaries, and venules (McCaslin et al., 2011).

Functionally, astrocytes maintain CNS homeostasis by regulating ion balance, neurotransmitter uptake, and synaptic signalling. They are electrically coupled into a syncytium via gap junctions, enabling the spread of calcium waves and long-range

signalling across the brain (Sofroniew & Vinters, 2010). Astrocytes are also critical for maintaining BBB integrity by secreting basement membrane proteins (e.g., laminins) and releasing signalling molecules that influence endothelial cells and pericytes, thereby preserving the CNS-specific properties of these cells within the BBB (Yao et al., 2014). Astrocytes interact closely with endothelial cells and pericytes. Mounting evidence highlights that the principal functional interaction of astrocytes at the BBB is with endothelial cells, primarily through the secretion of paracrine factors that influence endothelial tight junctions, barrier properties, and inflammatory responses (Manu et al., 2023). In addition, astrocytes contribute to nutrient transport by regulating the uptake of glucose and glutamate—both vital for healthy brain function (Lee et al., 2017).

Within the NVU, astrocytes play a key role in regulating cerebral blood flow: they help maintain the resting tone of arterioles by releasing vasoactive agents such as prostaglandin E2 and ATP, and act as intermediaries in neurovascular coupling by relaying signals from active neurons to vascular mural cells (Mishra, 2017). Astrocytes also serve an important role in glymphatic waste clearance. Together, these functions underscore the diverse and multifaceted roles astrocytes play in supporting both vascular and neuronal homeostasis in the CNS.

Thus, dysfunction of astrocytes has been increasingly recognised as a key contributor to brain disorders, including neurodegenerative disease progression, as impairments in neurotransmitter recycling, calcium signalling, and metabolic support can disrupt synaptic integrity and promote neuronal vulnerability (Brandebura et al., 2023).

Microglia

Microglia, the brain's resident immune cells, patrol the cerebral microenvironment, enabling rapid responses to pathogens, injury, and other disturbances. Microglia are

responsible for the clearance of microbes, dead cells, redundant synapses, protein aggregates, and various particulate or soluble antigens that may pose a threat to CNS homeostasis. In addition to their phagocytic functions, microglia serve as the primary source of proinflammatory cytokines in the brain, positioning them as key mediators of neuroinflammation. Through cytokine signalling and cellular crosstalk, microglia can initiate, amplify, or modulate a wide range of responses within the neurovascular unit and the broader neural environment (Colonna & Butovsky, 2017).

In the early phase of systemic inflammation, microglia physically associate with the vasculature, where they express the tight junction protein to help maintain endothelial integrity; however, in prolonged inflammatory exposure, microglia shift to a reactive phenotype and begin to phagocytose astrocytic endfeet, leading to the disruption of the glio-vascular interface and subsequent compromise of BBB integrity (Haruwaka et al., 2019). Microglia can also influence vascular tone and adjust cerebral blood flow in response to metabolic demands or vascular stress. Experimental ablation or inhibition of microglia leads to impaired vasodilation and reduced cerebral blood flow responses, indicating that microglia are critical for normal neurovascular coupling activity (Csaszar et al., 2022).

Notably, microglia have emerged as a key player in the pathogenesis of AD. Genome-wide association studies (GWAS) revealed that most AD risk genes are predominantly or exclusively expressed in microglia, underscoring their significance in AD progression and treatment strategies (Sun et al., 2024). *APOE*, a key genetic risk factor for AD, is highly expressed in astrocytes under normal conditions but is also upregulated in reactive microglia in disease states, highlighting the critical interplay between microglia and astrocytes in AD pathology (Parhizkar & Holtzman, 2022).

Single-Cell Technologies: Deciphering Brain Complexity

Table 2. Comparison of bulk RNA sequencing, single-cell RNA sequencing, and single-nucleus RNA sequencing.

	Bulk RNA-seq	**scRNA-seq**	**snRNA-seq**
Input	Tissues/Cell populations	Dissociated cells	Isolated nuclei
Output	Average gene expression profile of each sample	Gene expression profile of each cell	Gene expression profile of each nucleus
Data Structure	Sample x Gene counts matrix	Cell x Gene counts matrix	Nucleus x Gene counts matrix
Tissue Requirement	Homogenous tissues	Fresh tissues	Frozen tissues (e.g. human post-mortem brain)
Usage	Difference between sample conditions	Investigate cellular heterogeneity	Investigate cellular heterogeneity
Advantages	Less expensive and easier to handle	Cell-type specific studies and deeper insights	Cell-type specific studies and deeper insights
Disadvantages	Masking cellular heterogeneity	Stochastic noise	Stochastic noise; missing cytoplasmic RNA

Bulk RNA-seq, Bulk RNA sequencing; scRNA-seq, single-cell RNA sequencing; snRNA-seq, single-nucleus RNA sequencing.

Bulk RNA-sequencing (Bulk RNA-seq) allowed researchers to investigate gene expression levels at a tissue or cell population, enabling identification of the difference between conditions such as disease compared to control tissue. However, bulk RNA-seq masks cell-to-cell variability and limits the identification of rare cell types and cell-type-specific studies. The rapid development of single-cell technologies has enabled the identification of novel cell types and subtypes in tissues, the investigation of cell-type-specific changes in response to diseases, and deeper insights into dysregulated molecular networks and potential pathogenic mechanisms (Table 2). In the case of frozen

human post-mortem tissue, single-nucleus RNA sequencing (snRNA-seq) is typically used as an alternative to single-cell RNA sequencing (scRNA-seq) since defrosting tissue leads to cell lysis whilst nuclei and their contents are preserved.

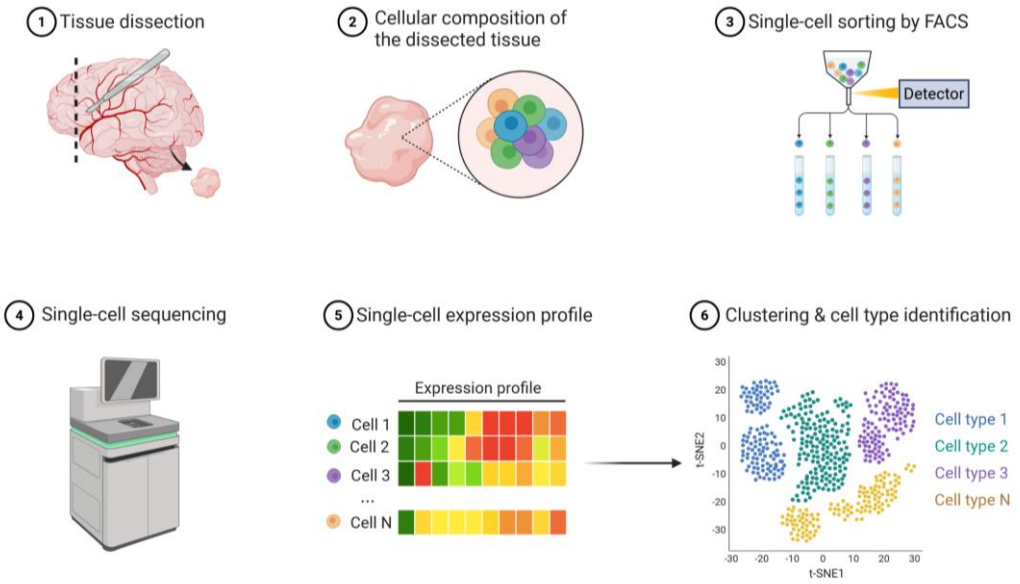

Figure 4. Overall process of single-cell RNA sequencing.

Reprinted from "Single-Cell Sequencing", by BioRender.com (2024). Retrieved from https://app.biorender.com/biorender-templates

Following tissue dissection, isolation of single cells and sequencing, raw sequencing reads are preprocessed (aligning reads to the reference genome, assigning reads to individual cells, and quantifying gene expression), quality controlled and normalised followed by various types of analyses (Figure 4).

While single-cell approaches provide unparalleled resolution of cellular heterogeneity, the single-cell data is often sparse and noisy due to technical dropout and low mRNA content per cell. Furthermore, single-cell analysis methods may lead to very high false discovery rates. scRNA-seq differential expression models that treat individual cells as independent can artificially inflate statistical power by ignoring the biological dependence between cells

from the same individual—a phenomenon known as pseudoreplication. This can lead to an increased risk of false positives, as intra-individual variation is mistakenly interpreted as a true biological signal (Murphy & Skene, 2022). To address these limitations and improve statistical robustness, many studies employ a pseudobulk approach. A pseudobulk gene expression matrix is generated by aggregating the counts across cell types in each sample, enabling the application of well-established bulk RNA-seq analysis tools while retaining the cellular resolution offered by scRNA-seq and avoiding false discovery (Murphy & Skene, 2022).

A recent study evaluated the robustness of pseudobulk analysis for identifying differentially expressed genes (DEGs) by comparing it with bulk RNA-seq and scRNA-seq analysis. The study reported that pseudobulk captured the majority of DEGs identified by bulk RNA-seq and more closely mirrored bulk DEG profiles than single-cell analysis using the Wilcoxon test in Seurat (Liu et al., 2023). Pseudobulk offers a more robust and quantitatively reliable approach for DEG detection than direct single-cell methods. However, single-cell approaches retain a key advantage, preserving cell-level resolution and subtle cellular states that are lost in aggregated data. These complementary strengths suggest that integrating both pseudobulk and single-cell methods may offer the most comprehensive strategy—leveraging the statistical power of pseudobulk methods for differential gene expression testing while preserving the cellular heterogeneity and discovery potential offered by single-cell methods.

Table 3. Comparison of 10x Genomics and Parse Bioscience (SPLiT-seq).

	10x Genomics	**Parse Bioscience (SPLiT-seq)**
Method	Microfluidics-based partitioning of cells into droplets for barcoding and library preparation	Combinatorial barcoding of fixed cells without physical partitioning
Sample Multiplexing	Limited (up to 16 samples)	High (up to 96 samples)
Library Efficiency	Higher cell recovery and valid reads (exonic)	Lower recovery and more invalid reads (intronic)
Gene Detection Sensitivity	Detect fewer genes per cell	Detect 1.2 times more genes per cell
Rare Cell Type Detection	Less sensitive	Better detection of rare cell populations
Clustering Quality	Moderate	More distinct clusters
Marker Gene Expression	Higher for canonical markers	Lower

10x Genomics and Parse Biosciences (SPLiT-seq) are two leading platforms for single-cell RNA sequencing, each with unique strengths and applications. 10x Genomics uses a microfluidics-based approach to partition individual cells into droplets, where barcoding and library preparation occur within each droplet. This method physically isolates each cell, allowing for high-efficiency capture and processing. In contrast, Parse uses combinatorial barcoding of fixed and permeabilised cells without physically isolating individual cells. Instead of droplets, Parse uses a series of split-pool steps across multi-well plates to assign unique barcodes, enabling high-throughput sample processing (Table 3).

Parse offers several advantages, including greater sensitivity for detecting lowly expressed genes and rare cell populations, as well as the ability to multiplex up to 96 samples in a single run, making it particularly well-suited for high-throughput discovery

studies. Sample multiplexing is a method that enables multiple biological samples to be processed together in a single experiment. This approach enhances efficiency and lowers overall costs by increasing throughput while minimising resource use and preparation time. Additionally, because all samples are handled under identical conditions, sample multiplexing helps to reduce batch effects and improve data consistency. However, its protocol yields lower cell recovery efficiency compared to 10x Genomics droplet-based methods. 10x Genomics demonstrates superior library efficiency and more reliable detection of canonical marker genes, making it ideal for studies focused on classical cell-type annotation (Xie et al., 2024). While both platforms generate high-quality single-cell transcriptomic data, their unique strengths suggest that platform selection should be guided by the specific goals of the study—whether that is maximising sensitivity and detecting rare cell populations (Parse), or optimising cell recovery and robust marker-based analysis (10x).

Single-Cell Transcriptomic Studies of Human Cerebrovasculature

The cerebral vasculature plays an essential role in maintaining brain function and homeostasis. Advances in single-cell transcriptomic technologies have enabled researchers to uncover the cellular heterogeneity of the human cerebrovasculature and characterise transcriptional changes associated with disease. These insights have deepened our understanding of neurovascular interactions and the molecular mechanisms underlying cerebrovascular and neuropsychiatric disorders, while also revealing potential therapeutic targets.

I reviewed recent research on single-cell transcriptomic studies of human brain vasculature: covering various brain regions—from foetal to adult—and including individuals without neurological disorders, patients with arteriovenous malformations (AVM), and, predominantly, individuals with AD (Table 4).

Table 4. Overview of single-cell/nucleus transcriptomic studies of human cerebrovasculature.

Study	**Sample Source**	**Number of Cells/Nuclei**	**Sample Cohort**
(Garcia et al., 2022)	*Ex vivo*: human temporal cortex *In silico*: vascular nuclei from post-mortem human brains across seven different brain regions - prefrontal cortex, mid-temporal cortex, angular gyrus, entorhinal cortex, thalamus, hippocampus, and mammillary body	*Ex vivo*: 84,350 profiled nuclei (including 4,992 vascular nuclei) *In silico*: 11,689 vascular nuclei	*Ex vivo*: 7 samples of healthy tissue distal to epileptic foci *In silico*: control individuals without neurological pathology from 219 published datasets
(Winkler et al., 2022)	Adult human cerebral cortex and arteriovenous malformations (AVM)	181,388 cells	5 normal cerebral cortex and 5 AVM tissues from adult human
(Yang et al., 2022)	Post-mortem human hippocampus and superior frontal cortex	143,793 nuclei	25 samples of 9 individuals with AD and 8 individuals with no cognitive impairment
(Sun et al., 2023)	Six brain regions: the prefrontal cortex (area BA9), the hippocampus, the mid-temporal cortex, the angular gyrus, the entorhinal cortex, and the thalamus	22,514 cerebrovascular nuclei	725 post-mortem brain samples of 220 individuals with AD and 208 age-matched controls
(Is et al., 2024)	Human temporal cortex	78,396 nuclei	12 donors with AD and 12 age- and sex-matched control
(Wälchli et al., 2024)	Developing foetal brains Adult control brains: temporal lobe Adult diseased brains: including brain vascular malformations and brain tumours	606,380 cells	117 samples of 8 human foetuses and 61 adult brain samples
(Tsartsalis et al., 2024)	Entorhinal, somatosensory, prefrontal cortex, and other cortical regions	> 100,000 cerebrovascular nuclei	Integrated with public data to yield 77 samples of 36 non-diseased controls and 41 AD donors

Garcia et al. (2022) addressed the challenge of low vascular cell abundance in brain tissue by developing a blood vessel enrichment protocol, using dextran-based density ultracentrifugation to isolate microvessel-enriched fractions from homogenised fresh human brain tissue. This study enriched for endothelial, mural, and fibroblast cells, while also capturing parenchymal cells. Using both experimental enrichment from fresh surgical cortex samples and *in silico* sorting from post-mortem data (ROSMAP), they captured 4,992 canonical vascular nuclei from 84,350 *ex vivo* profiled nuclei, as well as an additional 11,689 canonical vascular nuclei from post-mortem tissue. The study revealed transcriptional zonation of endothelial and mural cells along the arteriovenous axis, and further examined Huntington's disease (HD), showing that HD brains exhibit increased innate immune signalling and reduced expression of tight junction proteins, indicative of BBB breakdown. The study also examined other datasets, including samples from the prefrontal cortex, and found that the *in silico* dataset showed consistent cell types across experimental platforms and sample cohorts.

Winkler et al. (2022) performed single-nucleus RNA sequencing of human cerebrovascular cells to characterise vascular cell types and transcriptional changes associated with brain arteriovenous malformations. This study enriched for cerebrovascular cells through a microdissection-based isolation of blood vessels. Using fresh surgical resections from patients with AVM and control tissue from epilepsy-related lobectomies, the authors profiled a total of 181,388 nuclei. To validate and spatially contextualise their findings, the authors also applied spatial transcriptomics to cortical AVM tissue. These data confirmed vascular gene expression with cerebrovascular cells organised into anatomically and molecularly distinct vascular compartments, such as arteries, capillaries, and veins. However, the focus on a single vascular pathology—arteriovenous malformation—may limit the generalisability of the findings to other neurovascular conditions, and the study did not focus on any specific cortical region, instead isolating the region containing the AVM.

Yang et al. (2022) developed VINE-seq, a novel protocol optimised to isolate cerebrovascular nuclei from frozen human brain tissue. This method overcomes the challenge of removing the extracellular matrix that surrounds microvessels without damaging the nuclei by using a gentle dissociation approach. Applying this method, they profiled 143,793 single-nucleus transcriptomes from the hippocampus and superior frontal cortex of individuals with AD and controls. They identified a broad range of cerebrovascular and associated cell types, including endothelial cells, mural cells, fibroblasts, astrocytes, and microglia, and characterised AD-related transcriptomic changes within these populations. The study highlighted widespread dysregulation of pathways involved in immune signalling, extracellular matrix remodelling, and BBB integrity, providing new insights into cerebrovascular dysfunction in AD.

Building on this foundation, Sun et al. (2023) substantially expanded the scope by conducting a comprehensive, multi-region single-nucleus transcriptomic analysis of the human cerebrovasculature in AD. Profiling 22,514 vascular nuclei from six brain regions—including the prefrontal cortex, hippocampus, mid-temporal cortex, angular gyrus, entorhinal cortex, and thalamus—from 220 individuals with AD and 208 age-matched controls. The study revealed 2,676 cell-type-specific differentially expressed genes in AD, many of which were enriched in pathways related to immune signalling, cell adhesion, extracellular matrix organisation, and BBB integrity. Tsartsalis et al. (2024) further advanced this work by performing a single-nucleus RNA sequencing analysis of over 100,000 brain vascular nuclei from different cortical regions, including the entorhinal, somatosensory, and prefrontal cortex, combining 44 newly generated samples with publicly available data for a total of 77 donors (41 AD donors and 36 controls). This study identified endothelial cells as particularly enriched for AD genetic risk loci and highlighted endothelial pathways related to angiogenesis, inflammation, and Aβ clearance as potential therapeutic targets for slowing or preventing AD progression. Most recently, Is et al. (2024) focused on the gliovascular unit in the temporal cortex, analysing 78,396 nuclei

from 12 individuals with AD and 12 controls. They identified pericytes as a key site of transcriptional perturbation and validated a disrupted VEGFA-SMAD3 signalling axis between astrocytes and pericytes.

Wälchli et al. (2024) constructed the most extensive single-cell atlas of the human brain vasculature to date, profiling 606,380 cells from 117 samples spanning foetal development, adult controls, and multiple vascular-dependent brain pathologies. These included brain vascular malformations and tumours such as AVM, gliomas, metastases, and meningiomas. The study achieved unprecedented resolution of endothelial heterogeneity, identifying 44 transcriptionally distinct endothelial subclusters that were organised along the arteriovenous axis, including arterial, capillary, venous, and angiogenic states. To spatially validate these findings, the authors applied spatial transcriptomics, confirming the localisation of endothelial subtypes along the arteriovenous axis and demonstrating spatial reorganisation of vascular gene expression in pathological tissues, marked by the disruption of normal zonation patterns.

Finally, a prefrontal cortex-specific single-cell dataset has recently been reported but this only had a small representation of vascular cells. The study performed integrated snRNA-seq and spatial transcriptomics to generate a high-resolution transcriptomic atlas of the human dorsolateral prefrontal cortex, using tissue from 10 neurotypical adult donors. A total of 54,394 nuclei passed quality control for snRNA-seq, and vascular cell types—including endothelial cells and mural cells—were present but constituted only a small proportion of the dataset (Huuki-Myers et al., 2024).

These single-cell studies have collectively shown that the cerebrovasculature has molecularly well-defined vascular cell types and cell subtypes. A key recurring theme across these studies is the breakdown of the BBB in disease, characterised by transcriptional changes in endothelial cells and pericytes. There was also evidence of activation of immune signalling, reflecting a shift toward a pro-inflammatory vascular phenotype, and by dysregulation of NVU, including disrupted astrocyte-vascular

interactions, in the context of disease. This highlights the biological relevance of BBB and NVU impairment across a range of neuropathological conditions.

Problem Statement

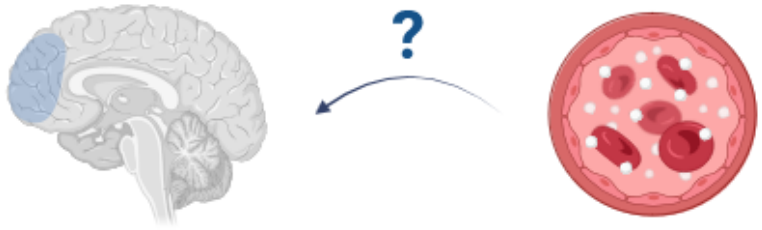

Figure 5. Vascular risk factors (hypertension and diabetes) may affect executive function primarily through their effects on the vasculature of the prefrontal cortex.

Created with BioRender.com.

The brain vasculature, which is the interface between the vascular system and the brain, is essential to brain homeostasis and health and ensures normal neurological function. Diabetes and hypertension are known to increase the risk of dementia, but the underlying mechanism is not well understood (Takeda et al., 2020). The prefrontal cortex, a brain region involved in executive functions, is particularly vulnerable to vascular pathology and dementia. Several potential pathophysiological mechanisms linking vascular pathology in diabetes or hypertension and brain dysfunction have been proposed including endothelial dysfunction, abnormal clotting, oxidative stress, inflammation, and BBB breakdown (Hosoki et al., 2023). To reveal the relationship between vascular risk factors and brain dysfunction and gain a deeper understanding of pathogenic mechanisms, a molecular investigation of brain vascular cells, including endothelial cells and mural cells, is necessary.

While several single-cell transcriptomic studies have been published on the human brain vasculature, they have not addressed the impact of major vascular risk factors such as

hypertension and diabetes. Moreover, few studies have focused specifically on the prefrontal cortex, and none have provided a detailed analysis of its vascular cell populations, limiting our understanding of region-specific vascular alterations in the context of disease. Thus, a focused investigation of the brain vasculature in the human prefrontal cortex under conditions of hypertension and diabetes is needed.

Research Hypothesis and Objectives

In this study, I will use single-cell technologies to gain a better insight into which specific cell types are perturbed and which molecular pathways are altered in T2DM or hypertension that could lead to brain dysfunction and predispose to neurodegeneration.

My hypothesis is that vascular risk factors for dementia, specifically diabetes and hypertension, alter signalling pathways in brain vascular cells to affect neuronal function and ultimately lead to cognitive decline and brain atrophy. Furthermore, these changes are expected to be discernible from significant alterations in gene expression.

To test my hypothesis, I have specific objectives for the following chapters:

- Chapter 1. Single-Cell Atlas of the Human Prefrontal Cortex
  a) Identify and annotate different cell types of the human prefrontal cortex from post-mortem tissue of donors with or without diabetes and hypertension from snRNA-seq data
  b) Compare the relative abundance of different cell types across conditions via cell proportion analysis to distinguish cellular composition changes from transcriptomic changes

- Chapter 2. Deciphering Dysregulated Pathways in Hypertension and Diabetes
  a) Identify differentially expressed genes in the main cell types of the human prefrontal cortex
  b) Use gene ontology (GO) analysis to understand dysregulated pathways

- Chapter 3. Cell-Type-Specific Dysregulated Gene Networks in Hypertension
  a) Evaluate co-expression networks by using weighted gene co-expression network analysis (WGCNA)
  b) Predict transcription factors (TFs) that regulate gene expression

- Chapter 4. Investigating Cellular Crosstalk in Hypertension
  a) Investigate altered cell-cell communications between cell types
  b) Prioritise ligands that are most likely to causally explain the observed differential gene expression

- Chapter 5. Cell-Type Enrichment of Disease Risk Genes
  a) Identify cell-type-disease associations by combining GWAS summary statistics and snRNA-seq data
  b) Functional enrichment analysis of cell-type-disease-linked genes

Chapter 1. Single-Cell Atlas of the Human Prefrontal Cortex

Introduction

The prefrontal cortex (PFC) is one of the most evolved brain regions and is particularly developed in humans, displaying a striking increase in size compared to non-human primates. According to Brodmann, the human PFC accounts for 29% of the cerebral cortex, compared to 17% in chimpanzees and 11.5% in rhesus monkeys. This expansion encompasses both the grey and white matter, and is mostly driven by an increase in the number of dendrites and axons, and the glial density, rather than the number of neurons. This increase reflects greater local and long-range connectivity, which can support complex cognitive functions (Levy, 2024).

The PFC plays a key role in higher-order cognitive and executive functions, including decision-making, working memory, attention, and reasoning. It is interconnected with other brain regions exerting top-down control. The PFC, as part of the frontoparietal network, exhibits much higher energy demand than sensory-motor networks (Castrillon et al., 2023). It may therefore be particularly dependent on a healthy vasculature to support its activity.

Dysfunction of the PFC or its associated networks is a key feature of many neuropsychiatric disorders (Friedman & Robbins, 2022; Kolk & Rakic, 2022). The PFC is particularly vulnerable to neurodegeneration and PFC atrophy can be considered as an important predictor of Alzheimer’s disease and symptoms in amyotrophic lateral sclerosis-frontotemporal dementia (ALS-FTD) (Burgmans et al., 2009; Ratti et al., 2021).

Previous studies have already profiled human brain vasculature of different brain regions using single-cell technology. Whilst some studies included the PFC, these have only contained a limited number of nuclei, or the PFC has not been the main region of interest (Table 4).

In this chapter, I aim to create a single-nucleus atlas of the prefrontal cortex using samples from 48 control and hypertensive/diabetic individuals without neurological disorders. The PFC was selected as the brain region of interest because of its early involvement in a range of neurodegenerative disorders and also due to the availability of good-quality post-mortem samples. Donor selection and sample processing for sequencing was undertaken by another DPhil student in the Cader Lab, Gabriel Rocha. Samples were obtained from 4 different brain banks to have sufficient numbers of donors for this study (see Methods).

By analysing the single-nucleus dataset comprised of parenchymal and vascular fractions, I aim to identify and characterise distinct cell-type groups including vascular, glial, and neuronal cell types. I will also plan to perform cell subtype analysis to determine whether endothelial populations from venous, arterial and capillary can be distinguished. Similarly for mural cells, I will attempt to identify vascular smooth muscle and pericytes. Cell proportion analysis will be performed to compare the relative abundance of different cell types across conditions, helping to distinguish cellular composition changes from transcriptomic changes. This chapter will highlight unique cell-type-specific marker genes and provide a framework for subsequent pathological analysis in the following chapters.

Methods

Donor Selection

48 donors were selected from four brain banks: Bristol, Newcastle, Edinburgh, and Netherlands on the basis of a diagnosis of diabetes, hypertension or donors without these diagnoses (Table S 1). Donors were excluded if they had significant neurodegenerative conditions (e.g. Alzheimer's disease, Parkinson's disease) and severe or moderate small vessel disease. Medical information including co-morbidities, medication, and cause of death was extracted where possible (Table S 2 - Table S 6).

Single-Nucleus RNA Sequencing

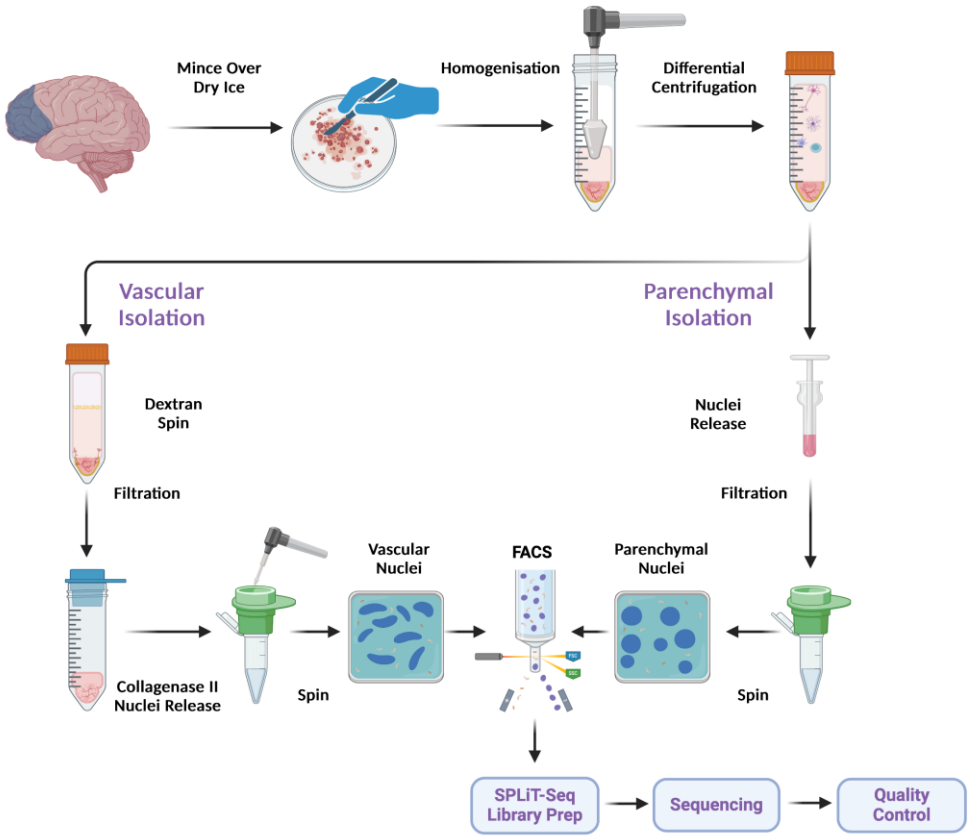

Figure 6. Overall workflow of single-nucleus RNA sequencing of human prefrontal cortex.

Created by Gabe Rocha (Cader Lab, Oxford).

Gabe Rocha in the Cader Lab performed SPLiT-seq (Parse Bioscience) on the samples (Figure 6). This is a split pool combinatorial barcoding method, which was applied to nuclei extracted from 0.5 – 1 g of human prefrontal cortex from each of 48 donor post-mortem brains. The dissociation protocol separates parenchymal and vascular fractions to yield 96 samples in total. 32 libraries were prepared using the Parse barcoding kit, from the 96 samples—16 vascular and 16 parenchymal. Each library has the representation of all 16 samples. 8 sub-libraries (4 vasculature and 4 parenchyma) were then sequenced at NovoGene.

Quality Control

Sequencing data was de-multiplexed and aligned to the human reference genome (GRCh38) by Novo Nordisk. The Splitpipe pipeline from Parse Bioscience was used for the reads alignment, transcript counting, and sample deconvolution. The SPLiT-seq protocol employs both poly(T) and random hexamer priming, enabling capture of a broad range of RNA types. While the majority of captured transcripts are mRNA, other RNA types (e.g., long non-coding RNA and additional RNA biotypes) are also detected. The protocol exhibits a 3′ bias; however, coverage across the full length of many transcripts is still achieved. Novo Nordisk then provided the gene counts matrix; the dataset contains a total of 796,410 nuclei (464,426 nuclei from vasculature and 331,984 nuclei from parenchyma) and 62,710 genes, including both protein-coding and non-coding genes.

Four donors – Donor 1, 4, 9, and 49 were identified with less than 1,500 nuclei recovery in parenchymal samples and therefore removed from the dataset (Figure S 3). I further removed the low-quality sample Donor 33, which showed signs of potential batch effects (Figure S 5). Nuclei outliers with a low or extremely high number of expressed genes (< 200 or > 13,000), a high ratio of mitochondrial genes (> 10%), or potential doublets (scrublet score > 0.2) were removed using the Seurat package (v5.1.0) in R (v4.1.1) (Satija et al., 2015).

47,239 nuclei from the vascular fraction identified as neurons, oligodendrocytes, and oligodendrocytes progenitor cells; 1,699 nuclei from the parenchymal fraction identified as fibroblast and mural cells; the low-quality cluster (labelled as ‘MC29’ on the UMAP plot) which was highly expressing mitochondrial genes (*MT-RNR2, MT-RNR1, MT-ND5, MT-CO1, MT-ND4*) were removed from the dataset (Figure S 6). This resulted in a filtered gene count matrix of 671,162 high-quality single nuclei (370,530 nuclei from vasculature and 300,632 nuclei from parenchyma).

Dimensionality Reduction, Clustering, and Cell Annotation

Single-nucleus RNA sequencing data was processed using Seurat R package (v5.1.0) (Satija et al., 2015). snRNA-seq data is characterised by significant cell-to-cell variation due to biological heterogeneity and technical artefacts. One of the most common technical confounders is the sequencing depth (the total number of reads obtained) across individual nuclei which can obscure true biological heterogeneity. To address this challenge, I used SCTransform normalisation (v0.4.1), an alternative method to the traditional workflow (NormaliseData, FindVariableFeatures, and ScaleData). SCTransform uses regularised negative binomial regression to model gene expression and computes Pearson residuals to effectively account for sequencing depth and preserve biological heterogeneity for downstream analysis (Hafemeister & Satija, 2019).

Principal component analysis (PCA) dimensionality reduction was run with default parameters to project genes into the principal component (PC) space. The first 35 PCs were used to capture the majority of variation in the data. Cells were clustered using the Louvain method with a resolution of 1.0, resulting in 43 clusters (Figure S 2).

For each cluster, the Wilcoxon rank sum test was used to identify cluster-specific differentially expressed genes. FindAllMarkers was run with the following parameters: 1) only return positive markers 2) only test genes that are detected in at least 25% of the cells in either of the populations 3) Log_2FoldChange (Log_2FC) > 0.25 or < -0.25. Then, I imported the top 20 marker genes (ranked by Log_2FC with adjusted p-values < 0.05) for each cluster and annotated cell types using published marker genes in PanglaoDB (Franzen et al., 2019).

Cell Proportion Analysis

Speckle R package (v1.4.0) was used to analyse the differences in cell type proportions (Phipson et al., 2022). The propeller function tests whether there is a difference in the cell type proportions between the two groups in each category (hypertension, diabetes, age, and sex). A t-test is used to calculate p-values. Benjamini and Hochberg false discovery rates (FDR) were calculated to account for multiple testing of cell types.

Endothelial and Mural Cell Subtype Analysis

To further investigate cell subtypes in major vascular cell types (endothelial cells and mural cells), I isolated EC and MC separately from the Seurat object, resulting in 164,221 EC nuclei and 122,516 MC nuclei respectively (Satija et al., 2015). SCTransform normalisation and variance stabilisation were run with default parameters (Hafemeister & Satija, 2019). PCA was run with default parameters to project genes into PC space, and then the first 35 PCs were selected. The EC dataset was clustered using the Louvain method with a resolution of 0.3, resulting in 13 clusters (Figure S 7); the MC dataset was clustered with a resolution of 0.1, resulting in 5 clusters (Figure S 8).

For each cluster, the Wilcoxon rank sum test was used to identify cluster-specific differentially expressed genes. FindAllMarkers was run with the following parameters: 1) only return positive markers 2) only test genes that are detected in at least 25% of the cells in either of the populations 3) Log_2FoldChange (Log_2FC) > 0.25 or < -0.25. Then, I imported the top 20 marker genes (ranked by Log_2FC with adjusted p-values < 0.05) for each cluster and annotated EC subtypes and MC subtypes using published datasets (Kalucka et al., 2020; Trimm & Red-Horse, 2023; Vanlandewijck et al., 2018; Wälchli et al., 2024); (Gastfriend et al., 2021; Sun et al., 2023; Yang et al., 2022).

Results

43 donors from the starting sample of 48 were retained in the analysis. The 5 removed donors were Donor 1 (93, F, diabetic/non-hypertensive), Donor 4 (71, M, diabetic/non-hypertensive), Donor 9 (80, F, diabetic/non-hypertensive), Donor 33 (73, F, hypertensive/non-diabetic), and Donor 49 (78, M, diabetic/non-hypertensive). Of these, Donors 1, 4, 9, and 49 were excluded for low nuclei recovery, and Donor 33 for batch effects and sample quality concerns. Of the retained 43 donors, the age range was 60 – 101 years. 22 donors were in the older age group (> 80) and 21 donors were in the younger age group (≤ 80). There were 26 males and 17 females.

Donors had a diagnosis of hypertension or diabetes coded in their records. In some cases, information on hypertension diagnosis was initially missing but based on their use of anti-hypertensive treatments, patients medical records were re-checked and a medical diagnosis of hypertension was confirmed.

27 donors had hypertension and 16 donors did not; 20 donors had diabetes and 23 did not. 13 donors had both hypertension and diabetes; whilst 9 had neither (Figure 7). Anti-hypertensive treatments recorded for the donors included beta-blockers, calcium channel blockers, angiotensin-converting enzyme inhibitors (ACE-I) and angiotensin II receptor blockers (ARB), alpha-blockers, thiazide, hydralazine, and spironolactone (Table S 3). Treatments for diabetes for the donors included insulin, metformin, thiazolidinediones, and sulfonylureas (Table S 4).

Further data on the donors including other medical history, cause of death, and the use of other medications are provided in Table S 1, Table S 2, Table S 5, and Table S 6.

a

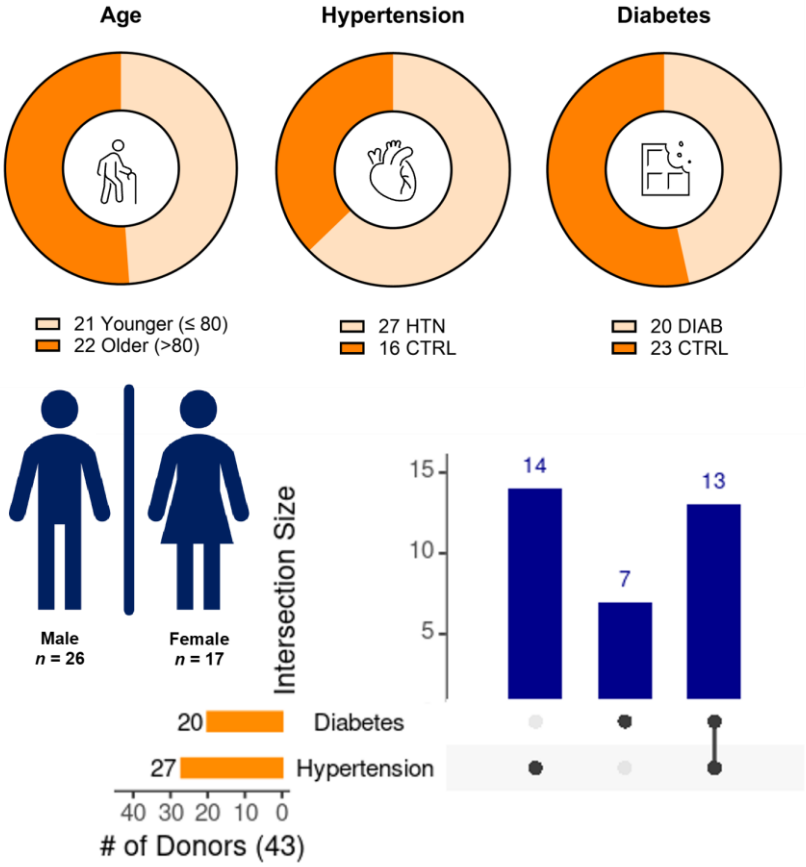

b

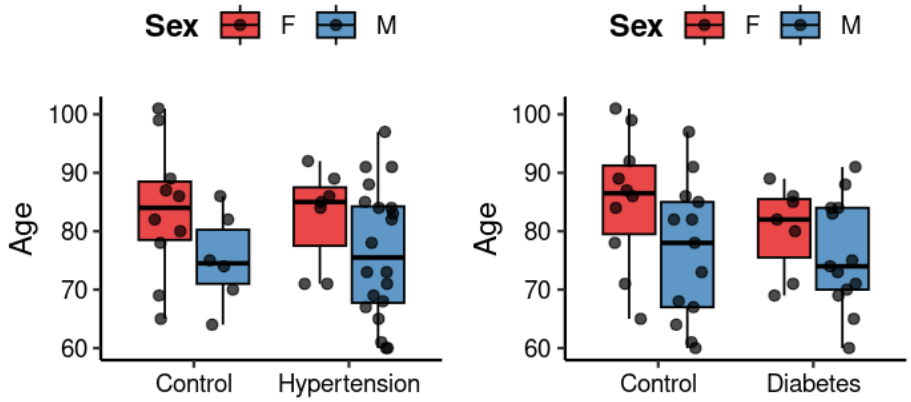

Figure 7. Donor demographics and clinical characteristics.

*(**a**) Overview of donor age, sex, and clinical diagnosis (n = 43). (**b**) Age and sex distribution of donors across hypertension and diabetes groups. Boxes represent the interquartile range (IQR), horizontal lines indicate the median, and whiskers extend to 1.5 × IQR.*

HTN, Hypertension; CTRL, Control; DIAB, Diabetes.

The snRNA-seq data from 43 donors encompassing 671,162 high-quality single nuclei (370,530 nuclei from vasculature and 300,632 nuclei from parenchyma) was clustered and visualised on a UMAP plot (Figure S 1; Figure S 2). 43 clusters were initially identified, and based on cell marker expression, I reduced this to 11 main cell-type clusters (Figure 8).

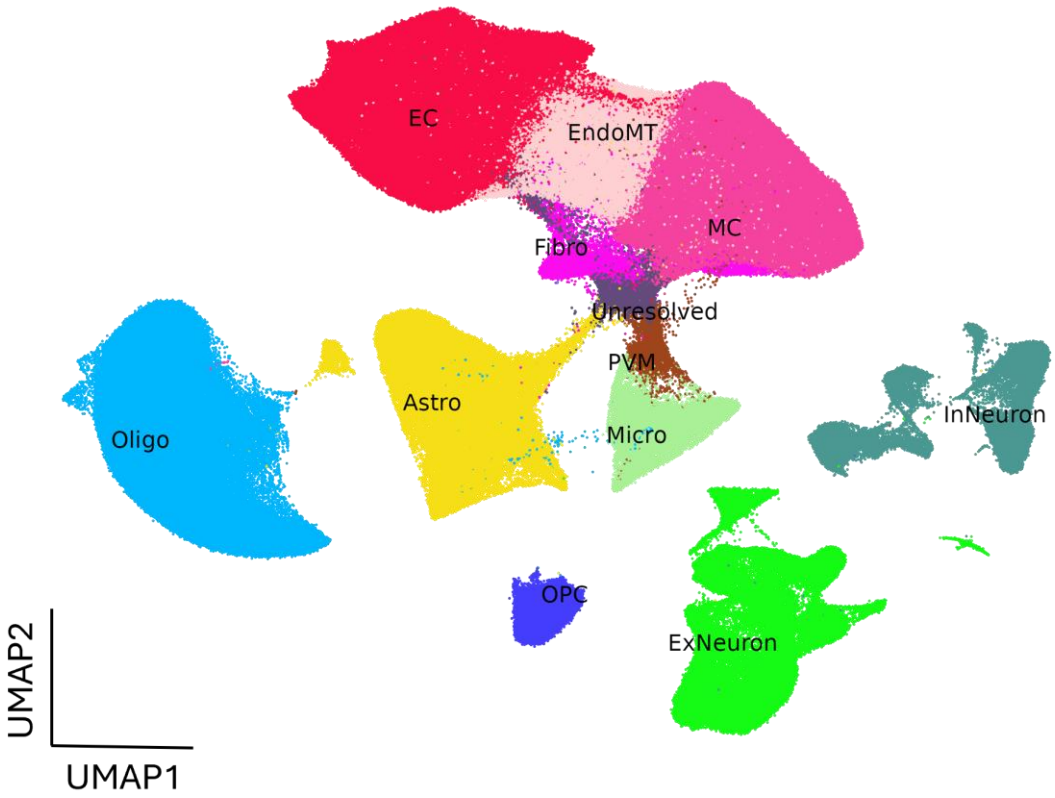

Figure 8. UMAP of 671,162 nuclei from post-mortem human prefrontal cortex of 43 donors.

Coloured by cell types. EC, Endothelial Cells; EndoMT, Endothelial-Mesenchymal Transition Cells; MC, Mural Cells; Fibro, Fibroblasts; Astro, Astrocytes; Oligo, Oligodendrocytes; OPC, Oligodendrocyte Progenitor Cells; Micro, Microglia; PVM, Perivascular Macrophages; ExNeuron, Excitatory Neurons; InNeuron, Inhibitory Neurons.

All the main brain cell types were identified including neurons, glia, vascular cells and fibroblasts.

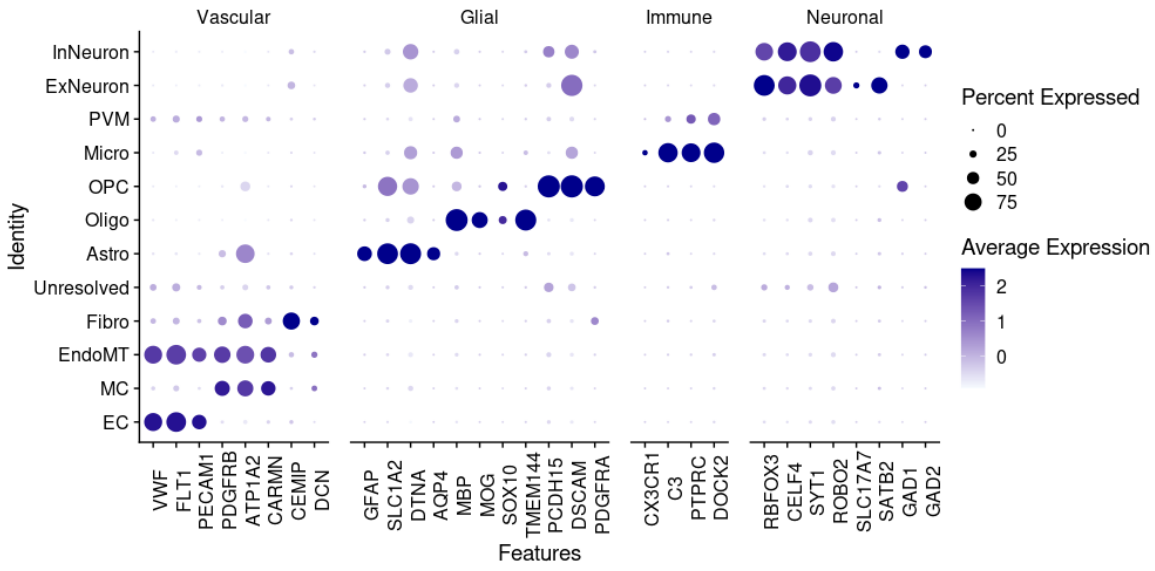

Figure 9. Cell type-specific marker expression in main cell clusters from snRNA-seq dataset.

The dot plot shows the expression of vascular, glial, immune, and neuronal markers across annotated cell types. The size of each dot indicates the percentage of nuclei within a cluster expressing the gene, while the colour scale represents the average expression level (scaled).

EC expressed *VWF, FLT1, PECAM1* (Figure 9). Mural cells (MC) include both pericytes and vascular smooth muscle cells—and both these cell subtypes expressed *PDGFRB, ATP1A2, CARMN*. I also found a cell population expressing markers of both EC and MC, and the Cader group has previously identified in another human prefrontal cortex single-cell dataset (personal communication, manuscript in preparation). This population has been termed endothelial-mesenchymal transition cells (EndoMT) expressing marker genes of both EC and MC and appears to represent a transitional cell population of EC differentiating into MC. The other cell types in the vascular fraction included fibroblasts (Fibro) which expressed *CEMIP, DCN* and perivascular macrophages (PVM) which expressed *PTPRC* and *DOCK2*.

Astrocytes (Astro) were identified by their expression of *GFAP, SLC1A2, DTNA, AQP4.* Oligodendrocytes (Oligo) expressed *MBP, MOG, SOX10, TMEM144*, and oligodendrocyte

progenitor cells (OPC) expressed *PCDH15, DSCAM, PDGFRA*. Microglia (Micro) were characterised by expressing *CX3CR1* and *C3.* Neurons expressed general neuronal marker genes including *RBFOX3, CELF4, SYT1, ROBO2*. Furthermore, neurons were divided into excitatory neurons (ExNeuron), which expressed *SLC17A7* (i.e. VGLUT1 encoding gene)*, SATB2*, and inhibitory neurons (InNeuron), which specifically expressed *GAD1, GAD2*. To provide a comprehensive overview of marker genes across cell types, I listed the top 10 marker genes for each cell type in Table S 7, ranked by Log_2FC with adjusted p-values < 0.05.

However, one cell cluster from the vascular compartment remains unresolved due to the lack of clear correspondence between its top 20 marker genes (*EYS, LINC01320, ENSG00000231918, AGBL1, ENSG00000248752, CCDC26, ADAMTSL1, LINC02055, PKN2-AS1, MIR3681HG, ENSG00000254186, ENSG00000285939, ENSG00000286481, RUNX1, RARB, SPAG16, ENSG00000228566, NELL1, ENSG00000229618, SGO1-AS1*) and characterised cell types from published studies. Notably, this gene expression profile lacked overlap with any key vascular, glial, immune, and neuronal marker genes. Instead, this cluster was characterised by expressing long non-coding RNA genes *LINC01320, LINC02055, PKN2-AS1, CCDC26, SGO1-AS1* and transcriptional regulation genes *RUNX1, RARB*. There was a larger proportion of unresolved cell type in the control samples (5.3% in control and 1.2% in hypertension), although this was not significant (see below). But this cluster had a high proportion of mitochondrial reads (15.4%), which is substantially above the threshold (10%) for high-quality nuclei. The mean number of transcripts per nucleus was only 1,110, and the mean number of genes detected per nucleus was 910. These characteristics may indicate low-quality nuclei or potential debris; hence, this unresolved cluster was removed from further analysis.

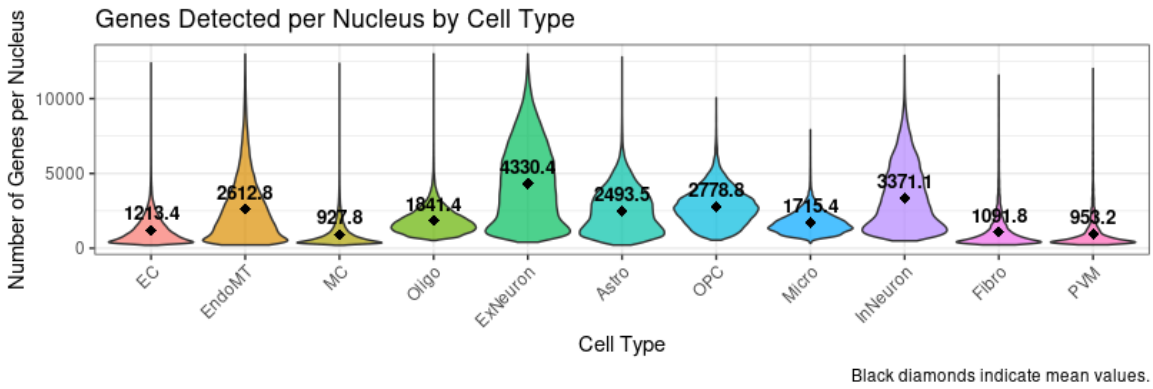

Figure 10. Genes detected per nucleus across cell types.

The unresolved cluster was excluded from the figure.

I evaluated the number of genes detected per nucleus across the cell types (Figure 10). On average, gene detection using SPLiT-seq (Parse Bioscience) ranged from 953 genes per nucleus in PVM to 4,330 genes per nucleus in ExNeuron. This represents an almost four-fold difference in gene expression. Overall, more genes per nucleus were detected in neuronal cell types, whereas fewer genes per nucleus were detected in vascular cell types. Among vascular cell types, EndoMT showed the highest number of genes detected per nucleus, which aligns with the transitional nature of these cell populations undergoing highly dynamic and transcriptionally active processes.

A previously published study using 10x Genomics on human brain vasculature reported lower gene detection with 712 genes per nucleus in endothelial cells, 856 genes per nucleus in neurons, 768 genes per nucleus in astrocytes (Yang et al., 2022).

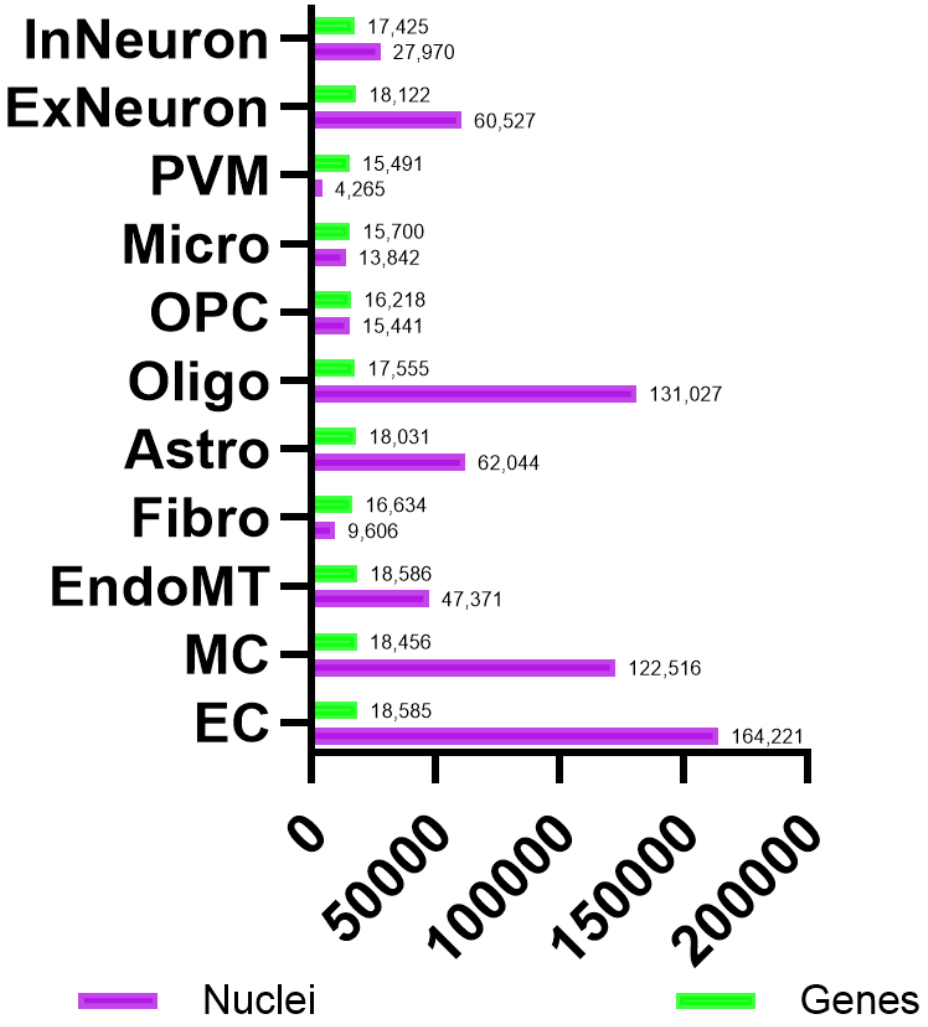

Figure 11. Number of nuclei and expressed protein-coding genes in each cell type.

Purple bars indicate the total number of nuclei assigned to each cell type. Green bars indicate the number of protein-coding genes detected in each cell type, defined as genes with expression counts > 10 across all nuclei in that cell type. The unresolved cluster was excluded from the figure.

The most abundant nuclei in our samples were identified as EC with 164,221 nuclei, while the least abundant were PVM with 4,265 nuclei. Protein-coding genes expressed by a cell type were broadly similar, ranging from 15,491 – 18,485 genes per cell type (Figure 11).

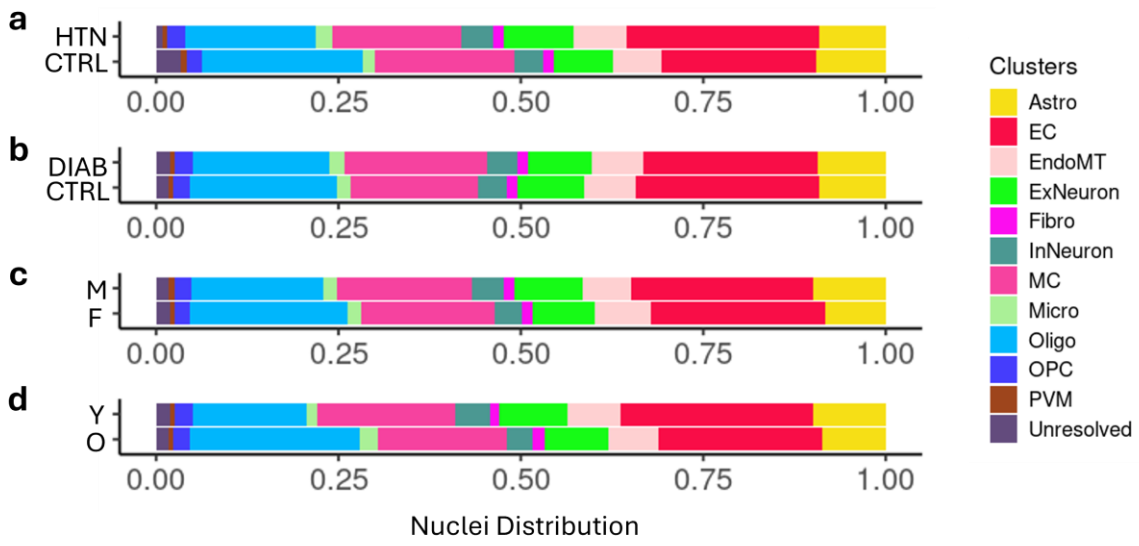

*Figure 12. Proportions of cell types in hypertension (**a**), diabetes (**b**), sex (**c**), and age (**d**) categories.*

Significant differences (t-test, FDR < 0.05) were labelled with an asterisk (*). HTN, Hypertension; CTRL, Control; DIAB, Diabetes; M, Male; F, Female; Y, Younger; O, Older.

Neurodegenerative disorders and systemic disorders leading to end-organ damage might be expected to lead to loss of cells and perhaps selective loss if particular cell types are vulnerable. Conditions such as hypertension and diabetes are both associated with cognitive decline and brain volume loss, which may be due to cell loss (Antal et al., 2022; Beauchet et al., 2013). Having defined the cell populations, I therefore assessed whether there was any significant difference in cell type proportion based on donor features.

There is no statistically significant difference (FDR < 0.05) in cell type proportions in each category – hypertension, diabetes, sex, and age (Figure 12). The lack of significant differences in cell proportions suggests that in this cohort, there is no selective loss of one cell type over the other.

Whilst no differences were statistically significant, some of the differences were nevertheless interesting and may merit further investigation with larger sample sizes since the lack of significance is likely due to high variability between donor samples. For

example, there was a difference between young and old with older donors (>80 years) having 21.3% oligodendrocytes compared to younger donors 14.2%. There was an apparent decrease in EC proportion from 26.2% to 23.0%. In hypertension, there was 26.7% EC compared to 21.1% in controls.

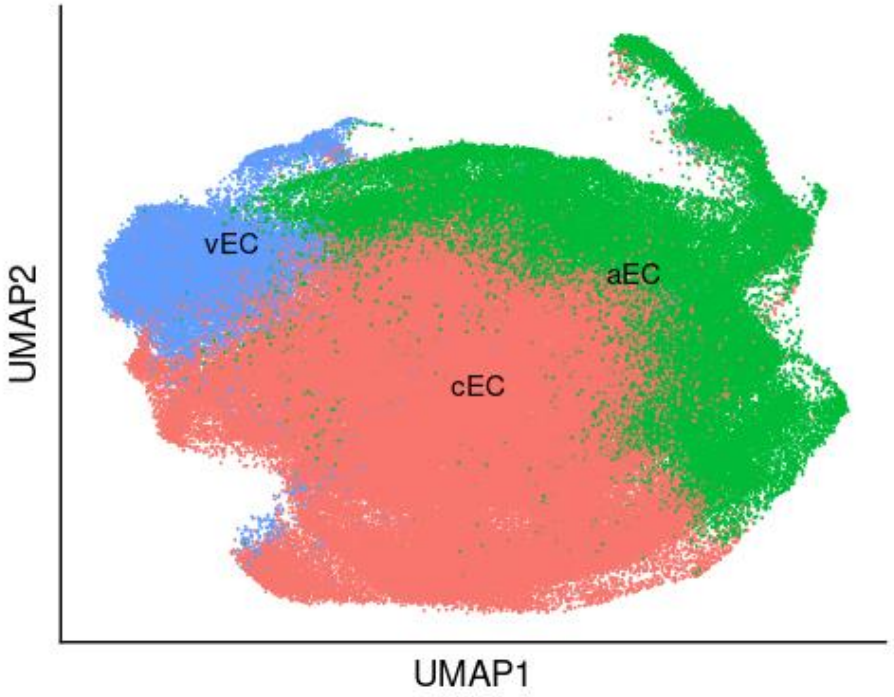

Figure 13. UMAP of 164,221 EC subtypes nuclei.

Coloured by cell types. aEC, Arterial Endothelial Cells; cEC, Capillary Endothelial Cells; vEC, Venous Endothelial Cells.

The brain microvasculature, similar to other vascular beds, is comprised of a hierarchy of interconnected terminal arterioles, capillaries, and post-capillary venules. A study in 2018 defined the molecular profiles of endothelial cells for these different vessels in detail (Vanlandewijck et al., 2018). To investigate whether the single-cell atlas obtained in this study also exhibited arteriovenous zonation, I performed subclustering of the EC population. 13 subclusters within the EC population were identified and based on specific marker expression, Clusters 4 and 12 were grouped together as venous EC, Clusters 0, 1, 5, 6, 7, 9, 10, 11 were capillary EC and Clusters 2, 3, 8 were identified as arterial EC (Figure S 7). There were 100,073 capillary endothelial cells, 15,945 venous endothelial cells, and 48,203 arterial endothelial cells (Figure 13).

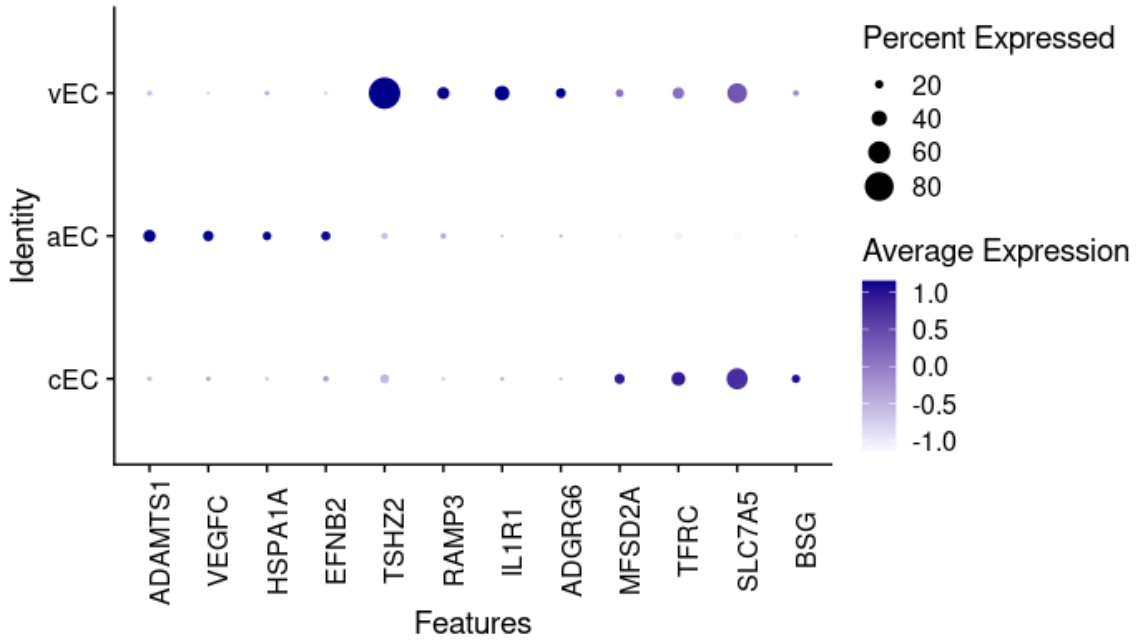

Figure 14. Cell type-specific marker expression in EC subtype clusters from snRNA-seq dataset.

The dot plot shows the expression of EC subtype markers across annotated cell subtypes. The size of each dot indicates the percentage of nuclei within a cluster expressing the gene, while the colour scale represents the average expression level (scaled).

Arterial EC expressed *ADAMTS1, VEGFC, HSPA1A, EFNB2* (Figure 14). Venous EC were characterised by expression of *TSHZ2, RAMP3, IL1R1, ADGRG6*, and capillary EC exhibited high expression of *MFSD2A, TFRC, SLC7A5, BSG*.

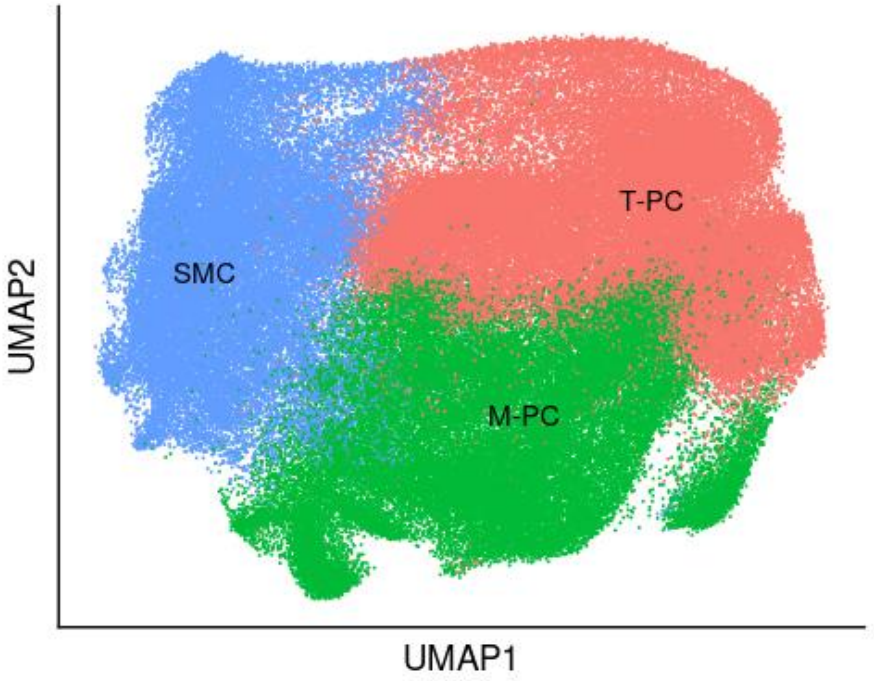

Figure 15. UMAP of 122,516 MC subtypes nuclei.

Coloured by cell types. SMC, Smooth Muscle Cells; M-PC, Matrix Pericytes; T-PC, Transport Pericytes.

Mural cells, which play an important role in regulating blood flow through the interaction with endothelial cells and maintaining blood-brain barrier integrity, are comprised of vascular smooth muscle cells and pericytes (Siekmann, 2023). To better understand the heterogeneity within mural cells, I performed subclustering of the MC population. Five subclusters within the MC population were identified and based on marker gene expression, Cluster 2 as smooth muscle cells, Clusters 0, 1, 3, 4 were grouped as pericytes (Figure S 8). Pericytes can be further divided into transport pericytes (Clusters 0 and 4) and matrix pericytes (Clusters 1 and 3). Matrix pericytes are a subtype of pericytes enriched for genes involved in extracellular matrix organisation, and transport pericytes are enriched for genes involved in small-molecule transmembrane transport. There were 30,461 vascular smooth muscle cells (SMC), 50,404 transport pericytes (T-PC), and 41,651 matrix pericytes (M-PC) (Figure 15).

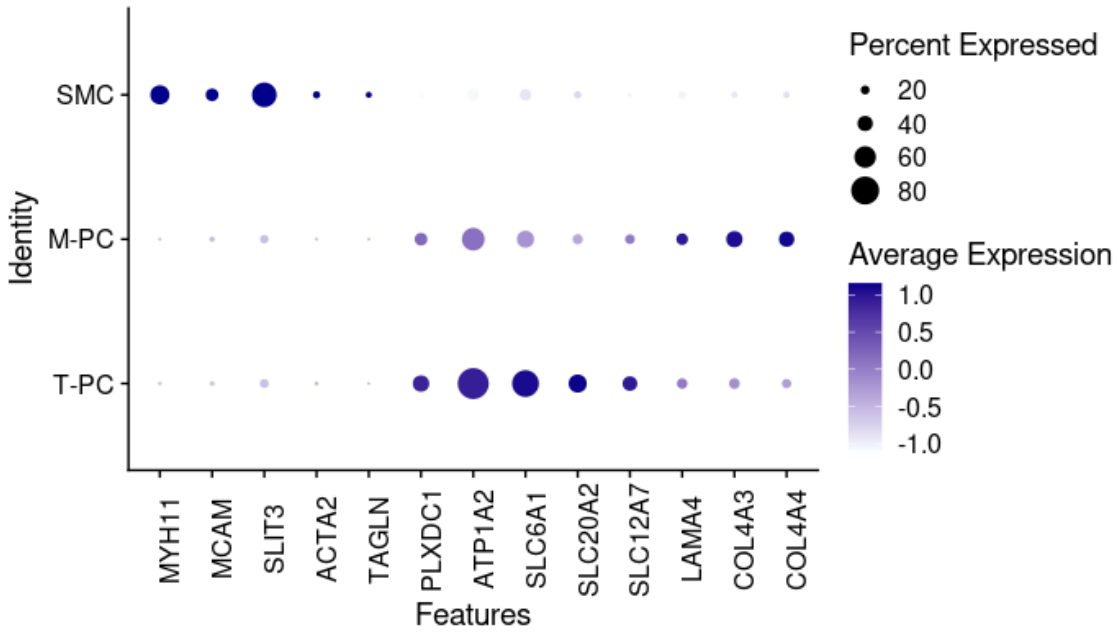

Figure 16. Cell type-specific marker expression in MC subtype clusters from snRNA-seq dataset.

The dot plot shows the expression of MC subtype markers across annotated cell subtypes. The size of each dot indicates the percentage of nuclei within a cluster expressing the gene, while the colour scale represents the average expression level (scaled).

Vascular smooth muscle cells expressed *MYH11, MCAM, SLIT3, ACTA2, TAGLN* (Figure 16). Pericytes expressed *PLXDC1, ATP1A2, SLC6A1, SLC20A2, SLC12A7, LAMA4, COL4A3, COL4A4*. The pericytes cell population can be further divided into T-PC and M-PC based on differential marker gene expression: T-PC exhibited high expression of *PLXDC1, ATP1A2, SLC6A1, SLC20A2, SLC12A7*, whereas M-PC showed elevated expression of *LAMA4, COL4A3, COL4A4*.

Discussion

In this chapter, I generated a large-scale single-nucleus atlas of the human prefrontal cortex vasculature from 48 donors, including both control and hypertensive/diabetic individuals but without neurological disorders and severe cerebrovascular disease, as determined from clinical diagnosis recorded in the brain bank medical records. The rationale for excluding donors with neurological disorders was to avoid results being confounded by changes due to these other disease processes. Conversely, we may have selected donors relatively protected from neurodegenerative/cerebrovascular processes. Nevertheless, the samples provide a means to understand how cardiovascular disorders such as hypertension and diabetes might affect human brain cortical tissue.

The samples were processed using a technique that allowed high yield and simultaneous isolation of both parenchymal and vascular cell types. This is undertaken at the tissue processing step and two fractions are then available from each donor for Parse Split-Seq barcoding, library preparation and then sequencing (Rosenberg et al., 2018). This work was undertaken by another student in the Cader lab, with barcoding/library preparation and quality control assessment undertaken by Novo Nordisk. I received sequencing data which I then subjected to further careful selection of donors and nuclei to ensure only high-quality data was retained for analysis.

Overall the sample and sequencing quality was very high. I identified a small number of donors which were poor quality and these were excluded from the analysis. This reduced the number of non-hypertension subjects from 20 to 16. Using snRNA-seq, I obtained 671,162 high-quality single nuclei derived from 43 donors after strict quality controls. These nuclei were derived from both parenchymal and vascular compartments: 370,530 nuclei from the vasculature and 300,632 nuclei from the parenchyma. This dataset covers 11 diverse cell types—including vascular, neuronal, immune, and glial cell populations—thereby providing a comprehensive architecture of human brain vasculature.

However, one cell cluster from the vascular compartment remained unresolved. This ‘Unresolved’ cluster was characterised by highly expressing long non-coding RNA genes and transcriptional regulation genes. It represents only a small fraction of the overall sample but interestingly it was present in control as well as hypertension or diabetes samples. But this cluster had a high proportion of mitochondrial reads (15.4%), which is substantially above the threshold (10%) for high-quality nuclei; it might just have been low-quality nuclei or potential debris. Hence, this unresolved cluster was removed from further analysis.

Overall, more genes per nucleus were detected in neurons, whereas fewer genes per nucleus were detected in EC and MC. This may reflect that neurons exhibit complex transcriptional activity compared to brain vascular cell types. Despite this, the total number of protein-coding genes expressed per cell type was broadly similar. This indicates that although individual EC and MC nuclei express fewer genes, the heterogeneity within the EC and MC populations contributes to a more comprehensive gene expression profile at the population level.

My analysis showed that SPLiT-seq (Parse Biosciences) detected a higher number of genes per nucleus across various cell types compared to the published study using 10x Genomics on human brain vasculature (Yang et al., 2022). This finding aligns with a recently published comparative study showed that Parse detected nearly twice the number of genes per cell compared to 10x Genomics in mouse thymus tissue (Filippov et al., 2024). This highlights that Parse generally detects more genes per cell or nucleus compared to 10x Genomics.

Recent single-cell studies have revealed how age and sex influence the cellular composition and molecular profiles of the human brain. For instance, a single-cell multi-omic analysis of the human dorsolateral prefrontal cortex examined only neuronal populations and reported age-related shifts in cell-type proportions, most notably a selective reduction in inhibitory interneurons in older individuals (70 - 74 years old)

compared to younger individuals (23 - 30 years old) (Chien et al., 2024). Although no significant sex-related differences in cell-type composition were observed, the study identified cell-type-specific sex differences in gene expression and DNA methylation.

In my study, cell proportion analysis revealed no statistically significant difference in the abundance of cell types in the prefrontal cortex vasculature across different conditions (hypertension, diabetes, sex, and age). This suggests the overall cellular composition is relatively stable across the conditions being compared. One possible explanation for not observing significant differences across age groups is that the sample cohort (60 - 101 years) represents a much older population, in which age-related changes in cellular composition may have already occurred earlier in life. Since the donors do not have neurological disorders or moderate-to-severe small vessel disease, significant compositional changes may not be expected. While the overall cellular architecture of the PFC remains stable, the conditions may still affect gene expression within each cell type, leading to functional changes. To further investigate this, I will perform differential gene expression analysis in each cell type across the conditions in the following chapter.

I performed cell subtype analysis of endothelial and mural cells to refine the vasculature landscape further. Endothelial and mural cells exhibit a gradual phenotypic change along the arteriovenous axis of the human brain vasculature, referred to as zonation (Vanlandewijck et al., 2018). This transcriptional gradient indicates the expected functional specialisation of each cell subtype, identifying three endothelial cell subtypes – arterial, capillary, and venous. A recent study, analysing 143,793 single-nucleus from 25 hippocampus and superior frontal cortex samples of 9 individuals with AD and 8 individuals with no cognitive impairment, identified a small cluster of endothelial tip cells outside conventional zonation (571 nuclei, around 0.1%) highly expressing *PLAUR* and *LAMB1* (Yang et al., 2022). However, my study didn't detect endothelial tip cells – with expression of *PLAUR* and *LAMB1* at 5.67% and 2.17% of EC, respectively. Endothelial tip cells lead sprouting angiogenesis and sense the environment for guidance cues, which

are typically found in regions undergoing active angiogenesis (Dallinga et al., 2015). The absence of the endothelial tip cell population in my dataset may reflect differences in methodology in isolating vascular fractions, or it may reflect the types of donors or differences in the brain region examined. Hence the prefrontal cortex vasculature may be more stable compared to the hippocampus which may have a more active angiogenesis process (Fournier & Duman, 2012).

With mural cell populations, three subtypes were identified – smooth muscle cells, transport pericytes, and matrix pericytes. While Yang et al. (2022) managed to cluster 34,508 nuclei into transport pericytes, matrix pericytes, and two subclusters of smooth muscle cells—arterial smooth muscle cells (aSMC) and arteriolar smooth muscle cells (aaSMC)—my analysis yielded only one SMC subcluster. This SMC cluster highly expressed *MYH11* and showed clear segregation on the UMAP plot (Figure S 9). Yang's study did not describe *MYH11* as one of the aSMC marker genes. However, searching for this gene on their published gene expression profile revealed *MYH11* was exclusively expressed in their aSMC cluster. This suggests that my *MYH11*-expressing SMC cluster represents arterial SMCs. Yang's study also reported *SLIT3* as an aaSMC specific marker but again searching their gene expression profile showed that *SLIT3* was highly expressed in both their aSMC and aaSMC clusters (Figure S 9). Similarly, I found *SLIT3* was expressed in my SMC cluster.

Single-nucleus RNA sequencing is a powerful tool to decipher human brain complexity, but my study has some limitations. First, we used single-nucleus which, unlike single-cell RNA sequencing, only captures nuclear RNA, which may miss the cytoplasmic transcriptome. Second, we used post-mortem human brain tissues from brain banks that may have had these tissues for several years leading to degraded RNA which can affect the quality of captured transcripts. Nevertheless, we found that sample quality was overall excellent, leading to high-quality sequencing. To further address this issue, I performed strict quality control to remove the low-quality donors and nuclei from the dataset.

Additionally, due to the stochastic nature of single-cell datasets and technical artefacts, real biological variability and experimental variability can be ambiguous (Hsu & Moses, 2022). To minimise this impact, I checked for batch effects and used SCTransform to apply variance stabilisation.

In summary, this chapter enhances our understanding of the landscape of the human prefrontal cortex vasculature and establishes a foundation for more in-depth single-cell analyses. Moving forward, differential gene expression analysis and functional enrichment analysis using the pseudobulk dataset will provide insights into gene expression changes within each cell type and identify key signalling pathways altered by two vascular risk factors—hypertension and diabetes.

Chapter 2. Deciphering Dysregulated Pathways in Hypertension and Diabetes

Introduction

Hypertension and type 2 diabetes mellitus have detrimental effects on the vasculature, resulting in the development of various cardiovascular diseases and dysfunction. Long-term exposure to elevated blood pressure and hyperglycaemia can lead to endothelial dysfunction, disruption of the BBB, impairment of the NVU, inflammation, and increased vascular permeability. These have also been suggested as the initial pathogenetic features of vascular dementia and Alzheimer's disease (Nagai et al., 2022). Midlife hypertension and the persistence of elevated blood pressure from midlife into late life are both associated with increased dementia risk (McGrath et al., 2017). Also, midlife diabetes and longer duration of uncontrolled diabetes are associated with greater late-life cognitive decline (Rawlings et al., 2014). Brain imaging studies have found that midlife hypertension and diabetes are associated with altered brain structures and executive function (Veldsman et al., 2020). These studies suggest that early diagnosis and management of hypertension and T2DM are critical for reducing the risk of brain dysfunction later in life.

Investigating cellular or molecular changes in the brain associated with these conditions may provide an understanding of why cognitive decline develops and may suggest therapeutic targets to protect brain health. Molecular profiling of post-mortem tissue from patients with disease can provide this type of data, and also has the advantage that human tissue is being examined. Surprisingly, the number of such studies in relation to hypertension and diabetes is limited. In the case of hypertension, there are no other transcriptomic studies, either bulk or single-cell RNA-sequencing of the human brain. With regard to diabetes, only bulk RNA sequencing has been performed to study transcriptomic

changes across various brain regions in T2DM tissues (Z. Zhou et al., 2019). However, bulk transcriptomic approaches do not capture cell-type-specific mechanisms underlying neurovascular dysfunction—which is now possible through the advent of single-cell technology.

In this chapter, I will investigate cell-type-specific transcriptional changes in the brain associated with hypertension and T2DM using differential gene expression analysis. Then, functional enrichment analysis will be performed to further explore dysregulated signalling pathways. Since this study focuses on hypertensive and diabetic patients who do not have neurological disorders or severe cerebrovascular disease, it will allow us to explore early molecular or cellular changes in the prefrontal cortex before significant brain dysfunction develops.

Methods

Pseudobulk and Differential Gene Expression Analysis

A pseudobulk gene expression matrix was generated by aggregating the counts across cell types in each sample. Then, I identified differentially expressed genes between the control group and the patient group using DESeq2 (v1.44.0) which is based on the negative binomial distribution: (1) the covariates, including age (as continuous variables), sex, hypertension, and diabetes were controlled in the model (2) estimateSizeFactors were applied to account for sequencing depth (3) only protein-coding genes from biomaRt (v2.60.1) were extracted and low counts genes in the matrix were filtered (rowSums < 10) (4) lfcShrink (type = "ashr") was used for visualisation and ranking genes (Durinck et al., 2005; Durinck et al., 2009; Love et al., 2014; Stephens, 2017).

ggplot2 R package (v3.5.1) was used for DEG visualisation (Valero-Mora, 2010). Two DEG selection criteria were used: (1) adjusted p-values < 0.05 (2) $Log_2FC > 0.2$ or < -0.2. The top 10 up or downregulated DEGs were labelled on the volcano plot. UpSetR R package (v1.4.0) was used for the visualisation of intersecting DEGs among cell types (Conway et al., 2017).

Pathway and Process Enrichment Analysis

Genes with $Log_2FC > 0.2$ or $Log_2FC < -0.2$ with adjusted p-values < 0.05 were used for subsequent GO analysis (Biological Processes only). GO analysis was performed using clusterProfiler package (v4.12.6) with the associated annotation packages annotationDBI (v1.68.0) and org.Hs.eg.db (v3.2.20) (Wu et al., 2021; Yu et al., 2012). UpSetR R package (v1.4.0) was used for the visualisation of intersecting GO terms among cell types (Conway et al., 2017).

To further refine the DEG list and ensure biological relevance and representation, an additional percentage expression filtering step was applied to perform functional enrichment analysis including GO analysis. First of all, I subset the Seurat object to include the corresponding cell type only which has a reasonable number of DEGs in the previous analysis (EC – 164,221 nuclei, MC – 122,516 nuclei, Astro – 62,044 nuclei, EndoMT – 47,371 nuclei, ExNeuron – 60,527 nuclei, cEC – 100,073 nuclei, vEC – 15,945 nuclei, aEC – 48,203 nuclei, SMC – 30,461 nuclei). Then, the SCT assay counts matrix was extracted and I calculated the percentage of nuclei expressing each gene in the corresponding cell type (a gene is considered expressed if its count > 0). Genes with less than 5% expression in the corresponding cell type were excluded from the final DEG list.

ggplot2 R package (v3.5.1) was used for the refined DEG visualisation (Valero-Mora, 2010). Three DEG selection criteria were used: (1) adjusted p-values < 0.05 (2) $Log_2FC > 0.2$ or < -0.2 (3) Expression > 5%. The top 10 up or downregulated DEGs were labelled on the volcano plot. Then, the final DEG list (adjusted p-values < 0.05 & $|Log_2FC| > 0.2$ & Expression > 5%) was used for GO analysis and additional pathway and process enrichment analysis in Metascape (v.3.5.20240901) (Y. Zhou et al., 2019). UpSetR R package (v1.4.0) was used for the visualisation of intersecting GO terms among cell types, and Complex Heatmap R package (v2.22.0) was used for the visualisation of genes from those dysregulated pathways (Conway et al., 2017; Gu, 2022). Pathway and process enrichment analysis carried out with the following ontology sources in Metascape: GO Biological Processes, KEGG (Kyoto Encyclopedia of Genes and Genomes) Pathway, Reactome Gene Sets, CORUM (Comprehensive Resource of Mammalian Protein Complexes), Canonical Pathways, and WikiPathways (Y. Zhou et al., 2019). All genes in the genome were used as the enrichment background. Terms (p-value < 0.01 & Count ≥ 3 & Enrichment Factor > 1.5) were grouped into clusters based on the membership similarities. Kappa scores were used to cluster similar terms based on overlapping genes (similarity > 0.3). The most statistically significant term within a cluster

was chosen to represent the corresponding cluster. A subset of enriched terms was selected to visualise in the network plot.

Results

a

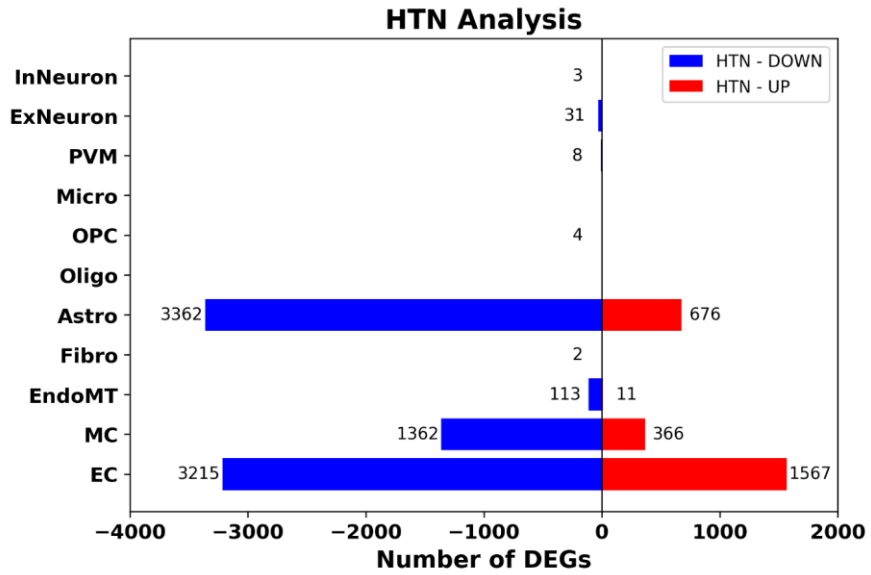

b

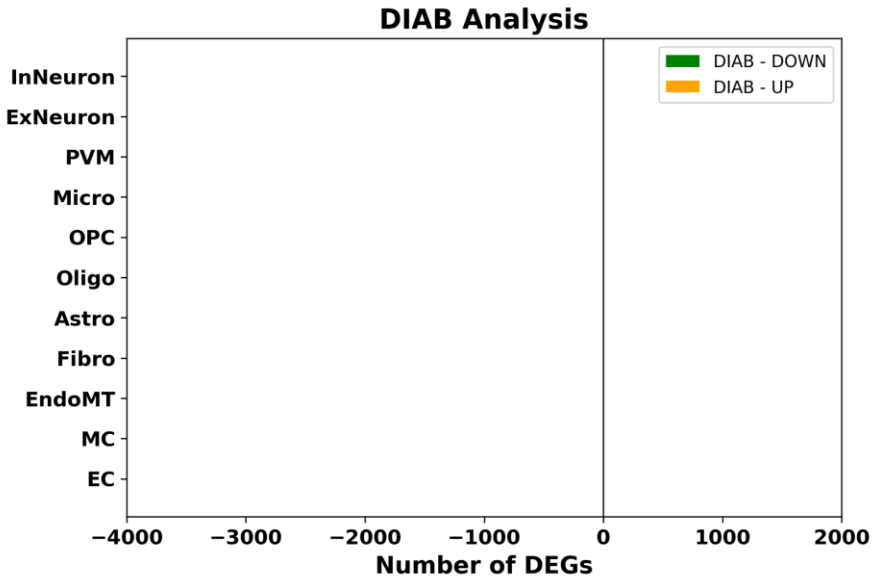

*Figure 17. Number of upregulated and downregulated DEGs in hypertension (**a**) and diabetes (**b**) in each cell type.*

*(**a**) Upregulated DEGs in hypertension were labelled in red colour and downregulated DEGs in hypertension were labelled in blue colour (adjusted p-values < 0.05 & $|Log_2FC| > 0.2$). (**b**) Upregulated DEGs in diabetes were labelled in orange colour and downregulated DEGs in diabetes were labelled in green colour (adjusted p-values < 0.05 & $|Log_2FC| > 0.2$).*

To study gene expression changes in each cell type associated with diabetes or hypertension, differential gene expression analysis was performed using the medical diagnosis provided with each donor sample. From the single-nucleus expression dataset, pseudobulk gene expression levels were generated and differentially expressed genes in each of the major cell types were determined using DESeq2 (v1.44.0). A regression model was used for the analysis with the covariates being age (as a continuous variable), sex, hypertension, and diabetes.

Hypertension showed substantial gene expression changes across multiple cell types with a high number of differentially expressed genes in endothelial cells, mural cells, and astrocytes, the majority of which were downregulated (Figure 17). However, no significant DEGs were detected in type 2 diabetes, despite its well-established association with cognitive decline (Rawlings et al., 2014).

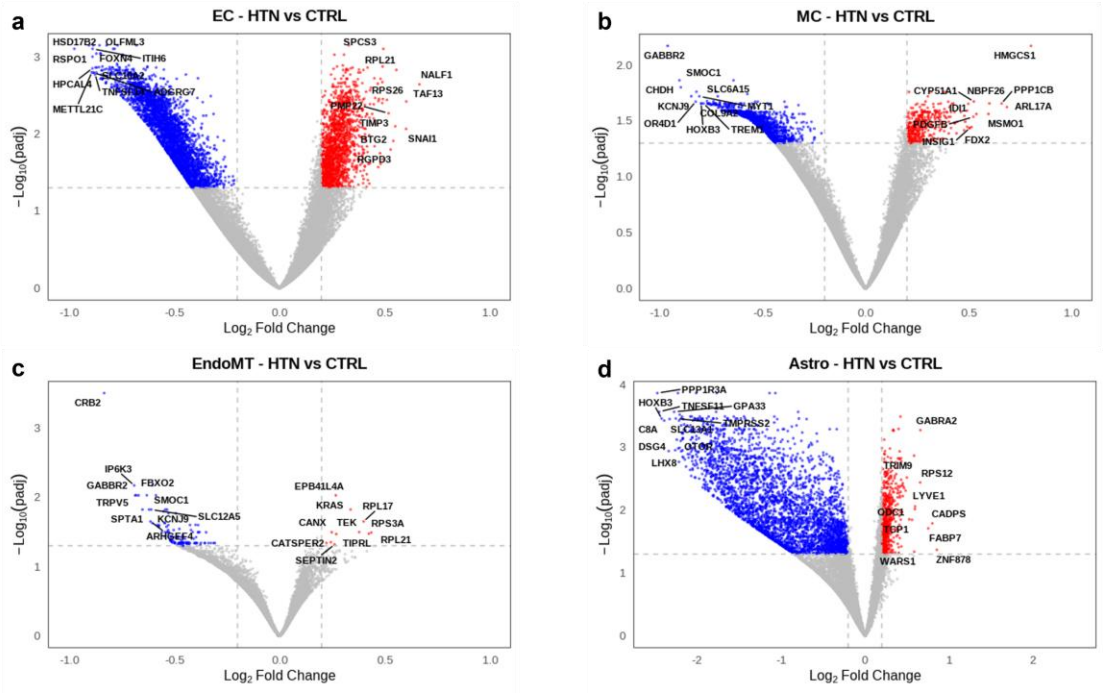

*Figure 18. Volcano plots show DEGs in hypertensive donors (n = 27) compared to non-hypertensive donors (n = 16) in EC (**a**), MC (**b**), EndoMT (**c**), and Astro (**d**).*

X-axis: Log_2FC (hypertensive relative to control); Y-axis: $-Log_{10}$(padj)-values. Horizontal dashed line represents a cutoff of adjusted p-values < 0.05, and vertical dashed lines represent Log_2FC cutoffs of > 0.2 or < -0.2. Genes meeting both cutoffs are represented by red circles (upregulated) and blue circles (downregulated). Top 10 up or downregulated DEGs (based on $|Log_2FC|$) were labelled.

Whilst the number of significant genes changed in hypertension was substantial, the fold changes were modest, ranging from - 2.47 to + 0.85 (Figure 18). Nevertheless, whilst this might suggest that the effects of hypertension on individual genes are relatively subtle, given the number of genes changed, the overall effect on the tissue may be profound.

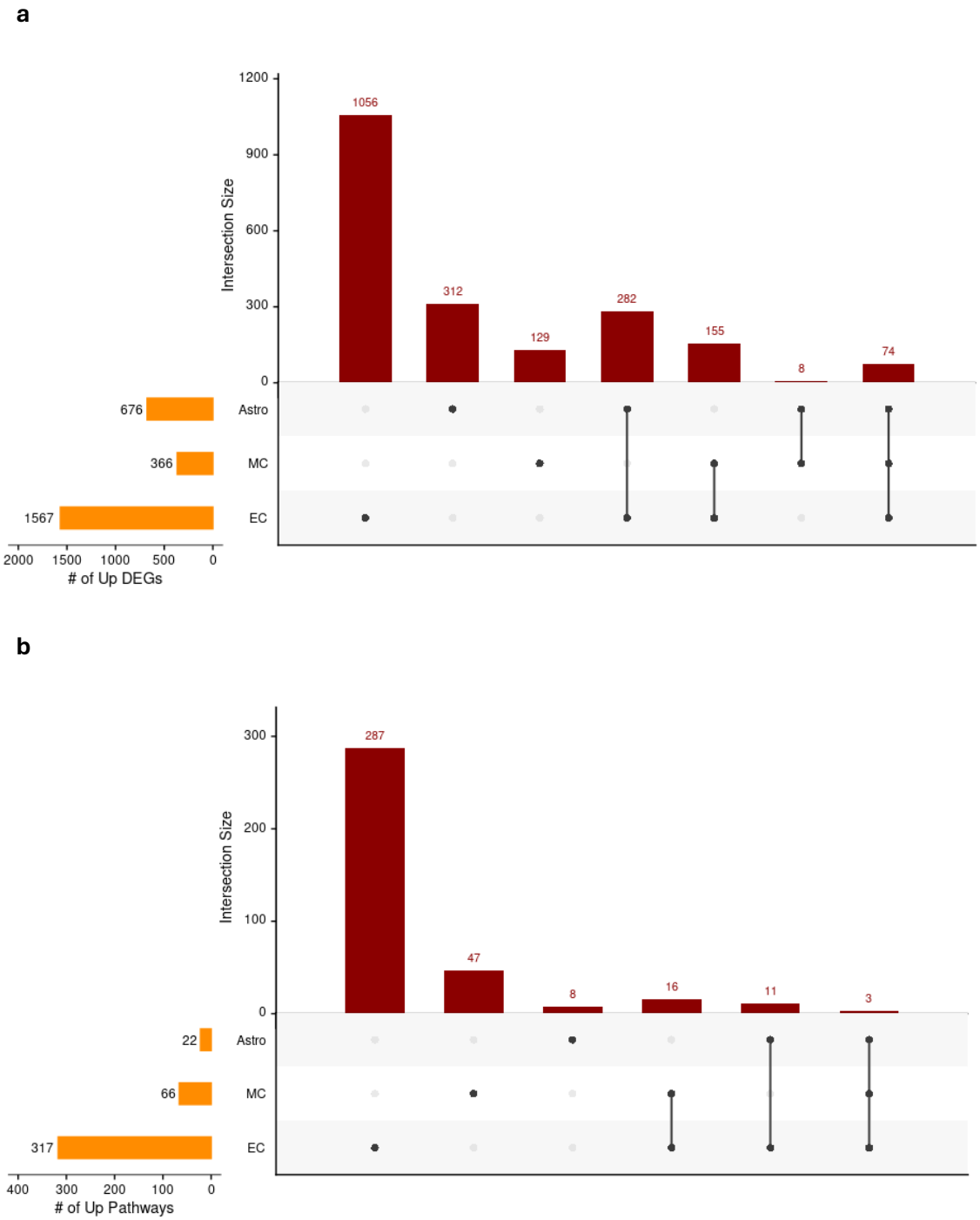

*Figure 19. Upset plot of the intersection of upregulated DEGs (**a**) and GO terms (**b**) among EC, MC, and Astro.*

Horizontal bars represent the total number of upregulated DEGs/GO terms in each cell type, and vertical bars indicate the number of upregulated DEGs/GO terms unique to or shared between specific cell types (denoted by the dots below the bars).

Hypertension may be inducing differential and specific effects on each cell type, or there may be a common response of cells to hypertension. To further investigate these possibilities, the overlap of DEGs and GO terms among cell types was evaluated. The upregulated and downregulated DEGs were considered separately since upregulated DEGs were found for EC, MC and astrocytes and downregulated DEGs were found for EC, MC, EndoMT and astrocytes.

EC had the highest percentage of upregulated DEGs which were unique, with 67% of EC upregulated genes (1,056 genes), whilst MC had the lowest proportion of unique DEGs, with 35% of MC upregulated genes (129 genes) uniquely identified. Astrocytes had 46% of upregulated DEGs (312 genes) unique to astrocytes (Figure 19a).

There were many genes that were shared between two cell types. Hence, 282 upregulated DEGs were shared exclusively between EC and Astro; 155 upregulated DEGs were shared exclusively between EC and MC; only 8 upregulated DEGs were shared exclusively between MC and Astro. However, 74 upregulated DEGs were identified across the three cell types.

It is possible that the common effects of hypertension are easier to detect at the pathway level. Therefore, I performed GO analysis to categorise all the upregulated genes into biologically meaningful terms and included only the Biological Process (BP) category to focus on functional pathways. Among the upregulated GO terms, 91% of EC upregulated GO terms (287 GO terms), 71% of MC upregulated GO terms (47 GO terms), and 36% of Astro upregulated GO terms (8 GO terms) were exclusively identified in the respective cell types. Hence, it appears that for EC and MC, the majority of pathways affected were unique to that cell type. Astrocytes, on the other hand, had a majority of pathway changes shared by other cell types.

16 upregulated GO terms were shared exclusively between EC and MC; 11 upregulated GO terms were shared exclusively between EC and Astro; but there was no overlap

between MC and astrocytes (Figure 19b). Only 3 upregulated GO terms were identified across three cell types.

Interestingly, the common upregulated GO terms were protein polyubiquitination and protein catabolic process, which may reflect potential stress response and inflammatory signalling in hypertension (Table 5). EC had the most upregulated genes belonging to these pathways, suggesting that in hypertension, these signalling pathways in EC were particularly affected.

Table 5. List of common upregulated GO terms in EC, MC, and Astro in hypertension.

GO ID	*Description*	*Cell Type*	*Upregulated / Total*	*p.adjust*
GO:0000209	Protein Polyubiquitination	**EC**	**53/244**	**1.19E-08**
		MC	**17/244**	**0.00264**
		Astro	**22/244**	**0.0178**
GO:0043161	Proteasome-Mediated Ubiquitin-Dependent Protein Catabolic Process	**EC**	**103/439**	**1.36E-20**
		MC	**20/439**	**0.0266**
		Astro	**45/439**	**2.11E-07**
GO:0048193	Golgi Vesicle Transport	**EC**	**64/294**	**1.15E-10**
		MC	**19/294**	**0.00264**
		Astro	**27/294**	**0.00511**

For each GO term, "Upregulated / Total" indicates the number of upregulated genes detected in the cell type divided by the total number of genes annotated to that GO term in the background gene set. Adjusted p-value (p.adjust) reflects the statistical significance of enrichment after multiple testing correction. Only GO terms significantly enriched in all three cell types are shown.

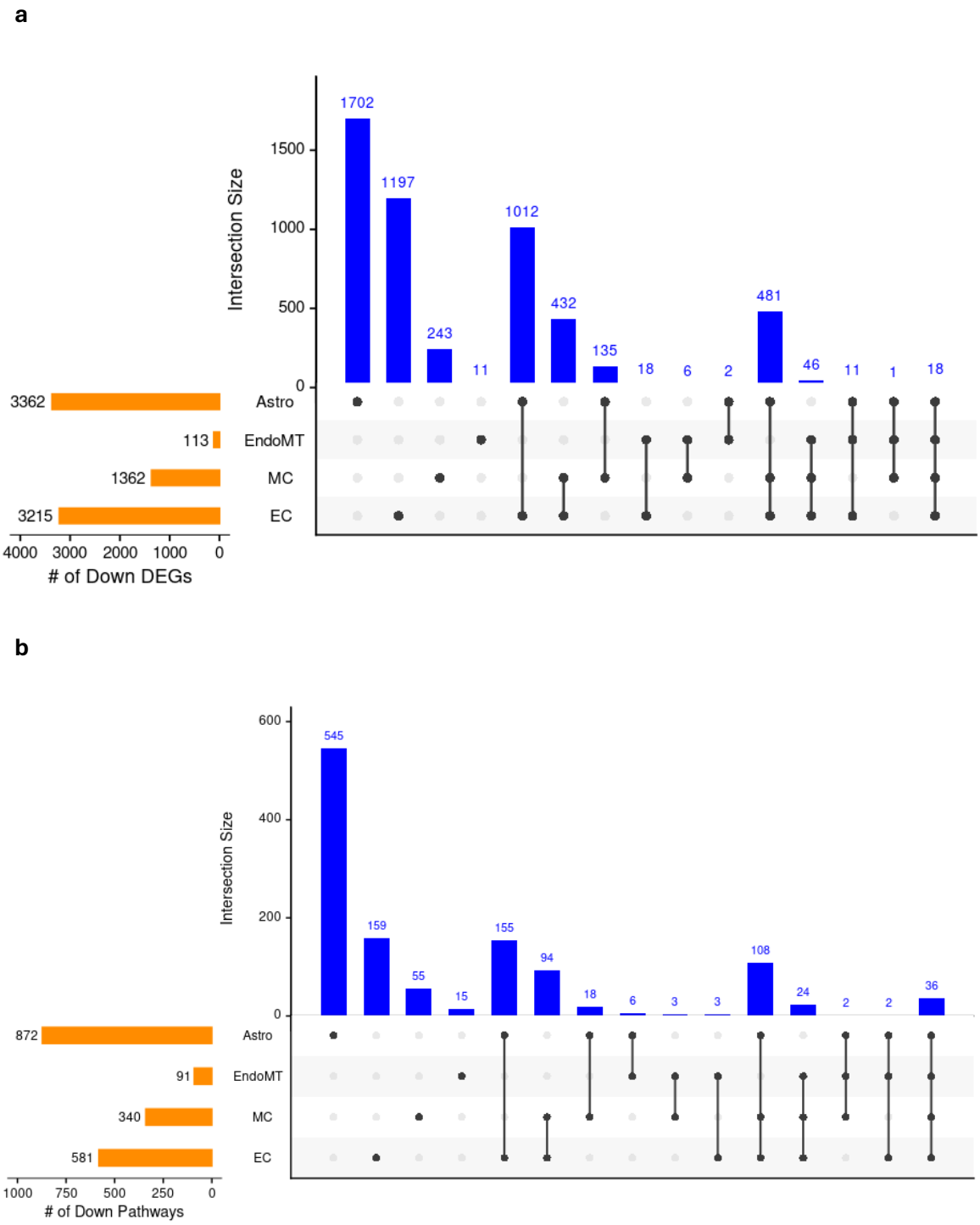

*Figure 20. Upset plot of the intersection of downregulated DEGs (**a**) and GO terms (**b**) among EC, MC, EndoMT, and Astro.*

Horizontal bars represent the total number of downregulated DEGs/GO terms in each cell type, and vertical bars indicate the number of downregulated DEGs/GO terms unique to or shared between specific cell types (denoted by the dots below the bars).

Among the downregulated DEGs, 51% of Astro downregulated genes (1,702 genes), 37% of EC downregulated genes (1,197 genes), 18% of MC downregulated genes (243 genes), and 10% of EndoMT downregulated genes (11 genes) were uniquely identified in the respective cell types (Figure 20a). As with upregulated DEGs, there was substantial overlap between EC and other cell types. 481 downregulated DEGs were identified across EC, MC, and Astro; 46 downregulated DEGs were identified across EC, MC, and EndoMT; 18 downregulated DEGs were identified across four cell types.

At the pathway level, downregulated pathways were much more likely to be shared with at least one other cell type. For example, 27% of EC unique downregulated pathways were unique in contrast to the 91% unique upregulated pathways (Figure 20b). Interestingly, 36 downregulated GO terms were identified across four cell types (Table 6) and were related to neuronal development, ion transport, synaptic transmission, cognitive function, and cell-cell adhesion. Hence, it appears that hypertension induces relatively cell-type-specific upregulation of pathways and conversely has broader downregulation of pathways shared across cell types.

Table 6. List of common downregulated GO terms in EC, MC, EndoMT, and Astro in hypertension.

GO ID	Description	Cell Type	Downregulated / Total	p.adjust
GO:0001654	Eye Development	**EC**	**85/385**	**0.00370**
		MC	**47/385**	**0.000741**
		EndoMT	**10/385**	**0.00579**
		Astro	**95/385**	**0.000304**
GO:0006813	Potassium Ion Transport	**EC**	**92/241**	**1.16E-15**
		MC	**54/241**	**2.82E-13**
		EndoMT	**6/241**	**0.0483**
		Astro	**70/241**	**1.95E-05**
GO:0006814	Sodium Ion Transport	**EC**	**87/254**	**8.96E-12**
		MC	**49/254**	**8.54E-10**
		EndoMT	**7/254**	**0.0210**
		Astro	**92/254**	**4.76E-12**
GO:0006820	Monoatomic Anion Transport	**EC**	**49/147**	**2.13E-06**
		MC	**22/147**	**0.00508**
		EndoMT	**7/147**	**0.00262**
		Astro	**52/147**	**1.14E-06**
GO:0007157	Heterophilic Cell-Cell Adhesion via Plasma Membrane Cell Adhesion Molecules	**EC**	**22/52**	**0.000108**
		MC	**14/52**	**0.000190**
		EndoMT	**4/52**	**0.0112**
		Astro	**17/52**	**0.0223**
GO:0007409	Axonogenesis	**EC**	**125/427**	**1.31E-11**
		MC	**71/427**	**4.61E-11**
		EndoMT	**14/427**	**4.73E-05**
		Astro	**93/427**	**0.0132**
GO:0007611	Learning or Memory	**EC**	**85/276**	**4.88E-09**
		MC	**54/276**	**5.31E-11**
		EndoMT	**7/276**	**0.0248**
		Astro	**70/276**	**0.00126**
GO:0010975	Regulation of Neuron Projection Development	**EC**	**124/452**	**1.38E-09**
		MC	**64/452**	**3.02E-07**
		EndoMT	**17/452**	**8.68E-07**
		Astro	**95/452**	**0.0272**
GO:0015698	Inorganic Anion Transport	**EC**	**60/179**	**6.47E-08**
		MC	**27/179**	**0.00118**
		EndoMT	**6/179**	**0.0198**
		Astro	**58/179**	**4.31E-06**

GO ID	*Description*	*Cell Type*	*Downregulated / Total*	*p.adjust*
GO:0030516	Regulation of Axon Extension	**EC**	**24/90**	**0.0364**
		MC	**14/90**	**0.0298**
		EndoMT	**4/90**	**0.0383**
		Astro	**24/90**	**0.0493**
GO:0031346	Positive Regulation of Cell Projection Organisation	**EC**	**80/353**	**0.00253**
		MC	**44/353**	**0.000796**
		EndoMT	**11/353**	**0.000891**
		Astro	**76/353**	**0.0334**
GO:0034329	Cell Junction Assembly	**EC**	**120/444**	**7.38E-09**
		MC	**64/444**	**1.56E-07**
		EndoMT	**9/444**	**0.0248**
		Astro	**105/444**	**0.000632**
GO:0042391	Regulation of Membrane Potential	**EC**	**162/433**	**5.47E-27**
		MC	**90/433**	**4.46E-20**
		EndoMT	**9/433**	**0.0228**
		Astro	**127/433**	**1.03E-09**
GO:0042461	Photoreceptor Cell Development	**EC**	**15/48**	**0.0406**
		MC	**12/48**	**0.00145**
		EndoMT	**4/48**	**0.00870**
		Astro	**15/48**	**0.0479**
GO:0043010	Camera-Type Eye Development	**EC**	**70/338**	**0.0371**
		MC	**41/338**	**0.00236**
		EndoMT	**8/338**	**0.0221**
		Astro	**85/338**	**0.000393**
GO:0048588	Developmental Cell Growth	**EC**	**63/231**	**6.61E-05**
		MC	**37/231**	**1.98E-05**
		EndoMT	**6/231**	**0.0424**
		Astro	**54/231**	**0.0232**
GO:0048592	Eye Morphogenesis	**EC**	**41/157**	**0.00503**
		MC	**29/157**	**1.95E-05**
		EndoMT	**8/157**	**0.000721**
		Astro	**42/157**	**0.00697**
GO:0048593	Camera-Type Eye Morphogenesis	**EC**	**34/127**	**0.00881**
		MC	**27/127**	**3.37E-06**
		EndoMT	**7/127**	**0.00131**
		Astro	**34/127**	**0.0162**

GO ID	Description	Cell Type	Downregulated / Total	p.adjust
GO:0048880	Sensory System Development	**EC**	**90/395**	**0.000966**
		MC	**49/395**	**0.000362**
		EndoMT	**10/395**	**0.00606**
		Astro	**97/395**	**0.000304**
GO:0050767	Regulation of Neurogenesis	**EC**	**86/381**	**0.00177**
		MC	**47/381**	**0.000584**
		EndoMT	**10/381**	**0.00573**
		Astro	**83/381**	**0.0204**
GO:0050769	Positive Regulation of Neurogenesis	**EC**	**52/232**	**0.0255**
		MC	**30/232**	**0.00568**
		EndoMT	**7/232**	**0.0153**
		Astro	**57/232**	**0.00788**
GO:0050770	Regulation of Axonogenesis	**EC**	**52/155**	**6.88E-07**
		MC	**27/155**	**0.000121**
		EndoMT	**9/155**	**7.67E-05**
		Astro	**44/155**	**0.00184**
GO:0050772	Positive Regulation of Axonogenesis	**EC**	**22/76**	**0.0214**
		MC	**14/76**	**0.00782**
		EndoMT	**4/76**	**0.0248**
		Astro	**24/76**	**0.00861**
GO:0050804	Modulation of Chemical Synaptic Transmission	**EC**	**153/487**	**4.83E-17**
		MC	**95/487**	**1.21E-19**
		EndoMT	**11/487**	**0.00664**
		Astro	**110/487**	**0.00220**
GO:0050890	Cognition	**EC**	**91/317**	**4.35E-08**
		MC	**58/317**	**1.24E-10**
		EndoMT	**7/317**	**0.0433**
		Astro	**75/317**	**0.00497**
GO:0051960	Regulation of Nervous System Development	**EC**	**119/461**	**1.17E-07**
		MC	**58/461**	**4.79E-05**
		EndoMT	**12/461**	**0.00163**
		Astro	**97/461**	**0.0250**
GO:0051962	Positive Regulation of Nervous System Development	**EC**	**77/280**	**4.53E-06**
		MC	**41/280**	**4.54E-05**
		EndoMT	**9/280**	**0.00309**
		Astro	**62/280**	**0.0369**

GO ID	Description	Cell Type	Downregulated / Total	p.adjust
GO:0060560	Developmental Growth Involved in Morphogenesis	**EC**	**67/234**	**5.95E-06**
		MC	**39/234**	**4.37E-06**
		EndoMT	**6/234**	**0.0433**
		Astro	**60/234**	**0.00255**
GO:0061564	Axon Development	**EC**	**136/479**	**1.31E-11**
		MC	**77/479**	**2.80E-11**
		EndoMT	**16/479**	**5.38E-06**
		Astro	**105/479**	**0.00684**
GO:0071805	Potassium Ion Transmembrane Transport	**EC**	**85/217**	**3.18E-15**
		MC	**52/217**	**5.90E-14**
		EndoMT	**6/217**	**0.0332**
		Astro	**61/217**	**0.000213**
GO:0090596	Sensory Organ Morphogenesis	**EC**	**67/269**	**0.000588**
		MC	**39/269**	**9.82E-05**
		EndoMT	**8/269**	**0.00827**
		Astro	**72/269**	**0.000215**
GO:0098656	Monoatomic Anion Transmembrane Transport	**EC**	**44/125**	**1.76E-06**
		MC	**19/125**	**0.00952**
		EndoMT	**6/125**	**0.00606**
		Astro	**42/125**	**6.37E-05**
GO:0098742	Cell-Cell Adhesion via Plasma-Membrane Adhesion Molecules	**EC**	**98/278**	**2.95E-14**
		MC	**52/278**	**6.77E-10**
		EndoMT	**10/278**	**0.000797**
		Astro	**76/278**	**6.71E-05**
GO:0099177	Regulation of Trans-Synaptic Signalling	**EC**	**153/488**	**4.83E-17**
		MC	**95/488**	**1.21E-19**
		EndoMT	**11/488**	**0.00664**
		Astro	**110/488**	**0.00238**
GO:0150063	Visual System Development	**EC**	**86/389**	**0.00340**
		MC	**47/389**	**0.000906**
		EndoMT	**10/389**	**0.00579**
		Astro	**95/389**	**0.000445**

GO ID	*Description*	*Cell Type*	*Downregulated / Total*	*p.adjust*
GO:1902476	Chloride Transmembrane Transport	**EC**	**40/98**	**7.09E-08**
		MC	**15/98**	**0.0257**
		EndoMT	**4/98**	**0.0470**
		Astro	**38/98**	**4.74E-06**

For each GO term, "Downregulated / Total" indicates the number of downregulated genes detected in the cell type divided by the total number of genes annotated to that GO term in the background gene set. Adjusted p-value (p.adjust) reflects the statistical significance of enrichment after multiple testing correction. Only GO terms significantly enriched in all four cell types are shown.

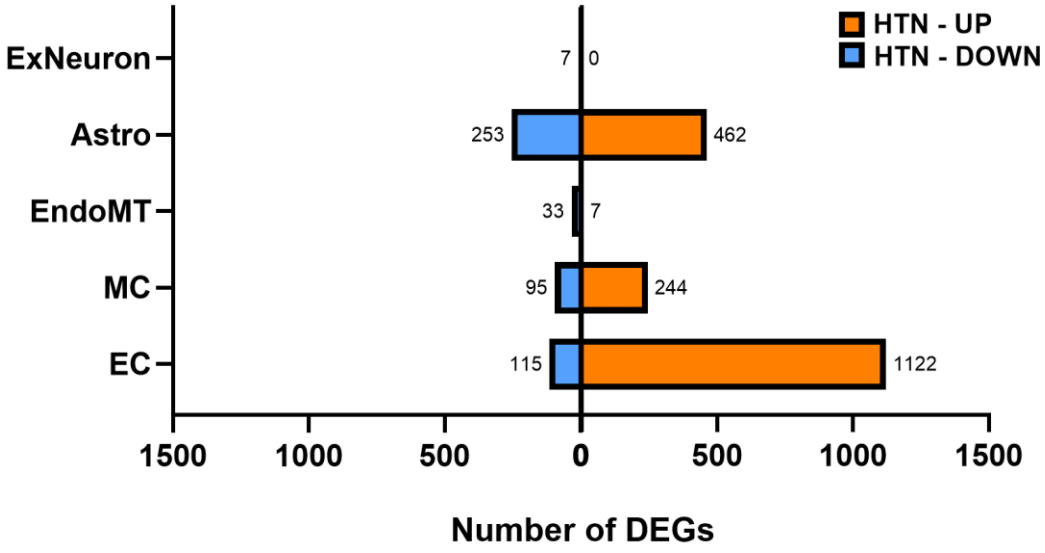

Figure 21. Number of refined upregulated and downregulated DEGs in hypertension in the selected cell types.

Upregulated DEGs in hypertension were labelled in orange colour and downregulated DEGs in hypertension were labelled in light blue colour (adjusted p-values < 0.05 & $|Log_2FC| > 0.2$ & Expression > 5%).

The increased sensitivity afforded by single-cell RNA sequencing means that even genes with low levels of expression in a cell type can be identified as differentially expressed where biological replicates (number of donors) are sufficient. For a gene to be biologically important to a particular cell type or tissue, we might expect a minimum proportion of cells of that type to express the gene. To help identify the gene changes with the most biological and disease relevance, I restricted the DEG set to genes with at least 5% expression in the affected cell type. Applying this filtering step resulted in a substantial reduction of downregulated genes compared to upregulated genes (Figure 21). Since hypertension leads to a downregulation of many genes, this can cause more downregulated genes to be filtered out. Still, many DEGs from endothelial cells, mural cells, and astrocytes were identified, but most were upregulated.

Table 7. List of downregulated genes in ExNeuron DEG analysis in hypertension.

Genes	baseMean	LFC	padj	Regulation	% Expression
SNCB	399.75	-0.51	0.00057	Downregulated	5.40
SYNGR1	1014.69	-0.36	0.0024	Downregulated	13.64
SPOCK2	708.56	-0.35	0.0093	Downregulated	6.69
PDZD4	469.06	-0.31	0.017	Downregulated	6.05
MEF2D	684.85	-0.27	0.0029	Downregulated	6.01
LZTS3	1090.73	-0.24	0.0078	Downregulated	17.42
FAIM2	1600.50	-0.24	0.025	Downregulated	21.38

baseMean, the average of normalised counts across all samples, providing an overall measure of its expression level prior to fold change calculation; LFC, Log_2FoldChange; padj, adjusted p-values.

Hypertension did not appear to substantially affect gene expression in neuronal populations. Nevertheless, 7 genes were significantly downregulated (Table 7). Interestingly, *SNCB* encodes beta-synuclein that protects the CNS from alpha-synuclein, which is linked to Parkinson's disease and dementia with Lewy bodies (Li et al., 2024). *SYNGR1*, which is associated with presynaptic vesicles in neurons, is a potential susceptibility gene for schizophrenia and bipolar disorder (Verma et al., 2005). Extracellular matrix (ECM) gene *SPOCK2* and PDZ domain-containing protein coding gene *PDZD4* were also identified as the downregulated genes in ExNeuron. *MEF2D* is the myocyte enhancer factor 2 (MEF2) transcription factors family, playing an important role in neuronal development, synaptic plasticity, learning and memory formation (Lisek et al., 2023). *LZTS3* is known to regulate dendritic spine morphogenesis and post-synapse assembly. Notably, *FAIM2* was also found in the downregulated gene list, which encodes Fas apoptotic inhibitory molecule and plays an important role in neuronal survival and neuroprotection (Komnig et al., 2016).

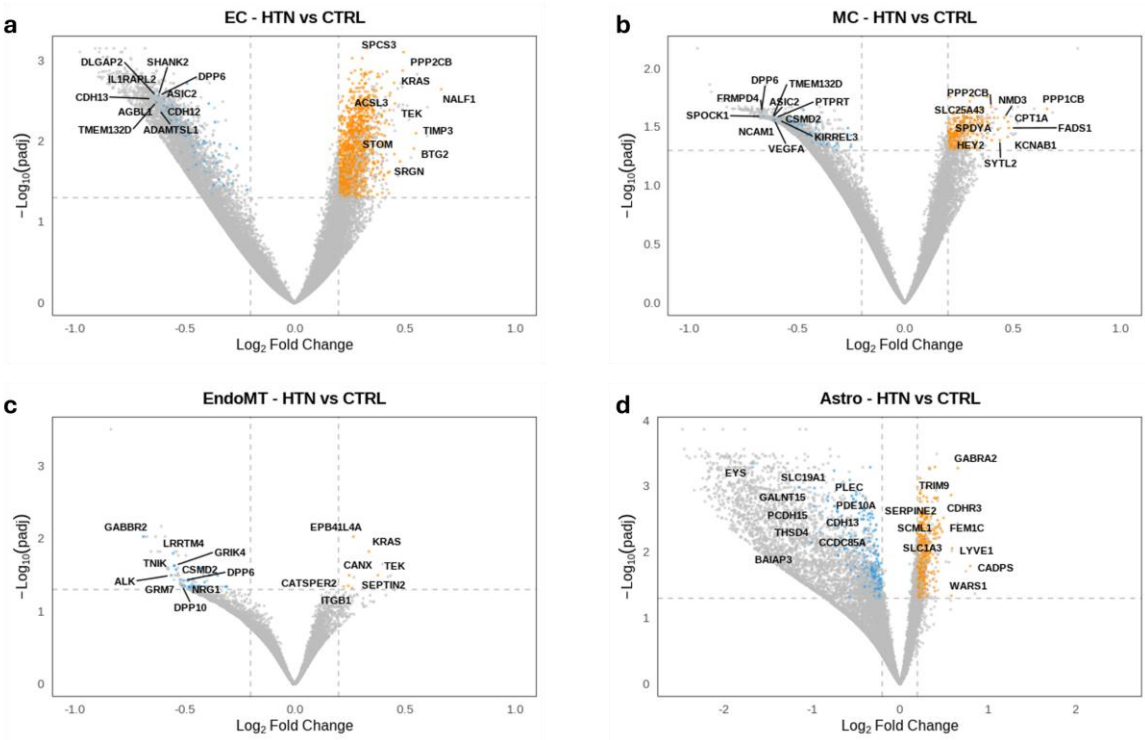

*Figure 22. Volcano plots show refined DEGs in hypertensive donors (n = 27) compared to non-hypertensive donors (n = 16) in EC (**a**), MC (**b**), EndoMT (**c**), and Astro (**d**).*

X-axis: Log_2FC (hypertensive relative to control); Y-axis: $-Log_{10}$(padj)-values. Horizontal dashed line represents a cutoff of adjusted p-values < 0.05, and vertical dashed lines represent Log_2FC cutoffs of > 0.2 or < -0.2. Genes meeting cutoffs (adjusted p-values < 0.05 & $|Log_2FC| > 0.2$ & Expression > 5%) are represented by orange circles (upregulated) and light blue circles (downregulated). Top 10 up or downregulated DEGs (based on $|Log_2FC|$) were labelled.

Even after applying 5% gene expression filtering, similar sets of the top 10 upregulated and downregulated genes were observed across cell types in the volcano plots (Figure 22). For instance, *TIMP3,* which encodes a protein that plays an important function in maintaining the ECM, was still identified in the top upregulated gene list of EC (Figure 22a). However, *SRGN,* which is a shear-stress-responsive gene, and *TEK*, which participates in the development and remodelling of the vascular system, were newly identified in the top 10 upregulated gene list of EC. *IL1RAPL2* (|LFC| = 0.66), which is associated with X-linked non-syndromic cognitive disability, was identified as the top downregulated gene in EC. Protein phosphatase gene *PPP1CB* (|LFC| = 0.66) was identified as the top upregulated gene in MC (Figure 22b). Notably, *VEGFA,* which plays a

crucial role in endothelial-mural cell interaction, was newly identified as one of the top 10 downregulated genes in MC. The EndoMT DEG list was quite similar, but after filtering, *TEK* (|LFC| = 0.38) was the top upregulated gene and GABA-B receptor gene *GABBR2* (|LFC| = 0.69) was the top downregulated gene (Figure 22c). Additionally, glutamate receptor genes *GRIK4, GRM7* and neuregulin gene *NRG1* were identified from the top downregulated gene list in EndoMT. In astrocytes, *CADPS* (|LFC| = 0.80), calcium-dependent secretion activator gene, was identified as the top upregulated gene. GABA-A receptor gene *GABRA2* and glutamate transporter *SLC1A3* were also significantly upregulated in Astro (Figure 22d). *EYS* (|LFC| = 1.67), which encodes a large extracellular protein including multiple epidermal growth factor-like and LamG domains, was identified as the most downregulated gene in astrocytes.

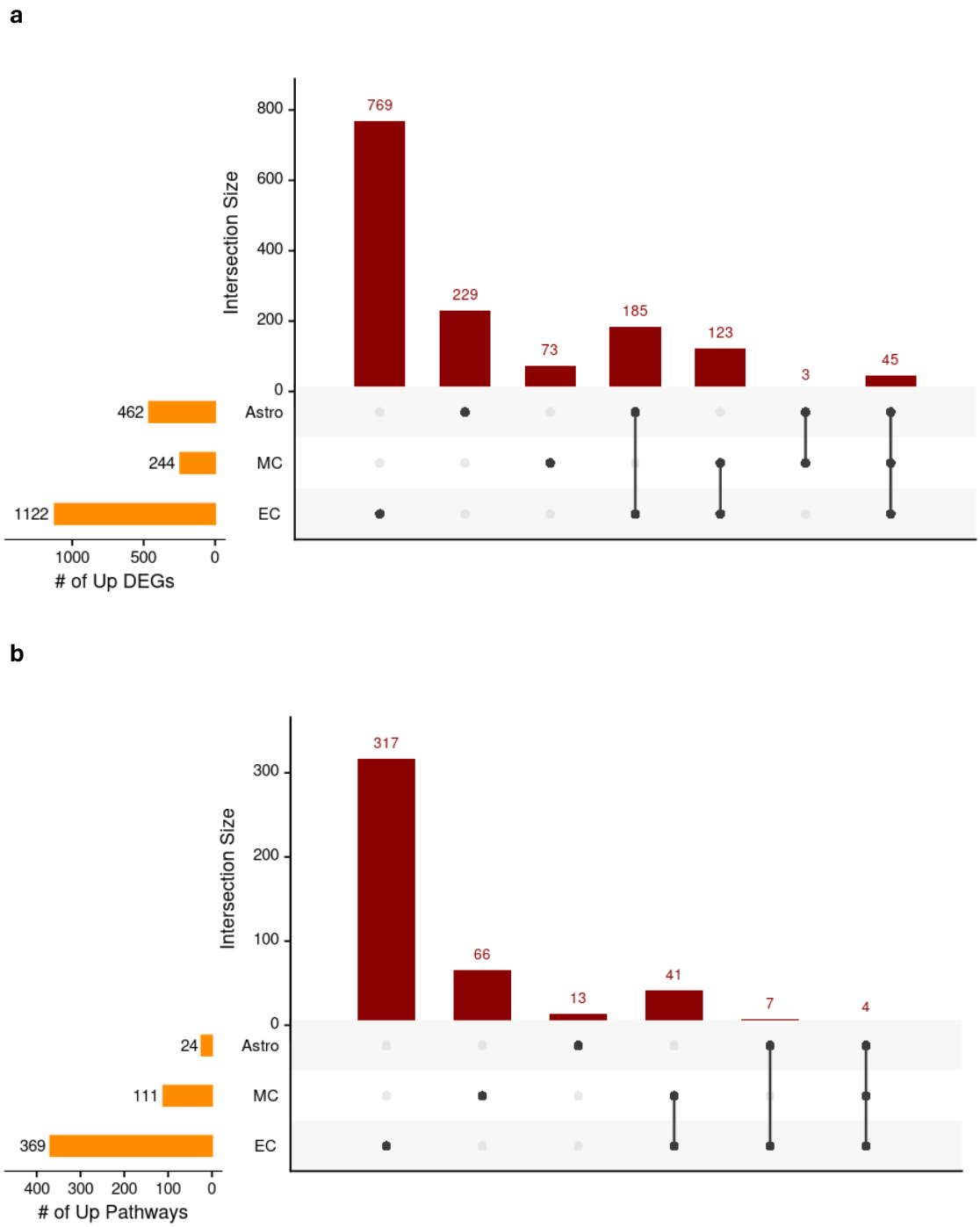

*Figure 23. Upset plot of the intersection of refined upregulated DEGs (**a**) and GO terms (**b**) among EC, MC, and Astro.*

Horizontal bars represent the total number of upregulated DEGs/GO terms in each cell type, and vertical bars indicate the number of upregulated DEGs/GO terms unique to or shared between specific cell types (denoted by the dots below the bars).

Among the upregulated DEGs, 69% of EC upregulated genes (769 genes), 50% of Astro upregulated genes (229 genes), and 30% of MC upregulated genes (73 genes) were uniquely identified in the respective cell types (Figure 23a). 45 upregulated DEGs were identified across three cell types.

Among the upregulated GO terms, 86% of EC upregulated GO terms (317 GO terms), 59% of MC upregulated GO terms (66 GO terms), and 54% of Astro upregulated GO terms (13 GO terms) were exclusively identified in the respective cell types (Figure 23b). 4 upregulated GO terms were identified across three cell types, which were the same signalling pathways we saw before the 5% expression filtering (Table 8).

Table 8. List of refined common upregulated GO terms in EC, MC, and Astro in hypertension.

GO ID	*Description*	*Cell Type*	*Upregulated / Total*	*p.adjust*
GO:0000209	Protein Polyubiquitination	**EC**	**51/267**	**3.75E-11**
		MC	**13/267**	**0.00114**
		Astro	**17/267**	**0.0194**
GO:0007264	Small GTPase-Mediated Signal Transduction	**EC**	**55/500**	**0.000730**
		MC	**18/500**	**0.0123**
		Astro	**26/500**	**0.0302**
GO:0048193	Golgi Vesicle Transport	**EC**	**53/294**	**3.45E-09**
		MC	**15/294**	**0.00224**
		Astro	**26/294**	**0.000269**
GO:0051056	Regulation of Small GTPase-Mediated Signal Transduction	**EC**	**33/304**	**0.0235**
		MC	**13/304**	**0.0196**
		Astro	**19/304**	**0.0278**

For each GO term, "Upregulated / Total" indicates the number of upregulated genes detected in the cell type divided by the total number of genes annotated to that GO term in the background gene set. Adjusted p-value (p.adjust) reflects the statistical significance of enrichment after multiple testing correction. Only GO terms significantly enriched in all three cell types are shown.

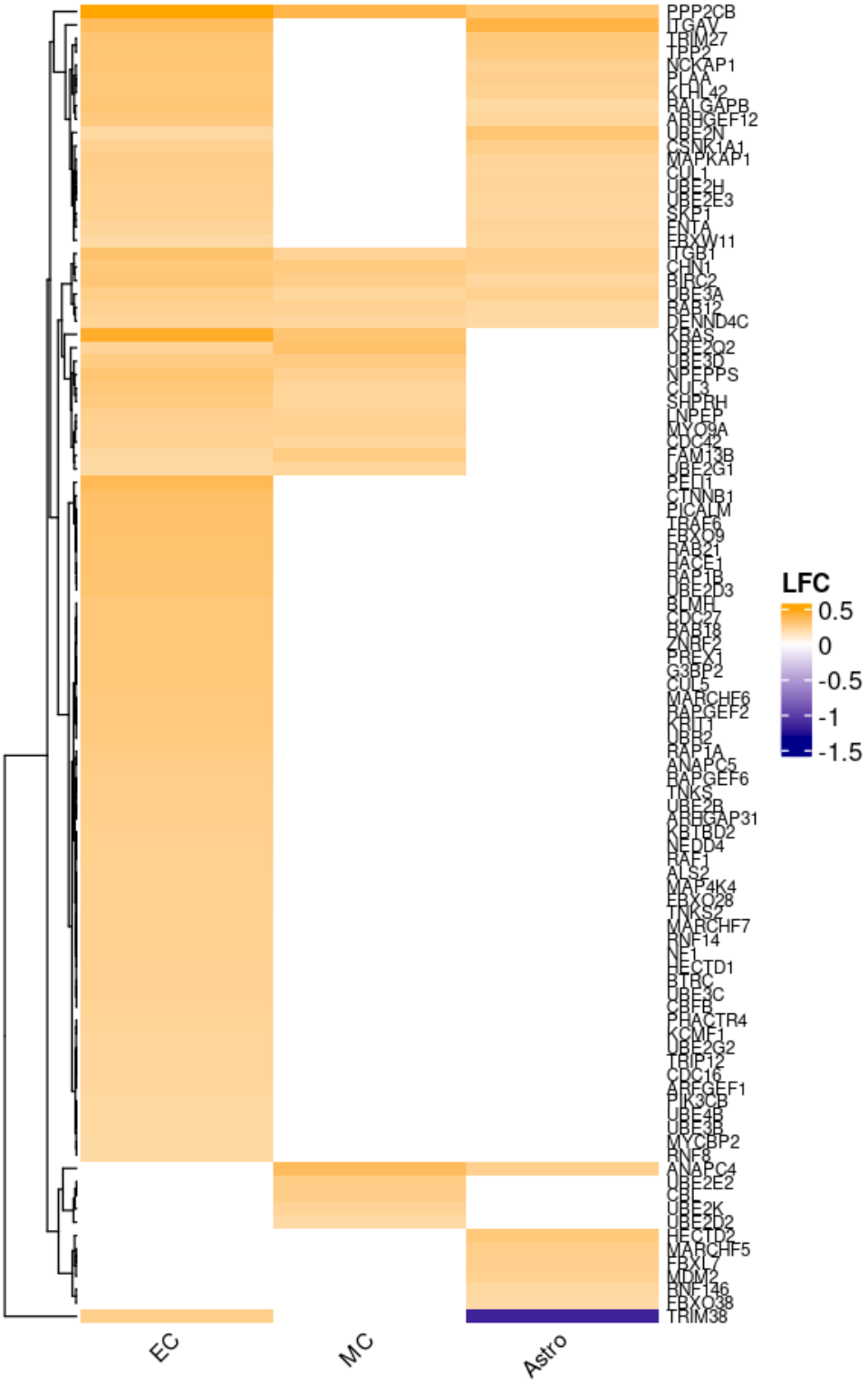
PPP2CB
ITGAV
TRIM27
TPP2
NCKAP1
PLAA
KTN1
KTN1
RALGAPB
ARHGEF12
UBE2N
CSNK1A1
MAPKAP1
CUL1
UBE2H
UBE2E3
SKP1
ENTA
FBXW11
ITGB1
CHN1
BIRC2
UBE3A
RAB12
DENND4C
KRAS
UBE2O2
UBE3D
NPEPPS
CUL3
SHPRH
LNPEP
MYO9A
CDC42
FAM13B
UBE2G1
PELI1
CTNNB1
PICALM
TRAF6
FBXO9
RAB21
HACE1
RAP1B
UBE2D3
BLMH
CDC27
RAB18
ZNRF2
PREX1
G3BP2
CUL5
MARCHF6
RAPGEF2
KBTBD7
UBR2
RAP1A
ANAPC5
RAPGEF6
TNKS
UBE2B
ARHGAP31
KBTBD2
NEDD4
RAF1
ALS2
MAP4K4
FBXO28
TNKS2
MARCH7
RNF14
NF1
HECTD1
BTRC
UBE3C
CBFB
PHACTR4
KCMF1
UBE2G2
TRIP12
CDC16
ARFGEF1
PIK3CB
UBE4B
UBE3B
MYCBP2
RNF8
ANAPC4
UBE2E2
CBL
UBE2K
UBE2D2
HECTD2
MARCHF5
FBXL7
MDM2
RNF146
FBXO38
TRIM38
LFC
0.5
0
-0.5
-1
-1.5
EC
MC
Astro

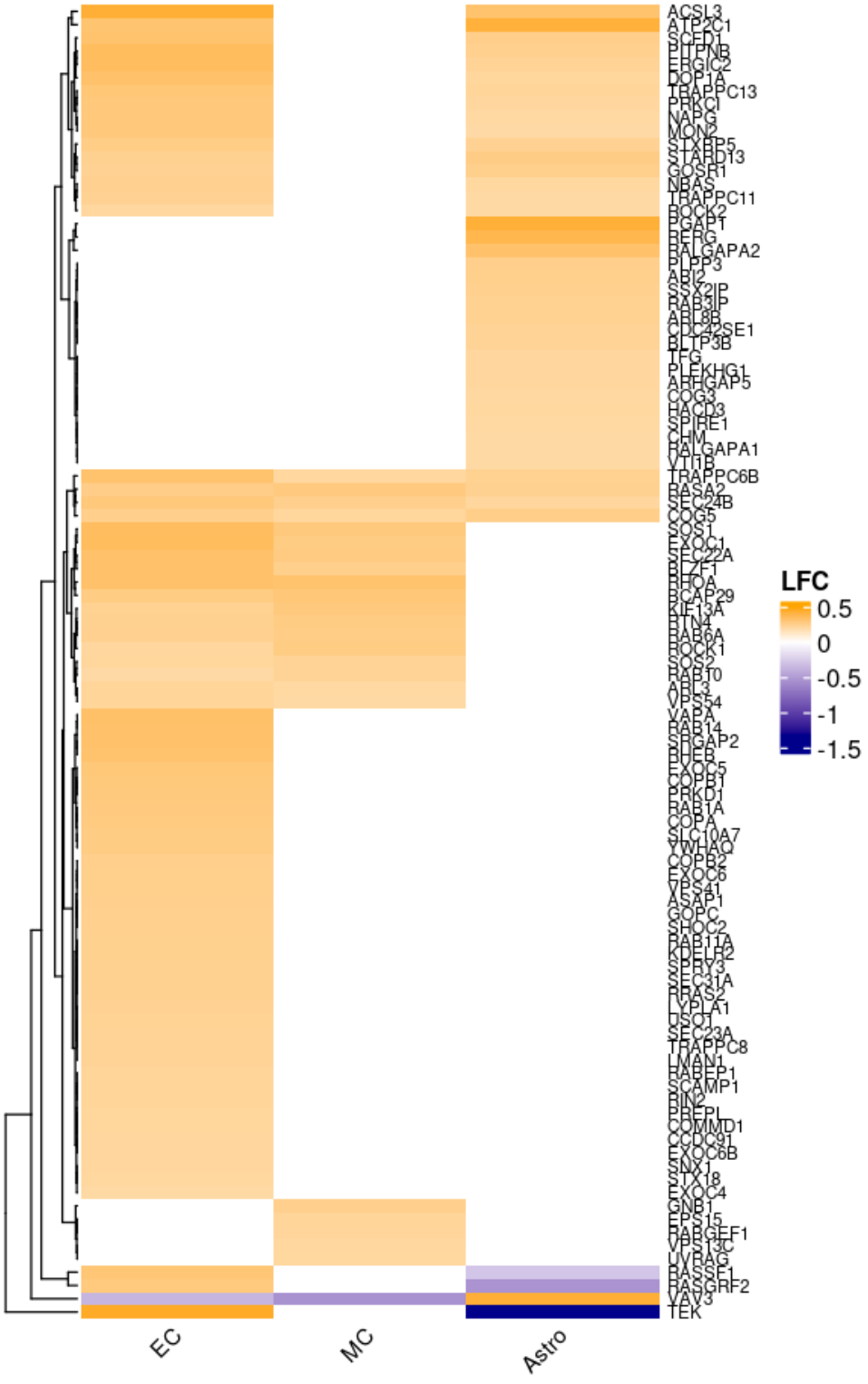

Figure 24. Heatmap of dysregulated genes from common upregulated pathways across EC, MC, and Astro in hypertension.

Rows represent genes and columns represent cell types. 197 genes included were derived from common upregulated pathways across three cell types (EC, MC, and Astro), with the colour scale indicating the Log_2FoldChange (LFC). Due to the large number of genes, the heatmap was split into two panels for clarity.

To determine whether the same genes drive the enrichment of these common upregulated pathways across different cell types or distinct genes contribute to the same signalling pathways, I listed the genes contributing to each common upregulated GO term in each cell type. 197 genes were identified and labelled with their corresponding LFC values from DEG analysis on the heatmap (Figure 24). Interestingly, although the same signalling pathways were enriched across EC, MC, and Astro, the involved genes were distinct, and many EC-unique genes were identified, suggesting the key and active role of EC in these pathways.

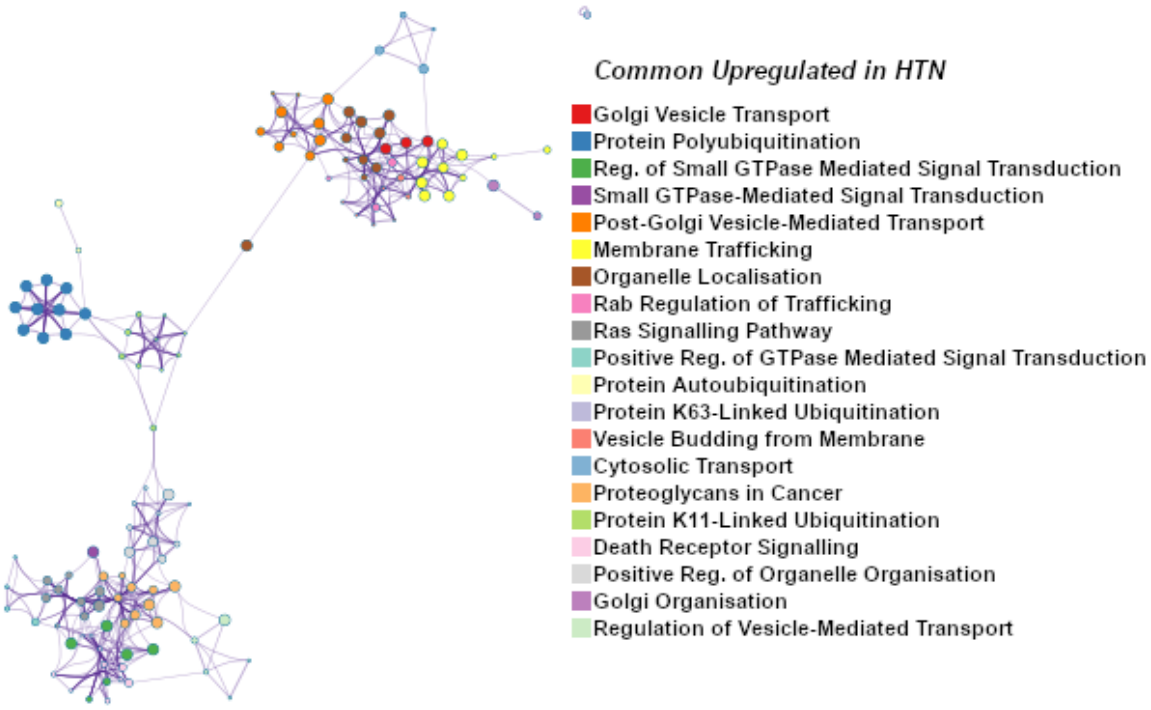

Figure 25. Network plot of enriched terms from dysregulated genes of common upregulated pathways across EC, MC, and Astro in hypertension.

Each node represents an enriched term and terms with a similarity > 0.3 are connected by edges. Node size indicates the number of genes in the term overlapping with the input gene list. The most statistically significant term per cluster was labelled from the top 20 clusters.

The network plots provided a comprehensive overview of biological processes and pathways associated with these 197 differentially expressed genes in hypertension. The most significant enrichment was *Golgi Vesicle Transport (GO:0048193)* (64 genes) followed by *Protein Polyubiquitination (GO:0000209)* (61 genes) and *Regulation of Small GTPase Mediated Signal Transduction (GO:0051056)* (42 genes) (Figure 25). The other upregulated enriched terms were all related to these processes and suggest significant alterations in protein biology and intracellular trafficking.

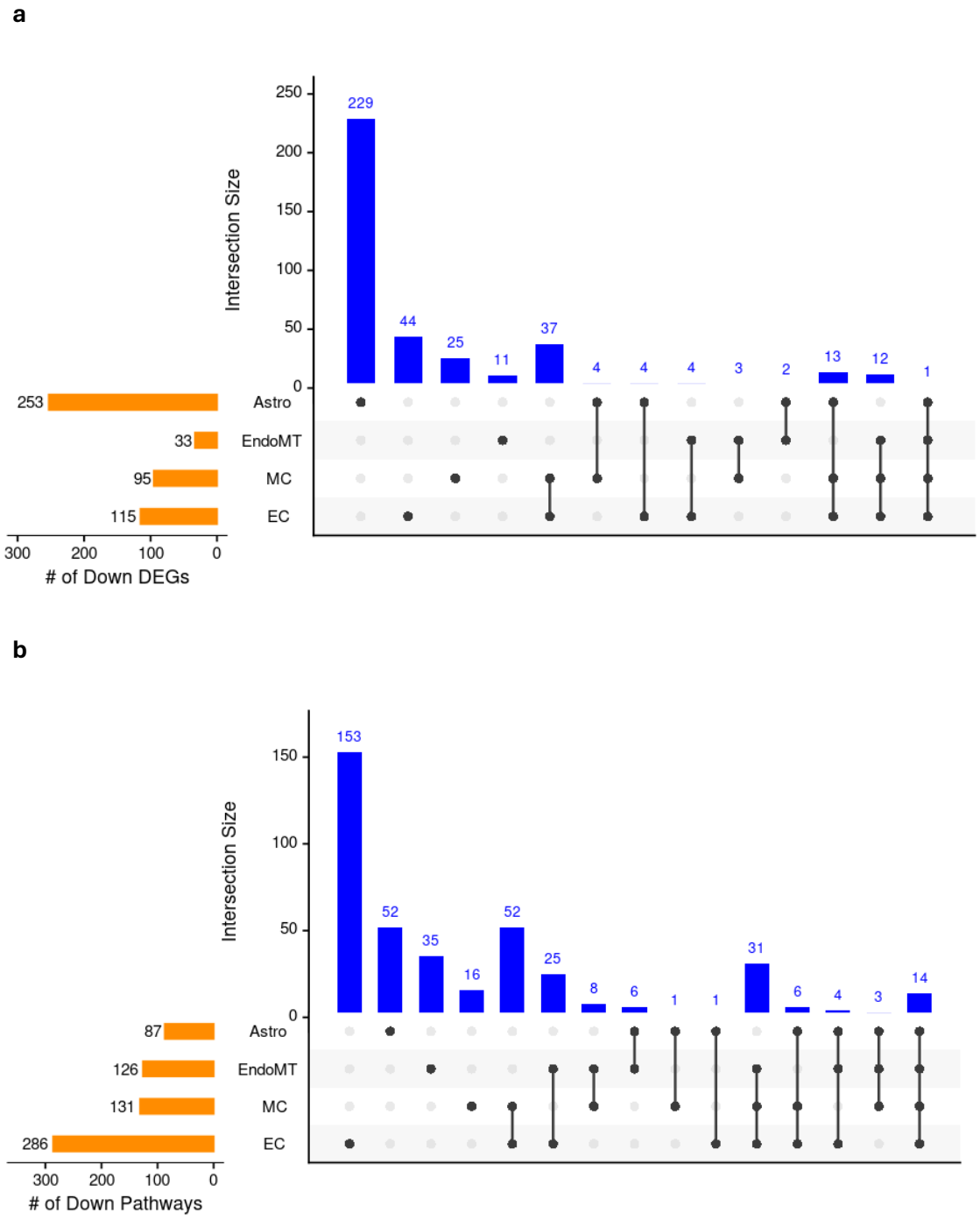

*Figure 26. Upset plot of the intersection of refined downregulated DEGs (**a**) and GO terms (**b**) among EC, MC, EndoMT, and Astro.*

Horizontal bars represent the total number of downregulated DEGs/GO terms in each cell type, and vertical bars indicate the number of downregulated DEGs/GO terms unique to or shared between specific cell types (denoted by the dots below the bars).

Among the downregulated DEGs, 91% of Astro downregulated genes (229 genes), 38% of EC downregulated genes (44 genes), 26% of MC downregulated genes (25 genes), and 33% of EndoMT downregulated genes (11 genes) were uniquely identified in the respective cell types (Figure 26a). 12 downregulated DEGs were identified across EC, MC, and EndoMT. Interestingly, 1 downregulated DEG (*NRG1*) was identified across four cell types. The 5% expression filtering has resulted in highlighting altered genes in astrocytes that were mostly unique changes in astrocytes, whilst the majority of EC and MC changes were not unique. Indeed, 37 downregulated DEGs were shared exclusively between EC and MC.

Among the downregulated GO terms, 53% of EC downregulated GO terms (153 GO terms), 60% of Astro downregulated GO terms (52 GO terms), 28% of EndoMT downregulated GO terms (35 GO terms), and 12% of MC downregulated GO terms (16 GO terms) were uniquely identified in the respective cell types (Figure 26b). Interestingly, 14 downregulated GO terms were identified across four cell types, which were the signalling pathways we saw before the 5% expression filtering, including neuronal development, synaptic transmission, and cell-cell adhesion (Table 9).

Table 9. List of refined common downregulated GO terms in EC, MC, EndoMT, and Astro in hypertension.

GO ID	*Description*	*Cell Type*	*Downregulated / Total*	*p.adjust*
GO:0007409	Axonogenesis	**EC**	**13/455**	**0.000127**
		MC	**13/455**	**2.20E-05**
		EndoMT	**7/455**	**0.000209**
		Astro	**25/455**	**1.93E-06**
GO:0007411	Axon Guidance	**EC**	**9/234**	**0.000340**
		MC	**9/234**	**0.000114**
		EndoMT	**3/234**	**0.0412**
		Astro	**14/234**	**0.000425**
GO:0007416	Synapse Assembly	**EC**	**16/208**	**2.84E-11**
		MC	**13/208**	**6.97E-08**
		EndoMT	**9/208**	**6.25E-06**
		Astro	**13/208**	**0.00545**
GO:0007612	Learning	**EC**	**7/153**	**0.000813**
		MC	**7/153**	**0.000474**
		EndoMT	**3/153**	**0.0176**
		Astro	**9/153**	**0.0269**
GO:0010975	Regulation of Neuron Projection Development	**EC**	**16/460**	**5.77E-06**
		MC	**11/460**	**0.000535**
		EndoMT	**10/460**	**8.10E-07**
		Astro	**21/460**	**7.17E-05**
GO:0016358	Dendrite Development	**EC**	**10/235**	**7.17E-05**
		MC	**6/235**	**0.0195**
		EndoMT	**7/235**	**1.08E-05**
		Astro	**12/235**	**0.00456**
GO:0031346	Positive Regulation of Cell Projection Organisation	**EC**	**12/360**	**0.000316**
		MC	**8/360**	**0.00808**
		EndoMT	**6/360**	**0.000518**
		Astro	**15/360**	**0.00475**
GO:0050770	Regulation of Axonogenesis	**EC**	**8/156**	**0.000165**
		MC	**6/156**	**0.00345**
		EndoMT	**6/156**	**1.87E-05**
		Astro	**14/156**	**1.93E-06**
GO:0050772	Positive Regulation of Axonogenesis	**EC**	**5/78**	**0.00200**
		MC	**4/78**	**0.0127**
		EndoMT	**3/78**	**0.00466**
		Astro	**9/78**	**0.000295**

GO ID	*Description*	*Cell Type*	*Downregulated / Total*	*p.adjust*
GO:0050919	Negative Chemotaxis	**EC**	**3/47**	**0.0228**
		MC	**3/47**	**0.0265**
		EndoMT	**2/47**	**0.0228**
		Astro	**6/47**	**0.00327**
GO:0051960	Regulation of Nervous System Development	**EC**	**17/468**	**1.92E-07**
		MC	**10/468**	**0.00278**
		EndoMT	**8/468**	**4.45E-05**
		Astro	**17/468**	**0.00334**
GO:0051962	Positive Regulation of Nervous System Development	**EC**	**15/294**	**4.84E-08**
		MC	**9/294**	**0.000535**
		EndoMT	**6/294**	**0.000209**
		Astro	**11/294**	**0.0419**
GO:0097485	Neuron Projection Guidance	**EC**	**9/234**	**0.000400**
		MC	**9/234**	**0.000114**
		EndoMT	**3/234**	**0.0412**
		Astro	**14/234**	**0.000425**
GO:0098742	Cell-Cell Adhesion via Plasma-Membrane Adhesion Molecules	**EC**	**20/279**	**2.55E-13**
		MC	**14/279**	**1.64E-08**
		EndoMT	**7/279**	**0.000186**
		Astro	**14/279**	**0.00194**

For each GO term, "Downregulated / Total" indicates the number of downregulated genes detected in the cell type divided by the total number of genes annotated to that GO term in the background gene set. Adjusted p-value (p.adjust) reflects the statistical significance of enrichment after multiple testing correction. Only GO terms significantly enriched in all four cell types are shown.

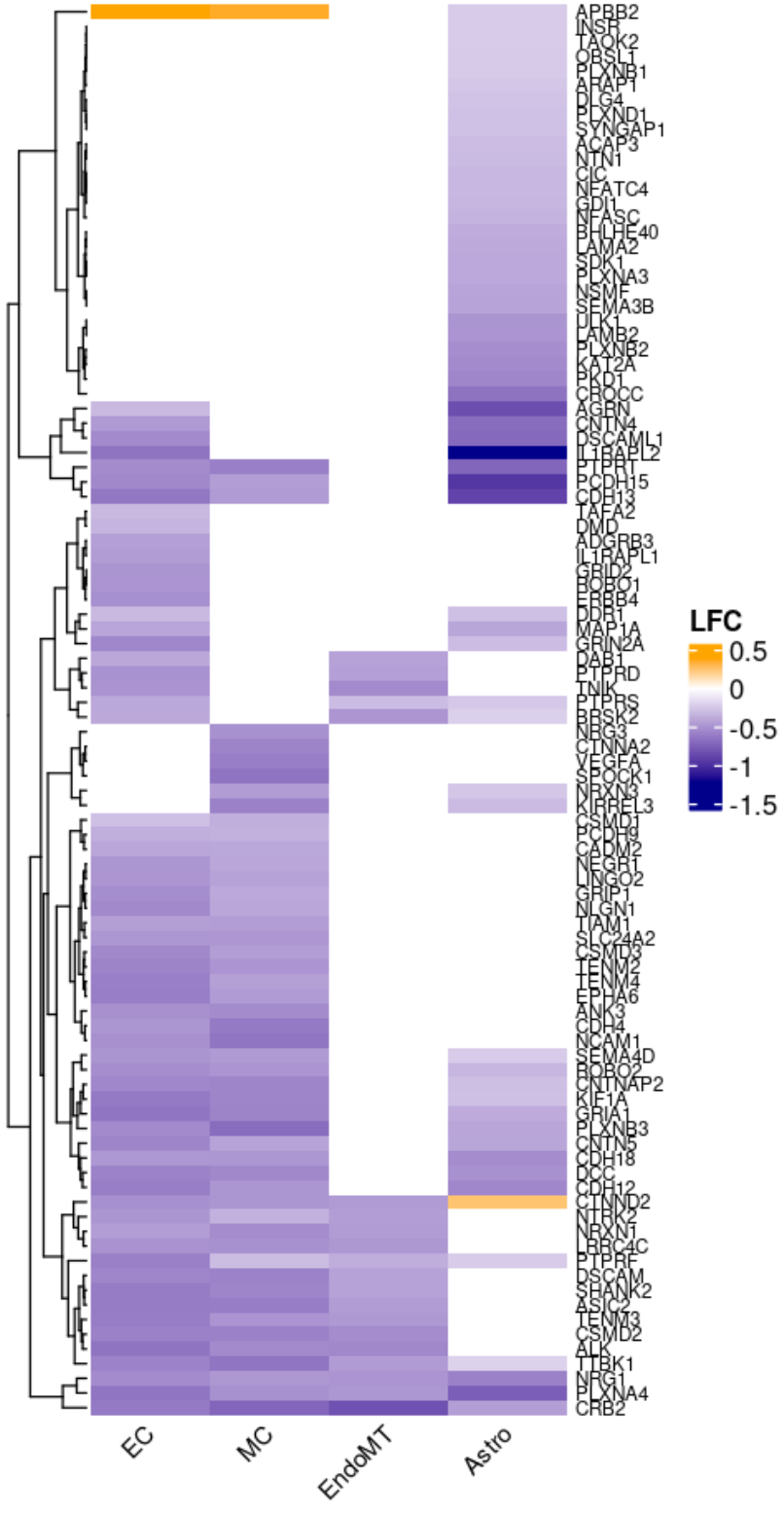

Figure 27. Heatmap of dysregulated genes from common downregulated pathways across EC, MC, EndoMT, and Astro in hypertension.

Rows represent genes and columns represent cell types. 96 genes included were derived from common downregulated pathways across four cell types (EC, MC, EndoMT, and Astro), with the colour scale indicating the Log_2FoldChange (LFC).

Examining the genes contributing to each common downregulated GO term in each cell type, 96 genes were identified (Figure 27). Although the same signalling pathways were enriched across cell types, the genes driving these pathways were not identical. While some genes were shared among cell types, astrocytes also exhibited a set of distinct genes that were not found in vascular cell types, several signalling molecules or receptors conspicuously downregulated only in astrocytes including semaphorin-plexins and the insulin receptor. There was extensive overlap in pathway genes between EC and MC. With the exception of EndoMT, each cell type did have a unique set of gene changes. This suggests the unique role of each cell type and cell-type-specific regulatory mechanisms in hypertension.

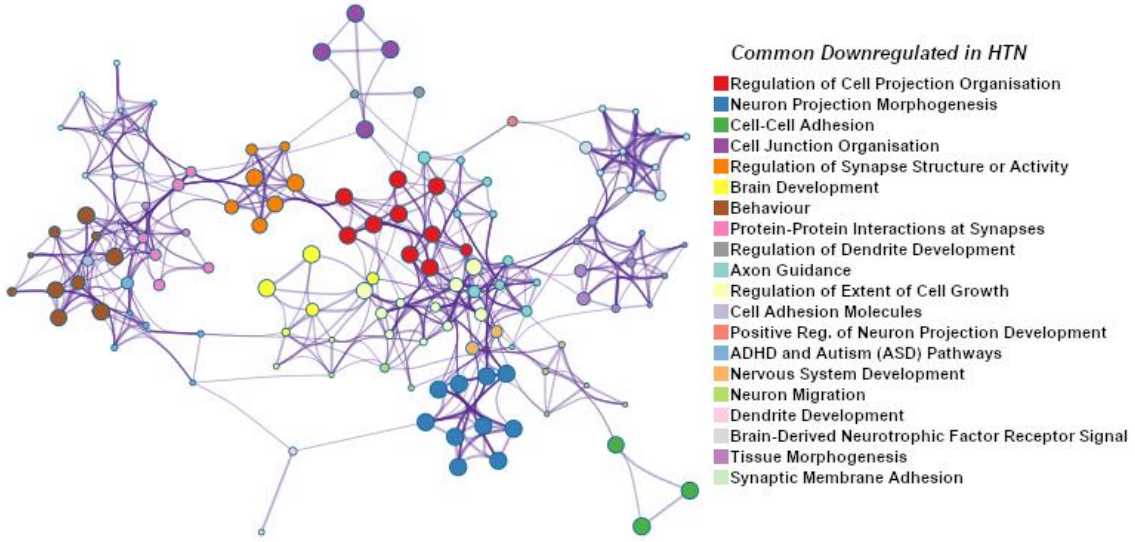

Figure 28. Network plot of enriched terms from dysregulated genes of common downregulated pathways across EC, MC, EndoMT, and Astro in hypertension.

Each node represents an enriched term and terms with a similarity > 0.3 are connected by edges. Node size indicates the number of genes in the term overlapping with the input gene list. The most statistically significant term per cluster was labelled from the top 20 clusters.

The most significant enrichment from 96 genes of common downregulated pathways across EC, MC, EndoMT, and Astro in hypertension was *Regulation of Cell Projection Organisation (GO:0031344)* (50 genes) followed by *Neuron Projection Morphogenesis (GO:0048812)* (41 genes) and *Cell-Cell Adhesion (GO:0098609)* (42 genes). All the other downregulated enriched terms were mainly related to these same processes (Figure 28).

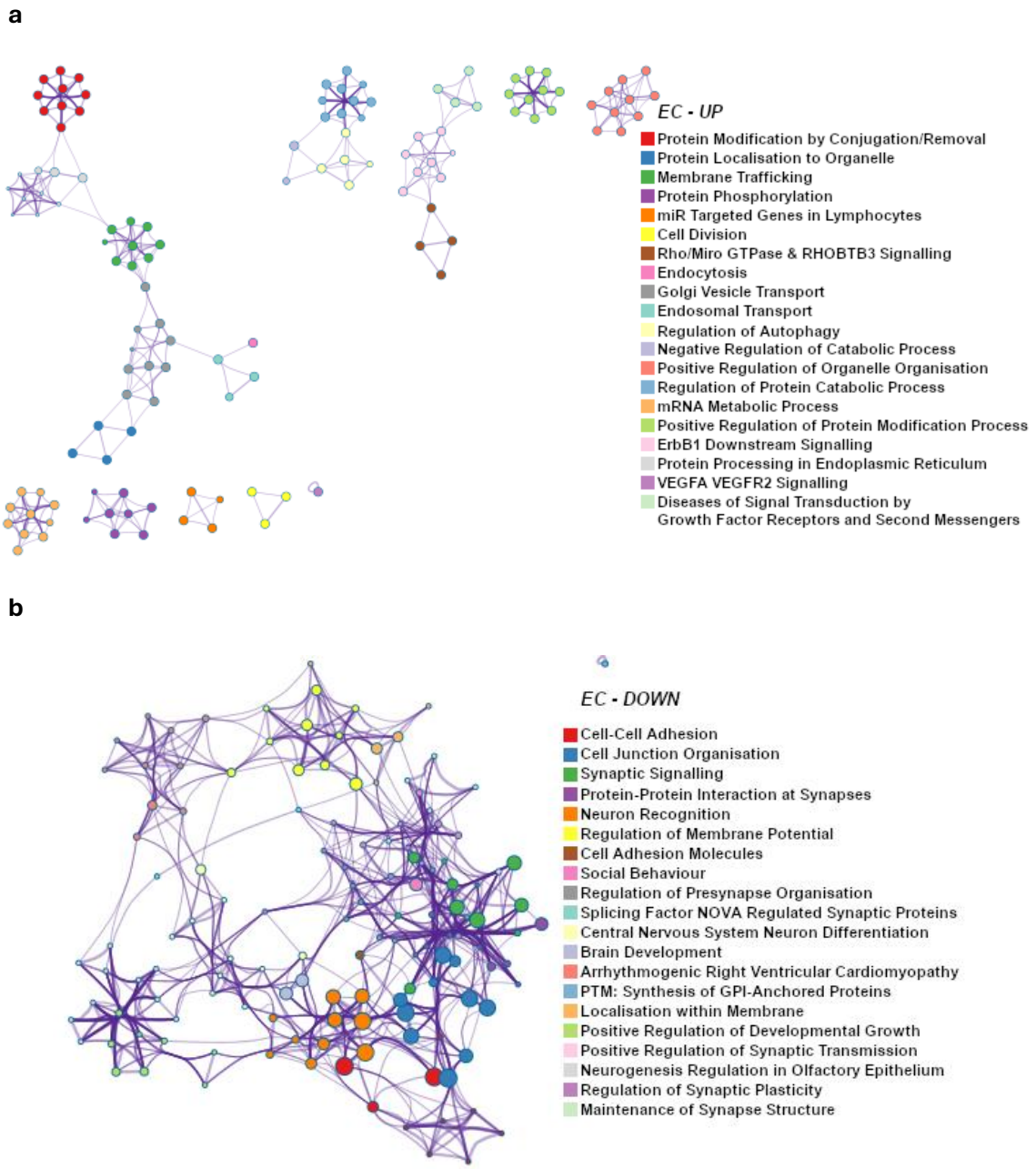

*Figure 29. Network plot of enriched terms from EC upregulated (**a**) and downregulated (**b**) genes in hypertension.*

Each node represents an enriched term and terms with a similarity > 0.3 are connected by edges. Node size indicates the number of genes in the term overlapping with the input gene list. The most statistically significant term per cluster was labelled from the top 20 clusters.

Additionally, I examined the DEGs of each cell type individually to dissect cell-type-specific disturbed functional modules and signalling pathways in hypertension. The pathways in each cell type were almost the same as the common pathways identified across cell types (Figure S 13; Figure S 14; Figure S 15). However, *Regulation of*

Autophagy (GO:0010506) (54 genes) was uniquely identified as one of the most significant enrichments from EC upregulated genes (Figure 29a). *VEGFA VEGFR2 signalling* (*WP3888*) (55 genes) was also uniquely identified as the significant enrichment from EC and Astro upregulated genes (Figure S 15).

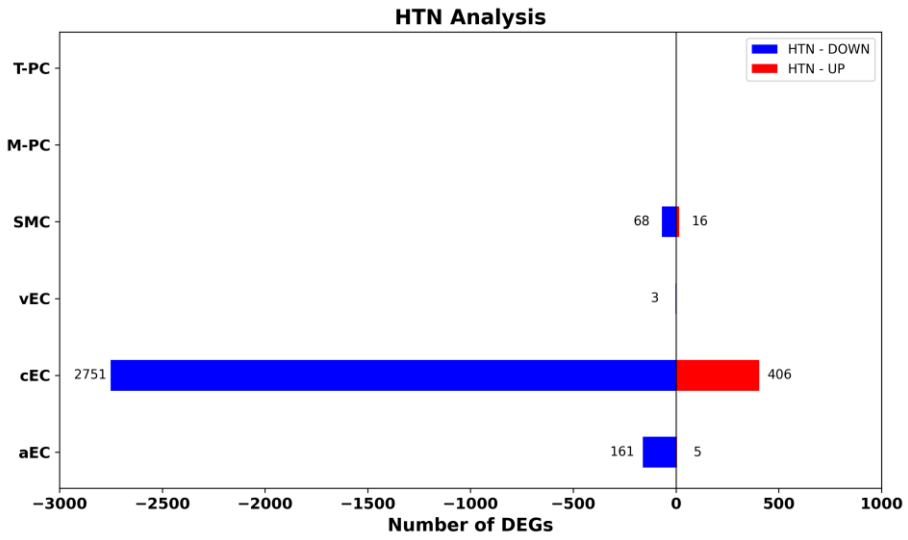

Figure 30. Number of upregulated and downregulated DEGs in hypertension in each EC and MC subtype.

Upregulated DEGs in hypertension were labelled in red colour and downregulated DEGs in hypertension were labelled in blue colour (adjusted p-values < 0.05 & $|Log_2FC| > 0.2$).

To further explore the transcriptional changes in hypertension within major vascular cell types, I performed differential gene expression analysis at the cell subtype level. Interestingly, a large number of DEGs were identified in cEC, some DEGs in aEC, and the majority of them were downregulated (Figure 30). SMC is the only mural cell subtype that showed DEGs, and no significant DEGs were identified in M-PC and T-PC.

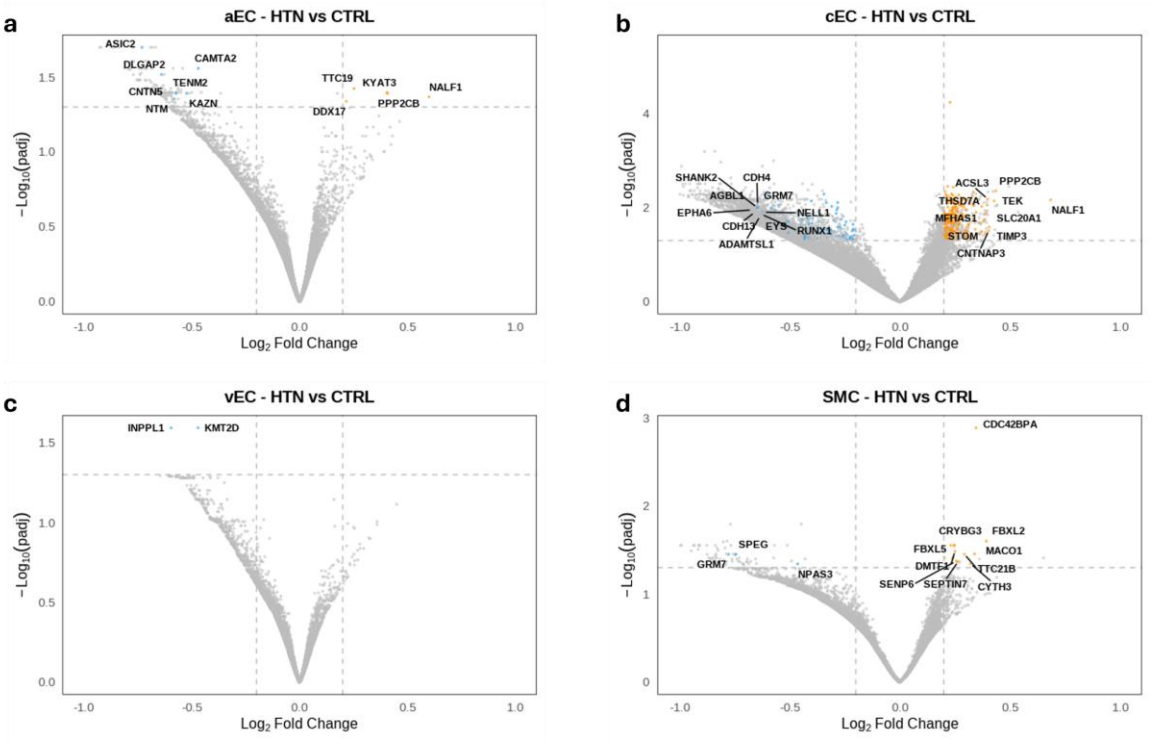

*Figure 31. Volcano plots show refined DEGs in hypertensive donors (n = 27) compared to non-hypertensive donors (n = 16) in aEC (**a**), cEC (**b**), vEC (**c**), and SMC (**d**).*

X-axis: Log_2FC (hypertensive relative to control); Y-axis: $-Log_{10}$(padj)-values. Horizontal dashed line represents a cutoff of adjusted p-values < 0.05, and vertical dashed lines represent Log_2FC cutoffs of > 0.2 or < -0.2. Genes meeting cutoffs (adjusted p-values < 0.05 & $|Log_2FC| > 0.2$ & Expression > 5%) are represented by orange circles (upregulated) and light blue circles (downregulated). Top 10 up or downregulated DEGs (based on $|Log_2FC|$) were labelled.

An additional filtering step (Expression > 5%) was added to ensure biological relevance and representation. This significantly reduced the number of DEGs: 5 upregulated and 7 downregulated genes in aEC, 250 upregulated and 130 downregulated genes in cEC, 2 downregulated genes in vEC, and 13 upregulated and 3 downregulated genes in SMC (Figure 31). A similar top DEGs list was identified, as in the volcano plots without applying 5% expression cut-off (Figure S 20). *NALF1*, the top upregulated gene in EC, was also identified as the top upregulated gene in aEC (|LFC| = 0.60) and cEC (|LFC| = 0.68). However, there were some newly identified interesting top DEGs: glutamate receptor gene *GRM7* was significantly downregulated in both cEC and SMC. Also, transcription factor gene *RUNX1*, which is a key regulator in angiogenesis, was one of the top downregulated genes in cEC.

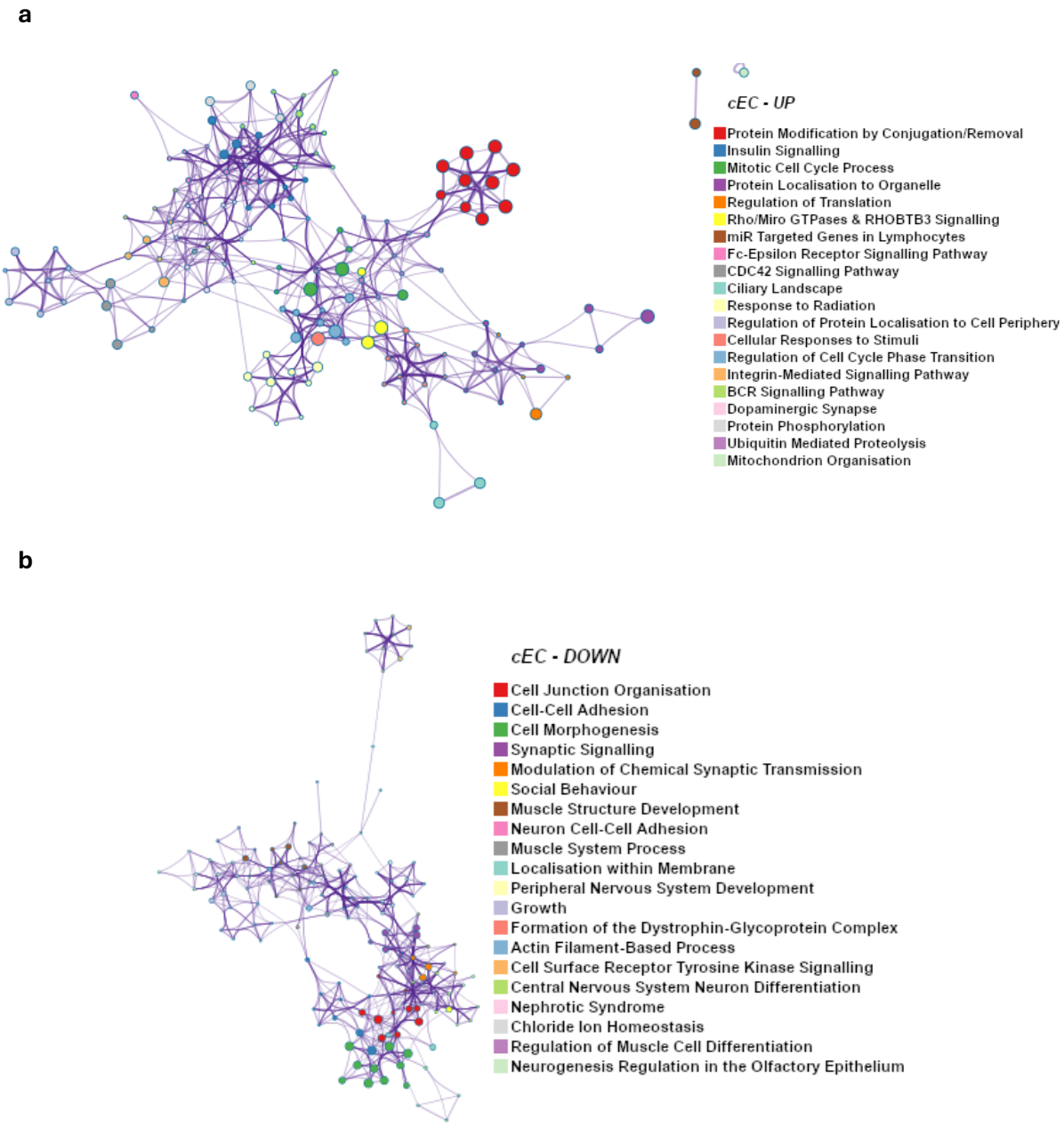

*Figure 32. Network plot of enriched terms from cEC upregulated (**a**) and downregulated (**b**) genes in hypertension.*

Each node represents an enriched term and terms with a similarity > 0.3 are connected by edges. Node size indicates the number of genes in the term overlapping with the input gene list. The most statistically significant term per cluster was labelled from the top 20 clusters.

Given the significant number of DEGs identified in cEC, I created the network plot to visualise the enriched terms. The most significant enrichment from cEC upregulated genes was *Protein Modification by Small Protein Conjugation or Removal (GO:0070647)*

(29 genes) followed by *Insulin Signalling (WP481)* (12 genes) and *Mitotic Cell Cycle Process (GO:1903047)* (20 genes). The upregulated enriched terms in cEC were mainly related to signal transduction, protein processing, metabolic processes, and cell cycle regulation (Figure 32a). The most significant enrichment from cEC downregulated genes was *Cell Junction Organisation (GO:0034330)* (25 genes) followed by *Cell-Cell Adhesion (GO:0098609)* (23 genes) and *Cell Morphogenesis (GO:0000902)* (23 genes). The downregulated enriched terms in cEC were mainly related to cell adhesion, synaptic signalling, muscle-related processes, neuronal development and differentiation (Figure 32b).

Discussion

From differential gene expression analysis, it is striking that no significant DEGs were identified in diabetes. This is very surprising given the established evidence that diabetes causes a vasculopathy in many other organs such as the heart and kidneys. One previous study using laser capture microdissection identified diabetes-associated changes in brain vasculature, but this study used a small number of lateral temporal cortex samples (Bury et al., 2021). Another study has investigated the transcriptomic change of 304 T2DM samples and 608 non-diabetic control samples across 13 brain regions: caudate and hippocampus revealed significant numbers of DEGs; however, no DEGs were identified from the frontal cortex which aligns with our findings (Z. Zhou et al., 2019).

It is also possible that my study is not sufficiently powered to detect transcriptomic changes associated with diabetes, but if this is the case, then diabetes-associated changes must be relatively subtle. A further limitation is that we obtained single-cell data from nuclei, not whole cells. It is possible that the nuclear transcriptome does not reflect diabetes-induced changes. It is also possible that the effects of diabetes are not mediated by gene expression changes and instead are at the protein level or metabolic changes. However, it would be surprising that significant alterations to protein signalling or metabolism would not then lead to secondary gene expression changes. It may also be the case that the donors for this study had well-controlled diabetes which meant that any end-organ effects were limited. Nevertheless, the consistency of the lack of effect with other transcriptomic studies suggests that the prefrontal cortex appears to be protected from diabetes-associated pathology.

In contrast, hypertension showed more substantial changes in the transcriptome of vascular cell types (endothelial cells, mural cells, and endothelial-mesenchymal transition cells) and astrocytes. This suggests that hypertension hugely impacts molecular and

cellular function in the prefrontal cortex, potentially leading to NVU dysfunction, impaired executive function, and even brain atrophy. This finding aligns with the previous brain imaging study that hypertensive patients show smaller prefrontal cortex and underlying white matter volumes compared to normotensive controls (Hung et al., 2024).

The differential gene expression analysis in hypertension revealed the greatest number of DEGs in EC – 4,782 DEGs, followed by 4,038 DEGs in Astro, 1,728 DEGs in MC, and 124 DEGs in EndoMT. Whilst the majority of DEGs were downregulated in hypertension, these mostly affected genes were not abundantly expressed by that cell type. By restricting to only those genes with at least 5% expression in a cell type, the picture is reversed and hypertension predominantly leads to gene upregulation. Upregulated pathways across EC, MC, and Astro were mainly related to protein processing, intracellular transport, and organelle organisation. Upregulated autophagy signalling was also observed in EC. This suggests a cellular stress response and cellular remodelling in hypertension, reflecting the attempts to maintain cellular homeostasis. This finding aligns with the widely accepted concept that hypertension develops as a result of chronic physiological maladaptation against various stressors which include mechanical stresses, neurohormonal factors, bioactive substances derived from adipose tissue, immune cells, skeletal muscle and endothelial cells, and intracellular accumulation of metabolites, toxic molecules and dysfunctional organelles (Cicalese et al., 2021).

At an individual gene level, there were some interesting changes observed; among the most upregulated genes in hypertensive endothelial cells was *TIMP3*. A previous mouse model study has shown that *TIMP3* is important for maintaining vascular health and preserving arterial ECM in response to angiotensin II stimuli in hypertension (Basu et al., 2013). This may suggest that *TIMP3* was upregulated to protect the brain vasculature from hypertensive-induced stress.

SRGN, a shear-stress-responsive gene in EC*,* was also one of the most significantly upregulated genes in hypertensive endothelial cells. This finding aligns with a previously

published mouse study reported that *Srgn* was significantly increased in atherosclerotic plaques induced by abnormal shear stress, and the positive correlation between *SRGN* and atherosclerosis was demonstrated (Ma et al., 2020). This suggests that *SRGN* is a key gene that responds to abnormal wall shear stress in EC, and its upregulation is deleterious to vascular stability.

VEGFA, which plays a key role in regulating the interaction between endothelial cells and mural cells, was identified as one of the most downregulated genes in MC. A study has suggested that dysregulated VEGF signalling can limit pericyte migration and reduce vessel coverage, contributing to vascular leakage (Darden et al., 2019). This suggests poor cell-cell communication between MC and EC, and even leaky vasculature in hypertension. *VEGFA* was not significantly dysregulated in endothelial cells and astrocytes, but instead, I found *VEGF-VEGFR2 signalling* (*WP3888*) was a significant enrichment from EC and Astro upregulated genes. This could imply increased sensitivity to VEGF signalling or potential activation of downstream targets—which might then be a compensation for reduced VEGF signalling from MC. A mouse study has shown that increased astrocyte-derived VEGFA signalling drives BBB disruption in CNS inflammatory disease such as multiple sclerosis (Argaw et al., 2012). Overall, the data suggests altered VEGFA signalling in hypertension, contributing to changes in BBB function and NVU stability.

FABP7, which plays an important role in lipid metabolism, neuroinflammation, and synaptic regulation, was one of the top upregulated genes in astrocytes. *FABP7* appears to be a low-expressed gene in astrocytes based on other prefrontal cortex single-nucleus studies (Chatzinakos et al., 2023). However, in neurodegenerative conditions, it may be upregulated. Several studies have investigated the role of astrocytic *FABP7* in neurological disorders. For example, in an amyotrophic lateral sclerosis (ALS) mouse model study, *Fabp7* was upregulated in astrocytes, triggering pro-inflammatory NF-κB response and contributing to motor neuron toxicity (Killoy et al., 2020). In an AD mouse

model, *Fabp7* brain expression was upregulated, specifically in astrocytes surrounding amyloid plaques. A similar result was also observed in the astrocytes derived from human induced pluripotent stem cell (iPSC) lines obtained from healthy individuals, where increased *FABP7* was induced via adenoviral vectors, leading to inflammation involving enhanced NF-κB signalling (Hamilton et al., 2024). Collectively, this suggests that upregulated astrocytic *FABP7* expression can lead to neuroinflammation that may cause neuronal dysfunction. However, in my dataset, *FABP7* expression was only 0.26% in astrocytes and an average expression of 22.63 at the pseudobulk level, with a LFC of 0.75. This suggests that whilst it was significantly upregulated in hypertension, only a minority of astrocytes have been activated in this way so the biological importance is not clear.

Despite the widespread changes in vascular cells and astrocytes, surprisingly the changes in neurons were minimal. This may reflect the selection of donors, excluding significant neurodegenerative disorders. Furthermore, whilst cortical atrophy is a consequence of hypertension (Gonzalez et al., 2015), it may be that surviving cells are resilient and hence not exhibiting transcriptomic changes. It is also possible that the changes are relatively subtle and pseudobulk gene expression analysis is too conservative to detect changes. The genes which were significantly downregulated in excitatory neurons are therefore particularly interesting.

For instance, *SNCB,* which encodes beta-synuclein that has a neuroprotective role against alpha-synuclein, was identified as one of the most significantly downregulated genes in hypertension. Whilst the accumulation of alpha-synuclein is the key characteristic of PD and DLB (Li et al., 2024), a significant decrease in beta-synuclein expression, especially in the frontal and temporal cortex, is identified in DLB (Beyer et al., 2010).

SYNGR1 is associated with presynaptic vesicles in neurons, is a susceptibility gene for schizophrenia and bipolar disorder and was significantly downregulated in the dorsolateral prefrontal cortex of schizophrenia patients (Santarelli et al., 2019; Verma et al., 2005).

Interestingly, in a recent study, mice exposed to the neurotoxicant paraquat, and had significantly downregulated *LZTS3,* which encodes a postsynaptic protein, in the cerebellum (Uchewa et al., 2025).

FAIM2 encodes an anti-apoptotic protein that protects neurons from Fas-induced apoptosis *Faim2*-deficient mice showed greater dopaminergic neuron loss compared to controls (Komnig et al., 2016). In the mouse stroke model, *Faim2* deficiency led to more severe brain damage, increased neuronal apoptosis, and worse neurological impairment compared to controls (Reich et al., 2011). These studies highlight a neuroprotective role of *FAIM2* and suggest that *FAIM2* downregulation in hypertension can lead to increased vulnerability to neuronal death.

The most notable transcriptomic changes were detected in hypertensive endothelial cells, highlighting the high vulnerability of EC to hypertensive stress. Brain endothelial cells are key components of the BBB, protecting the brain from pathogens and facilitating nutrient delivery to maintain brain homeostasis and function (Chen et al., 2020). A single-nucleus study has shown that the gene expression pattern of Alzheimer's brain endothelial cells was dramatically altered and characterised by upregulated protein-folding genes (Bryant et al., 2023). This aligns with the upregulated protein-processing genes observed in EC in my study.

Among EC downregulated genes in hypertension were genes related to cell adhesion. Reduced cell-cell adhesion in endothelial cells may lead to BBB leakage and impaired NVU integrity in hypertension. Interestingly, a mouse hypertensive model using angiotensin II (Ang II) demonstrates increased BBB permeability mediated by Ang II type

1 receptor activation, leading to transcytotic and paracellular leakage without degrading tight junction proteins (Fleegal-DeMotta et al., 2009). This may suggest that hypertension-induced BBB impairment is driven by both dysregulated cell-cell adhesion signalling and Ang II.

The significant downregulation of genes in EC involved in synaptic structure/function and neuronal guidance was unexpected and has not been well explored in EC. It is possible that the downregulation of 'neuronal' genes in endothelial cells may merely represent a byproduct of altered signalling from the local environment. However, this seems unlikely, given that neuronal gene expression was largely unaffected by hypertension. Furthermore, there is some literature related to these 'neuronal' genes in EC, which include an important vascular role of neurexins (NRXN), a family of presynaptic cell adhesion proteins connecting neurons at the synapse. For instance, blocking neurexin with a monoclonal antibody inhibited angiogenesis in a chicken chorioallantoic membrane model, and neurexin inhibition also affected vascular tone in chicken arteries (Bottos et al., 2009). The dual role of neurexins suggests shared molecular cues between nervous and vascular systems. Furthermore, glutamate and GABA receptors have also been shown to have functional roles in EC. However, these roles may be very different to those described for neurons. A mouse model study has shown that *Gabrb3*^{ECKO} mice (*Gabrb3* was selectively knocked out in endothelial cells) developed hypertension, suggesting that endothelial GABA signalling plays an important role in vascular homeostasis (Agrud et al., 2022). *GRIN2D*, a glutamate-dependent NMDA receptor, has been identified as a tumour-specific endothelial marker in colorectal cancer, playing a crucial role in angiogenesis and vascularisation (Ferguson et al., 2016). These prior studies suggest that the 'neuronal/synaptic' genes may have additional roles in vascular cells, and their downregulation may contribute to impaired vascular homeostasis and even NVU instability.

The changes in genes regulating synapses and neuronal guidance were not just confined to EC. Common downregulated GO terms across vascular and glial cell populations (EC, MC, EndoMT, and Astro) were also enriched for ion transport, neurodevelopment, cell-cell adhesion, and synaptic function. Amongst these *NRG1* was notably downregulated across cell types. *NRG1* signalling is known to have multiple functions in neurons and glial cells, and also cytoprotective properties in human brain endothelial cells (Lok et al., 2009). An *in vivo* study has shown that *NRG1* treatment increased BBB integrity after brain injury (Lok et al., 2012). In a human cerebral malaria study, *NRG1* was shown to protect brain endothelial cells and also neuroglial cells from cell death (Liu et al., 2018). Downregulation of *NRG1* could therefore lead to potential BBB leakage and NVU dysfunction in hypertension.

In addition to *NRG1*, there were several other signalling molecules that were downregulated in hypertension. This was particularly true for astrocytes, where significantly downregulated DEGs included *SEMA3B* and *NTN1*. Sema3B, which is a key axon guidance cue, is known to affect the integrity of neuron dendritic structure, suggesting that reduced Sema3B signalling may lead to damaged dendritic spines that can cause cell-cell communication dysfunction in NVU (Du et al., 2022). However, Sema3B signalling also has anti-angiogenic activity, which can repel endothelial cells and induce apoptosis, suggesting its downregulation could alter vascular remodelling (Iragavarapu-Charyulu et al., 2020). Studies on the role of astrocytic *SEMA3B* are limited, and further investigations using *in vitro* co-culture models (including endothelial cells, astrocytes, and neurons) are needed. *NTN1* (Netrin 1) is known as a neuron survival factor, playing a key role in axon growth and neuronal migration by actively interacting with its receptors—including DCC (Zhu et al., 2025). A mouse model study has investigated the role of astrocytic *NTN1* in blood vessel homeostasis; interestingly, *NTN1* depletion in astrocytes led to leaky BBB in the cortex (Yao et al., 2020). This suggests that

the downregulation of *NTN1* in astrocytes can have widespread effects on the NVU in hypertension.

Cell-subtype differential gene expression analysis of EC and MC further revealed that the detected changes in EC were mainly driven by capillary endothelial cells, and some DEGs were also identified from arterial endothelial cells; the main changes in MC were attributed to smooth muscle cells. The lack of changes in arterial EC is surprising since it might be expected that increased blood pressure would have the most impact on arteries and arterioles (Figure 3). The burden on capillary EC may instead suggest that changes in EC are due to non-pressure-related effects or perhaps these EC are the least resilient to even the small increase in blood pressure that will be transmitted through in patients with hypertension.

An ageing-focused single-cell study of mouse hippocampal brain endothelial cells has shown that capillary EC exhibited the greatest transcriptional changes when compared with arterial and venous EC in normal ageing, especially upregulated immunity and oxidative stress response pathways (Chen et al., 2020). This suggests that the capillary endothelial cells are vulnerable to both age-related circulatory cues and hypertension-induced stress.

I performed pseudobulk gene expression analysis which allows the assessment of the effect of a condition on specific cell types whilst keeping the risk of false discovery reduced (Squair et al., 2021). Conversely, more subtle changes in gene expression that might be detected using single-cell differential gene expression methods such as MAST, may be missed (Finak et al., 2015). Future work with this dataset could explore this analysis and whether it might reveal changes in diabetes and also in hypertension in cell types not obviously affected in the pseudobulk expression analysis.

In summary, this chapter identified significant transcriptomic changes from endothelial cells, mural cells, and astrocytes in hypertension. These genes are normally considered important for neuronal function, but in vascular cells, they are likely to lead to altered BBB and NVU integrity. It is also possible that downregulation of ligands and receptors may alter cell-cell signalling. Moving forward, I will use cell-cell communication analysis as a tool to reveal the crosstalk between cell types and dissect dysregulated gene networks in these key cell types using WGCNA, especially looking into ‘neuronal’ genes from synaptic-related pathways.

Chapter 3. Cell-Type-Specific Dysregulated Gene Networks in Hypertension

Introduction

The previous chapter revealed that endothelial cells, especially capillary endothelial cells, were identified as a key cell type in the prefrontal cortex and showed a substantial number of DEGs in the context of hypertension. Interestingly, many EC downregulated genes were involved in synaptic signalling pathways, highlighting a set of genes involved in endothelial cell biology beyond their known traditional functions in neurons.

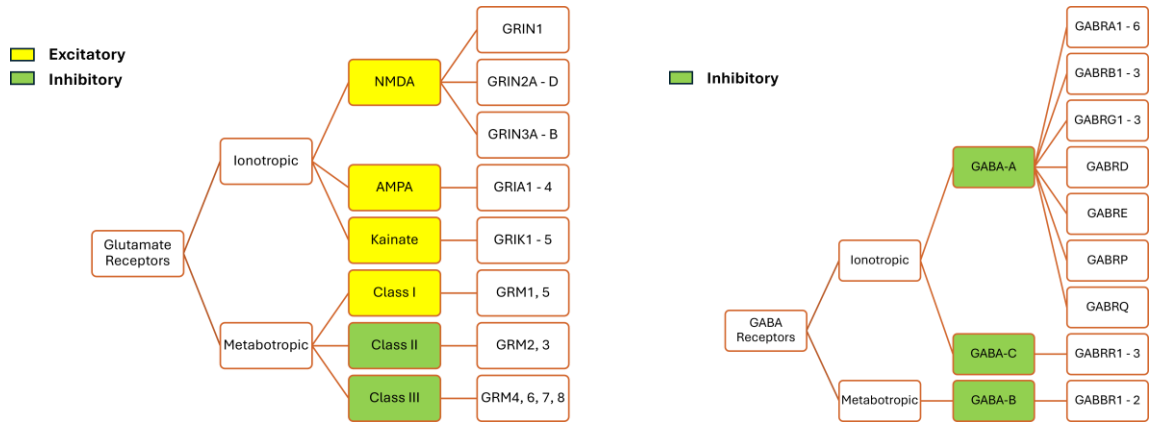

Figure 33. List of glutamate and GABA receptor subtypes.

Excitatory receptors were highlighted in yellow and inhibitory receptors were highlighted in green.

Among the genes expressed in prefrontal cortex endothelial cells and downregulated were glutamate receptors—including ionotropic and metabotropic receptors—and γ-aminobutyric acid (GABA) receptors, particularly GABA-A receptors (Figure 33). Previous studies have identified functional roles for these receptors in endothelial cells. For example, a study has suggested that telencephalic endothelial cells utilise novel GABA signalling distinct from traditional neuronal GABA signalling, and can modulate neuronal migration with a significant role in brain development and neuropsychiatric disease (Li et

al., 2018). The study showed that endothelial-specific loss of *Gabrb3* affected brain development and lead to behavioural dysfunction; additionally this mouse developed hypertension, suggesting that endothelial GABA signalling plays an important role in both the brain and the vasculature (Agrud et al., 2022; Li et al., 2018). Another mouse model study found glutamate activates endothelial NMDA receptors to enhance vessel-associated migration of cortical GABA interneurons (Leger et al., 2020).

Given that endothelial cells are the interface between the blood and parenchymal cells, the utilisation of ligand-gated receptors to enable EC to serve as a key signal transduction platform is not surprising. By integrating various chemical and physical stimuli through increasing intracellular Ca^{2+} concentration, such receptors would generate output to serve a range of functions (McCarron et al., 2017). A recent investigation revealed that brain capillary endothelial cells can control blood flow through Ca^{2+} signals, which can drive nitric oxide synthesis and selectively increase blood flow, enabling blood delivery to small clusters of neurons (Longden et al., 2021). Notably, endothelial Ca^{2+} waves can be evoked by synaptic activity (synaptically released glutamate and GABA), and elevated Ca^{2+} can lead to vasodilation via nitric oxide production and the activation of calcium-activated potassium channels (Moccia et al., 2023). These studies highlight the role of endothelial cells beyond the known traditional role as barriers but also as key mediators in the neurovascular unit.

A striking finding from the DEG analysis was the number of neuronal/synaptic genes that were downregulated. Given the pervasive changes, it suggests an alteration in a shared gene expression program due to hypertension. Indeed, gene expression in a cell typically shows co-correlated expression patterns which implies a coordination of those genes. Gene co-expression networks (GCNs) can be constructed from transcriptomic data and they reflect shared regulatory mechanisms or functional relationships among genes, often controlled by common transcription factors, signalling pathways, or epigenetic

modifications. Furthermore, changes in these co-expression networks under different physiological or pathological conditions can reveal key molecular drivers of cell-state transitions, disease mechanisms, and potential therapeutic targets (Langfelder & Horvath, 2008).

Several methods exist for the construction and analysis of GCNs. Weighted Gene Co-expression Network Analysis (WGCNA) is one of the most commonly used and identifies modules of highly correlated genes, WGCNA uses Pearson correlations and identifies gene modules by applying hierarchical clustering to a topological overlap matrix derived from the correlations (Langfelder & Horvath, 2008). The modules are summarised using module eigengene (the first principal component), which captures the main gene expression patterns within a module. Further enrichment analysis on module genes can link these modules into meaningful biological pathways, and module-trait correlation analysis can reveal how specific modules are associated with particular biological conditions. Also, WGCNA can identify hub genes (genes with high connectivity within a module) to highlight key molecules underlying biological processes.

Combining WGCNA with transcriptomic data can uncover GCNs that are not evident from individual gene analysis (e.g. differential gene expression analysis) which focuses on isolated gene changes. In my dataset, a substantial amount of differentially expressed genes was identified across cell types from the DEG analysis in hypertension, making it challenging to interpret the biological meanings in a systematic way. WGCNA can help address this challenge by identifying gene modules that get involved in the shared dysregulated pathways and hub genes that may drive the transcriptomic changes observed in hypertension.

Where GCNs are observed, they may be driven by transcription factors inducing or repressing sets of genes. TFs act as master regulators of gene expression by binding to

response elements within gene regulatory regions including promoters and enhancers, to orchestrate precise gene expression programs. TFs play a key role in determining cell identity and driving processes such as development and cell-type-specific functions, and their mutations have been linked to numerous diseases (Lambert et al., 2018). In the context of gene network level dysregulation, investigating TFs provides a way to uncover upstream regulators that may coordinate the transcriptomic changes observed.

However, TF gene activity isn't always reflected by mRNA expression levels, so inferring TF activity levels indirectly from the single-nucleus dataset is needed. BITFAM is a statistical model designed to infer TF activities from single-cell datasets by analysing known TF genes and target genes from the published ChIP-seq databases (Gao et al., 2021). Given the substantial transcriptomic changes observed in endothelial cells, TF inference analysis is essential to prioritise key TF genes and uncover key regulatory mechanisms that drive the gene expression changes in hypertension.

In this chapter, my aim is to characterise the change in neuronal genes and their associated gene networks, I will use WGCNA as a tool to build co-expression networks in endothelial cells, astrocytes, and vascular smooth muscle cells. Following network construction, module-trait correlation analysis will be conducted to determine which co-expression gene networks are highly associated with hypertension. Furthermore, TF inference analysis will be performed specifically in endothelial cells to reveal key molecular drivers and identify potential therapeutic targets.

Methods

Investigating Glutamate and GABA Receptor Gene Expression Level in EC

Genes encoding GABA and glutamate receptors were extracted from the hypertension DEG table to investigate the transcriptomic changes in those genes associated with hypertension. Only significant genes (adjusted p-values < 0.05 & |LFC| > 0.2) were listed in the tables.

Then, the percentage of nuclei expressing each glutamate and GABA receptor gene in the hypertensive endothelial cells and control (non-hypertensive) endothelial cells was calculated: the SCT assay counts matrices of HTN EC (110,403 nuclei) and CTRL EC (53,818 nuclei) were extracted separately, and a gene was considered expressed in a nucleus if its count > 0. Then, the mean expression for non-zero counts (nuclei where the gene was expressed) was calculated for each gene.

Weighted Gene Co-expression Network Analysis (WGCNA)

WGCNA was performed on pseudobulk gene expression data for each of the main cell types affected by hypertension—namely EC, astrocytes and vascular smooth muscle cells. Only protein-coding genes from biomaRt (v2.62.0) were extracted (Durinck et al., 2005; Durinck et al., 2009). Outlier genes and donors were removed using the built-in function (Langfelder & Horvath, 2008) and the PCA method respectively. DESeq2 R package (v1.46.0) was used to organise the count data and metadata for downstream analysis (Love et al., 2014). Then, I further removed genes with counts less than 15 in more than 75% of the samples. DESeq2 vst() function was used to normalise and transform the data, ready to construct the network.

Table 10. Summary of WGCNA preprocessing steps and network parameters across the datasets.

Dataset	Genes Removed	Genes After Filtering	Outlier Donors Removed	Donors After Filtering	Soft Threshold Power	merge Cut Height
EC Combined	7,365	11,881	Donor 29 (78, F, non-DIAB/non-HTN)	42	10	0.25
EC HTN	7,087	12,159	None	27	10	0.25
EC CTRL	8,043	11,203	Donor 29 (78, F, non-DIAB/non-HTN)	15	10	0.25
Astro Combined	8,038	11,208	None	43	10	0.25
Astro HTN	7,967	11,279	None	27	10	0.25
Astro CTRL	7,936	11,310	None	16	10	0.25
SMC Combined	14,381	4,865	None	43	10	0.25
SMC HTN	14,423	4,823	None	27	10	0.25
SMC CTRL	13,909	5,337	None	16	10	0.25

Outlier genes and donor samples were removed using the built-in WGCNA function and PCA, respectively. Genes with counts less than 15 in more than 75% of samples were further excluded. A soft-threshold power (β) was applied to construct a weighted network adjacency matrix. A mergeCutHeight was applied to merge similar gene modules based on module eigengene similarity.

WGCNA unsigned network construction was performed by calculating pairwise positive and negative gene co-expression correlations using the Pearson correlation.

To maximise a model fit R^2 under a scale-free topology model defined by the presence of a few highly connected hubs and many nodes with few connections, a soft-threshold

power β was applied to generate a weighted network adjacency matrix, reflecting connection strength between genes.

From the given adjacency matrix, the corresponding topological overlap matrix (TOM) was calculated and then the TOM dissimilarity matrix (1-TOM) was used to construct distinct modules using linkage hierarchical clustering (a module is a group of gene profiles that are highly correlated). A module eigengene (ME) is the standardised gene expression profile for a given module. To further merge the clusters into more condensed and meaningful modules based on pairwise eigengene correlations, I set the mergeCutHeight as 0.25 (the height corresponds to a correlation of over 75%) (Table 10). The grey module, which represents a group of genes that do not belong to any co-expression module, was omitted from further analysis. chooseTopHubInEachModule() built-in function in WGCNA R package was used to export the top hub gene in each module.

To determine if the identified modules were associated with hypertension and diabetes, I further performed the module-trait correlation analysis. The donor's hypertension and diabetes status were binarised, with hypertension diagnosis as 1 and non-hypertensive controls as 0. Similarly, donors with diabetes were labelled as 1 and non-diabetic control donors as 0. Then, Pearson correlation coefficients were calculated between module eigengenes (the first principal component of gene expression within a module) and binarised traits, and student's t-distribution was used to calculate p-values.

Module genes were used for subsequent GO enrichment analysis. The GO analysis was performed using clusterProfiler R package (v4.12.6) with the associated annotation R packages annotationDBI (v1.68.0) and org.Hs.eg.db (v3.2.20) (Wu et al., 2021; Yu et al., 2012). To reduce the redundancy in GO terms and retain the most statistically significant representative terms, I applied semantic similarity filtering using the simplify() function in clusterProfiler (v4.12.6). GO terms with a semantic similarity > 0.7 were collapsed into a single representative GO term with the lowest adjusted p-value. The final set of GO terms was used for downstream visualisation.

For the hub gene network visualisation, I exported the module network in edge and node list files in a Cytoscape (v3.10.2) format (Shannon et al., 2003). Thresholds were selected for edge weights to facilitate visualisation. Furthermore, only nodes representing genes with at least 5% expression in the cell type of interest were selected.

Transcription Factor Activity Inference in Endothelial Cells

To infer transcription factor that may be responsible for the altered gene expression in endothelial cells, I used the BITFAM (v1.2.0) R package, a computational framework that estimates TF activities from single-cell/nucleus RNA sequencing data (Gao et al., 2021). TF analysis is computationally intensive and I therefore restricted the dataset to capillary endothelial cells as these were identified as the key cell type affected by hypertension; Seurat object raw counts table with protein-coding genes only (19,246 genes x 100,073 nuclei) for the downstream analysis. The raw gene counts table was pre-processed using the BITFAM_preprocess() function, which included normalisation, identification of highly variable genes, and standardisation. Candidate TFs in BITFAM were selected based on the following criteria: (1) only TFs that were among the most variably expressed genes (2) TFs must have corresponding ChIP-seq data available in the Gene Transcription Regulation Database (GTRD) (Yevshin et al., 2019), and (3) the TF has at least 10 target genes among the most variably expressed genes. I applied the BITFAM model to infer TF activities across capillary endothelial cells, resulting in 187 TF genes.

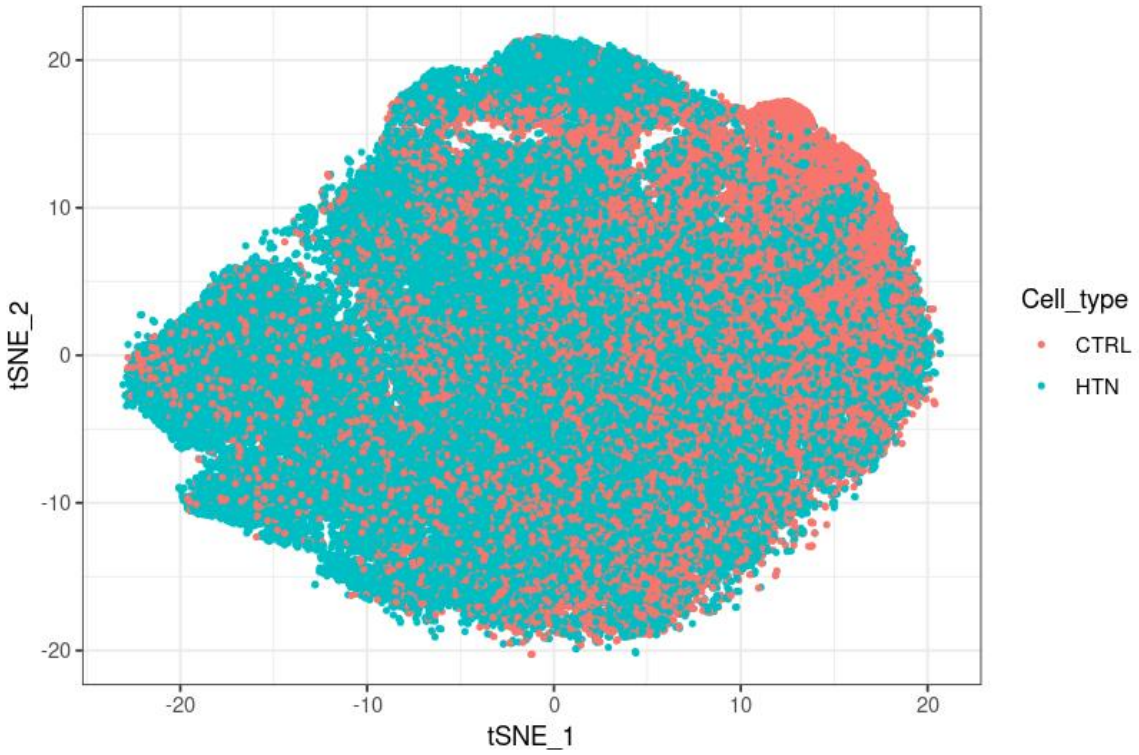

Figure 34. t-SNE of inferred transcription factor activities in capillary endothelial cells. Cells were labelled based on the hypertension status.

The inferred TF activity scores were extracted and I further visualised the patterns of TF activity using t-SNE dimensionality reduction (Figure 34). Then, I applied a random forest algorithm to identify key TFs associated with hypertension. The cell-type binary annotation was created: hypertensive nuclei as 1 and control nuclei as 0. The inferred TF activity scores were combined with this binary annotation, and a random forest model was trained (HTN was the dependent variable and the TF activity scores were predictors). After training, feature importance scores were extracted and the most influential TFs associated with hypertension were identified based on the ranking. Then, the activity values of the top influential TFs were visualised using boxplots in ggplot2 (v.3.5.1) (Valero-Mora, 2010). A t-test was used to determine the statistical difference between the two groups.

Results

a

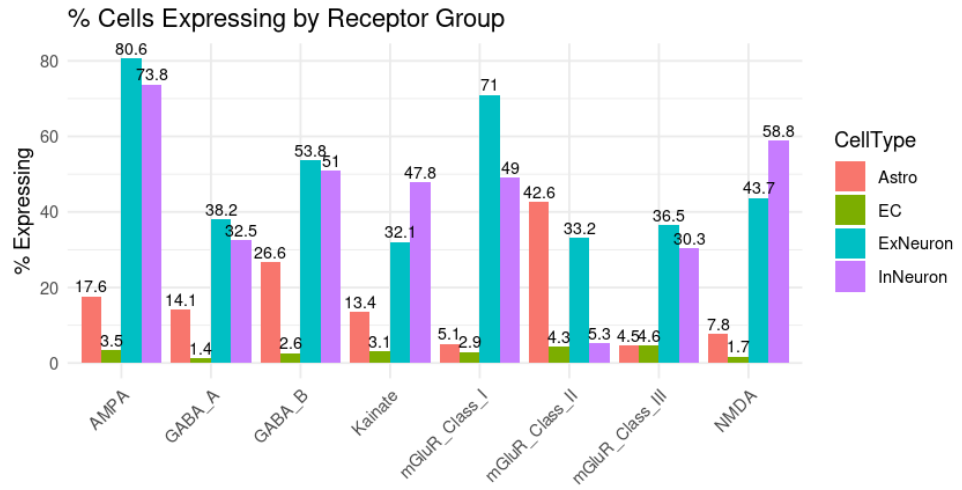

b

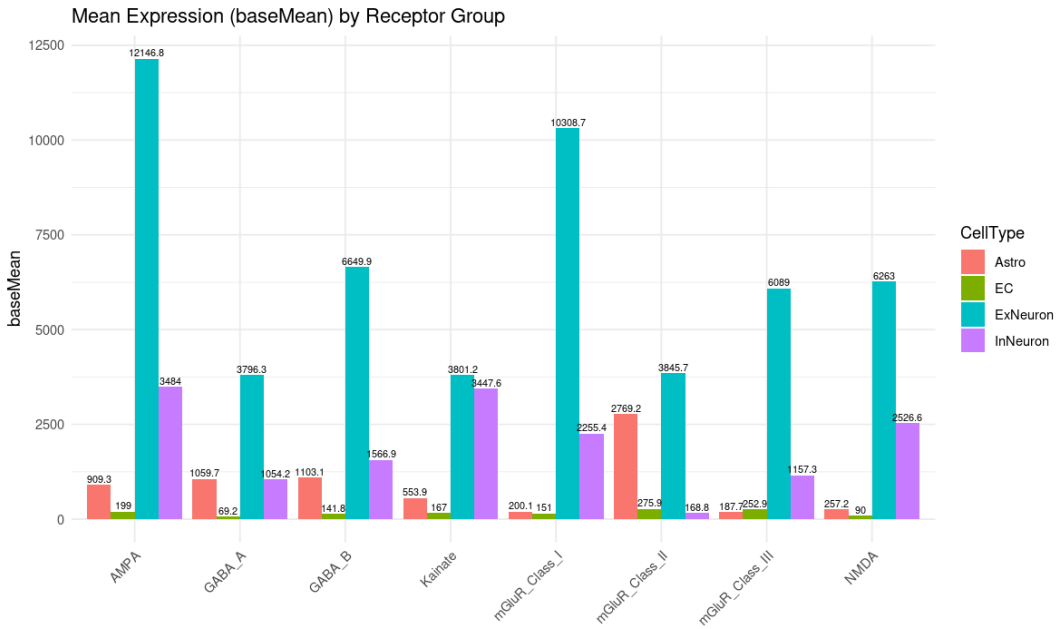

*Figure 35. Cell type-specific percentage of nuclei expressing (**a**) and pseudobulk baseMean expression (**b**) of GABA and glutamate receptor genes.*

baseMean indicates the average of normalised counts across all samples. Genes with negligible or no expression (e.g., GABRP, GABRQ, GABRE, GRIN3B, GRM2, GRM6, and all GABA-C genes) were excluded.

Emerging evidence suggests the role of ‘neuronal’ genes, including GABA and glutamate receptor genes, in endothelial cells. I focused on GABA and glutamate receptors as an exemplar to better understand how hypertension affects these genes in endothelial cells.

Overall, the proportion of EC expressing these genes was low, with a mean percentage expression of 1.52% for GABA receptors and 3.04% for glutamate receptors (Figure 35). Similarly, the pseudobulk baseMean expression levels were 78.89 and 167.02, respectively, where baseMean represents the average of normalised counts across all samples, as calculated by DESeq2. This contrasts with excitatory neurons, which exhibited the highest levels of receptor expression, with 40.23% of cells expressing GABA receptors and 49.02% expressing glutamate receptors, and corresponding baseMean expression levels of 4176.76 and 7042.92, respectively. In inhibitory neurons, 34.94% of cells expressed GABA receptors and 51.13% expressed glutamate receptors, with baseMean expression levels of 1122.54 and 2597.93, respectively. Astrocytes showed lower expression, with 15.80% of cells expressing GABA receptors and 11.94% expressing glutamate receptors, and baseMean expression levels of 1065.49 and 556.29, respectively.

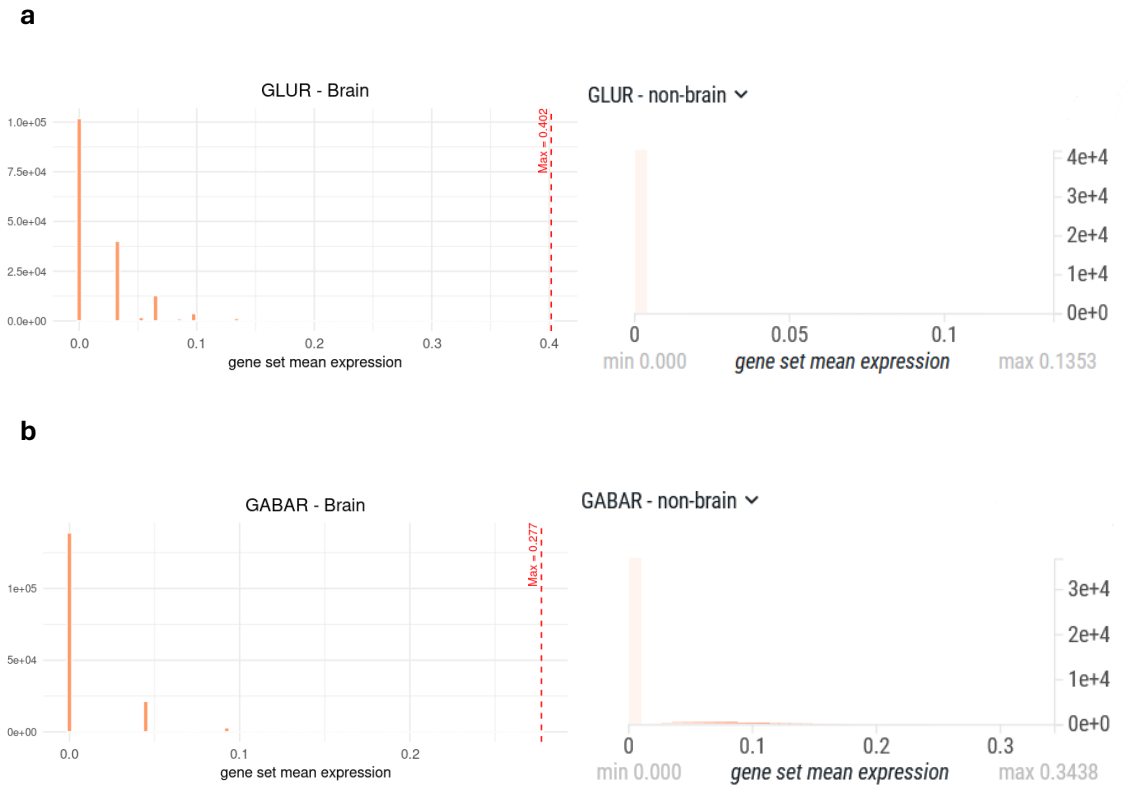

*Figure 36. Distribution of glutamate (**a**) and GABA (**b**) receptor gene expression across individual endothelial cells from brain and non-brain tissues.*

*(**a**) Left panel: Brain endothelial cells; right panel: non-brain endothelial cells. (**b**) Left panel: Brain endothelial cells; right panel: non-brain endothelial cells.*

Each histogram shows the distribution of mean gene set expression per cell. The x-axis indicates the mean expression of the respective receptor gene set in a single cell; the y-axis shows the number of cells with that level of gene set expression. Gene sets consist of known glutamate or GABA receptor genes (excluding those with negligible expression: e.g., GABRP, GABRQ, GABRE, GRIN3B, GRM2, GRM6, and GABA-C genes). Data for brain endothelial cells were generated in this study; data for non-brain endothelial cells were derived from the multi-organ vascular cell atlas published by Barnett et al. (2024).

I also examined glutamate and GABA receptor expression in other non-brain vascular cells from a recently published multi-organ single-cell vascular atlas (Barnett et al., 2024). Non-brain endothelial cells from Barnett et al. (2024) were compared to my own brain EC dataset, rather than to the brain data from their study, to maintain consistency with the core dataset used throughout this thesis and to take advantage of the greater number of nuclei in my samples. Expression of these receptor genes was overall low in both brain and non-brain vascular cells (Figure 36). In the non-brain endothelial cells (a total of

42,510 cells), GABA and glutamate receptor gene expression was extremely low or nearly undetectable at the single-cell level. However, brain endothelial cells exhibited higher levels of gene set expression per nucleus compared to non-brain vascular cells. Hence GABA and glutamate receptor gene expression is a specific feature of brain endothelial cells.

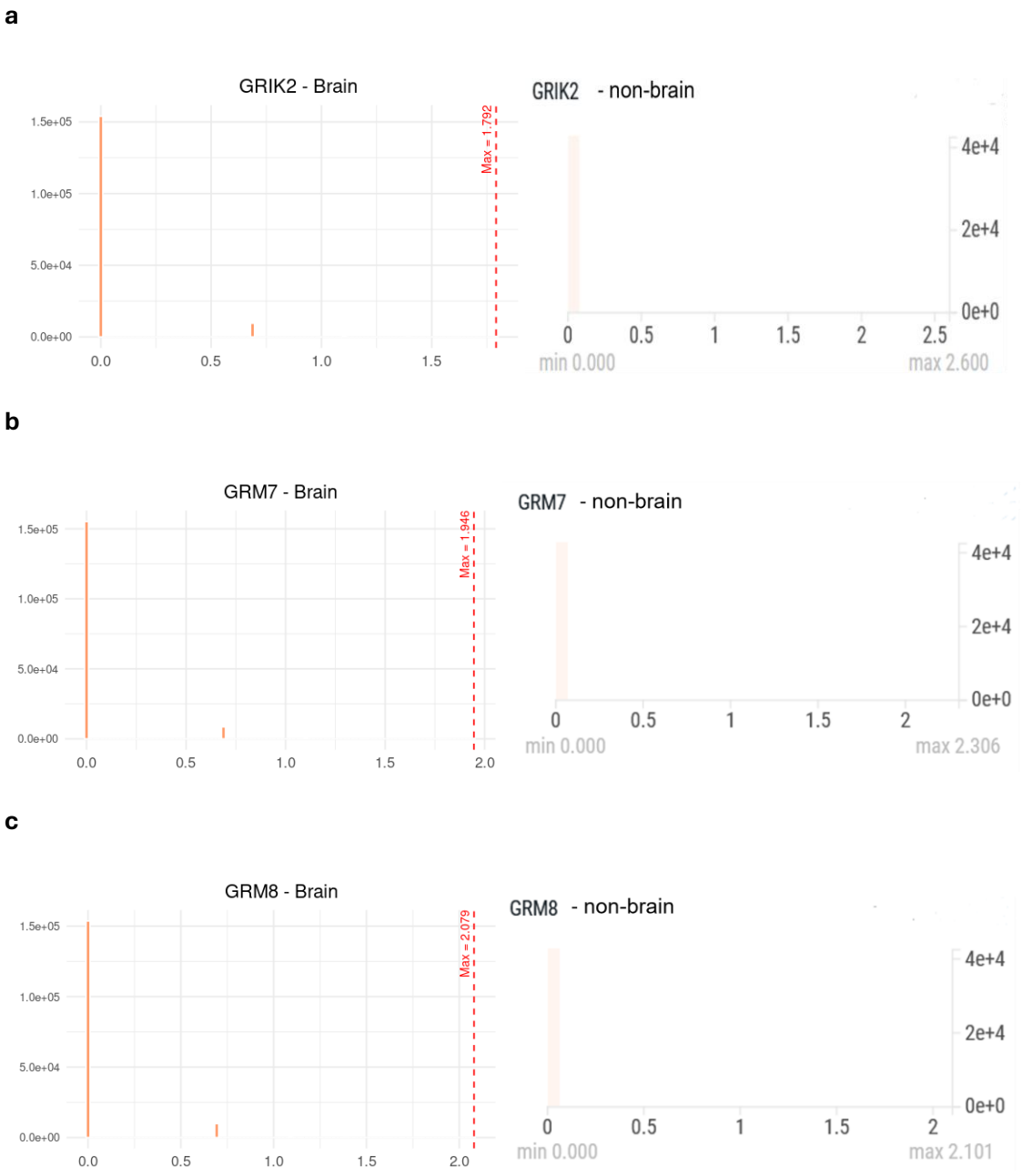

*Figure 37. Distribution of GRIK2 (**a**), GRM7 (**b**), GRM8 (**c**) gene expression across individual endothelial cells from brain and non-brain tissues.*

*(**a**) Left panel: Brain endothelial cells; right panel: non-brain endothelial cells. (**b**) Left panel: Brain endothelial cells; right panel: non-brain endothelial cells. (**c**) Left panel: Brain endothelial cells; right panel: non-brain endothelial cells.*

Each histogram shows the distribution of gene expression per cell. The x-axis indicates the expression of the respective gene in a single cell; the y-axis shows the number of cells with that level of gene expression. Data for brain endothelial cells were generated in this study; data for non-brain endothelial cells were derived from the multi-organ vascular cell atlas published by Barnett et al. (2024).

Table 11. List of dysregulated GABA and glutamate receptor genes in EC DEG analysis in hypertension.

Gene	baseMean	LFC	padj	Regulation	% Expression
GABRA1	16.40	-0.65	0.0018	Downregulated	0.38
GABRA2	64.68	-0.56	0.0046	Downregulated	1.28
GABRA3	64.12	-0.64	0.0022	Downregulated	1.44
GABRA4	23.04	-0.46	0.013	Downregulated	0.49
GABRA5	22.32	-0.69	0.0022	Downregulated	0.50
GABRA6	47.50	-0.53	0.013	Downregulated	0.98
GABRB1	151.95	-0.60	0.0029	Downregulated	2.74
GABRB2	89.18	-0.64	0.0027	Downregulated	1.74
GABRB3	153.31	-0.53	0.0076	Downregulated	2.88
GABRG1	20.04	-0.69	0.0030	Downregulated	0.44
GABRG2	43.88	-0.54	0.0070	Downregulated	0.93
GABRG3	199.42	-0.59	0.0047	Downregulated	3.79
GABRD	3.84	-0.64	0.0069	Downregulated	0.09
GRIN2A	201.33	-0.56	0.0033	Downregulated	3.75
GRIN2B	202.33	-0.64	0.0034	Downregulated	3.80
GRIN2C	12.04	-0.48	0.0193	Downregulated	0.24
GRIN2D	22.28	-0.55	0.0028	Downregulated	0.53
GRIN3A	51.36	-0.57	0.0072	Downregulated	1.12
GRIA1	140.36	-0.65	0.0025	Downregulated	2.65
GRIA2	105.00	-0.49	0.010	Downregulated	1.76
GRIA4	151.62	-0.56	0.0037	Downregulated	2.81
GRIK1	156.61	-0.49	0.0071	Downregulated	3.10
GRIK2	**370.48**	**-0.43**	**0.019**	**Downregulated**	**6.53**
GRIK3	86.26	-0.59	0.0046	Downregulated	1.78
GRIK4	182.73	-0.55	0.0072	Downregulated	3.40
GRIK5	38.72	-0.50	0.0061	Downregulated	0.83
GRM1	118.64	-0.56	0.0056	Downregulated	2.41
GRM5	183.45	-0.55	0.0045	Downregulated	3.46
GRM4	44.32	-0.51	0.012	Downregulated	0.99
GRM7	**321.38**	**-0.61**	**0.0033**	**Downregulated**	**5.80**
GRM8	**392.94**	**-0.34**	**0.030**	**Downregulated**	**7.09**

baseMean, the average of normalised counts across all samples, providing an overall measure of its expression level prior to fold change calculation; LFC, Log_2FoldChange; padj, adjusted p-values.

Genes with over 5% expression in EC were highlighted in bold.

In hypertension compared to control, there was a significant downregulation (adjusted p-value < 0.05) across all these genes in endothelial cells at the pseudobulk level. Specifically, this included ionotropic GABA-A receptors, ionotropic NMDA receptors, ionotropic AMPA receptors, ionotropic kainate receptors, and metabotropic class I and III glutamate receptors were significantly downregulated in hypertensive endothelial cells

(Table 11). *GRIK2, GRM7, GRM8* were more highly expressed in the brain endothelial cell population compared to other glutamate and GABA receptor genes. In the multi-organ single cell atlas, expression of these genes was extremely low or nearly undetectable at the single-cell level in the non-brain endothelial cells, but detectable expression was observed in the brain EC (Figure 37).

While there are no previous studies linking *GRIK2* directly to endothelial function and evidence for a vascular role for *GRM7* and *GRM8* is also limited.

Table 12. The mean expression and expression percentage of GABA and glutamate receptor genes in hypertensive and control EC.

Gene	Mean Expression in HTN EC	Mean Expression in CTRL EC	Mean Expression Difference	% Expression in HTN EC	% Expression in CTRL EC	% Expression Difference
GABRA1	0.81	0.82	**-0.01**	0.31	0.51	**-0.20**
GABRA2	0.84	0.85	**-0.01**	1.10	1.63	**-0.53**
GABRA3	0.70	0.71	**-0.01**	1.16	2.00	**-0.84**
GABRA4	0.80	0.81	**-0.01**	0.43	0.61	**-0.18**
GABRA5	0.70	0.70	**0**	0.42	0.67	**-0.25**
GABRA6	0.70	0.70	**0**	0.84	1.28	**-0.44**
GABRB1	0.92	0.92	**0**	2.38	3.46	**-1.08**
GABRB2	0.87	0.87	**0**	1.48	2.28	**-0.80**
GABRB3	0.89	0.90	**-0.01**	2.48	3.69	**-1.21**
GABRG1	0.70	0.70	**0**	0.37	0.59	**-0.22**
GABRG2	0.82	0.83	**-0.01**	0.82	1.16	**-0.34**
GABRG3	0.88	0.91	**-0.03**	3.26	4.85	**-1.59**
GABRD	0.69	0.69	**0**	0.06	0.15	**-0.09**
GRIN2A	0.90	0.92	**-0.02**	3.23	4.82	**-1.59**
GRIN2B	0.89	0.91	**-0.02**	3.16	5.10	**-1.94**
GRIN2C	0.70	0.70	**0**	0.20	0.31	**-0.11**
GRIN2D	0.70	0.70	**0**	0.46	0.68	**-0.22**
GRIN3A	0.70	0.70	**0**	0.96	1.43	**-0.47**
GRIA1	0.88	0.90	**-0.02**	2.25	3.47	**-1.22**
GRIA2	0.92	0.95	**-0.03**	1.55	2.18	**-0.63**
GRIA4	0.90	0.91	**-0.01**	2.42	3.59	**-1.17**
GRIK1	0.83	0.84	**-0.01**	2.75	3.80	**-1.05**
GRIK2	0.93	0.95	**-0.02**	5.83	7.98	**-2.15**
GRIK3	0.83	0.83	**0**	1.49	2.39	**-0.90**
GRIK4	0.88	0.89	**-0.01**	2.87	4.48	**-1.61**
GRIK5	0.80	0.82	**-0.02**	0.74	1.03	**-0.29**
GRM1	0.84	0.84	**0**	2.08	3.10	**-1.02**
GRM5	0.90	0.91	**-0.01**	2.99	4.42	**-1.43**
GRM4	0.70	0.71	**-0.01**	0.83	1.31	**-0.48**
GRM7	0.91	0.92	**-0.01**	4.94	7.58	**-2.64**
GRM8	0.88	0.89	**-0.01**	6.46	8.37	**-1.91**

The mean expression for nuclei where the gene was expressed (a gene was considered expressed in a nucleus if its count > 0). "Mean Expression Difference" was calculated as the mean expression in HTN EC minus the mean expression in CTRL EC. "% Expression Difference" was calculated as the expression percentage in HTN EC minus the expression percentage in CTRL EC.

Genes with over 5% expression in EC were highlighted in bold.

On examining whether hypertension is associated with a change in mean expression at the single-cell level or a change in the percentage of nuclei expressing the gene, I found

the percentage of nuclei expressing genes was reduced in hypertensive endothelial cells (Table 12).

Evaluation of gene expression of GABA and glutamate receptor subtypes indicates that a subset of endothelial cells express these genes in control donors, and that only certain receptor subtypes are expressed at levels likely to be biologically meaningful. This may suggest that that some brain endothelial cells have undergone specialisation. The reduction in the proportion of endothelial cells expressing these genes in hypertension, rather than a decrease in mean expression at the single-cell level, may imply a reduction in the proportion of such specialised endothelial subpopulations. However, this interpretation should be made with caution given the stochastic nature of gene expression at the single-cell level.

a

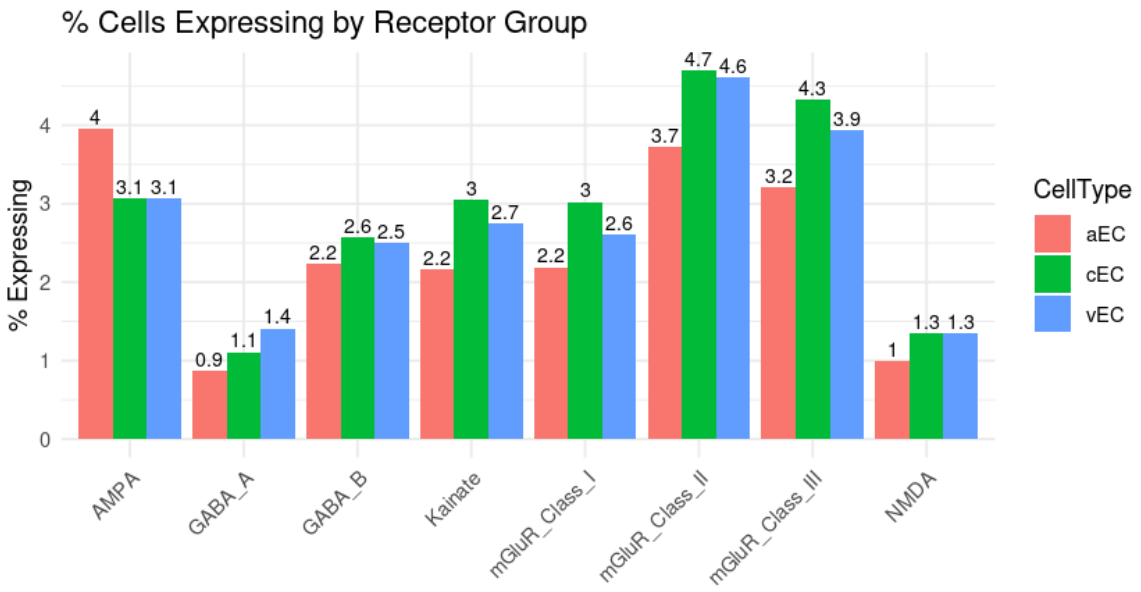

b

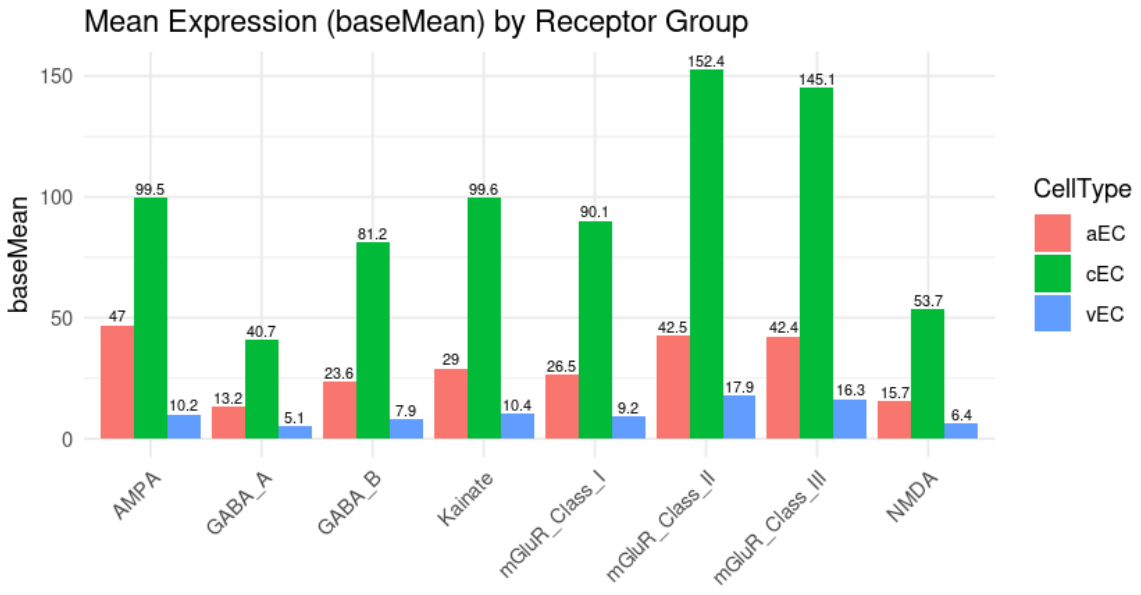

*Figure 38. EC subtype-specific percentage of nuclei expressing (**a**) and pseudobulk baseMean expression (**b**) of GABA and glutamate receptor genes.*

baseMean, the average of normalised counts across all samples. Genes with negligible or no expression (e.g., GABRP, GABRQ, GABRE, GRIN3B, GRM2, GRM6, and all GABA-C genes) were excluded.

The mean percentage of nuclei expressing GABA receptors was 1.30% in cEC, 1.61% in vEC, and 1.07% in aEC, while for glutamate receptors, the values were 2.82% in cEC, 2.72% in vEC, and 2.40% in aEC (Figure 38). These data suggest a consistent but low level of receptor expression across EC subtypes. Interestingly, while the proportion of expressing nuclei was similar across subtypes, pseudobulk baseMean expression levels were markedly higher in capillary EC, reaching 46.12 for GABA receptors and 94.57 for glutamate receptors. In contrast, vEC exhibited lower expression (GABA: 5.63, Glutamate: 10.49), and aEC showed intermediate levels (GABA: 14.70, Glutamate: 30.95). The class II and class III metabotropic glutamate receptors were the most expressed subgroup of glutamate receptors in terms of the highest proportion of endothelial nuclei expressing and the highest levels of expression. The class II and class III metabotropic glutamate receptors are G-protein-coupled receptors that primarily couple to Gi/o proteins, resulting in the inhibition of adenylyl cyclase, activation of potassium channels, and inhibition of voltage-gated calcium channels (Niswender & Conn, 2010). This may suggest that capillary EC may be positioned to respond to glutamate from adjacent neuronal activity to alter endothelial function.

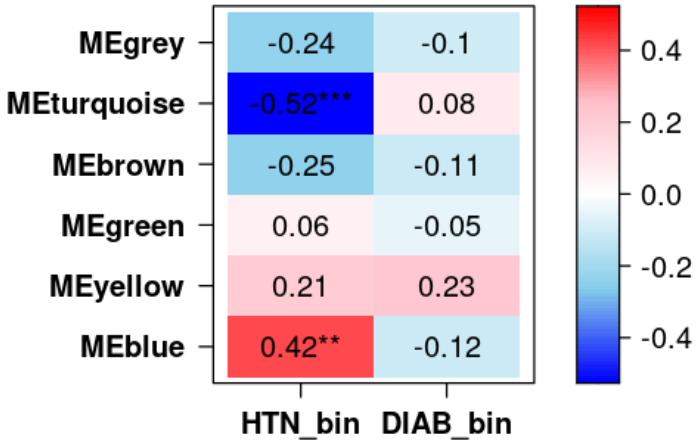

Figure 39. Heatmap of module-trait correlation with hypertension and diabetes in the combined EC dataset.

*The heatmap showed the correlation between gene co-expression modules and traits (hypertension and diabetes) in endothelial cells. Each row represents a gene co-expression module, and each column corresponds to trait. The colour scale represents Pearson correlation coefficients, ranging from -1 (labelled in blue, negative correlation) to +1 (labelled in red, positive correlation). Asterisks indicate statistical significance levels based on p-values from Pearson correlation tests: * ($p < 0.05$), ** ($p < 0.01$), and *** ($p < 0.001$).*

To help understand the pervasive reduction in neuronal/synaptic genes, I next examined gene co-expression networks. WGCNA was performed on the combined EC dataset, including both hypertension and non-hypertensive control samples, resulting in 5 co-expression modules (Table 13). The module-trait correlation analysis revealed that two modules (turquoise and blue) were significantly correlated with hypertension (Figure 39). As expected, no modules showed a significant correlation with diabetes, aligning with the findings from the previous chapter.

GO analysis was performed to infer the biological function of the modules, focusing on biological process (BP) GO terms (Figure 40). The blue module, which was positively correlated with hypertension, showed a significant enrichment in myelin-related GO terms. Traditionally, endothelial cells are not associated with myelination, suggesting that these myelin genes may be involved in alternative biological processes rather than myelination.

Interestingly, the turquoise module, which represents the neuronal gene network with the largest number of genes (3,749 genes), showed a strong negative correlation with hypertension.

Table 13. The number of genes and the hub gene in each module across the combined EC dataset (include both hypertensive and control samples), in the hypertensive EC dataset, and in the control EC dataset.

	Black	Blue	Brown	Green	Red	Turquoise	Yellow
EC - Combined	NA	298	158	23	NA	3,749	99
	NA	*NCAM1*	*TNS3*	*DNAJB1*	NA	*DCC*	*HERC6*
EC - HTN	108	1,230	578	388	146	2,697	446
	HERC6	*NAP1L1*	*PLPPR4*	*TNS3*	*SNAP23*	*DCC*	*CSDE1*
EC - CTRL	NA	880	647	NA	NA	3,211	240
	NA	*SEC24B*	*KIF1A*	NA	NA	*GALNTL6*	*MFN1*

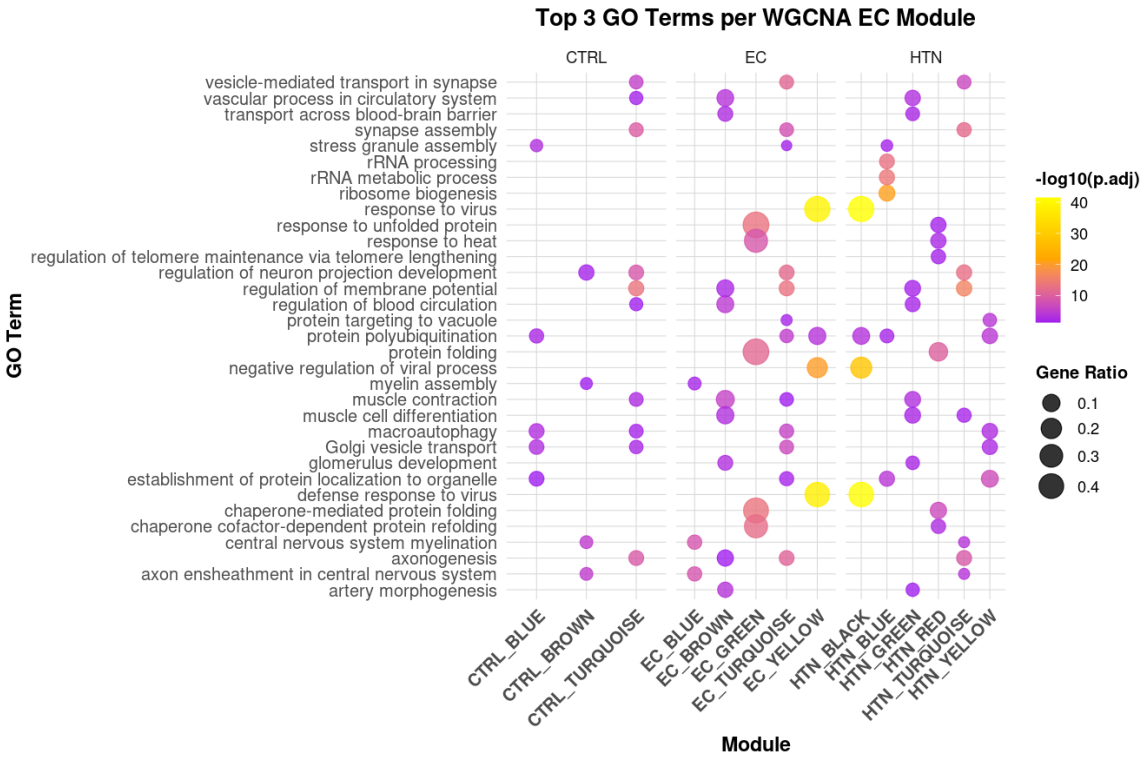

Figure 40. Dot plot of functional profiles for genes in each module from WGCNA in the EC datasets.

The dot plot was divided into three panels: the left panel corresponds to the CTRL EC dataset, the middle panel represents the combined EC dataset (including both hypertension and non-hypertensive control samples), and the right panel shows results from the HTN EC dataset. The dot size represents the gene ratio (proportion of module genes associated with each GO term), and the colour scale indicates -log10(adjusted p-value).

To investigate how neuronal gene networks were altered in hypertensive endothelial cells, I further performed WGCNA separately on the hypertensive endothelial cells and non-hypertensive control endothelial cells, resulting in 7 modules in the HTN EC dataset and 4 modules in the CTRL EC dataset (Table 13). Among the identified modules, the turquoise modules emerged as the module of interest in both the control and hypertension datasets (Figure 40). Additionally, I found *rRNA metabolic process* and *ribosome biogenesis* were unique to the hypertension-specific modules. This may suggest an alteration in ribosomal function and protein synthesis in endothelial cells, which might indicate stress responses in hypertension.

Table 14. Network connectivity in the turquoise modules of HTN EC and CTRL EC.

Weight Cutoff	*# of Genes in HTN EC*	*# of Genes in CTRL EC*	*# of Edges in HTN EC*	*# of Edges in CTRL EC*	*Mean # of Edges per Gene in HTN EC*	*Mean # of Edges per Gene in CTRL EC*
0.52	0	691	0	10,253	0.0	14.8
0.48	155	1,100	157	59,527	1.0	54.1
0.44	596	1,321	5,943	155,131	10.0	117.4
0.40	851	1,510	33,812	292,040	39.7	193.4

The 'Mean # of Edges per Gene' was calculated by dividing the total number of edges by the total number of genes at each weight cut-off.

I analysed the connectivity of genes within the turquoise modules, the module of interest containing neuronal genes, by examining the number of genes, edges (i.e. connections), and mean connection per gene at different weight cut-offs (Table 14). A significant loss of network connectivity in hypertension was observed, with the maximum weight value being 0.504 in the hypertension turquoise module and 0.535 in the control turquoise module. This weaker 'neuronal' network connectivity in hypertension aligns with the results from DEG analysis and provides evidence that the downregulation of 'neuronal' genes was not purely an isolated transcriptional change but was also accompanied by a collapse in 'neuronal' co-expression networks and the associated regulatory factors.

a

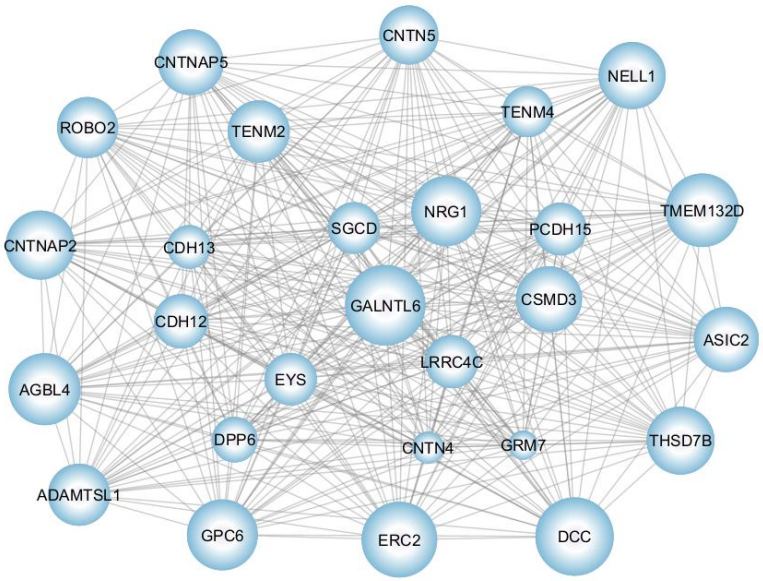

b

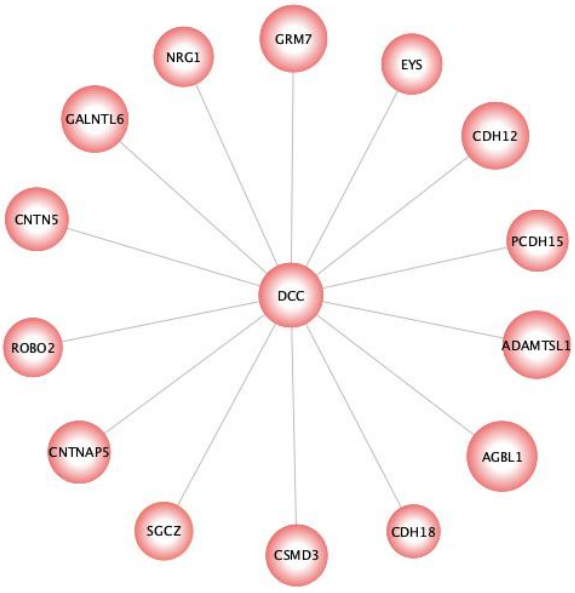

*Figure 41. The hub network in the EC CTRL turquoise (**a**) and the HTN turquoise (**b**) module.*

*(**a**) Edges with weights above 0.48 from TOM were included. Nodes represent genes with a minimum of 300 edges with at least 5% expression in endothelial cells. The size of each node was proportional to the number of edges, reflecting its connectivity within the network. Downregulated DEGs in hypertension were labelled in blue colour.*

*(**b**) Edges with weights above 0.48 from TOM were included. Nodes represent genes with at least 5% expression in endothelial cells. The size of each node was proportional to |LFC| value from the DEG analysis. Downregulated DEGs in hypertension were labelled in red colour.*

To investigate key genes in the ‘neuronal’ gene networks, I visualised the hub gene networks in the CTRL and HTN turquoise modules. To ensure only strong co-expression relationships and key hub genes were visualised in the control turquoise module, I included edges with weights above 0.48 and nodes with a minimum of 300 edges and at least 5% expression in EC (Figure 41a). The size of each node was proportional to the number of edges to reflect the connectivity within the network. Interestingly, the key hub genes (27 genes total) were all identified as downregulated genes in hypertension from the DEG analysis and these genes were all positively correlated with each other. *GALNTL6* was the most connected hub gene and the other hub genes can be grouped into cell adhesion genes (*CNTNAP2, CNTNAP5, CNTN4, CNTN5, CDH12, CDH13, PCDH15*), ECM genes (*NELL1*, *GPC6*, *ADAMTSL1*), axon guidance and neuronal genes (*ROBO2, TENM2, TENM4, DCC, GRM7*, *ASIC2*, *DPP6*, *LRRC4C, TMEM132D, NRG1, ERC2*).

Surprisingly, only the *DCC*-centred network remained in the hypertension turquoise module, and 15 hub genes were all downregulated DEGs in hypertension from the DEG analysis and these hub genes were all positively correlated with each other (Figure 41b). *GALANTL6* was also present but it lost its central network position. Other hub genes that were retained included cell adhesion (*CNTNAP5, CNTN5, CDH12, PCDH15*), the ECM (*ADAMTSL1*) and neuronal genes (*DCC, GRM7, ROBO2, NRG1*).

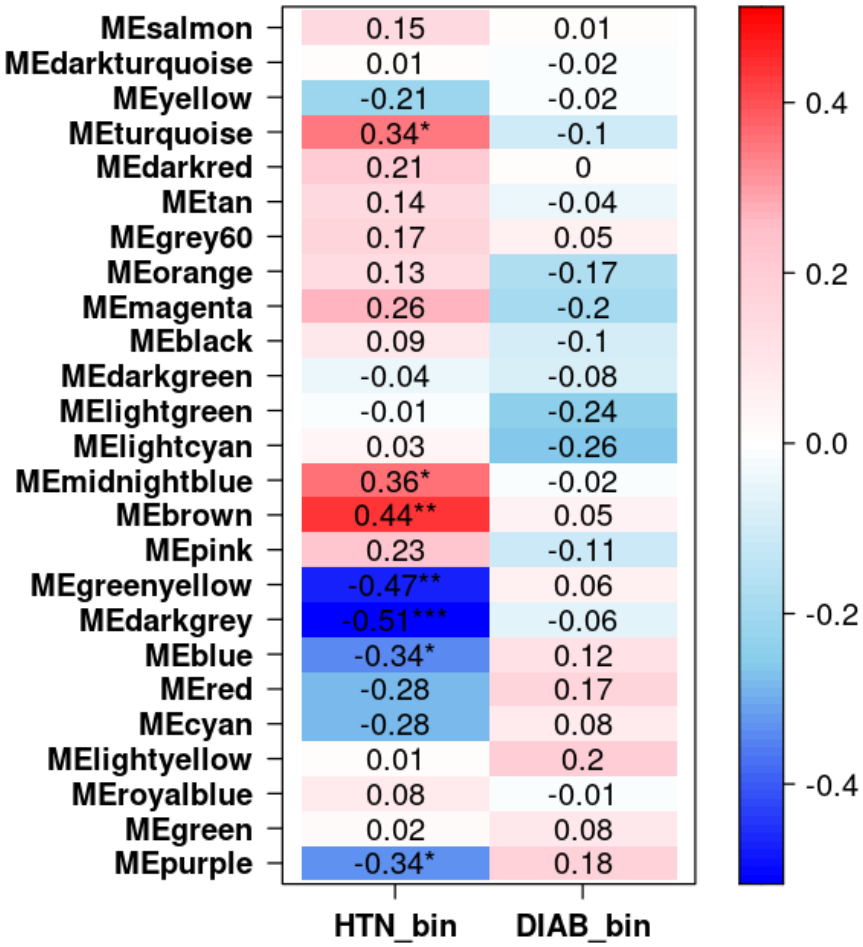

Figure 42. Heatmap of module-trait correlation with hypertension and diabetes in the Astro dataset.

*The heatmap showed the correlation between gene co-expression modules and traits (hypertension and diabetes) in astrocytes. Each row represents a gene co-expression module, and each column corresponds to traits. The colour scale represents Pearson correlation coefficients, ranging from -1 (labelled in blue, negative correlation) to +1 (labelled in red, positive correlation). Asterisks indicate statistical significance levels based on p-values from Pearson correlation tests: * ($p < 0.05$), ** ($p < 0.01$), and *** ($p < 0.001$).*

In the previous chapter, cell-type-specific gene dysregulation was identified in astrocytes and vascular smooth muscle cells in addition to EC. Hence, I examined GCNs in astrocytes and vascular smooth muscle cells. 25 modules were identified in the astrocytes dataset, a greater number than observed in endothelial cells (Table S 8). This may indicate the higher transcriptional heterogeneity of astrocytes and a broader range of biological functions. I further investigated the correlations between modules and traits. As expected, no modules were significantly correlated with diabetes (Figure 42). But three

modules (turquoise, midnightblue, brown) were positively correlated with hypertension and four modules (greenyellow, darkgrey, blue, purple) exhibited negative correlations with hypertension.

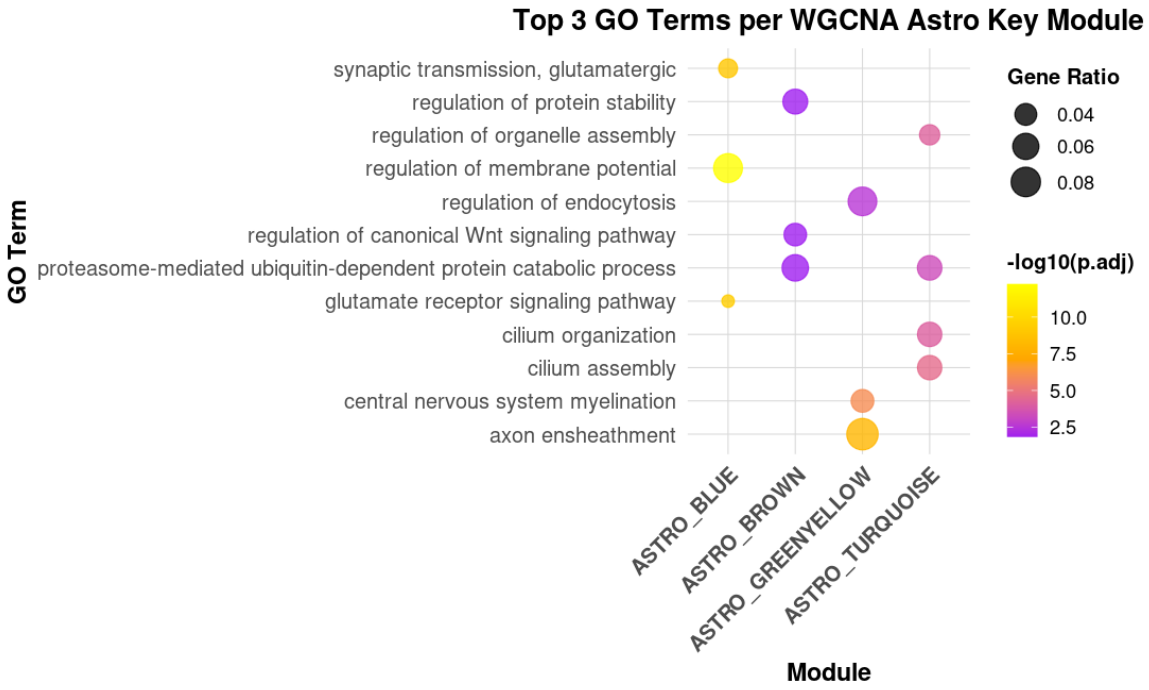

Figure 43. Dot plot of functional profiles for genes in each module from WGCNA in the Astro dataset.

The dot size represents the gene ratio (proportion of module genes associated with each GO term), and the colour scale indicates -log10(adjusted p-value).

Four modules showed significantly enriched GO terms, no GO terms were identified from the midnightblue (80 genes), darkgrey (26 genes), and purple (175 genes) modules (Figure 43). This may be due to these module genes with limited functional annotations in GO BP databases or the small gene set size of the modules. Interestingly, two positively correlated modules: the turquoise module, enriched for cilium and organelle assembly, and the brown module, enriched for protein catabolic processes and Wnt signalling; two negatively correlated modules: the greenyellow module, enriched for myelination-related processes, and the blue module, enriched for glutamate signalling and synaptic transmission, mirroring the turquoise ‘neuronal’ module detected in endothelial cells. Although the EC blue and astrocyte greenyellow myelination modules contained 170 and 298 genes respectively, only 35 genes were shared between them.

a

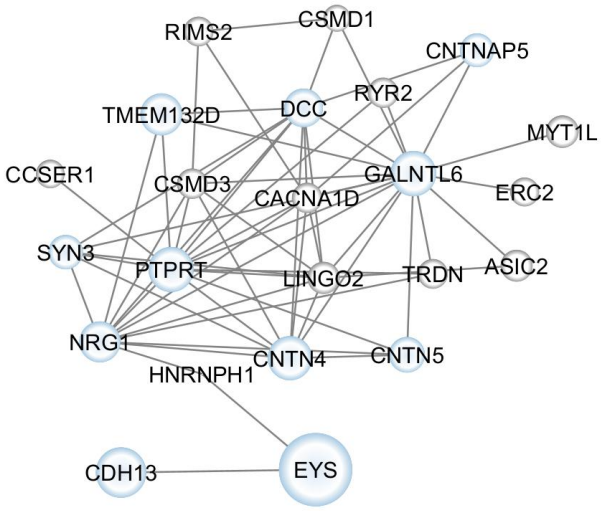

b

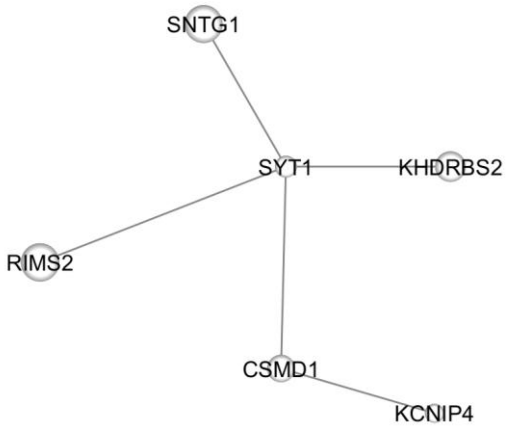

*Figure 44. The hub network in the Astro CTRL blue (**a**) and the HTN red (**b**) module.*

Edges with weights above 0.30 from TOM were included. Nodes represent genes with at least 5% expression in astrocytes. The size of each node was proportional to |LFC| value from the DEG analysis. Downregulated DEGs in hypertension were labelled in blue colour, and non-significant genes were labelled in dark grey.

To investigate how 'neuronal' gene networks were altered in hypertensive astrocytes, I further performed WGCNA separately on the hypertensive astrocytes and non-

hypertensive control astrocytes, resulting in 28 modules in the HTN Astro dataset and 26 modules in the CTRL Astro dataset (Table S 8). Among the identified modules, the red module from the HTN Astro dataset and the blue module from the CTRL Astro emerged as the modules of interest, enriched in synaptic-related pathways (Figure S 27).

The maximum weight in astrocyte networks didn't exceed 0.40, indicating overall weaker co-expression relationships in astrocytes (Figure 44). I extracted hub gene networks using a weight cut-off of 0.30. To ensure biological relevance, I applied the 5% expression cut-off, resulting in 23 genes in the Astro CTRL blue module and only 6 genes in the HTN red module. In the CTRL module, 11 out of 23 hub genes were downregulated DEGs in hypertension and the gene networks hugely overlapped with the EC 'neuronal' gene networks. Notably, the hub genes from the Astro HTN module, which were all non-significant genes in hypertension, were distinct from the Astro CTRL and also EC 'neuronal' modules. As with the EC network, the astrocyte network shows a large gene network collapse in hypertension astrocytes.

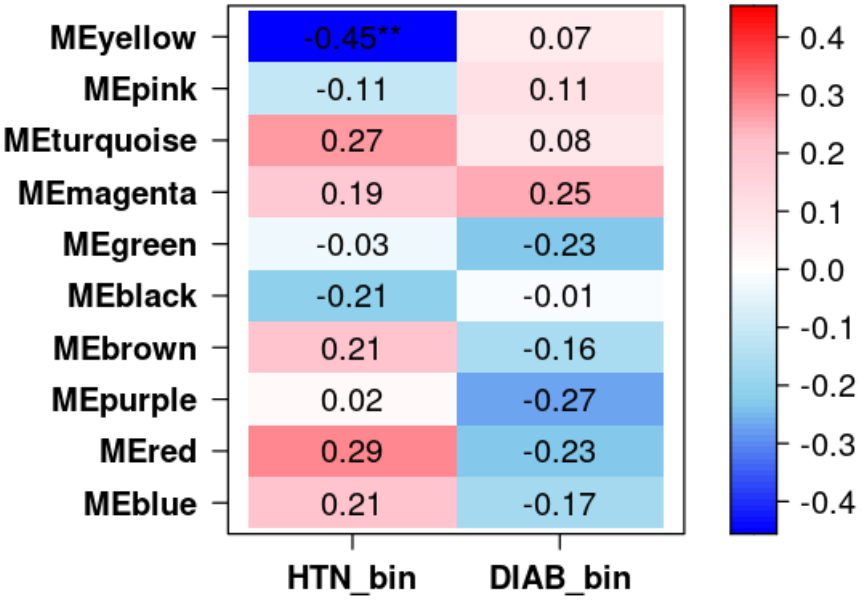

Figure 45. Heatmap of module-trait correlation with hypertension and diabetes in the SMC dataset.

*The heatmap showed the correlation between gene co-expression modules and traits (hypertension and diabetes) in vascular smooth muscle cells. Each row represents a gene co-expression module, and each column corresponds to traits. The colour scale represents Pearson correlation coefficients, ranging from -1 (labelled in blue, negative correlation) to +1 (labelled in red, positive correlation). Asterisks indicate statistical significance levels based on p-values from Pearson correlation tests: * ($p < 0.05$), ** ($p < 0.01$), and *** ($p < 0.001$).*

In the vascular smooth muscle cells dataset, 10 modules were identified (Table S 9). Interestingly, from the module-trait correlation analysis, only one module (yellow, 449 genes) exhibited a significant negative correlation with hypertension (Figure 45). As expected, there were no significant correlations identified in diabetes.

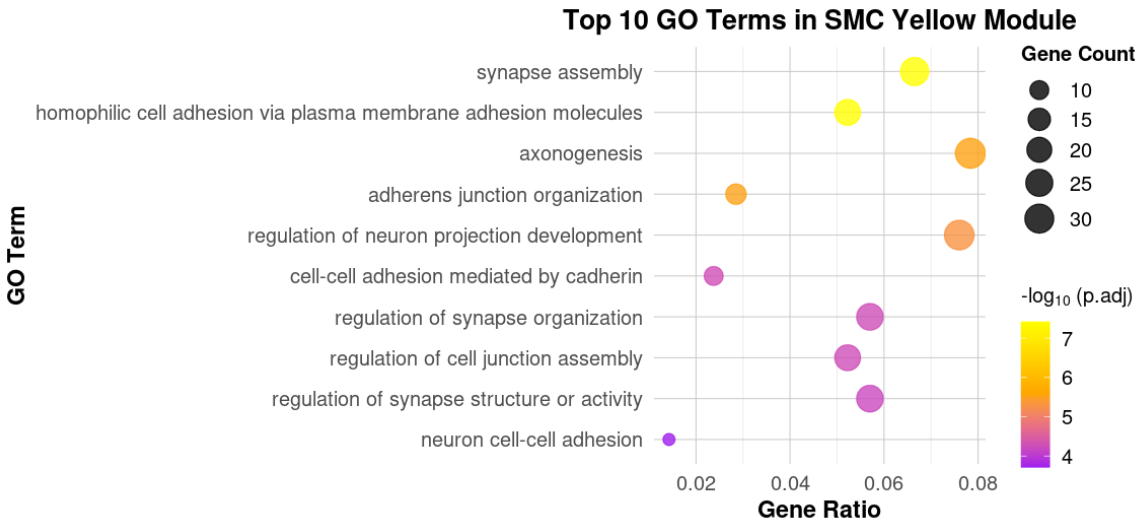

Figure 46. Dot plot of top 10 GO terms in the SMC yellow module.

The x-axis indicates the Gene Ratio, representing the proportion of genes in the module associated with each GO term. The dot size corresponds to the number of genes (Gene Count) mapped to each term. The colour scale represents -log₁₀(adjusted p-value).

Interestingly, enriched GO terms in the SMC yellow module overlapped with those enriched in the EC turquoise module, including cell adhesion and axon/synaptic-related pathways (Figure 46). This suggests a shared gene network regulatory mechanism between endothelial cells and smooth muscle cells.

a

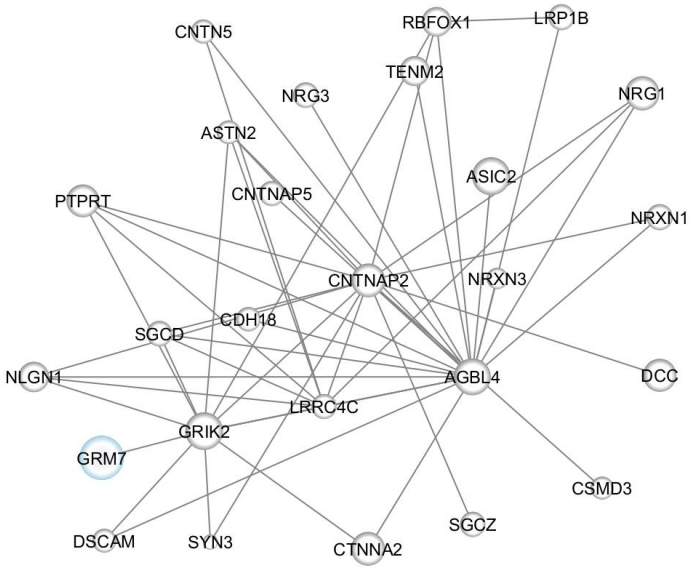

b

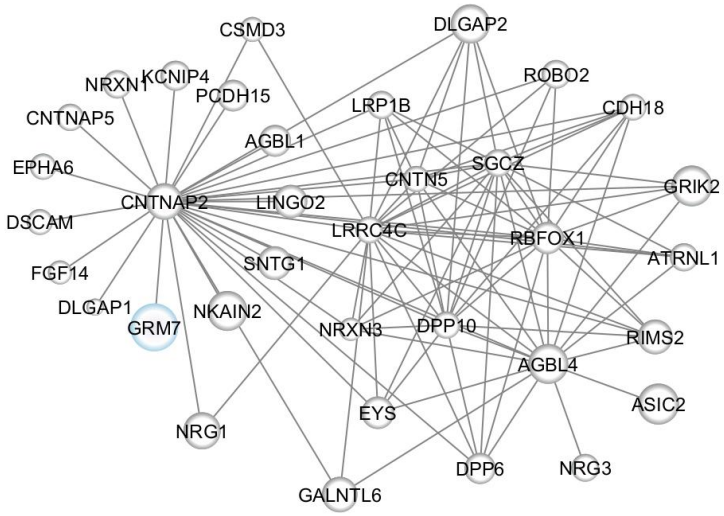

*Figure 47. The hub network in the SMC CTRL brown (**a**) and the HTN brown (**b**) module.*

Edges with weights above 0.40 from TOM were included. Nodes represent genes with at least 5% expression in smooth muscle cells. The size of each node was proportional to |LFC| value from the DEG analysis. Downregulated DEGs in hypertension were labelled in blue colour, and non-significant genes were labelled in dark grey.

Examining hypertension and control donors separately, identified 11 modules in the HTN SMC dataset and 8 modules in the CTRL SMC dataset (Table S 9). Among the identified modules, the brown modules from the HTN SMC dataset and the CTRL SMC emerged as the modules of interest, enriched in cell adhesion and synaptic-related pathways (Figure S 30). Interestingly, a *CNTNAP2*-centred hub gene networks were identified in both modules and the hub genes were overlapped with those in the EC turquoise module, further confirming the shared mechanism between EC and SMC.

I extracted the hub gene networks, including edges that passed a 0.40 weight cut-off and nodes with at least 5% expression. An equal similar number of nodes, 26 and 35 genes respectively, were present in this module from both control and hypertension, contrasting with core network collapse present in EC and Astrocytes. Only one DEG, *GRM7* was present in this network (Figure 47). However, the total number of genes belonging to the ‘neuronal’ modules differed substantially: 333 genes in the HTN module and 622 genes in the CTRL module.

Table 15. List of top 10 influential TFs distinguishing HTN cEC and CTRL cEC.

Rank	**TF**
1	*MBL2*
2	*PHF21A*
3	*TBX1*
4	*YBX3*
5	*OVOL3*
6	*RFX7*
7	*TBPL1*
8	*NR2F2*
9	*DLX6*
10	*TRIM22*

TFs were ranked by their importance scores derived from the random forest model trained to classify cEC as HTN (labelled as 1) or CTRL (labelled as 0).

Next, I performed transcription factor inference analysis to identify candidate TF genes that may be mediating the molecular changes observed in hypertensive capillary endothelial cells (which is the key cell type in the EC populations), and ranked the top 10 influential TF genes based on the importance scores derived from the random forest model (Table 15).

First, I examined their presence within the EC modules from WGCNA, which can allow for the identification of potential TFs that may play central regulatory roles within co-expression networks. In the combined EC dataset, *PHF21A* and *RFX7* were found in the turquoise module, *TBPL1* in the blue module, and *NR2F2* in the brown module. In the HTN EC dataset, *YBX3* was found in the blue module and *NR2F2* in the green module. In the CTRL EC dataset, *PHF21A* was found in the turquoise module, *TBPL1* in the brown module, and *NR2F2* in the brown module.

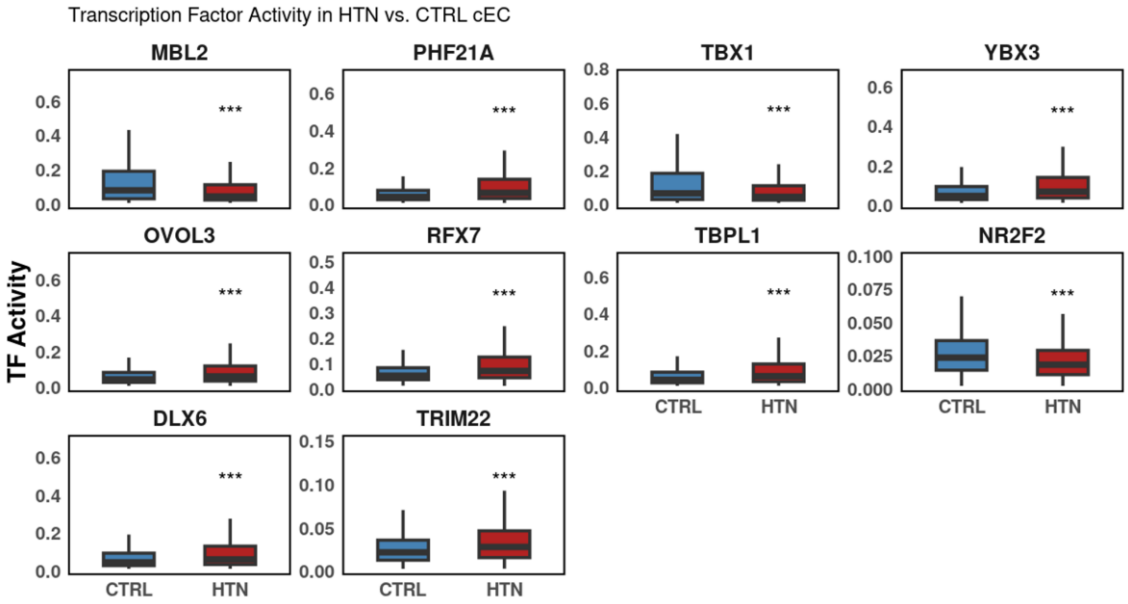

Figure 48. The activity of the most influential TFs in HTN and CTRL cEC.

*Boxplots represent the activity of the most influential transcription factors in HTN and CTRL cEC. Red represents HTN cEC and blue represents CTRL cEC. A t-test was performed to determine whether there was a significant difference between conditions (*** indicates p < 0.001, ** indicates 0.001 < p < 0.01, * indicates 0.01 < p < 0.05, n.s. indicates not significant).*

Then, I assessed the activity values of TFs in two conditions. It was shown that *MBL2, TBX1, NR2F2* were significantly reduced while *PHF21A, YBX3, OVOL3, RFX7, TBPL1, DLX6, TRIM22* showed significantly increased activity in hypertension (Figure 48).

Discussion

I found broad classes of GABA and glutamate receptor genes were all significantly downregulated in hypertensive endothelial cells. *GRIK2, GRM7, GRM8* were the most expressed whilst the other genes were minimally expressed. There is limited literature exploring the role of *GRIK2, GRM7, GRM8* in vascular biology. However, one study reported that *GRM7* and *GRM8* may be involved in the regulation of vascular calcification. *GRM7* and *GRM8* were identified as upregulated genes in the regression phase, which is a reversible window during which the vascular system begins to recover from vascular calcification (Jiang et al., 2013). In my study, the downregulation of *GRM7* and *GRM8* in hypertension was observed, suggesting a possible disruption of this protective mechanism. While these specific genes remain underexplored, a few studies have investigated the role of other glutamate receptor family members in vascular function. For example, loss of *GRM1* function reduced tumour-induced angiogenesis in murine models, highlighting a novel pro-angiogenic role of *GRM1* (Speyer et al., 2014). *GRIN2D* has been identified as a tumour-specific endothelial marker in colorectal cancer, playing a crucial role in angiogenesis and vascularisation (Ferguson et al., 2016). This may suggest a loss of glutamate receptor functions can lead to reduced angiogenesis in hypertension. Glutamate and GABA receptors have also been proposed to have a role in neurovascular coupling: endothelial Ca^{2+} waves were found to be evoked by synaptic activity (synaptically released glutamate and GABA), subsequently leading to vasodilation via nitric oxide production and the activation of calcium-activated potassium channels (Moccia et al., 2023).

Collectively, this may suggest a loss of glutamate and GABA receptor functions can lead to reduced angiogenesis and impaired neurovascular coupling. Whilst expression levels may be lower than in neurons, this does not preclude an important functional role in EC, which is supported by endothelial cell-specific knock-out studies of these genes. Several

studies have reported impaired angiogenesis and neurovascular coupling in hypertension. Impaired angiogenesis relates to a process known as microvascular rarefaction, where there is a reduced density of microvessels in various organs in hypertension which may in turn relate to reduced pro-angiogenic factor activity (Sane et al., 2004). For example, a study examined 82 hypertensive patients and 34 normotensive healthy individuals, and quantified the serum levels of angiogenic mediators using a combination of enzyme-linked immunosorbent assay (ELISA) and flow cytometry-based Cytometric Bead Array (CBA) techniques. Hypertensive patients showed an imbalance between pro- and anti-angiogenic factors, with increased serum endostatin, a known anti-angiogenic factor, and reduced angiogenin and basic fibroblast growth factor, indicating a systemic suppression of angiogenesis (Marek-Trzonkowska et al., 2015). A mouse model of systolic hypertension and atherosclerosis has shown that elevated blood pressure imposes chronic hemodynamic stress on cerebral vessels, initiating a cascade of cerebrovascular injury and NVU impairment, which can ultimately lead to cognitive decline, BBB leakage, and microvascular rarefaction (de Montgolfier et al., 2019). Based on my findings, the role of endothelial metabotropic glutamate receptors in impaired angiogenesis and neurovascular impairment merits further study.

The significant downregulation of these genes appeared to be related to a reduction in the number of cells expressing the gene rather than a reduction in the mean expression per cell. This might imply a loss of a unique cell population or a cell state due to hypertension. For example, hypertension may induce a de-differentiation of vascular smooth muscle cells, in which highly specialised contractile cells lose their phenotype and adopt a proliferative, migratory, and inflammatory state (Touyz et al., 2018). However, the UMAP plot of cells expressing these receptors was not a unique cluster. Instead, expression was dispersed across the whole EC cluster with capillary endothelial cells exhibiting the higher average expression levels. This suggests that there is no separate transcriptomic identity

of brain endothelial cells expressing these genes. Instead, it appears more likely that the reduced number of cells expression is a reflection of the stochastic nature of gene expression and its detection using single-cell methods.

It's interesting that glutamate and GABA receptors appear to be unique to brain endothelial cells, as no detectable expression was observed in the non-brain endothelial cell dataset (Barnett et al., 2024). However, it is important to note that the non-brain EC dataset used for comparison was generated using a different vascular extraction protocol and applied different thresholds during raw count processing, which may influence the detection of lowly expressed transcripts. Despite these methodological differences, the study did detect glutamate receptors, including *GRIK2, GRM7* and *GRM8* in brain EC but not in non-brain EC supports brain EC specialised to use these receptors. This should be examined more comprehensively in a future study, performing a single-cell RNA sequencing analysis of both brain and non-brain vasculature using a unified dissociation protocol and standardised preprocessing pipeline. This would enable a direct and quantitative comparison of glutamate and GABA receptor gene expression.

GCNs provide a means to understand cell type specific functions. Investigation of GCNs across EC, SMC and astrocytes revealed each cell type had different numbers of modules and module sizes. EC had the fewest whilst astrocytes had the most, which may relate to the highly diverse functions of astrocytes. However, the maximum topological overlap (TOM) weight in astrocytes was 0.36, with only 134 gene pairs exceeding the 0.3 threshold, while endothelial cells exhibited a higher maximum TOM weight of 0.54 with 344,714 gene pairs exceeding the 0.4 threshold, and vascular smooth muscle cells had a maximum TOM weight of 0.46 with 916 gene pairs exceeding the 0.4 threshold. This indicates an overall weaker co-expression relationship of networks in astrocytes but very

tight co-regulation in EC. Modules related to protein homeostasis and neuron/synapse pathways were identified across all three cell types.

Several modules in each cell type were significantly correlated with hypertension. In the vascular smooth muscle cells among the 10 identified modules, only one module (the 'synaptic' module) exhibited a significant negative correlation with hypertension. In EC, 2 of 5 modules were correlated, whilst in astrocytes, 7 out of 25 modules were correlated. This collectively underscores the importance of these cell types in hypertension-related effects on the brain. It also highlights the relevant functional processes involved.

Among the significantly correlated modules, the EC blue module, which was positively correlated with hypertension, showed significant enrichment in myelin-related GO terms. Traditionally, endothelial cells are not associated with myelination, suggesting that these myelin genes may be involved in alternative biological processes rather than myelination. Also, there was a possibility that this was merely a byproduct of signalling from the local environment. Further investigation is needed to determine the role of myelin genes in endothelial cells.

It was interesting that EC, astrocytes, and SMC from control donors, all had a 'synaptic' module GCN, with some genes being in common between the cell types. EC in particular had a very large 'synaptic' module with several thousand genes. There was also substantial overlap in hub genes. For example, *ASIC2, CNTN5, CNTNAP5, CSMD3, DCC, NRG1* were commonly identified across all three cell types; both EC and astrocytes contained key hub genes *CDH13, CNTN4, ERC2, EYS, GALNTL6, TMEM132D*; between EC and SMC, overlapping genes included *AGBL4, CNTNAP2, GRM7, LRRC4C, SGCD, TENM2*; *PTPRT* and *SYN3* were shared hub genes between SMC and astrocytes. This suggests a shared regulatory mechanism between these cell types. Nevertheless, other

members of the network differed and network topology also differed suggesting cell-type specific regulatory processes.

GALNTL6 was identified as the key hub gene from endothelial cells and also had a central position in the astrocyte network. This gene encodes the enzyme that plays a role in protein glycosylation; its functional role in these cell types remains unknown, suggesting that further investigation is needed.

A *CNTNAP2*-centred hub gene networks were identified in both EC turquoise and SMC brown modules and the hub genes overlapped. This suggests a commonly regulated GCN in the cells. *CNTNAP2* encodes a member of the neurexin family CASPR2 protein, a neuronal cell-adhesion molecule that is critical for neurodevelopment and neuronal function. However, it also has other non-neuronal functions including in smooth muscle cells and endothelial cells. Altered gut transit time and colonic motility patterns were observed in *Cntnap2* mutant mice, and *CNTNAP2* dysfunction has also been implicated in gastrointestinal motility deficits in autism (Robinson et al., 2023). A study on pseudoexfoliation syndrome reported that *CNTNAP2* is consistently expressed in vascular endothelial cells across multiple ocular regions and suggested a potential role in endothelial membrane stabilisation (Krumbiegel et al., 2011). Given the reported function of *CNTNAP2*, my analysis suggests that *CNTNAP2* is a key gene with potential effects across neurons, endothelial cells, and vascular smooth muscle cells.

A notable finding from the analysis is that the hub genes from endothelial cells are established risk genes in several neuropsychiatric disorders: *CNTN4*, *CNTNAP2* are autism risk genes and *NRG1* is a schizophrenia risk gene (Douet et al., 2014; Memis et al., 2022; Oguro-Ando et al., 2021). *CSMD1*, *THSD7B*, *ASIC2*, *CDH13*, *TENM2, CNTNAP2* are among 63 risk genes significantly associated with stress-related depression (Gal et al., 2024). These genes (e.g. *ROBO2*, *DCC, CNTNAP2*) are well-

known for their traditional roles in neurons in synapse development and axonal guidance. My analysis however suggests an important functional role for these genes in non-neuronal cell types to regulate vascular and astrocytic relevant processes related to vascular network development. This is not necessarily surprising that gene programs are re-purposed. This is conceptually appealing since blood vessel networks will need to mirror neural networks and hence should be able to respond to the same guidance cues.

Building on the earlier observation of 'neuronal' gene expression in vascular cells, the WGCNA analysis identified a broader set of such genes. Several studies provide support for these 'neuronal' genes playing an important role in the neurovasculature. In a rat model study, *Cntnap2* knock-out showed significantly increased BBB permeability and elevated oxidative stress markers (Memis et al., 2022). *ROBO2,* which encodes a transmembrane receptor protein, plays a key role in neuronal guidance. But genetic knockout of *Slit2* or its receptors *Robo1/Robo2* leads to reduced angiogenesis. Conversely, endothelial cell migration was strengthened by Slit2 signalling via Robo1/Robo2 (Rama et al., 2015). *DCC* encodes netrin 1 (*NTN1*) receptor, and netrin 1 increases nitric oxide (acts as a vasodilator) production in EC through a DCC-dependent ERK 1/2-eNOS signalling; interestingly, blocking *DCC* can inhibit nitric oxide production and angiogenesis (Nguyen & Cai, 2006). *NRG1* was shown to protect brain endothelial cells and also neuroglial cells from cell death in a human cerebral malaria study (Liu et al., 2018). Downregulation of *NRG1* could therefore lead to potential BBB leakage and NVU dysfunction in hypertension. The downregulation of these genes in hypertension suggests increased BBB permeability and reduced angiogenesis. A single-nucleus study has shown the role of EC pathology in Alzheimer's disease (AD), suggesting maintaining BBB integrity and restoring effective angiogenesis can potentially slow the progression of early AD (Tsartsalis et al., 2024).

Among the genes belonging to the turquoise module are signalling molecules such as *NRG1*, which are significantly expressed by glio-vascular cell types. In the vascular smooth muscle cell hub genes, ligands such as *NRG3* and the neurexin family members *NRXN1* and *NRXN3* were also identified. It is possible that these molecules not only exert local effects on adjacent vascular cells and astrocytes but also exert crosstalk effects on neurons. Whilst in the healthy brain such secreted ligands may help support both vascular and neuronal networks, in hypertension, the observed downregulation may affect neuronal function and viability. This could represent an additional mechanism by which hypertension contributes to cognitive decline beyond disruption of the blood-brain barrier.

Examining the control and hypertension donors separately allowed an evaluation of how the gene networks changed with the disease. A significant loss of ‘neuronal’ network connectivity in hypertension was observed in both EC and astrocytes. This weaker connectivity in hypertension aligns with the results from DEG analysis and also provides evidence that the downregulation of ‘neuronal’ genes was not purely an isolated transcriptional change but was also accompanied by a collapse in ‘neuronal’ co-expression networks. The collapse of this gene co-expression network is likely a consequence of the hypertension-induced gene downregulation. Notably, all the key hub genes in the EC neuronal module were downregulated in hypertension.

Interestingly, SMC did not show a significant downregulation of its brown module of any hub genes (*GRM7* being an exception) but instead, there was a large change in the network with the number of genes halving from 622 in the non-hypertensive control network to 333 genes in the hypertension network. It was also evident that gene relationships in the network changed. This may suggest altered signalling and regulatory activity in SMC not discernible from differential gene expression analysis.

Only a reduced *DCC*-centred network remained in the hypertension EC turquoise module. *DCC* gene encodes netrin 1 (*NTN1*) receptor; interestingly, the downregulation of

astrocytic *NTN1* was identified in the DEG analysis. This suggests a potential crosstalk between endothelial cells and astrocytes and reduced netrin signalling in hypertension that can contribute to BBB leakage and NVU dysfunction.

Transcription factor analysis revealed some TFs which could be responsible for the observed DEGs and the gene networks. I found *NR2F2* had downregulated TF activity values in hypertensive endothelial cells. Interestingly, *NR2F2* knockout *in vitro* increased inflammation and oxidative stress (Dougherty et al., 2023). This suggests that the loss of *NR2F2* is deleterious in hypertension. *NR2F2* was consistently identified in the brown module of the combined and control EC datasets, and the green module of the HTN EC dataset.

Among the significant TFs identified, *PHF21A, and RFX7* were part of the EC WGCNA neuronal module. The role of *PHF21A* in endothelial cells is largely unexplored, but *PHF21A* is known to function as a transcriptional repressor, and loss of its function can drive both intellectual disability and craniofacial anomalies in Potocki-Shaffer syndrome (Kim et al., 2012). *RFX7* on the other hand is widely studied in atherosclerosis, and plays a protective role in maintaining endothelial cell homeostasis and mitigating inflammation (Yu et al., 2022). *RFX7* predicted activity was increased in hypertensive capillary endothelial cells, possibly indicating a protective role against hypertension-induced stress in endothelial cells.

Inferring TF activity from single-nucleus data can allow me to detect potential regulatory drivers, but it comes with important caveats. Instead of mature mRNA, pre-mRNA (intronic reads) often directly correlates with ongoing TF activity, which can enhance accuracy (Xue et al., 2023). Also, single-cell RNA sequencing commonly suffers from high dropout rates and variability, causing many reads to come from only the most abundant transcripts. Thus, lowly expressed but crucial genes, especially TFs, are frequently

missed or inaccurately quantified (Pokhilko et al., 2021). Also, the TF prediction algorithm relies heavily on incomplete databases, and no single method consistently outperforms the others in accuracy (McCalla et al., 2023). Thus, integrating ATAC-seq and performing wet lab validation is necessary to improve transcription factor inference substantially.

In summary, this chapter highlighted the role of neuronal genes in endothelial cells, and its dysregulation can potentially lead to BBB impairment and reduced angiogenesis in hypertension. Interestingly, smooth muscle cells and astrocytes showed ‘neuronal’ hub gene networks similar to those in endothelial cells, suggesting a shared regulatory mechanism. However, in the context of hypertension, astrocytes showed a collapse of the networks while smooth muscle cells did not show a network collapse but instead a network reconfiguration.

This arising question from my analysis is why are we observing the changes in gene expression and why are there profound changes in gene networks. One possibility is that an altered signalling milieu due to hypertension is driving such changes. I will therefore next examine cell-cell communication using the single-nucleus dataset.

Chapter 4. Investigating Cellular Crosstalk in Hypertension

Introduction

Multicellular organisms rely on intricate cell-cell communication (CCC) networks to coordinate cell behaviours required for homeostasis, development, and response to physiological stressors. CCC operates through both direct contact and diffusible signals via ligand-receptor interactions, which initiate intracellular signalling cascades and transcriptional reprogramming. Disruption in these interactions has been implicated in a wide range of pathological conditions, including cancer and neurodegenerative diseases (Su et al., 2024).

Recent advances in single-cell transcriptomics have enabled the deconvolution of cellular crosstalk at unprecedented resolution, allowing for systematic inference of ligand-receptor activity between cell populations and revealing how CCC is altered in the context of disease. For instance, a recently published single-cell study of the human brain vasculature applied CCC analysis to uncover substantial ligand-receptor crosstalk between endothelial cells and surrounding perivascular cell populations, highlighting the endothelial cell population as a central signalling hub within the neurovascular unit. The study also identified elevated MHC class II signalling not only in EC-EC interactions but also in EC-perivascular crosstalk in the context of brain pathologies, including brain tumours and vascular malformations (Wälchli et al., 2024).

The most widely used computational tools for investigating CCC are CellChat and NicheNet. CellChat infers CCC based on the expression of ligand-receptor pairs and quantifies communication probability using a curated knowledge-based database. By organising ligand-receptor pairs into curated signalling pathways, CellChat enables pathway-level interpretation of CCC (Jin et al., 2021; Jin et al., 2024). It is particularly

effective at mapping the overall communication network and revealing the intercellular signalling landscapes. NicheNet extends CCC inference by linking ligands expressed in sender cell populations to observed gene expression changes in a receiver cell population. It does so by prioritising ligands whose predicted downstream target genes show the greatest overlap with differentially expressed genes in the receiver cell population. These predictions rely on a curated ligand-receptor-target database constructed from integrated prior knowledge (Browaeys et al., 2020; Sang-Aram et al., 2025). NicheNet is particularly effective at identifying condition-specific ligand activity that may drive transcriptional changes in a target cell population, helping to assess whether observed DEGs are likely caused by upstream ligand signalling. Together, these complementary tools provide a powerful strategy to dissect the complexity of CCC at single-cell resolution.

In the previous chapter, widespread transcriptional changes of gene networks were observed across multiple cell types in hypertension, particularly in endothelial cells and astrocytes. One possible driver of these profound changes is an altered cellular signalling environment. In this chapter, I will perform CCC analysis to explore how hypertension reshapes the intercellular signalling landscape and to evaluate whether the observed transcriptional changes are driven by upstream ligand signalling.

Methods

Mapping Communication Networks Using CellChat

CellChat R package (v2.1.2) uses known ligand-receptor interactions to predict cell-cell communication between cell types in the single-nucleus dataset (Jin et al., 2021; Jin et al., 2024). Two CellChat objects were created from the Seurat object (assay = 'SCT'): 52,123 genes x 418,449 hypertensive nuclei and 52,123 genes x 252,713 control (non-hypertensive) nuclei.

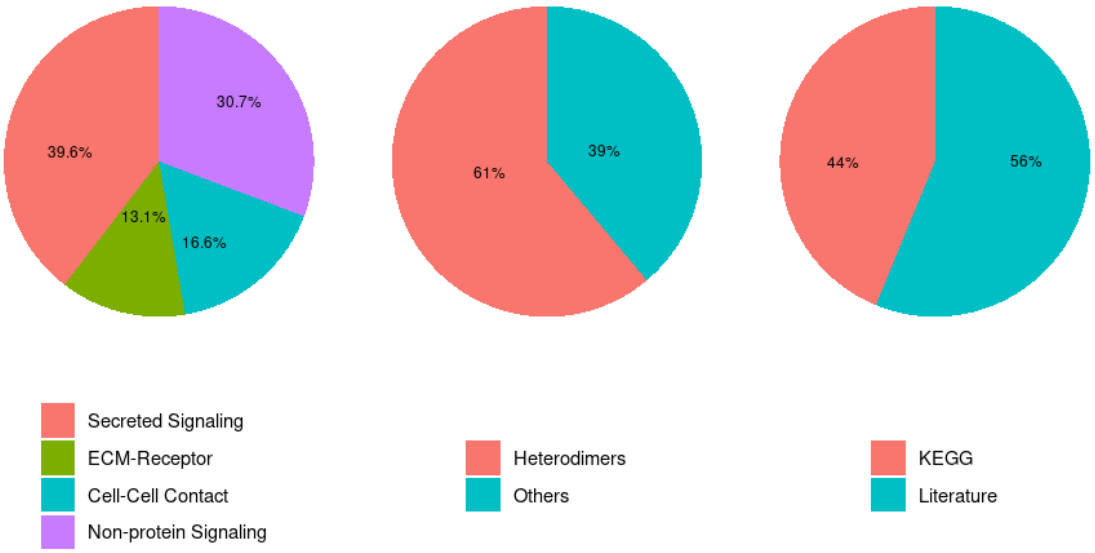

Figure 49. Pie chart of ligand-receptor interaction database from CellChat.

ECM, Extracellular Matrix.

CellChat database contains about 3,300 validated molecular interactions: 39.6% of secrete autocrine or paracrine signalling interactions, 30.7% non-protein signalling, 16.6% cell-cell contact interactions, and 13.1% ECM-receptor interactions (Figure 49). I set the human CellChat database for downstream cell-cell communication analysis.

Then, CellChat R package (v2.1.2) identified overexpressed ligands or receptors in each cell type (Wilcoxon rank sum test, $p < 0.05$) and then further identified overexpressed ligand-receptor interactions in the CellChat object. 2,562 highly variable ligand-receptor pairs were identified for signalling inference in the hypertension dataset and 2,505 highly variable ligand-receptor pairs in the control (non-hypertensive) dataset. Then, I projected gene expression data onto the protein-protein interaction (PPI) network. Using the projected data, I computed the communication probability and inferred the cellular communication network ('triMean', which approximates 25% truncated mean, is used for calculating the average gene expression per cell group; 'triMean' method performs well at predicting stronger interactions). The projected data reduced dropout effects of signalling genes, especially for possible zero expression of subunits of ligands or receptors. To ensure reliable detection of cell-cell communication and minimise noise, I filtered out the cell-cell communications if there were less than 10 nuclei in certain cell groups. Then, I summarised the communication probabilities of all ligand-receptor interactions associated with each signalling pathway to infer the cell-cell communication at a signalling pathway level. By counting the number of links or summarising the communication probability, CellChat calculated the aggregated cell-cell communication network.

For systematic analysis of complex intercellular communication networks, I used CellChat to further compute the network centrality scores to identify dominant senders, receivers, influencers, and mediators across all inferred communication networks. In a weighted-directed network (the weights as the computed communication probabilities), the out-degree (senders) was computed as the sum of communication probabilities of the outgoing signalling from a cell type; the in-degree (receivers) was computed as the sum of the communication probabilities of the incoming signalling to a cell type; the flow betweenness (mediators) measures the capability of a cell type as a gatekeeper to control communication flow between any two cell types; the information centrality (influencers) measures the global influence on the overall information flow.

I ran these CellChat pipelines on each dataset separately and then merged the hypertension and control (non-hypertensive) CellChat objects to perform the comparison analysis, which can identify major signalling changes across two biological conditions (hypertension and control). The merged CellChat object includes 1,439 signalling genes and 671,162 nuclei.

Prioritising Ligand-Receptor-Target Interactions Using NicheNet

To prioritise ligands that are most likely to causally explain the differential gene expression observed in hypertension, I applied NicheNet (v2.2.0), a computational method that integrates prior knowledge of ligand-receptor-target relationships to predict how ligands from sender cell populations influence gene expression in a receiver cell population (Browaeys et al., 2020; Sang-Aram et al., 2025). I performed two separate NicheNet analyses, using endothelial cells and astrocytes as the receiver cell type. In both analyses, the sender populations included all cell types except the ‘Unresolved’ cluster, allowing for the modelling of both paracrine and autocrine signalling. In NicheNet analysis, genes were considered expressed if they were detected in at least 5% of cells within each population, as determined using the get_expressed_genes() function with pct = 0.05. Based on this criterion, 5,496 genes were expressed in EC, and 6,643 genes were expressed in astrocytes.

For each receiver population, I first identified the set of expressed receptors, defined as genes in the ligand-receptor network that were also expressed in the receiver population. This resulted in 224 expressed receptors in EC and 259 expressed receptors in astrocytes, which were then used to filter the ligand-receptor network and define a list of potential ligands. I further refined this list by filtering for ligands expressed in the sender populations (sender-focused approach). For the EC analysis, 723 potential ligands were

identified, of which 321 were expressed in the sender populations; for astrocytes, 781 potential ligands were identified, of which 348 were retained after sender filtering.

The gene set of interest was defined as the differentially expressed genes (only genes expressed in at least 5% of the receiver cell type) between hypertensive and control conditions within the receiver population, obtained from the prior differential expression analysis. Originally, 1,237 DEGs were identified in EC and 715 in astrocytes. After intersecting with the NicheNet ligand-target matrix, 1,235 EC DEGs and 712 astrocyte DEGs were retained for ligand activity prediction. Background gene sets were composed of all genes expressed in the receiver population and present in the ligand-target matrix (5,274 genes for EC and 6,155 for astrocytes).

Ligand activity was assessed using the predict_ligand_activities() function, which ranks ligands based on how well their predicted target genes (as defined in the ligand-target matrix) overlap with the observed DEGs in the receiver population, relative to a background set of genes. For each ligand, NicheNet calculates AUPR, which is particularly useful when DEGs are sparse and evaluates the enrichment of true positive target genes among all predictions. NicheNet first binarises the gene set of interest by assigning a value of 1 to DEGs and 0 to background genes, generating an Observed Expression Pattern (OEP). This is then compared to each ligand's predicted target profile derived from the prior ligand-target matrix. AUPR is computed between the OEP and the predicted scores, and subsequently corrected for baseline enrichment by subtracting the expected AUPR under a random model, which is defined as the proportion of DEGs in the background gene set. Ligands are then ranked primarily based on their AUPR-corrected values, a normalised score that accounts for variability in gene set size and class imbalance.

Then, I selected the top 10 prioritised ligands based on their AUPR-corrected scores from the ligand activity analysis, ensuring that each ligand was also expressed in at least 5% of cells in the sender populations. For each of the 10 ligands, the top 100 predicted targets

with the highest regulatory potential scores were identified using the get_weighted_ligand_target_links() function. However, only those targets that overlapped with the predefined gene set of interest were retained. As a result, the final set included 63 ligand-target gene pairs in EC analysis, and 50 pairs in Astro analysis. I prepared the data for heatmap visualisation using the prepare_ligand_target_visualization() function, applying a quantile cutoff of 0.25 such that regulatory potential scores falling below the 25th percentile of all scores between the top-ranked ligands and their top predicted targets were set to zero. This filtering step reduced noise and enhanced interpretability by highlighting the most confident ligand-target interactions, resulting in 39 ligand-target pairs retained for visualisation in EC and 23 pairs in Astro.

To investigate through which receptors the top-ranked ligands may act on the receiver population, I assessed ligand-receptor interaction strengths using NicheNet's precompiled ligand-receptor matrix. These scores represent the prior likelihood of ligand-receptor binding and downstream signalling, derived from integrated pathway knowledge and protein-protein interaction data. The resulting interaction matrix was visualised as a heatmap, illustrating the predicted interaction potential between each ligand and its corresponding receptors.

Results

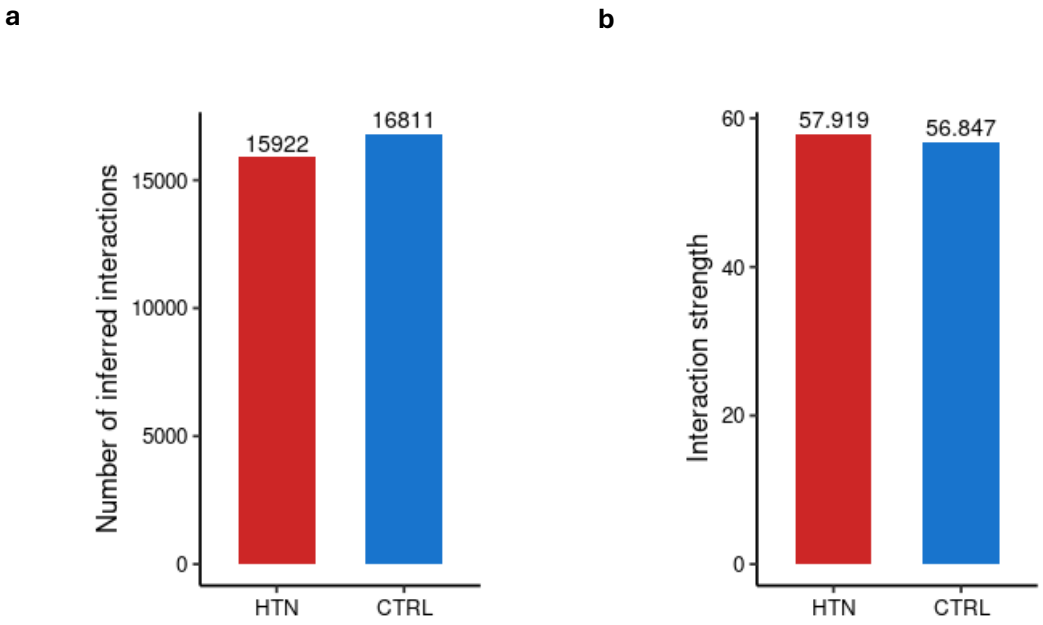

Figure 50. Summary of global cell-cell communication in hypertension (HTN) and control (CTRL) groups inferred by CellChat.

*(**a**) Bar plot showing the total number of inferred ligand-receptor interactions. (**b**) Bar plot showing the overall interaction strength.*

HTN and CTRL groups were analysed separately using CellChat. The number of interactions refers to the total number of significant ligand-receptor pairs detected across all cell-type pairs, while interaction strength reflects the sum of communication probabilities. The metrics were compared to assess global network features.

I compared the total number of inferred interactions and the interaction strength of the inferred cell-cell communication networks between HTN and CTRL. The analysis revealed that the total number of inferred interactions was reduced in HTN, while the interaction strength was slightly increased (Figure 50).

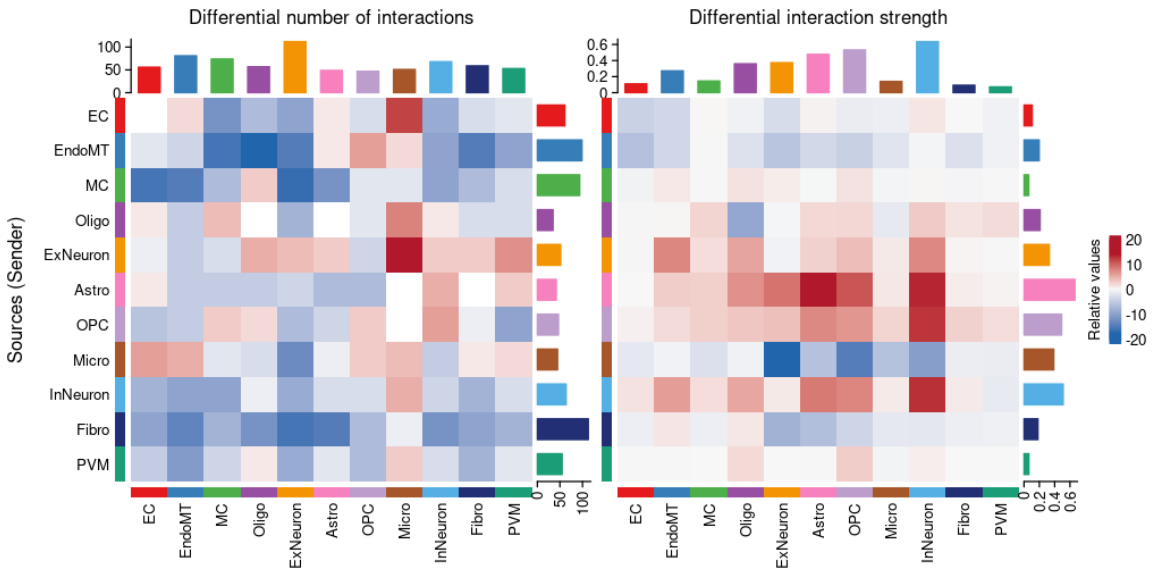

Figure 51. Heatmap of the differential number of interactions and interaction strength in the cell-cell communication network between HTN and CTRL.

The top-coloured bar plot indicates the absolute values of the sum of each column of the heatmap (incoming signalling), and the right-coloured bar plot indicates the absolute values of the sum of each row of the heatmap (outgoing signalling). The bar height indicates the degree of change in terms of the number of interactions or interaction strength between HTN and CTRL. In the heatmap, red represents increased signalling in HTN and blue represents decreased signalling in HTN.

To examine how intercellular signalling was altered in hypertension, differential interaction plots were generated. Overall, the total number of interactions was generally reduced in hypertension, indicating widespread attenuation of signalling connectivity across cell types (Figure 51). Notable exceptions to this trend included microglia, which showed an increase in incoming interactions specifically from excitatory neurons and endothelial cells. In addition, excitatory neurons exhibited an increased number of interactions with multiple target populations in hypertension.

However, differential interaction strength revealed a contrasting pattern. While the overall changes in interaction strength were subtle, certain cell populations showed notable increases. In particular, astrocytes showed increased interaction strength in autocrine signalling as well as enhanced interaction strength with OPC and inhibitory neurons, suggesting intensified glial and neuron-glial communication under hypertensive

conditions. Conversely, the interaction strength from microglia to excitatory neurons was substantially reduced in hypertension.

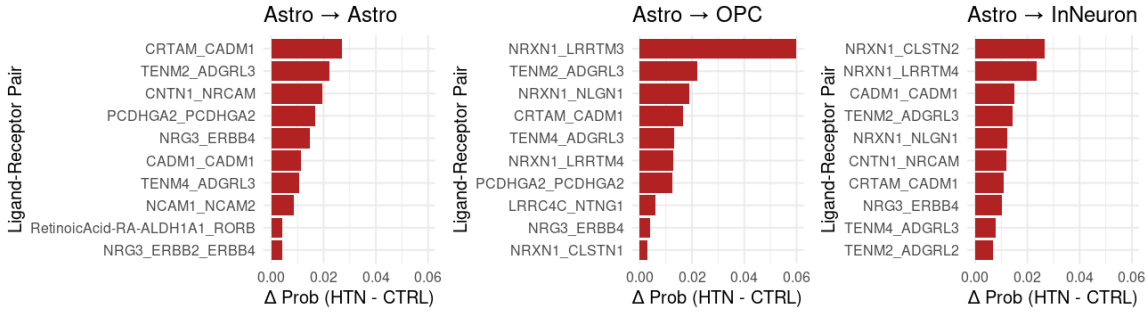

Figure 52. Increased astrocyte-derived ligand-receptor interactions in hypertension.

Bar plots show the top 10 ligand-receptor pairs with the largest increase in interaction strength (communication probability) in hypertension relative to control. The source population is astrocytes, and the target populations are astrocytes, oligodendrocytes progenitor cells, and inhibitory neurons. Bar height represents the difference in communication probability.

I examined the top 10 ligand-receptor pairs that were most increased in astrocyte-to-astrocyte, astrocyte-to-OPC, and astrocyte-to-InNeuron communication (Figure 52). TENM2-ADGRL3, CRTAM-CADM1, and NRG3-ERBB4 interactions were enriched in all three cell-type pairs. The NRXN1-LRRTM3, mediating communication from astrocytes to OPC, exhibited the largest increase in communication probability in hypertension. NRXN1 appeared repeatedly across multiple astrocyte-derived interactions, including both astrocyte-to-OPC and astrocyte-to-InNeuron.

Among the 30 ligand-receptor pairs examined, only 11 unique ligands (CRTAM, TENM2, CNTN1, PCDHGA2, NRG3, CADM1, TENM4, NCAM1, RA-ALDH1A1, NRXN1, LRRC4C) were identified. Interestingly, the vast majority of these ligand genes did not show significant changes in astrocyte differential expression analysis. The only exception was *CRTAM*, which was significantly downregulated in hypertension (LFC = -0.998, adjusted p-value = 0.024).

a

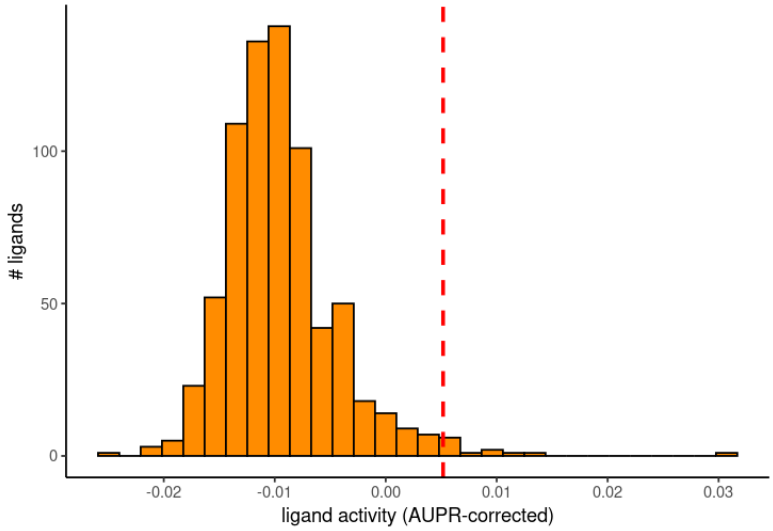

b

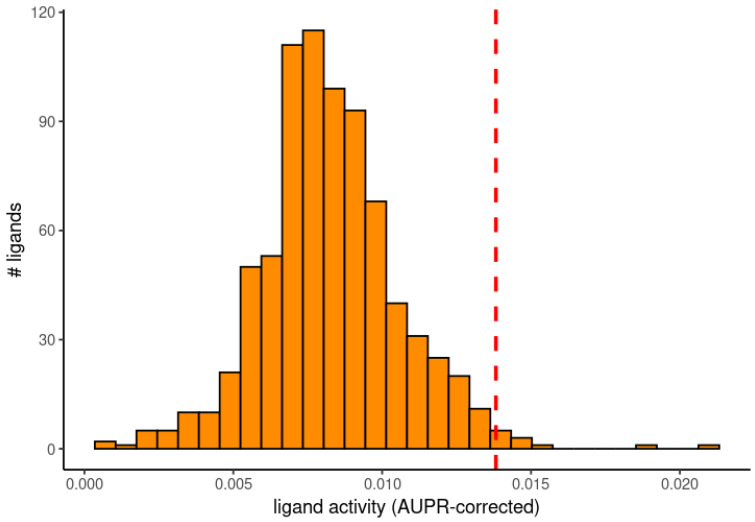

*Figure 53. Distribution of ligand activity scores with EC (**a**) and Astro (**b**) as the receiver.*

*Histogram showing the distribution of AUPR-corrected scores for all potential ligands evaluated by NicheNet, using endothelial cells (**a**) and astrocytes (**b**) as the receiver population. Ligand activity was quantified based on the enrichment of predicted target genes among observed DEGs. Higher AUPR-corrected scores indicate stronger ligand-target associations, while scores near zero reflect the level of association expected by random chance. The red dashed line marks the cutoff for the top 10 ranked ligands.*

To assess whether the observed DEGs in EC and astrocytes were likely driven by upstream ligand activity, I applied NicheNet ligand activity analysis. Histograms of AUPR-corrected scores showed that most potential ligands had values clustered around zero in

both EC and astrocytes, suggesting that the observed transcriptional changes were not strongly driven by ligand activity (Figure 53). The red dashed lines indicate the AUPR-corrected thresholds of the top 10 ligands, further highlighting the modest scores across the dataset.

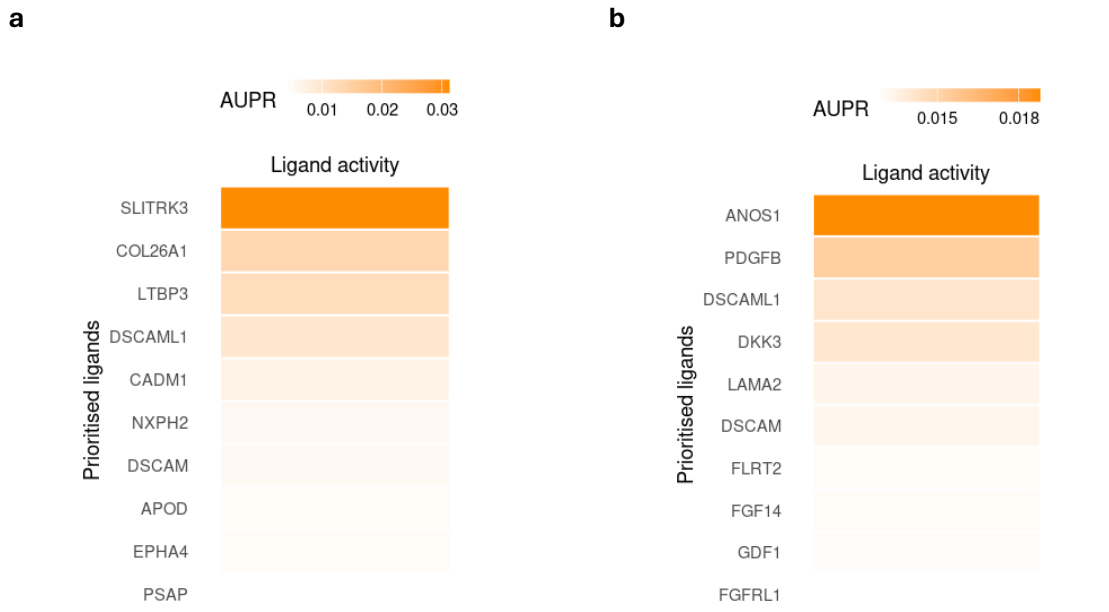

*Figure 54. Ligand activity scores for the top 10 prioritised ligands with EC (**a**) and Astro (**b**) as the receiver.*

*Heatmap displaying AUPR-corrected scores for the top 10 ligands ranked by NicheNet, using endothelial cells (**a**) and astrocytes (**b**) as the receiver population.*

Despite the low activity scores, I visualised the top 10 ligands (expressed in at least 5% of cells in one or more sender populations) with the highest ligand activity scores for each receiver population (Figure 54). In EC, SLITRK3, COL26A1, LTBP3, DSCAML1 were the highest-ranked ligands, and in astrocytes, ANOS1, PDGFB, DSCAML1, DKK3 were prioritised. DSCAML1 and DSCAM were identified in both EC and astrocyte analysis, indicating potential shared upstream signals influencing these two key cell types.

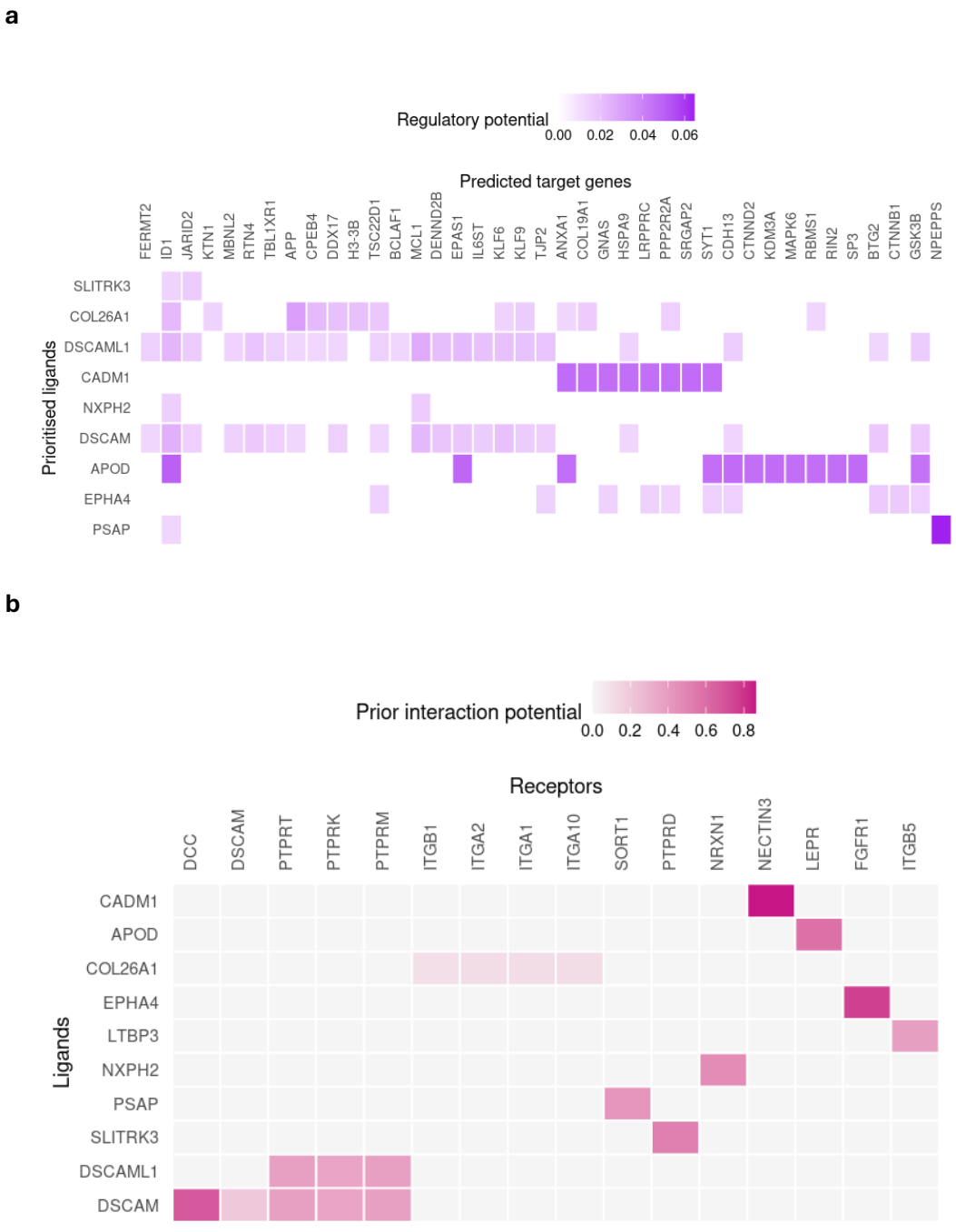

*Figure 55. Heatmap of predicted ligand-target (**a**) and ligand-receptor (**b**) interactions for the top 10 prioritised ligands with EC as the receiver.*

*Heatmap visualising regulatory potential scores between the top 10 prioritised ligands and their predicted downstream target genes (**a**) and interaction potential scores between the top 10 prioritised ligands and their corresponding expressed receptors (**b**) in EC. Each tile represents the predicted scores of a ligand-target pair, derived from NicheNet's curated databases. The colour scheme corresponds to the potential score.*

Ligands such as DSCAM, DSCAML1, CADM1, APOD exhibited strong regulatory potential, influencing a broad array of predicted downstream target genes in EC (Figure 55). In particular, DSCAM and DSCAML1, cell adhesion molecules, were linked to multiple receptors (including DCC), suggesting they may play a central role in mediating endothelial cell responses under hypertensive conditions.

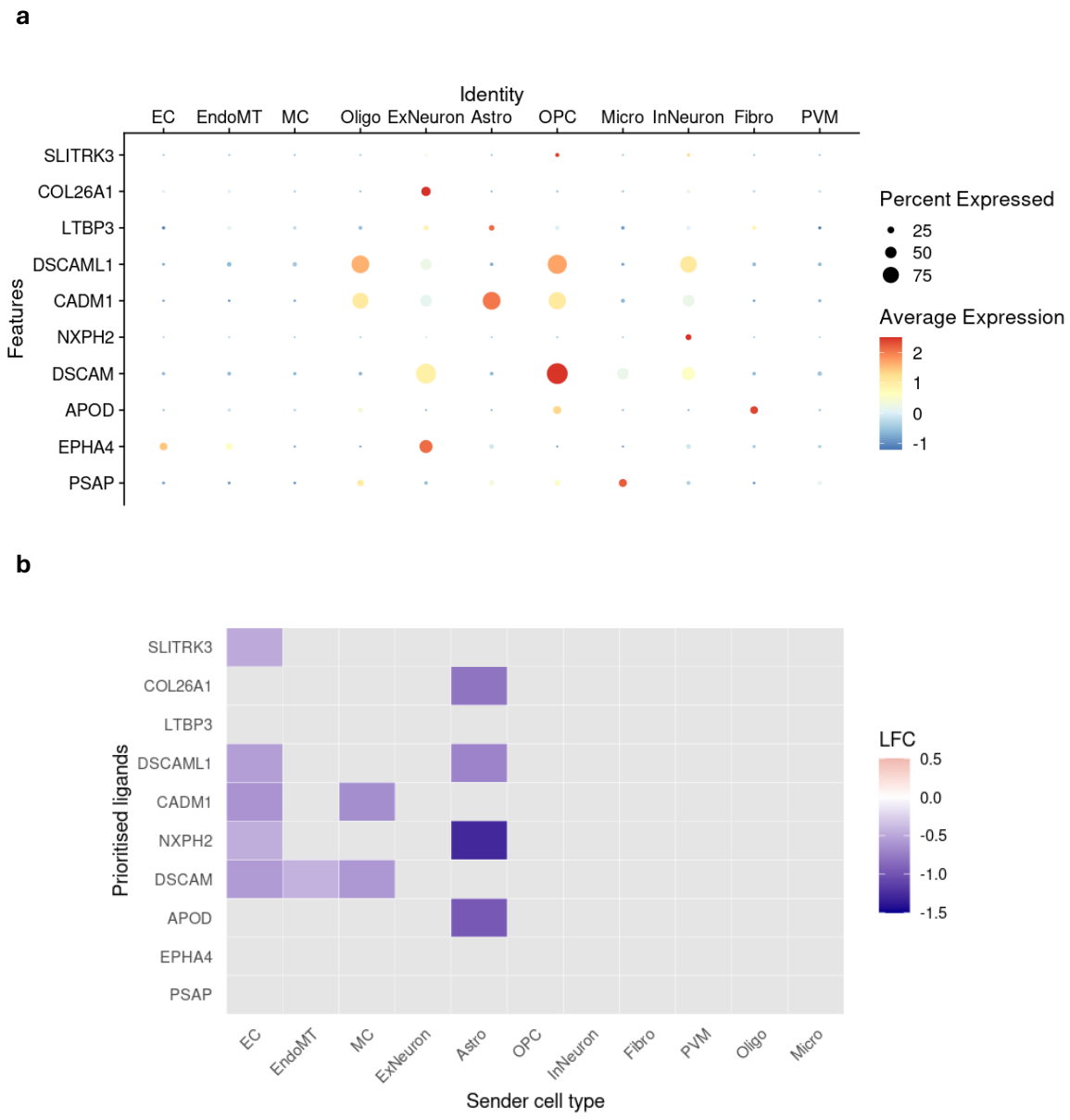

*Figure 56. Expression of top 10 prioritised ligands across sender cell populations (**a**) and differential expression of top 10 prioritised ligands across sender cell populations (**b**) with EC as the receiver.*

*(**a**) Dot plot showing the expression of the top 10 prioritised ligands across sender cell types. Each dot colour represents the average expression level and dot size represents the percentage of cells expressing the ligand within each cell type.*

*(**b**) Heatmap showing the log_2FoldChange (LFC) of the top 10 prioritised ligands across sender cell types in hypertensive versus control conditions. Only ligand-cell type pairs with statistically significant differential expression (p-adj < 0.05) were coloured, and non-significant pairs were shown in grey. The colour scheme represents the magnitude and direction of the regulation.*

To better understand the source and regulation of ligands predicted to act on endothelial cells, I examined their expression profiles and differential expression across sender cell populations. Interestingly, many of the top prioritised ligands were broadly expressed across non-vascular cell types, including glial populations and neurons (Figure 56). However, while several of these ligand genes were found to be downregulated in hypertension, their overall percentage of expression in the corresponding sender cell types remained relatively subtle.

a

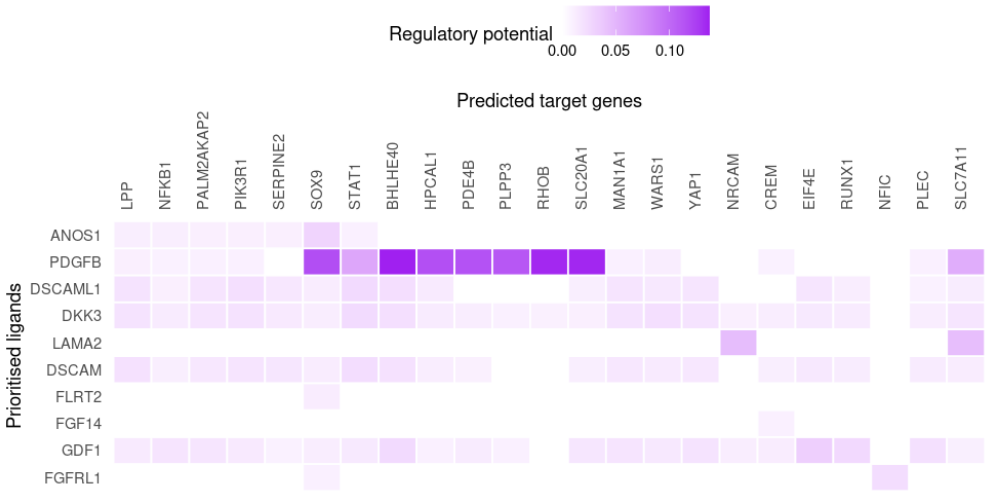

b

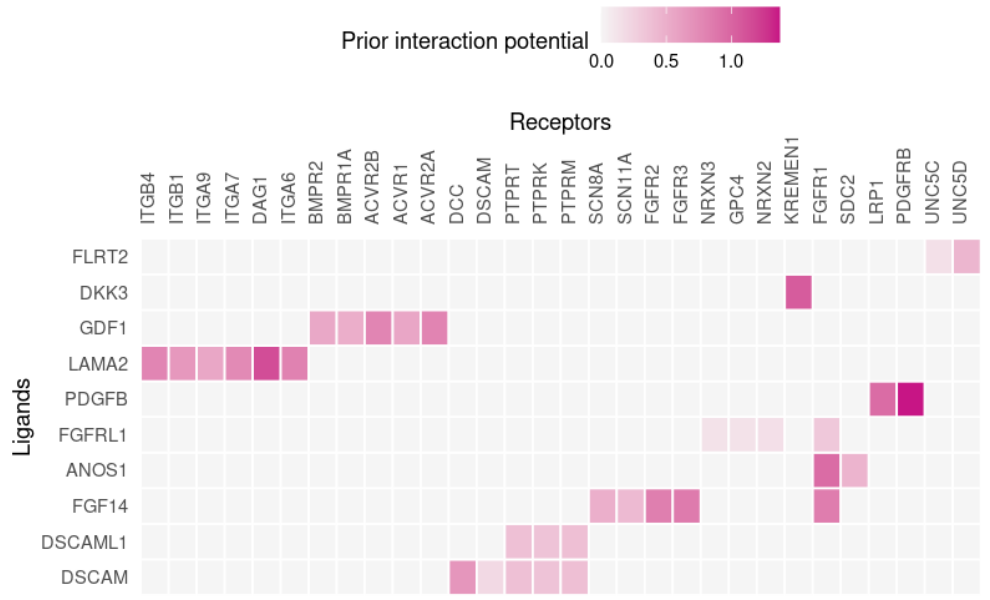

*Figure 57. Heatmap of predicted ligand-target (**a**) and ligand-receptor (**b**) interactions for the top 10 prioritised ligands with Astro as the receiver.*

*Heatmap visualising regulatory potential scores between the top 10 prioritised ligands and their predicted downstream target genes (**a**) and interaction potential scores between the top 10 prioritised ligands and their corresponding expressed receptors (**b**) in astrocytes. Each tile represents the predicted scores of a ligand-target pair, derived from NicheNet's curated databases. The colour scheme corresponds to the potential score.*

Among the top-ranked ligands, PDGFB, DSCAML1, DKK3, DSCAM, GDF1 exhibited strong regulatory potential for a range of target genes in astrocytes (Figure 57). Notably, PDGFB exhibited relatively higher regulatory potential scores for several target genes, including SOX9, BHLHE40, HPCAL1, PDE4B, PLPP3, RHOB, SLC20A1. The ligand-receptor analysis further revealed that these ligands were predicted to interact with a broad set of receptors in astrocytes.

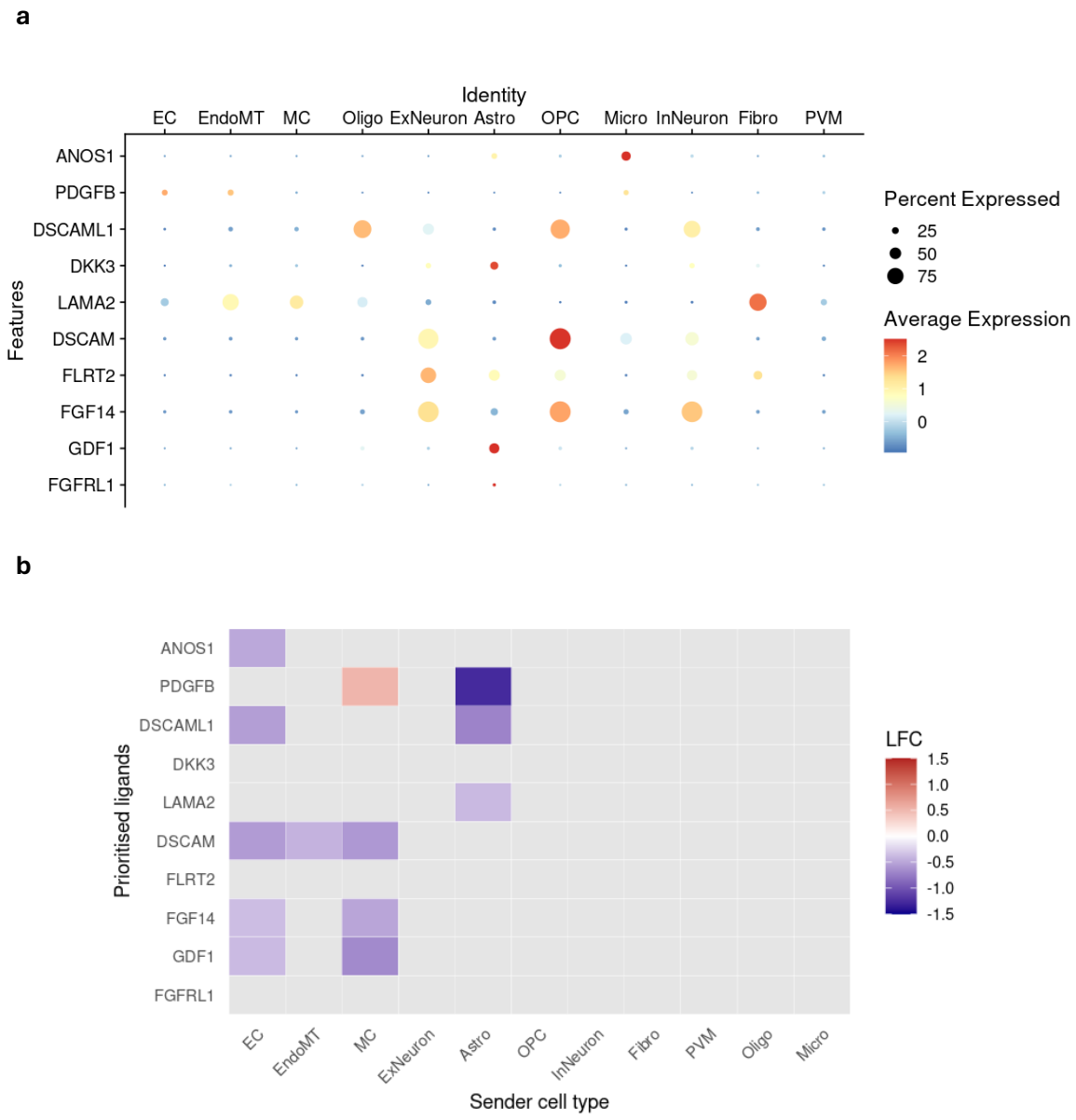

*Figure 58. Expression of top 10 prioritised ligands across sender cell populations (**a**) and differential expression of top 10 prioritised ligands across sender cell populations (**b**) with Astro as the receiver.*

*(**a**) Dot plot showing the expression of the top 10 prioritised ligands across sender cell types. Each dot colour represents the average expression level and dot size represents the percentage of cells expressing the ligand within each cell type.*

*(**b**) Heatmap showing the log_2FoldChange (LFC) of the top 10 prioritised ligands across sender cell types in hypertensive versus control conditions. Only ligand-cell type pairs with statistically significant differential expression (p-adj < 0.05) were coloured, and non-significant pairs were shown in grey. The colour scheme represents the magnitude and direction of the regulation.*

While most of these ligands were predominantly expressed in glial cells and neurons, *PDGFB* and *LAMA2* were more highly expressed in vascular cell types (Figure 58). Notably, differential expression analysis revealed that *PDGFB* was significantly upregulated in mural cells but downregulated in astrocytes, suggesting a potential shift in the source of PDGFB-mediated signalling in hypertension. However, the overall percentage of cells expressing *PDGFB* remained low.

Discussion

CellChat analysis revealed that the total number of interactions was reduced and interaction strength was increased overall in hypertension, suggesting complex signalling changes in hypertension. A notable exception was microglia which exhibited an increase in the number of incoming interactions, particularly from excitatory neurons and endothelial cells, whilst the interaction strength from microglia to excitatory neurons was reduced in hypertension. This may suggest a compensatory shift in microglial signalling dynamics in response to hypertensive-induced changes in the surrounding cellular communication landscape—which overall prevents any major activation of inflammatory pathways. This aligns with the lack of significant inflammatory pathway-associated DEGs in hypertension identified in my dataset.

Astrocytes exhibited increased autocrine signalling and their interactions with OPC and inhibitory neurons. TENM2-ADGRL3, CRTAM-CADM1, and NRG3-ERBB4 interactions were enriched in all three cell-type pairs. Additionally, NRXN1 signalling appeared repeatedly increased across multiple astrocyte-derived interactions. A mouse model study has previously shown that TENM2 signalling was upregulated in reactive astrocytes following mechanical brain injury (Tessarin et al., 2019). CRTAM signalling is primarily characterised in the context of immune responses, particularly in mucosal immunity, where it plays a critical role in the retention and function of intraepithelial T cells (Cortez et al., 2014). However, the role of CRTAM signalling in astrocytes remains underexplored. Given that *CRTAM* gene was significantly downregulated in hypertensive astrocytes, further investigation is needed. Interestingly, a single-nucleus RNA-seq study on AD has reported a marked downregulation of homeostatic genes such as *NRXN1*, *NRG3*, *ERBB4* in reactive astrocytes, suggesting a loss of their physiological support functions in AD (Dai et al., 2023). In my study, increased ligand-receptor signalling from astrocytes, particularly in interactions with OPC and inhibitory neurons was observed. This may reflect astrocytes

compensating for functional stress or altered environmental cues by enhancing these ligand-mediated pathways in hypertension.

NicheNet analysis showed that the observed transcriptional changes in endothelial cells and astrocytes were not strongly driven by ligand activity, as indicated by generally low ligand activity scores, but some signalling pathways are worth highlighting due to their potential relevance. DSCAML1 and DSCAM signalling were identified as decreased in both EC and astrocyte analysis, indicating potential shared upstream signals influencing these two cell types. A human iPSC study has shown that deletion of *DSCAM* from trisomy 21 endothelial cells reduced the secretion of sclerostin, which is upregulated in trisomy 21 and suppresses Wnt signalling required for normal cardiac, skeletal, and vascular development (McKean et al., 2024). My data suggest that decreased DSCAM signalling, accompanied by increased Wnt signalling, may reflect compensatory changes under hypertensive conditions. Wnt signalling has been reported as key regulator of blood pressure and vascular homeostasis (Abou Ziki & Mani, 2017). Additionally, dysregulation of Wnt signalling impairs astrocytic glutamate clearance, leading to neurotoxicity and exacerbating neurodegenerative processes in AD (Vallee et al., 2022). Collectively, this suggests altered DSCAM signalling through Wnt may play a key role in both vascular dysfunction and neurodegeneration.

Altered astrocyte PDGFB signalling was also identified and found to regulate a set of target genes, including *SOX9, BHLHE40, HPCAL1, PDE4B, PLPP3, RHOB, SLC20A1*. A mouse model study has shown that loss-of-function mutations in *PDGFB* cause vessel-associated calcifications in the brain, which in turn elicit a neurotoxic response in astrocytes and contribute to neuronal dysfunction (Zarb et al., 2019). This may suggest that disturbed PDGFB signalling in hypertension could contribute to reactive astrocyte responses, potentially through vascular dysfunction or changes in intercellular signalling.

Notably, PDGFB signalling has a well-established role in vascular biology, especially in endothelial-to-mural cell communication. It plays a key role in the recruitment of pericytes and vascular smooth muscle cells during angiogenesis. Endothelial cell-derived PDGFB acts as a chemoattractant for PDGFRB-expressing mural cells, facilitating BBB development and ensuring vascular stability (Gaengel et al., 2009; Hellström et al., 1999). Thus, altered PDGFB signalling may have broader impacts on the neurovascular unit.

The cell-cell communication analysis largely failed to explain the observed differentially expressed genes in hypertensive donors. The ligand-receptor pairs identified by CellChat as differential between hypertension and control were notably not the ligands and receptors identified as differentially expressed in my pseudobulk analysis. This may arise from CellChat relying on the Wilcoxon rank sum test to identify differentially expressed ligands and receptors at the single-cell level within each cell group without accounting for confounding factors (e.g. age, sex). As noted previously, single-cell level differential expression can be more sensitive but also subject to greater false discovery. Further studies are therefore required to validate the signalling changes identified through CellChat.

Similarly, NicheNet did not identify signalling pathways responsible for the differentially expressed genes such as the downregulation of neuronal/synaptic genes in endothelial cells. This may be due to many of the DEGs not being due to signalling alterations but instead due to other cellular changes such as epigenetic modification. Notably, several target genes identified from the cell-cell communication analysis were epigenetic factors (e.g., *SOX9*, *BHLHE40*). Furthermore, cell-cell communication analyses have a number of limitations.

While most CCC inference from single-cell data relies on co-expression analysis—linking the expression of a ligand in one cell type with the expression of its corresponding receptor in another—this approach inherently assumes that transcript abundance reflects

protein abundance and interaction potential. However, mRNA levels do not always correlate with protein expression, and the presence of ligand-receptor transcripts alone does not confirm functional communication between cells (Cheng et al., 2023). Furthermore, most CCC inference relies on curated ligand-receptor databases, which are compiled from heterogeneous data sources of varying quality and experimental validation. Also, the activation state of receptors, key entry points in signalling pathways, may not consistently align with the expression of downstream target genes (Devkota & Wuchty, 2020). NicheNet's ligand-target prior model aggregates evidence for regulatory potential without distinguishing between activating and inhibitory interactions, and the resulting regulatory scores are only comparable within a given ligand and not across different ligands (Sang-Aram et al., 2025). Moreover, CCC tools do not account for transcriptional heterogeneity within defined cell populations, potentially masking subpopulation-specific signalling changes.

Despite these limitations, analysing ligand-receptor-target expression remains a valuable tool for exploring intercellular signalling landscapes and providing a foundation for interpreting potential cell-cell interactions. As a future study, experimental follow-up is crucial to validate predicted interactions and elucidate their biological relevance.

Chapter 5. Cell-Type Enrichment of Disease Risk Genes

Introduction

Differential gene expression provides an understanding of how a disease affects the brain, and in the case of hypertension, this may represent decades of the brain exposed to high blood pressure and associated systemic signalling changes. One of the inherent limitations of human post-mortem studies is the inability to determine whether the observed changes are the primary contributors to disease or the consequences of disease pathology. Integrating genome-wide association studies (GWAS), which can identify genetic variants linked to traits, overcomes this limitation and can allow us to gain insights into early and potential causal molecular changes. Over 90% of trait-associated GWAS variants are found in non-coding regions, suggesting these variants mainly influence gene expression rather than directly altering protein structures (Wu et al., 2024).

Typical GWAS single-SNP analysis focuses on individual variants, which might fail to capture meaningful biological insights and can be difficult to interpret; however, gene and gene-set analysis, as more powerful alternatives, can aggregate signals from multiple SNPs to help infer biological effects of a disease (Tang et al., 2015). In gene analysis, individual variants are aggregated to the gene level, and the collective effects are assessed. In gene-set analysis, individual genes are aggregated to the predefined gene-set level, which can provide additional insight into biological and functional mechanisms.

MAGMA.Celltyping, a computational tool designed to perform cell-type-disease association analysis, builds on this concept by mapping genetic variants from GWAS onto single-cell gene expression profiles using gene-set analysis, uncovering how disease genetic risk converges on particular cell populations. This method is widely used to prioritise cell types that are critical to disease pathology. For instance, a schizophrenia

(SCZ) study has shown that the genomic loci implicated in SCZ consistently mapped onto pyramidal cells, medium spiny neurons, and certain interneurons. The identified cell-type-associated genetic risk did not overlap between cell types, suggesting that different cell types have biologically distinct roles in SCZ (Skene et al., 2018).

In this chapter, I will integrate published GWAS summary statistics of hypertension and other control traits with my snRNA-seq dataset to explore whether disease-associated gene sets converge on specific cell types, aiming to uncover early molecular signatures and decode cell-type-specific genetic susceptibility.

Methods

Cell-Type Enrichments of Disease-Associated Gene Sets

Table 16. List of GWAS summary statistics.

Study	Traits	Ancestry Group	Data Accession
(Keaton et al., 2024)	HTN – SBP	European	GCST90310294
(Keaton et al., 2024)	HTN – DBP	European	GCST90310295
(Keaton et al., 2024)	HTN – PP	European	GCST90310296
(Suzuki et al., 2024)	T2DM	European	DIAGRAM Consortium
(Traylor et al., 2019)	WMH	European	GCST007305
(Malik et al., 2018)	Stroke	European	GCST006906
(Trubetskoy et al., 2022)	SCZ	European	GCST90128471
(Bellenguez et al., 2022)	AD	European	GCST90027158 (GRCh 38)
(Meyers et al., 2023)	Migraine	European	GCST90271641

HTN, Hypertension; SBP, Systolic Blood Pressure; DBP, Diastolic Blood Pressure; PP, Pulse Pressure; T2DM, Type 2 Diabetes Mellitus; WMH, White Matter Hyperintensities; SCZ, Schizophrenia; AD, Alzheimer's Disease.

To identify cell types that were associated with different traits, following GWAS summary statistics were downloaded from GWAS Catalog (https://www.ebi.ac.uk/gwas/) and DIAGRAM Consortium (http://www.diagram-consortium.org/downloads.html) (Table 16).

First of all, MungeSumstats R package (v1.12.2) was used to manage GWAS datasets from different sources and prepare GWAS datasets for downstream analysis, ensuring consistency in column names and formats (Murphy et al., 2021). Then, MAGMA R package (v1.10) was used to map SNPs to genes (a window of 35 kb upstream and 10 kb downstream): the reference genome 'GRCh37' was utilised for all analyses except for AD GWAS summary statistics, which were mapped using 'GRCh38' (Tang et al., 2015) (Table 16).

CellTypeDataset (CTD) is a standardised data format created from EWCE R package (v1.10.2) that is used to represent the expression profiles of genes across different cell types (Skene & Grant, 2016). CTD was used to assess whether GWAS disease genes were enriched in specific cell types. Only control nuclei were used in each analysis to rule

out the confounding effects of disease-related changes. Control (non-hypertensive) nuclei were extracted and low-count genes (cutoff = 10) were removed from the single-nucleus dataset, resulting in 47,149 genes x 252,713 control nuclei. Then, I removed 2,781 uninformative genes which were not significantly differentially expressed across major cell types (adjusted p-values cutoff = 10^{-5}). A similar filtering step was also performed using the dataset with cell subtype labels (e.g., EC split into cEC, aEC, vEC; MC split into SMC, T-PC, M-PC; other cell types remained unchanged), resulting in the removal of 3,161 uninformative genes.

For T2DM analysis, non-diabetic nuclei were extracted and low-count genes (cutoff = 10) were removed, resulting in 47,638 genes x 355,748 non-diabetic nuclei. 2,470 genes that did not exhibit significant differential expression across major cell types were excluded from the diabetes analysis (adjusted p-values cutoff = 10^{-5}).

MAGMA.Celltyping R package (v2.0.14) was used to conduct cell-type-specific enrichment tests on GWAS summary statistics (Skene et al., 2018). The top 10% mode of cell-type-trait association uses only the top 10% of most cell-type-specific genes for each cell type to perform gene-set enrichment analysis (GSEA), discarding any gene-level weight data and treating genes as categorical data (in the gene list or not). MAGMA.Celltyping calculates the false discovery rate (FDR) using the Benjamini-Hochberg (BH) correction. I visualised the cell-type-trait association results using the Complex Heatmap R package (v2.22.0) (Gu, 2022).

Conditional Cell-Type Enrichment Analysis

Sometimes, a single cell type can dominate the signature and even overshadow other cell-type associations in MAGMA.Celltyping baseline analysis, making it difficult to determine whether other cell types are truly associated with the GWAS trait. Conditional

cell-type enrichment analysis in MAGMA.Celltyping (v2.0.14) addresses this issue by statistically controlling one or more cell types and assessing whether other cell types are significantly enriched. In the baseline analysis of major cell types, I identified a significant enrichment of vascular cell types (EC, MC, EndoMT, Fibro) in hypertension traits (SBP, DBP, PP), suggesting vascular cells were associated with the genetic architecture of hypertension. In the baseline analysis of cell subtypes, a significant enrichment of aEC, EndoMT, M-PC were identified across the hypertension traits. To identify which vascular cell type is the main driver of the enrichment signal and also check if other cell types were previously masked by dominant enrichment signals from vascular cell types, I performed conditional analysis using linear mode while maintaining the top 10% mode for enrichment testing (i.e. only the top 10% of genes were considered for enrichment tests).

Pathway Enrichment Analysis of Significant Disease-Associated Genes

MAGMA competitive gene-set analysis tests whether the genes in a gene set are more strongly associated with the phenotype of interest than other genes. MAGMA gene-set analysis directly uses the output from MAGMA gene analysis which tests the association of genes with phenotype. I used SNP-wise models to perform the gene analysis: SNP-wise models perform tests on mean SNP association using GWAS summary statistics and reference linkage disequilibrium (LD) panel (Tang et al., 2015). In this study, I defined significant disease-associated-cell-type genes as those with p-values less than 5×10^{-8} in the gene analysis results from the previous MAGMA.Celltyping analysis (see above). Significant genes were used for subsequent GO analysis (BP sub-ontology). The GO analysis was performed using clusterProfiler R package (v4.12.6) with the associated annotation R packages annotationDBI (v1.68.0) and org.Hs.eg.db (v3.2.20) (Wu et al., 2021; Yu et al., 2012). UpSetR R package (v1.4.0) and ggplot2 R package (v3.5.1) were used for the visualisation of intersecting genes and GO terms among different traits and cell types (Conway et al., 2017; Valero-Mora, 2010).

Overlapping genes between differentially expressed genes (at least 5% expression in the corresponding cell type) and significant GWAS were used for subsequent GO enrichment analysis. To reduce the redundancy in GO terms and retain the most statistically significant representative terms, I applied semantic similarity filtering using the simplify() function in clusterProfiler (v4.12.6) (Wu et al., 2021; Yu et al., 2012). GO terms with a semantic similarity > 0.7 were collapsed into a single representative GO term with the lowest adjusted p-value. The final set of GO terms was used for downstream visualisation.

To assess whether the overlap between differentially expressed genes (at least 5% expression in the corresponding cell type) and significant GWAS was statistically significant, I performed a hypergeometric test. The test was conducted using the phyper() function in R, with the total number of genes expressed (at least 5% expression in the corresponding cell type) used as the background. A one-sided test was applied to determine whether the observed overlap was enriched beyond random chance.

GWAS Gene Overlap with Cell Type-Specific Markers

The top 100 marker genes for each key vascular cell population (aEC, EndoMT, and M-PC) were identified using the FindMarkers function in Seurat (v5.1.0) with default parameters, and only positive markers were included (Satija et al., 2015). Hypertension GWAS genes were obtained from MAGMA gene-level analysis, using a significance threshold (p-value < 5×10^{-8}). Overlapping genes between hypertension GWAS genes and the top 100 cell type-specific marker genes (aEC, EndoMT, and M-PC) were subsequently used to generate a heatmap of expression across cell types (Kolde, 2018).

Results

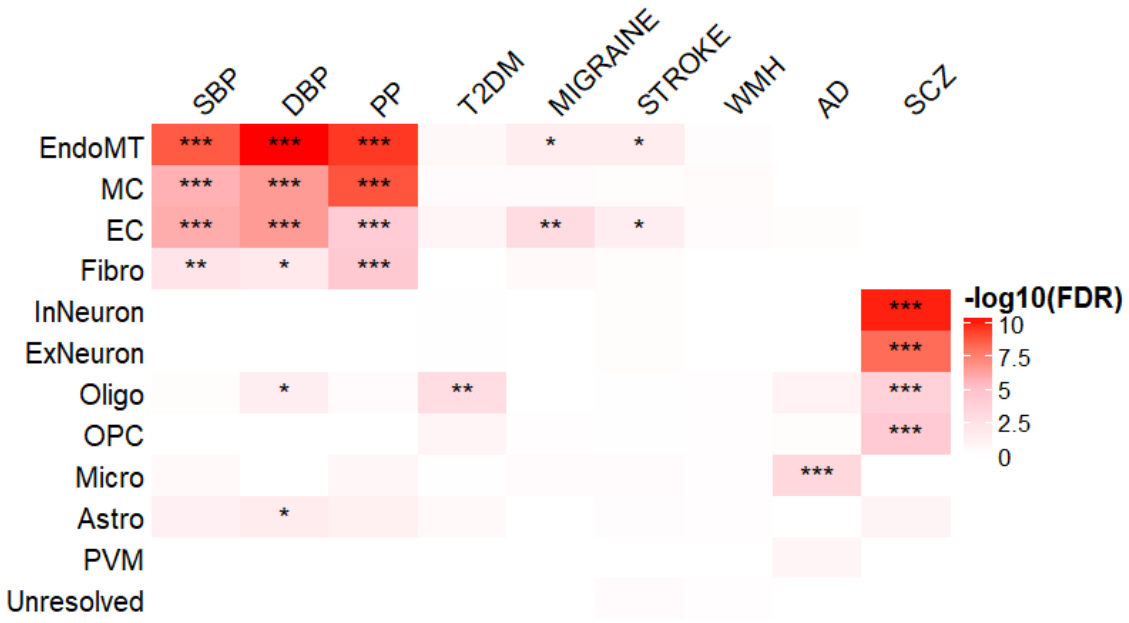

Figure 59. Heatmap of cell-type-disease association.

*Heatmap showing the enrichment of GWAS signals for traits across cell types. X-axis: traits; Y-axis: cell types (*** indicates FDR < 0.001, ** indicates 0.001 ≤ FDR < 0.01, * indicates 0.01 ≤ FDR < 0.05). SBP, Systolic Blood Pressure; DBP, Diastolic Blood Pressure; PP, Pulse Pressure; T2DM, Type 2 Diabetes Mellitus; WMH, White Matter Hyperintensities; AD, Alzheimer's Disease; SCZ, Schizophrenia.*

MAGMA identified a total of 2,531 unique genes associated with hypertension GWAS loci ($P < 5 \times 10^{-8}$) across three different blood pressure traits: 1,488 for systolic blood pressure (SBP), 1,432 for diastolic blood pressure (DBP), and 1,318 for pulse pressure (PP), a very large number reflecting the very many susceptibility loci associated with hypertension. Cell-type-disease association analysis results revealed that hypertension (SBP, DBP, PP) GWAS genes were mainly enriched in vascular cell types (EndoMT, MC, EC, and Fibro) (Figure 59). Additionally, DBP-specific GWAS genes were enriched in Oligo and Astro. Oligo was identified as the only significant cell type in T2DM. Migraine and stroke showed similar results—GWAS genes were enriched in EndoMT and EC. There was no statistically significant enrichment in WMH, and microglia was the only significant cell type in AD. SCZ-specific GWAS genes were highly enriched in neurons (ExNeuron and

InNeuron) and also enriched in two glial cell types—Oligo and OPC. This suggests trait-specific cell type vulnerability, where genetic risk factors converge on particular cell populations.

a

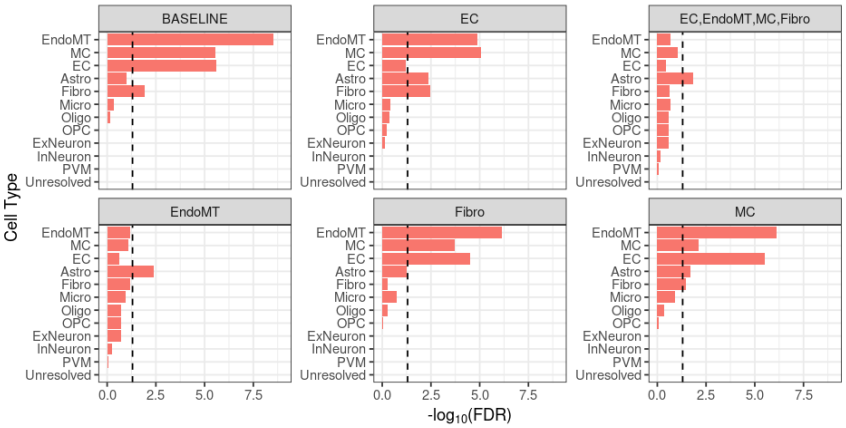

b

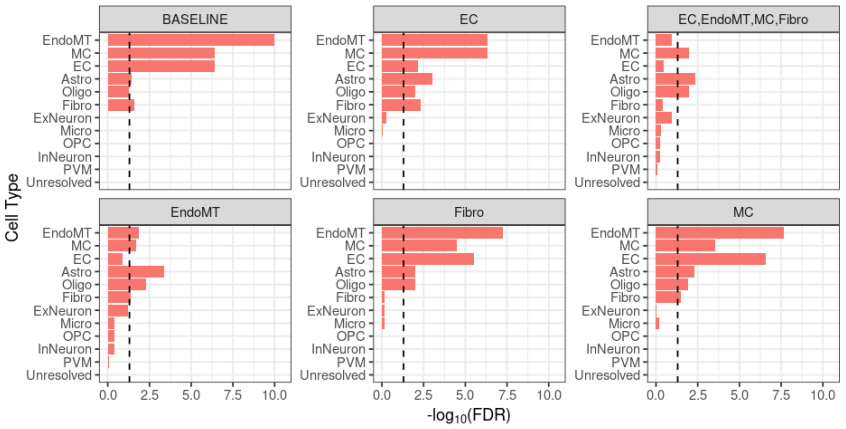

c

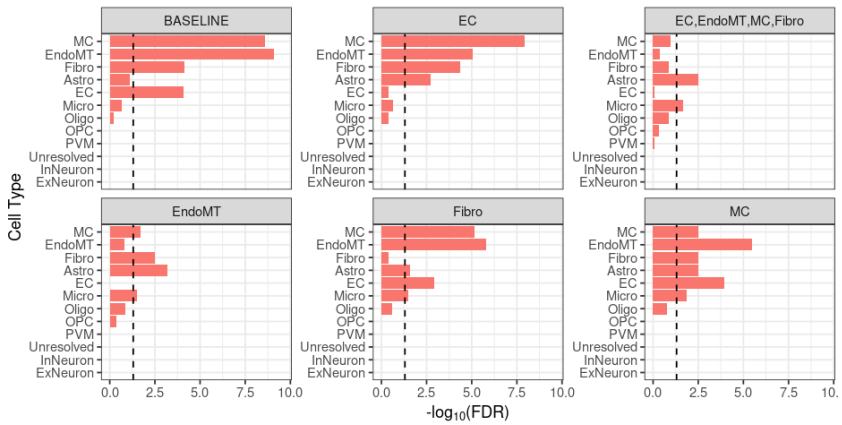

*Figure 60. Conditional cell-type enrichment analysis of SBP (**a**), DBP (**b**), and PP (**c**).*

Bar plots show the -log$_{10}$(FDR) for cell type enrichment across different conditional models: baseline, individual conditions, and the combined model (EC, EndoMT, Fibro, MC). FDR correction was performed using the Benjamini-Hochberg (BH) method. The top 10% mode was used for enrichment tests. The vertical dashed line indicates the significance threshold (FDR = 0.05).

The vascular cell types (EC, EndoMT, MC, Fibro) dominated the signals in hypertension GWAS (SBP, DBP, PP). However, this makes it difficult to decode whether other cell types are truly associated with hypertension, or whether some cell types appear enriched due to overlapping gene expression signatures with the top enriched cell types. Thus, I performed conditional cell-type enrichment across different conditional models, individually controlling for EC, MC, EndoMT, Fibro, and a combined model including all four cell types (Figure 60).

When conditioning on EndoMT, EC and MC signals decreased substantially. When conditioning on EC, EndoMT signals dropped but still remained significantly enriched, suggesting the EndoMT signature was not fully explained by the EC signature. However, MC signals remained largely unchanged after EC conditioning, indicating that MC enrichment was independent of the EC signature. A similar pattern was observed when conditioning on MC, EndoMT signals decreased but still remained significantly enriched, while EC enrichment remained stable. These suggest that EndoMT exhibited both EC and MC signatures, and EC and MC showed more independent signatures. Fibroblasts showed more overlaps with EndoMT and MC, but relatively less with EC.

Interestingly, a notable increase in enrichment signals from astrocytes was observed when conditioning on vascular cell types, indicating that astrocyte signals were previously masked by the stronger signals from the vascular cell types and suggesting that astrocyte-specific gene expression profiles may be associated with the hypertension GWAS. Also, significantly increased enrichment was observed for oligodendrocytes in DBP and microglia in PP, suggesting trait-specific genetic susceptibility of glial cell populations.

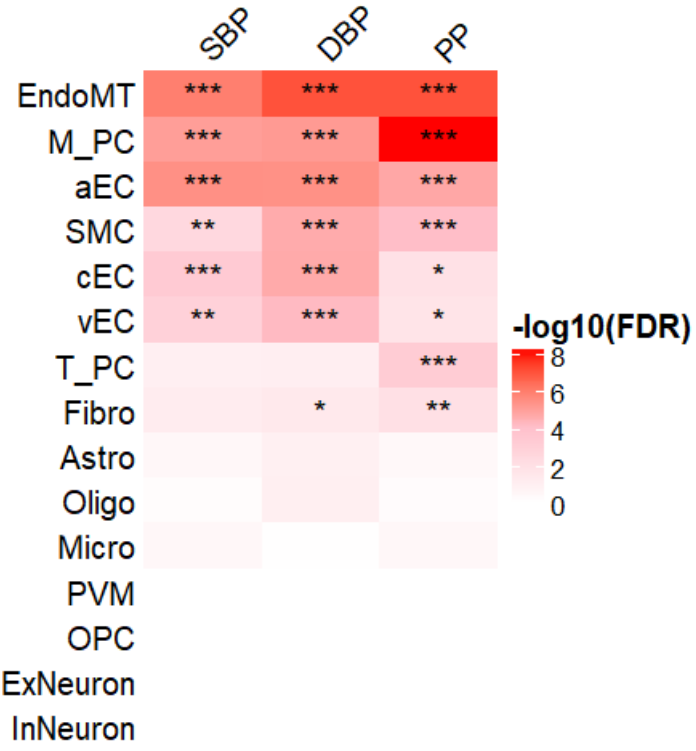

Figure 61. Heatmap of cell-subtype-hypertension association.

*Heatmap showing the enrichment of hypertension GWAS signals across cell subtypes. X-axis: traits; Y-axis: cell types (*** indicates FDR < 0.001, ** indicates 0.001 ≤ FDR < 0.01, * indicates 0.01 ≤ FDR < 0.05). SBP, Systolic Blood Pressure; DBP, Diastolic Blood Pressure; PP, Pulse Pressure.*

To further prioritise vascular subtypes in hypertension, endothelial cells were subdivided into arterial EC, capillary EC, venous EC; mural cells were classified into smooth muscle cells, transport pericytes, matrix pericytes. Then, I re-ran MAGMA.Celltyping analysis on this refined dataset. The analysis revealed significant enrichment of hypertension GWAS genes in endothelial and mural subtypes. EndoMT, M-PC, and aEC showed the strongest enrichment across all three blood pressure traits (Figure 61). Notably, T-PC showed enrichment only for PP. Conditioning on EndoMT, M-PC, and aEC produced similar results to conditioning on EndoMT, MC, and EC, attenuating the vascular signal while unmasking enrichment in astrocytes, microglia, and oligodendrocytes (Figure S 31).

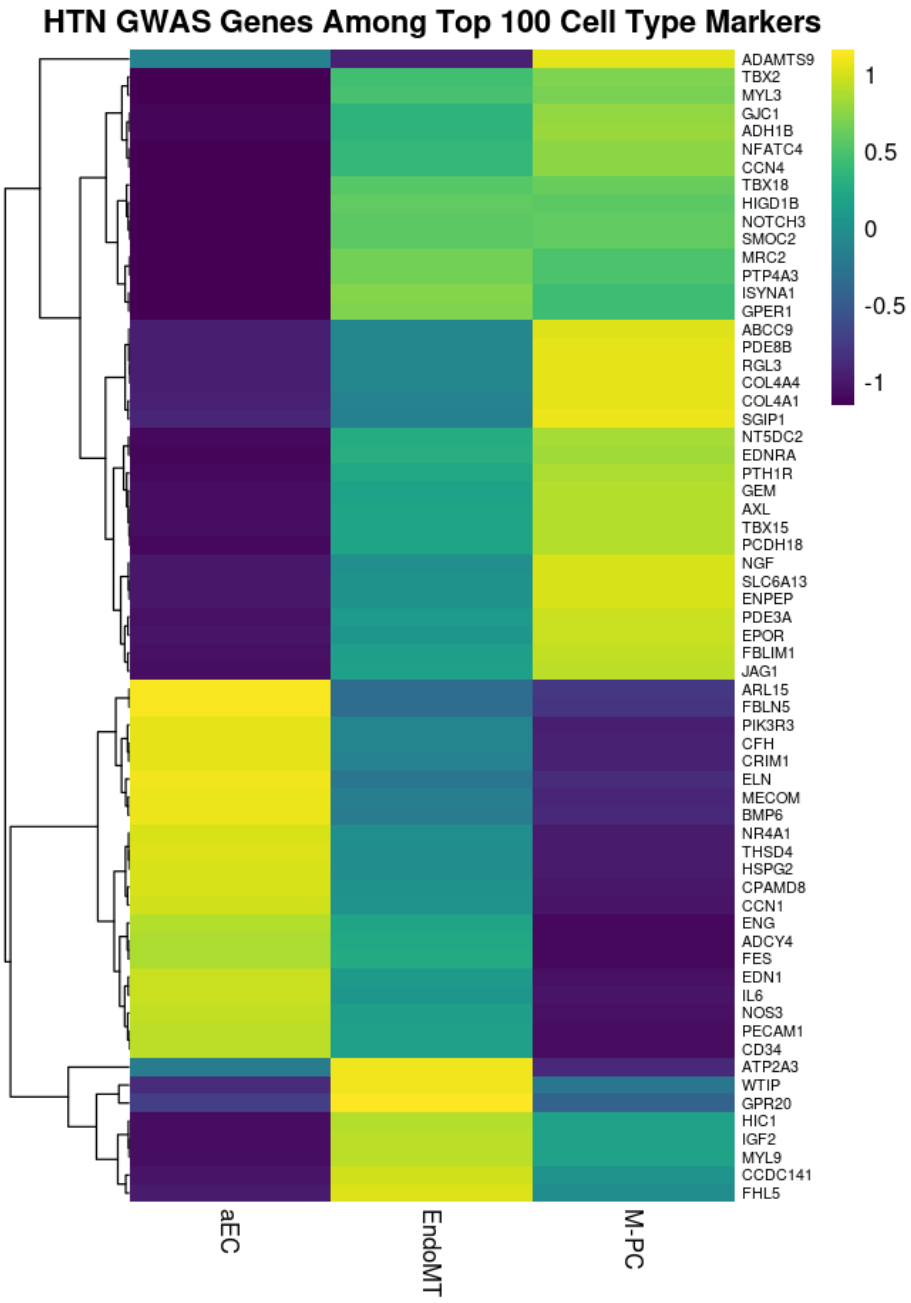

Figure 62. Expression heatmap of hypertension-associated GWAS genes overlapping top cell type-specific markers in aEC, EndoMT, and M-PC.

Only genes present in both the top 100 markers and the GWAS gene set ($p < 5 \times 10^{-8}$) were included. Rows represent genes, columns represent cell types, and colour represent scaled expression values.

I assessed the overlap between significant GWAS genes and the top 100 marker genes for aEC, EndoMT, and M-PC. A total of 21, 27, and 27 HTN-associated GWAS genes overlapped with the top markers in aEC, EndoMT, and M-PC, respectively. While the

number of overlapping genes was similar overall, the heatmap revealed broader expression patterns in EndoMT (Figure 62). This suggests that EndoMT may play a more active role in the pathogenesis of hypertension. Additionally, the heatmap revealed that each cell type had a unique gene set enriched.

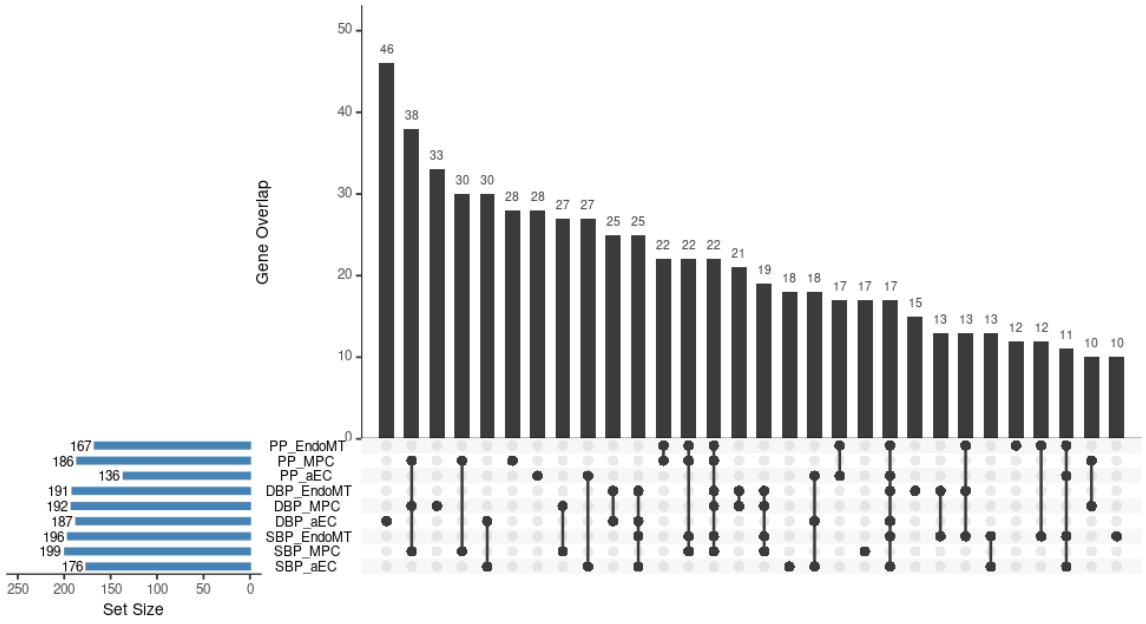

Figure 63. Upset plot of the intersection of significant GWAS genes among aEC, M-PC, and EndoMT across hypertension traits.

Horizontal bars represent the total number of significant GWAS genes associated with each trait-cell type combination, and vertical bars indicate the number of genes unique to or shared between specific groups (denoted by the dots below the bars). Significant GWAS genes were defined as those with p-values less than 5 x 10^{-8} in the MAGMA.Celltyping gene analysis. Only intersections involving at least 10 genes were shown.

I next assessed the overlap of significant hypertension GWAS genes across traits and key vascular cell types—aEC, M-PC, and EndoMT. The number of significant GWAS-identified hypertension-associated genes in vascular cell types showed a similar range overall (136 – 199 genes) (Figure 63). While there was substantial overlap in GWAS genes across traits and cell types, distinct gene sets were also observed in each cell type and trait combination.

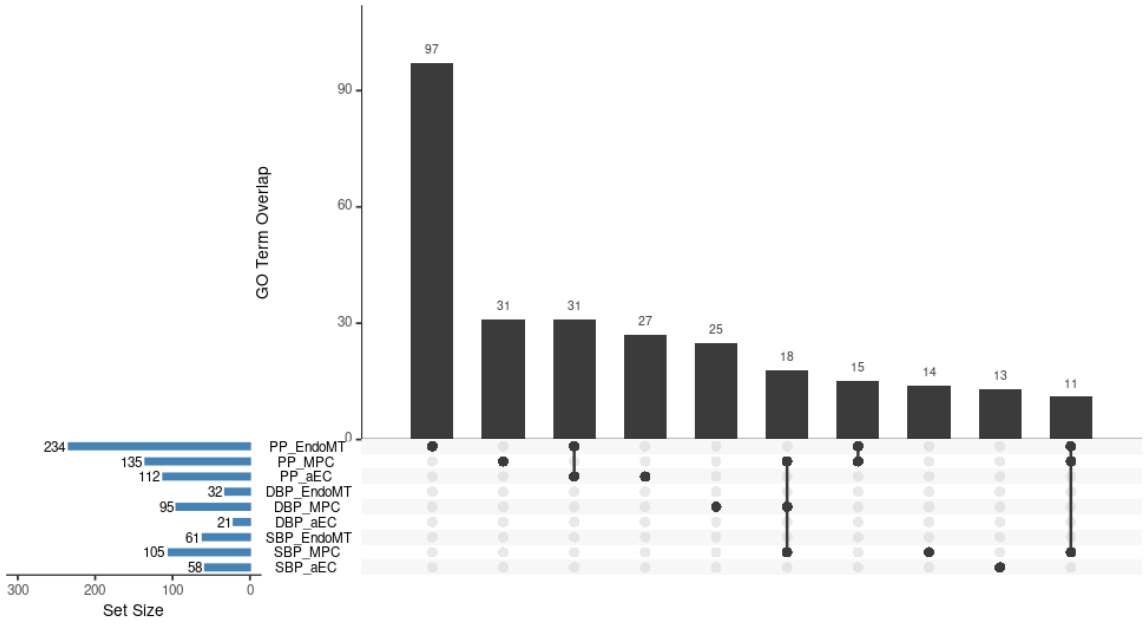

Figure 64. Upset plot of the intersection of GO terms among aEC, M-PC, and EndoMT across hypertension traits.

Horizontal bars represent the total number of GO terms associated with each trait-cell type combination, and vertical bars indicate the number of GO terms unique to or shared between specific groups (denoted by the dots below the bars). Only intersections involving at least 10 GO terms were shown.

To further understand the biological functions of the significant GWAS genes, I performed GO analysis for each cell type across the hypertension traits. The total number of enriched GO terms varied across groups, with PP_EndoMT showing the highest number of significant GO terms (234 GO terms), while DBP_aEC had the fewest (21 GO terms) (Figure 64). Interestingly, the largest overlaps involve aEC and EndoMT in the PP trait. Despite some shared pathways, the majority of cell type-trait combinations displayed distinct sets of enriched biological processes.

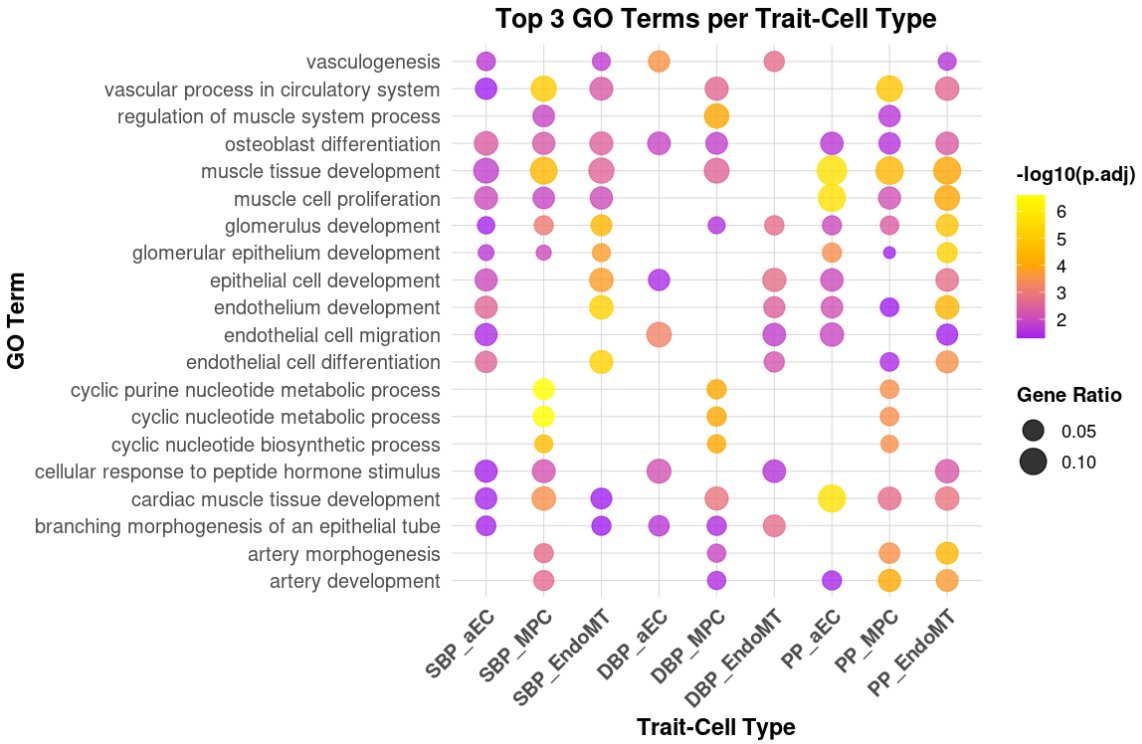

Figure 65. Dot plot of functional profiles for significant GWAS genes in each trait-vascular-cell type.

For each trait (SBP, DBP, PP), the top three significantly enriched GO terms per cell type (aEC, MPC, EndoMT) are shown. The dot size represents the gene ratio (proportion of genes associated with each GO term), and the colour scale indicates -log10(adjusted p-value).

Although the total number of significantly enriched GO terms varied across hypertension traits and vascular cell types, the top three most significant GO terms revealed strong convergence across groups (Figure 65). Processes related to vascular development, and endothelial and muscle-related differentiation consistently appeared in the top terms across all trait-cell type combinations, including aEC, M-PC, and EndoMT in SBP, DBP, and PP.

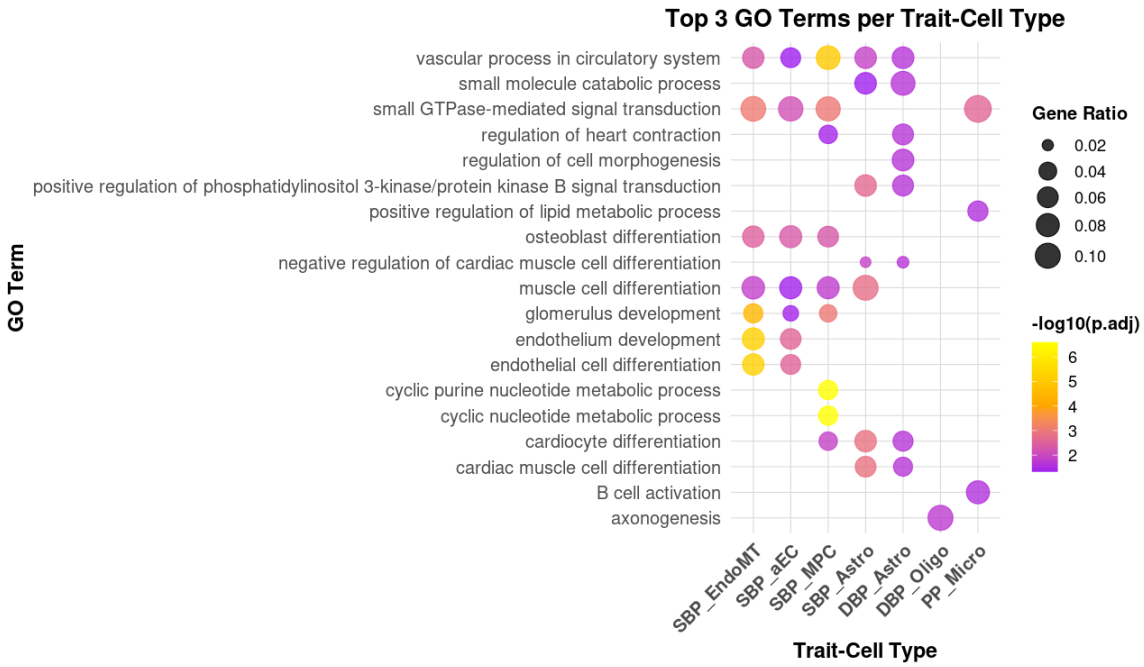

Figure 66. Dot plot of functional profiles for significant GWAS genes in each trait-cell type.

Dot plot showing the top three significantly enriched GO terms for each trait-cell type combination. Enrichment was performed using significant GWAS genes mapped to specific cell types (aEC, MPC, EndoMT, Astro, Oligo, Micro). Traits include SBP, DBP, and PP. The dot size represents the gene ratio (proportion of genes associated with each GO term), and the colour scale indicates -log10(adjusted p-value).

The number of significant GWAS genes was relatively consistent across glial cell types, ranging from 133 to 160 genes (Table S 10). Astrocyte hypertension GWAS genes were enriched for catabolic process, small GTPase signal transduction, and several pathways overlapped with those identified in vascular cell types. Microglia hypertension GWAS genes were uniquely enriched for B cell activation and lipid metabolic process, and oligodendrocytes hypertension GWAS genes were enriched for axonogenesis (Figure 66).

a

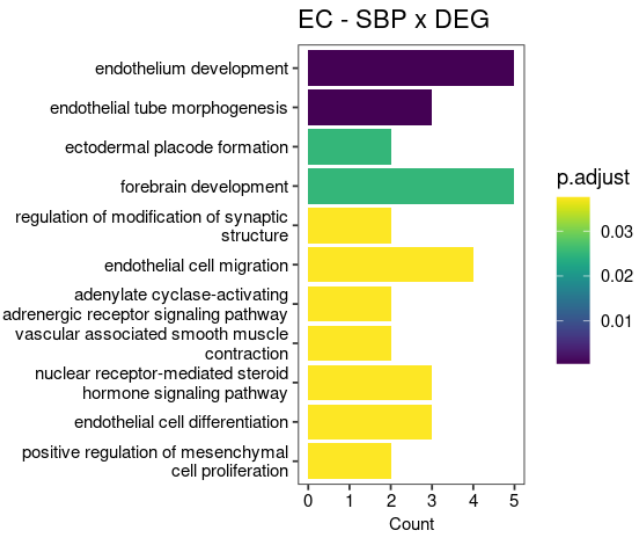

b

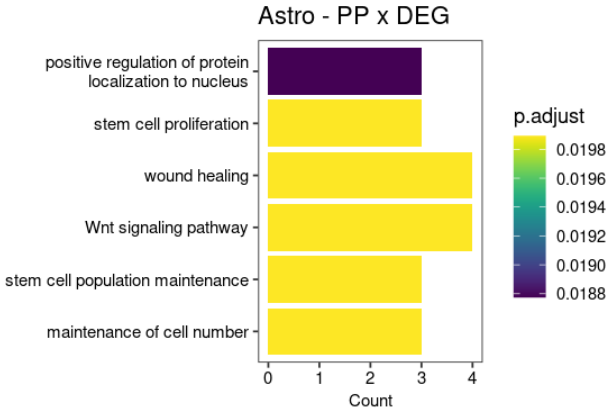

*Figure 67. Enriched Biological Process (BP) GO terms for overlapping genes between SBP-associated significant GWAS genes and HTN DEGs in endothelial cells (**a**); between PP-associated significant GWAS genes and HTN DEGs in astrocytes (**b**).*

The y-axis represents the GO terms, and the x-axis indicates the gene count associated with each term. The colour gradient corresponds to the adjusted p-value.

Since the number of differentially expressed genes in the aEC and M-PC subtypes was limited, I instead used broader EC and MC populations to assess the overlap between DEGs and significant hypertension GWAS genes. Only 5 overlapped genes (*NAB1,*

RHOA, VCL, ABO, HEY2) were identified in MC, no overlaps in EndoMT, 37 genes (3.0% of EC DEGs) in EC, 26 genes (3.6% of Astro DEGs) in Astro (Figure S 32).

Although there was no statistically significant enrichment between significant GWAS genes and DEGs in endothelial cells and astrocytes (Figure S 33), examining the identity of the overlapping genes remains valuable to help prioritise future studies. Enriched GO terms in endothelial cells included vascular development and differentiation, neurodevelopment, and adrenergic signalling pathways (Figure 67). GO analysis revealed that the overlapping genes between DEGs and significant GWAS genes from SBP, DBP, and PP shared similar GO terms (Figure S 34). Several genes within these pathways are worth highlighting *NCOA1, CTNNB1, RHOA, FOXP1, RAPGEF2* were associated with forebrain development, and *RHOA, KIF5B* were associated with regulation of modification of synaptic structure. Enriched GO terms in astrocytes included cellular maintenance and proliferation, and Wnt signalling pathway (*PLPP3, YAP1, FERMT2, ZNRF3*).

Discussion

Investigating GWAS gene enrichment in single-cell datasets is a powerful approach to understand pathogenic mechanisms and re-prioritise research efforts. This was particularly the case in AD where the enrichment of AD GWAS in microglia shifted the field to considering microglia and immune/inflammatory responses as central in AD (X. Liang et al., 2021; Nott & Holtman, 2023). It was therefore reassuring that I also observed the expected enrichment of AD GWAS in microglia in my single-nucleus dataset. Similarly as previously described, I found significant enrichment of SCZ GWAS genes in both inhibitory and excitatory neurons (Skene et al., 2018). This confirms the validity of the MAGMA.Celltyping approach and my prefrontal cortex single-nucleus dataset.

Hypertension is a multifactorial disease arising from the complex interplay between genetic, environmental, neural, renal, vascular, and immune mechanisms (Harrison et al., 2021). Interestingly, hypertension (SBP, DBP, PP) GWAS genes were strongly enriched in vascular cell types (EndoMT, MC, EC, and Fibro); and additionally DBP-associated GWAS genes were enriched in glial cell populations, oligodendrocytes and astrocytes. In the vascular subtypes, aEC and M-PC showed the strongest enrichment. This finding emphasises the role of vascular dysfunction in the pathogenesis of hypertension and extends this concept to the brain vasculature.

Since hypertension is a systemic disorder that is regulated by multiple organs, the role of brain vascular dysfunction should be considered within the broader physiological context, including the heart and kidneys, as a future study. The brain vascular system is not typically considered the causal organ in hypertension. However, it is interesting that endothelial-specific loss of *Gabrb3* affected brain development and led to hypertension (Agrud et al., 2022). A mouse model study has shown that EC-specific knockout of endothelin-1 leads to reduced blood pressure, highlighting the critical role of endothelial cells in maintaining vascular tone and systemic blood pressure (Kisanuki et al., 2010).

Also, another study has shown that EC-specific knockout of C-type natriuretic peptide in mice led to hypertension, impaired vasorelaxation, and increased endothelin-1 expression (Nakao et al., 2017). Caution is required with these studies as the hypertension could be due to non-specific effects of the knock-out. Nevertheless, the brain is a highly protected organ with multiple mechanisms in place to ensure sufficient vascular supply. It is therefore biologically plausible that genetic changes in the brain lead to a cascade of changes, including systemically, which raise blood pressure to ensure sufficient brain perfusion.

The MAGMA.Celltyping was performed only with brain cell types and other vascular beds were not included. It is therefore not possible to assess whether other vascular beds may have a stronger enrichment for hypertension GWAS genes than the brain. However, it is interesting that a tissue-specific analysis of hypertension GWAS loci, using FUMA—a web-based platform that maps genetic variants to genes and assesses their expression across tissues—also identified the brain as a significant contributor when considering a broader range of organs (Keaton et al., 2024).

Hypertension GWAS genes were highly enriched in the vascular cell types, but this may be due to overlapping gene expression signatures with the top enriched cell types. Conditional cell-type enrichment across different conditional models supported this. Interestingly, when conditioned on EndoMT, EC and MC signals decreased substantially, suggesting EndoMT as a critical cell state that is involved in the genetic risk architecture of hypertension.

Endothelial-to-mesenchymal transition is a biological process in which endothelial cells lose their typical features—such as intercellular adhesion and barrier integrity—and acquire mesenchymal cell traits including enhanced migration, contractility, and extracellular matrix production. EndoMT cell population exists as a continuum from partial EndoMT—where cells have both endothelial and mesenchymal features—to complete

EndoMT, characterised by the full acquisition of mesenchymal identity and loss of endothelial markers (Islam et al., 2021).

EndoMT plays essential roles during embryogenesis, such as in cardiac valve formation; however, it is now also recognised as a key contributor to pathological tissue remodelling in various diseases, including pulmonary hypertension, atherosclerosis, cerebral cavernous malformations, and lung fibrosis. EndoMT contributes to vessel wall thickening, neointimal formation, and loss of endothelial integrity—hallmarks of vascular remodelling in disease (Gorelova et al., 2021). In the context of disease, EndoMT is activated by inflammatory cytokines (e.g., IL-1β, TNF-α), disturbed shear stress, chronic TGF-β signalling, and Wnt signalling (Alvandi & Bischoff, 2021; Lu et al., 2019). Transcriptomic profiling has revealed that genes enriched in EndoMT are often involved in inflammation and fibrosis, which are highly relevant to the pathobiology of hypertension (Gorelova et al., 2021; Monteiro et al., 2021). Interestingly, angiotensin II can also induce EndoMT through the chromatin remodelling protein BRG1, contributing to fibrosis and cardiac dysfunction (Li et al., 2020). Collectively, these findings position EndoMT as a potential key contributor to the pathology of hypertension.

ATP2A3, WTIP, GPR20, HIC1, IGF2, MYL9, CCDC141, FHL5 exhibited selective enrichment in EndoMT relative to other key vascular cell populations such as aEC and M-PC. Among these genes, *MYL9* has previously been implicated in vascular injury and ageing, and was the only gene consistently differentially expressed across multiple post-injury time points in aged versus young rat arteries. Notably, *MYL9*, which encodes a protein involved in muscle contraction, was found to be upregulated not only in smooth muscle layers but also in the endothelial layer of aged arteries, implicating it in both contractile and endothelial remodelling processes (Shehadeh et al., 2011).

Despite the loss of significant enrichment signals in EC and MC on conditional analysis, they may still contribute to the pathogenesis of hypertension. EndoMT, EC and MC exist on a continuum; hence, genetic susceptibility could play a role in any of these cell types.

This suggests that genetic risk may not be confined to a single static cellular identity, but rather may exert its influence across a dynamic continuum of cell states.

Whilst vascular cell types dominated the hypertension GWAS enrichment, glial cell populations (astrocytes, oligodendrocytes, microglia) enrichment emerged when conditioning on vascular cell types. The biological processes involved were interesting. In astrocytes, pathways involved in catabolic processes, signal transduction, and cell differentiation were enriched; microglia uniquely showed enrichment for B cell activation and lipid metabolic process; oligodendrocytes were uniquely enriched for axonogenesis pathway.

Emerging evidence highlights the contribution of glial cell types, such as astrocytes, in mediating blood pressure. For instance, a study has shown that astrocytes act as intracranial baroreceptors, detecting reductions in cerebral perfusion pressure and activating central sympathetic circuits to elevate systemic arterial pressure and maintain brain blood flow. This process depends on calcium signalling and ATP release, forming a homeostatic feedback loop between the brain and the periphery (Marina et al., 2020). Also, angiotensin II has been shown to act on AT1 receptors expressed by astrocytes in the paraventricular nucleus of the hypothalamus, leading to inhibition of the astrocytic glutamate transporter GLT1. This inhibition results in elevated extracellular glutamate levels, which in turn activate extrasynaptic NMDA receptors on presympathetic neurons, increasing their excitability and driving enhanced sympathetic outflow and blood pressure (Stern et al., 2016).

Microglia, the brain’s resident immune cells, play a central role in driving neuroinflammation and enhancing neuronal excitability, both of which can contribute to elevated blood pressure. In hypertensive mice induced by angiotensin II or L-NAME, microglia in the paraventricular nucleus exhibited morphological activation and upregulation of inflammatory activation markers. Interestingly, targeted depletion of

microglia significantly attenuated neuroinflammation, suppressed NMDA receptor expression, reduced levels of vasopressin and norepinephrine, and ultimately lowered blood pressure. Conversely, the adoptive transfer of pre-activated microglia prolonged the pressor response to central angiotensin II (Shen et al., 2015).

Currently, there is limited direct evidence linking oligodendrocytes and hypertension; however, a brain imaging study has shown that hypertensive adults exhibit significantly reduced myelin content across multiple white matter regions, particularly in the corpus callosum, fronto-occipital fasciculus, temporal lobes, internal capsules, and corona radiata (Laporte et al., 2023). This reduction in myelin was independent of age, sex, and comorbidities, suggesting a direct relationship between elevated blood pressure and compromised cerebral white matter integrity (Laporte et al., 2023).

To further prioritise genes involved in hypertension pathology, I examined the overlap between differentially expressed genes and significant hypertension GWAS genes. The overlaps however were non-significant, suggesting the overlaps were occurring by chance. This is further supported by the finding that EndoMT, the cell population with the strongest genetic enrichment for hypertension, showed no overlap with differentially expressed genes, whereas capillary endothelial cells exhibited the largest number of DEGs. Therefore the observed DEGs are not likely due to changes caused by hypertension causal variants but instead are more likely secondary consequences of disease or long-term epigenetic changes. Nevertheless, the overlap helps with prioritising pathways for further study; for example, vascular development and differentiation, neurodevelopment, and adrenergic signalling pathway in EC.

Several genes are worth highlighting due to their known roles in vascular biology. Interestingly, small GTPases—which can be categorised into families like RhoA, Cdc42, and Rac1—are central regulators of endothelial migration and vascular health (Flentje et al., 2019). Interestingly, *RHOA* were found in both EC and MC overlapping gene sets, and

it was upregulated in EC and MC, suggesting widespread activation of the RhoA pathway in the hypertensive brain vasculature. Overactivation of RhoA leads to barrier dysfunction, vascular inflammation, and increased contractility (Yao et al., 2010). This supports a causal role of upregulated RhoA in driving hypertension. Unsurprisingly, there are more examples of the theme of deleterious and protective changes in hypertension. *MCL1*, which is essential for endothelial cell survival, was upregulated (Watson et al., 2016). *KLF7* promotes angiogenesis and endothelial survival, in part by activating NF-κB signalling pathway*,* which was upregulated in my study (Mao et al., 2023; Wu et al., 2022).

Astrocytes exhibited enrichment of the Wnt signalling pathway, with upregulation of genes including *PLPP3, YAP1, FERMT2, and ZNRF3*, suggesting activation of this pathway in the context of hypertension. A study has shown that astrocyte-derived Wnt secretions are essential for the maintenance of BBB integrity, suggesting astrocytic Wnt signalling may play a protective role (Guerit et al., 2021).

As with the DEGs, neuronal development and synaptic structure regulation were highlighted as enriched terms in EC. They have been assigned gene ontologies on the basis of functional studies in neurons and given these the types of genes involved (e.g. *CTNNB1, FOXP1, RAPGEF2*) which are expressed and functional in endothelial cells—it is more likely they regulate important aspects of vascular biology rather than mediating direct crosstalk with neurons. Their dysregulation in endothelial cells may thus impair the neurovascular unit by affecting BBB integrity and perfusion.

In summary, this chapter highlighted that hypertension-associated genetic risk converges on vascular cell types, especially EndoMT as a critical cell state, emphasising the role of vascular dysfunction in the pathogenesis of hypertension and even extending this concept to the brain vasculature. Furthermore, glial cells were also shown to be enriched for hypertension-associated genetic risk genes upon conditional analysis. Collectively, this suggests an important role of the brain in causing hypertension.

Conclusion & Future Studies

This study represents the first evaluation of the effects of hypertension and diabetes on the human prefrontal cortex at the single-cell level. It provides new insights into the role of these well-established vascular risk factors on brain dysfunction. Using a conservative analysis, we found that hypertension has pronounced effects on brain capillary endothelial cells and astrocytes. Surprisingly, substantial effects of diabetes were not evident. Hypertension induced unexpected transcriptomic changes in brain capillary endothelial cells, characterised by the downregulation of genes typically associated with neuronal function and synaptic organisation. Downregulation of these pathways was also observed in astrocytes and vascular smooth muscle cells, suggesting a common upstream driver across different cell types. Whilst hypertension GWAS candidate genes were strongly enriched in vascular cells, there was no significant overlap with differentially expressed genes, indicating that the observed transcriptomic changes are consequential rather than causal of hypertension. This means that with appropriate intervention, such as improved blood pressure control, it may be possible to prevent the molecular consequences of having hypertension.

We were able to achieve these insights by utilising a single-nucleus isolation method that efficiently extracted both parenchymal and vascular cell types. We thereby produced a large-scale single-nucleus atlas of the human prefrontal cortex comprised of 671,162 high-quality single nuclei from 43 donors. By capturing both parenchymal and vascular compartments, including vascular, neuronal, immune, and glial cell populations, the atlas provides a comprehensive architecture of the human brain vasculature. We were then able to test the hypothesis that vascular risk factors for dementia, specifically diabetes and hypertension, alter molecular pathways in brain vascular cells to affect neuronal function and ultimately lead to cognitive decline and brain atrophy. Furthermore, these

changes are expected to be discernible from significant alterations in gene expression. The findings partially support this hypothesis.

Differential gene expression analysis revealed the absence of transcriptomic changes in diabetes at the pseudobulk level, suggesting that the prefrontal cortex may be relatively protected from diabetes-associated pathology. In contrast, hypertension was associated with substantial transcriptomic alterations, particularly in vascular cell types (endothelial cells, mural cells, and endothelial-mesenchymal transition cells) and astrocytes, suggesting that hypertension hugely impacts molecular and cellular function in the glio-vasculature of the prefrontal cortex. Among endothelial cells, we found that capillary endothelial cells exhibited the most significant changes, while vascular smooth muscle cells were the only mural cell type that showed differential gene expression.

As key components of the BBB, brain endothelial cells protect the brain from pathogens and facilitate nutrient delivery to maintain brain homeostasis and neuronal function. A novel finding in my study is that hypertension downregulates genes related to cell adhesion, synaptic function and structure, and neuronal development in EC. This reduction in cell-cell adhesion points to potential BBB leakage and impaired barrier integrity in hypertension. Notably, the significant downregulation of genes in EC related to synaptic structure/function and neuronal guidance, which is unexpected and underexplored in EC. These changes were not limited to endothelial cells; mural cells, EndoMT, and astrocytes downregulated DEGs were also enriched for ion transport, neurodevelopment, cell-cell adhesion, and synaptic function. My analysis suggests that these traditional 'neuronal' genes may play important functional roles in non-neuronal cell types, particularly in regulating vascular and astrocytic processes related to vascular network development. This repurposing of gene programs is not entirely unexpected and is conceptually appealing since blood vessel networks will need to mirror neural networks and hence should be able to respond to the same guidance cues. However, further wet lab validation is needed to determine whether the downregulation of these 'neuronal'

genes in endothelial cells reflects a unique functional role or if this downregulation was merely a byproduct of signalling from the local environment.

A key recurring theme emerging from the findings is the inhibition of angiogenesis in hypertension. My finding suggests that this is driven by the downregulation of genes traditionally associated with neuronal function. Although expressed at lower levels in endothelial cells compared to neurons, genes such as *GABRB3, CNTNAP2, NRG1, ROBO2,* and *DCC* have all previously been reported to have roles in vascular integrity and angiogenesis. Their downregulation in hypertension suggests a widespread impairment in angiogenic signalling, which would be expected to contribute to NVU instability and reduced perfusion. These changes may then underlie brain atrophy and cognitive decline observed in hypertensive patients. Notably, a recent single-nucleus study has highlighted EC pathology in AD, further supporting the idea that maintaining BBB integrity and restoring effective angiogenesis can potentially slow the progression of early AD (Tsartsalis et al., 2024). Thus, targeting angiogenic pathways in EC may be an important strategy to shed light on preventing or slowing cognitive decline in hypertension.

The brain glio-vascular system also appears to play a central role in the development of hypertension. In particular, EndoMT emerged as a critical cell state involved in the genetic risk architecture of hypertension. This study also indicates the pivotal role of vascular dysfunction in the pathogenesis of hypertension, and even extends this concept to the brain vasculature. While hypertension is a systemic condition influenced by multiple organ systems, the contribution of brain vascular dysfunction should be considered within a broader physiological framework, including the heart and kidneys. However, the brain is a highly protected organ with stringent mechanisms to ensure adequate perfusion. It is therefore biologically plausible that genetic alterations in brain vasculature could initiate compensatory systemic responses, including elevated blood pressure, to preserve cerebral blood flow. It is important to note that the vasculature from other organs was not included in my study; therefore, as a future study, examining multiple vascular beds will be

essential to fully understand the organ-specific contributions to hypertension and to clarify whether the brain vasculature plays a central role in driving systemic blood pressure elevation.

There are many potential reasons for altered gene expression in disease states including genetic causation as well as direct and indirect consequences of disease processes which may include tissue injury or inflammation. Gene expression changes may also reflect epigenetic modifications from long-term exposure to a stimulus. In hypertension, despite treatment, blood pressure may not be adequately controlled, leading to cells being exposed to shear stress. It is also possible that signalling molecules implicated in causing hypertension, such as angiotensin II or endothelin, may persist despite treatment. Finally, the long-term drug treatments may also cause cellular changes. The findings from this study indicate that the molecular alterations observed in hypertensive prefrontal cortex are not due to hypertension GWAS genes. It was also not well-explained by altered cell-cell signalling. Therefore, chronic epigenetic changes seem a plausible hypothesis for the differentially expressed changes. As a future study, integrating multi-omic data, such as ATAC-seq and ChIP-seq, will be required to understand key drivers leading to transcriptional and functional changes in brain vascular and glial cells in hypertension.

There are many questions raised by this study which require future experiments to answer. For example, the lack of transcriptomic changes in diabetes is surprising and may be due to the conservative pseudobulk analysis we adopted. Single-cell analysis methods such as MAST may reveal more subtle transcriptomic changes (Finak et al., 2015). Furthermore, other brain regions may be more impacted by diabetes, and single-cell sequencing of regions such as the hippocampus or caudate should be undertaken.

Whilst we observed substantial transcriptomic changes associated with hypertension, the upstream mechanisms driving these alterations and their precise contribution to neurodegeneration and dementia remain unknown. This will likely require experiments in model systems, such as mouse models and human iPSC models, to test these

hypotheses. For example, if the downregulation of key genes in endothelial cells or astrocytes leads to altered trophic support of neurons, this could be tested by targeted genetic knockdown or knockout of selected genes, followed by assessment of neuronal function. We also have not established the driver of the hypertension-associated gene expression changes, and this might plausibly arise from the cerebral vessels exposed to the physical stressors of increased pressure or from changes in systemic signalling molecules such as angiotensin II. These could be investigated in model systems designed to mimic chronic exposures, in order to assess whether similar gene expression changes occur and whether these are accompanied by impaired brain function or neurodegeneration. This could then lead to a potential therapeutic target for preventing or slowing dementia progression.

Appendices

Appendix A. Supplementary Tables

Table S 1. Age, sex, BMI, and clinical diagnosis of donors (n = 43).

Donor	Age	BMI	Sex	HTN - Diagnosis	DIAB - Diagnosis
2	87	25.81	F	CTRL	CTRL
3	83	33.65	M	HTN	DIAB
5	89	NA	F	CTRL	CTRL
6	74	36	M	CTRL	DIAB
7	91	NA	M	HTN	CTRL
8	84	NA	M	HTN	DIAB
10	69	36.9	F	CTRL	DIAB
11	99	16.8	F	CTRL	CTRL
12	92	16.53	F	HTN	CTRL
13	71	31	F	HTN	CTRL
14	78	29.2	M	HTN	CTRL
15	68	25.1	M	HTN	CTRL
16	86	26.9	F	CTRL	DIAB
17	73	29.6	M	HTN	DIAB
19	80	NA	F	CTRL	DIAB
20	70	23.41	M	CTRL	DIAB
21	88	24	M	HTN	DIAB
22	97	22.6	M	HTN	CTRL
23	75	33.8	M	CTRL	DIAB
24	84	22	F	HTN	CTRL
25	86	15	M	CTRL	CTRL
26	82	20.8	M	CTRL	CTRL
27	71	40	M	HTN	DIAB
28	82	26	M	HTN	CTRL
29	78	29.5	F	CTRL	CTRL
30	73	NA	M	HTN	CTRL
31	69	25.6	M	HTN	DIAB
32	71	30.5	F	HTN	DIAB
34	65	34.2	F	CTRL	CTRL
35	61	32.7	M	HTN	CTRL
36	60	25.7	M	HTN	DIAB
37	101	21	F	CTRL	CTRL
38	82	NA	F	CTRL	DIAB
39	85	29	F	HTN	DIAB
40	86	23.8	F	HTN	CTRL
41	64	NA	M	CTRL	CTRL
42	67	NA	M	HTN	CTRL
43	89	30	F	HTN	DIAB
44	84	32	M	HTN	DIAB
46	65	32	M	HTN	DIAB
47	85	26.86	M	HTN	CTRL
48	60	40.1	M	HTN	CTRL
50	91	27	M	HTN	DIAB

NA, Non Applicable.

Table S 2. Cause of death of donors (n = 43).

Donor	Cancer	Infection	Kidney Disease	Heart Disease	Pulmonary Disease	Other
2		●			●	
3			●	●		
5		●				
6		●				
7				●		
8						●
10	●					
11					●	
12	●					
13		●				
14	●					
15						●
16	●					
17			●	●		
19				●	●	
20	●					
21			●	●		
22		●				
23	●					
24	●					●
25		●				●
26	●					
27	●					
28	●					
29	●					
30	●					
31				●		
32				●		
34	●					
35				●		
36				●		
37				●		
38	●					
39	●					
40	●					
41				●		
42	●					
43		●				
44	●					
46			●	●		●
47				●		
48		●		●	●	
50			●			

Table S 3. The use of hypertension medications of donors (n = 43).

Donor	Beta-Blockers	Calcium Channel Blockers	ACE-I/ARB	Alpha-Blockers	Thiazide	Hydralazine	Spironolactone
2							
3	●	●					
5							
6							
7	●		●	●			
8	●						
10	NA	NA	NA	NA	NA	NA	NA
11	NA	NA	NA	NA	NA	NA	NA
12	●	●					
13	●		●				●
14	●				●		
15	●		●				
16			●				
17	●		●	●			
19							
20							
21			●				
22			●				
23							
24	●		●				
25							
26							
27	●		●				
28			●				
29			●				
30	NA	NA	NA	NA	NA	NA	NA
31		●					
32			●	●			
34							
35					●		
36		●	●		●		
37	●						
38		●					
39	●						
40	NA	NA	NA	NA	NA	NA	NA
41							
42		●	●				
43	●		●		●		
44			●				
46	●		●			●	●
47	●		●		●		●
48		●					
50		●		●			

ACE-I, Angiotensin-Converting Enzyme Inhibitors; ARB, Angiotensin Receptor Blockers; NA, Non Applicable.

Table S 4. The use of diabetes medications of donors (n = 43).

Donor	Insulin	Metformin	Thiazolidinediones	Sulfonylureas	Others (Hypoglycaemics)
2					
3					
5					
6		●		●	
7					
8	●				
10	NA	NA	NA	NA	NA
11	NA	NA	NA	NA	NA
12					
13					
14					
15					
16					
17	●				
19					●
20				●	
21					
22					
23					
24					
25					
26					
27					
28					
29					
30					
31		●		●	
32	●	●		●	
34					
35					
36	●	●			
37					
38	●			●	
39	●	●			
40					
41					
42					
43		●			
44				●	
46	●				
47					
48					
50	●		●	●	

NA, Non Applicable.

Table S 5. The use of other medications of donors (n = 43).

Donor	Nitrates	Antiplatelet	Anticoagulant	Statin	Steroid	Pain Killers
2			●			●
3		●	●	●	●	
5						●
6		●		●		
7	●		●	●		
8			●		●	
10	NA	NA	NA	NA	NA	
11	NA	NA	NA	NA	NA	
12					●	●
13			●			●
14		●		●	●	●
15						
16	●	●		●		
17	●	●		●		●
19			●			
20					●	●
21			●	●		
22						
23		●				●
24		●				
25		●				●
26						●
27	●	●		●		
28		●			●	●
29				●		
30	NA	NA	NA	NA	NA	NA
31						
32				●		
34						
35						
36		●		●		●
37	●				●	●
38			●			●
39			●		●	●
40						●
41						
42		●		●		●
43	●		●			
44					●	●
46	●	●		●		
47	●	●	●	●		
48				●		
50		●		●		●

NA, Non Applicable.

Table S 6. Brain bank source, Braak stage, APOE status, and postmortem interval of donors (n = 43).

Donor	Brain Bank	Braak Lewy Body Stage	Braak Tangle Stage	APOE Status	Postmortem Interval (Hours)
2	Bristol	NA	3	APOE=2/3	NA
3	Bristol	0	2	APOE=3/3	NA
5	Newcastle	0	3	APOE=3/3	98
6	Newcastle	0	1	APOE=3/4	25
7	Newcastle	0	2	APOE=3/3	29
8	Edinburgh	0	1	NA	NA
10	Newcastle	0	1	APOE=3/3	16
11	Newcastle	0	3	APOE=3/3	19
12	Bristol	0	2	APOE=3/3	NA
13	Newcastle	0	0	APOE=3/3	72
14	Bristol	0	2	APOE=3/3	NA
15	Edinburgh	NA	NA	NA	NA
16	Newcastle	0	3	APOE=3/3	27
17	Newcastle	0	3	APOE=3/3	40
19	Newcastle	0	2	APOE=2/3	12
20	Bristol	NA	NA	APOE=3/3	NA
21	Newcastle	0	2	APOE=3/3	23
22	Newcastle	0	2	APOE=3/3	23
23	Newcastle	0	0	APOE=3/3	20
24	Netherlands	3	3	NA	NA
25	Netherlands	NA	NA	NA	NA
26	Bristol	NA	NA	APOE=3/3	NA
27	Newcastle	0	1	NA	25
28	Netherlands	NA	NA	NA	NA
29	Newcastle	0	2	APOE=2/3	23
30	Bristol	NA	NA	APOE=3/3	NA
31	Edinburgh	NA	NA	NA	NA
32	Edinburgh	NA	NA	NA	NA
34	Newcastle	0	1	NA	47
35	Edinburgh	NA	NA	NA	NA
36	Edinburgh	NA	NA	NA	NA
37	Netherlands	NA	NA	NA	NA
38	Bristol	NA	NA	APOE=3/3	NA
39	Netherlands	NA	NA	NA	NA
40	Newcastle	3	1	NA	22
41	Newcastle	0	1	NA	93
42	Newcastle	0	0	APOE=3/3	22
43	Netherlands	0	NA	NA	NA
44	Newcastle	1	2	NA	81
46	Newcastle	0	0	APOE=3/3	55
47	Bristol	NA	2	APOE=3/3	NA
48	Edinburgh	NA	NA	NA	NA
50	Newcastle	0	3	APOE=3/4	24

NA, Non Applicable.

Table S 7. Top 10 marker genes of each cell type.

Cell Type	Gene	Cell Type	Gene	Cell Type	Gene
EC	*FLT1*	MC	*CARMN*	EndoMT	*HEYL*
EC	*ENSG00000287338*	MC	*SLC38A11*	EndoMT	*COL6A2*
EC	*ABCB1*	MC	*SLC19A1*	EndoMT	*TBX2*
EC	*MECOM*	MC	*NOTCH3*	EndoMT	*CYSLTR2*
EC	*SMAD6*	MC	*RNF152*	EndoMT	*PEAR1*
EC	*ATP10A*	MC	*PTH1R*	EndoMT	*SLC12A7*
EC	*CP*	MC	*P2RY14*	EndoMT	*LAMC3*
EC	*VWF*	MC	*GJC1*	EndoMT	*SLC6A12*
EC	*CD34*	MC	*CRISPLD2*	EndoMT	*CSPG4*
EC	*ST8SIA6*	MC	*SLC6A12*	EndoMT	*GJC1*
Oligo	*PLP1*	OPC	*ENSG00000278254*	Astro	*ETNPPL*
Oligo	*ENSG00000286558*	OPC	*BEST3*	Astro	*AQP4*
Oligo	*OPALIN*	OPC	*FERMT1*	Astro	*GFAP*
Oligo	*MOG*	OPC	*COL20A1*	Astro	*SLC14A1*
Oligo	*ST18*	OPC	*LHFPL3*	Astro	*SLC1A2*
Oligo	*LINC01608*	OPC	*CACNG5*	Astro	*ADGRV1*
Oligo	*ERMN*	OPC	*MYT1*	Astro	*RGS20*
Oligo	*LINC01792*	OPC	*PDGFRA*	Astro	*PAX6*
Oligo	*MOBP*	OPC	*GALR1*	Astro	*LINC00499*
Oligo	*FOLH1*	OPC	*GPNMB*	Astro	*SLC39A12*
ExNeuron	*LINC02263*	InNeuron	*DLX6-AS1*	Fibro	*CEMIP*
ExNeuron	*CBLN2*	InNeuron	*GAD2*	Fibro	*FBLN1*
ExNeuron	*TESPA1*	InNeuron	*GAD1*	Fibro	*ABCA9*
ExNeuron	*ENSG00000235337*	InNeuron	*ABTB3*	Fibro	*FAM20A*
ExNeuron	*MCHR2*	InNeuron	*GRIN3A*	Fibro	*BICC1*
ExNeuron	*EPIC1*	InNeuron	*ENTPD3*	Fibro	*LINC01088*
ExNeuron	*CABP1*	InNeuron	*GRIK1*	Fibro	*ABCA10*
ExNeuron	*ENSG00000224819*	InNeuron	*GRIP1*	Fibro	*ABCA6*
ExNeuron	*NRGN*	InNeuron	*ANK1*	Fibro	*LAMB1*
ExNeuron	*ENC1*	InNeuron	*SLC35F4*	Fibro	*APOD*
Micro	*RGS1*	PVM	*PTPRC*	Unresolved	*EYS*
Micro	*ADAM28*	PVM	*IQGAP2*	Unresolved	*LINC01320*
Micro	*ENSG00000287684*	PVM	*MYO1F*	Unresolved	*ENSG00000231918*
Micro	*TLR2*	PVM	*CARD11*	Unresolved	*AGBL1*
Micro	*APBB1IP*	PVM	*AOAH*	Unresolved	*ENSG00000248752*
Micro	*CYBB*	PVM	*PIK3R5*	Unresolved	*CCDC26*
Micro	*ENSG00000287616*	PVM	*STAB1*	Unresolved	*ADAMTSL1*
Micro	*CSF3R*	PVM	*DOCK2*	Unresolved	*LINC02055*
Micro	*FGD2*	PVM	*TBXAS1*	Unresolved	*PKN2-AS1*
Micro	*SLC11A1*	PVM	*ARHGAP15*	Unresolved	*MIR3681HG*

Table S 8. The number of genes and the hub gene in each module in the astrocytes dataset.

Module	**# of Genes (Combined)**	**Hub Gene (Combined)**	**# of Genes (HTN)**	**Hub Gene (HTN)**	**# of Genes (CTRL)**	**Hub Gene (CTRL)**
Black	327	*CATSPERE*	411	*CATSPERE*	458	*LLGL2*
Blue	979	*KCNH5*	964	*SLC30A7*	1,518	*STK32B*
Brown	525	*TCF4*	684	*PDE9A*	1,075	*KIFC2*
Cyan	117	*SBNO2*	118	*MRPS6*	190	*TMED10*
Darkgreen	28	*TERF2IP*	43	*MSM01*	50	*SYNPO2*
Darkgrey	26	*FXYD6*	41	*ANKRD33B*	30	*DCAKD*
Darkorange	NA	NA	29	*ZNF846*	21	*MVD*
Darkred	31	*NFIA*	48	*PEX5*	66	*CCDC102B*
Darkturquoise	27	*CCDC6*	43	*FBXO34*	35	*INSIG1*
Green	390	*ELL2*	473	*PTGES3*	614	*PICALM*
Greenyellow	170	*FRMD4B*	179	*FRMD4B*	291	*FRMD4B*
Grey60	37	*ZNF706*	80	*FAM13A*	110	*MNAT1*
Lightcyan	69	*ZNF44*	98	*PLXND1*	112	*LDHA*
Lightgreen	34	*AKT3*	78	*ARHGEF11*	109	*MAP1LC3A*
Lightyellow	34	*PSMC4*	68	*NEO1*	78	*BCL3*
Magenta	229	*DNM1L*	211	*ARRDC3*	298	*EIF5B*
Midnightblue	80	*ATP13A4*	107	*CARF*	176	*TGFB2*
Orange	20	*MSMO1*	38	*PARD3*	27	*HNRNPK*
Pink	282	*KLF12*	277	*MICU3*	333	*TCERG1*
Purple	175	*ARL13B*	198	*PRPF38B*	297	*KCNJ10*
Red	329	*UBR3*	421	*CDH18*	464	*FAM20C*
Royalblue	32	*RFX2*	59	*CDK4*	68	*MINPP1*
Salmon	120	*TRIO*	158	*NRXN1*	221	*RANBP9*
Skyblue	NA	NA	25	*ZNF248*	NA	NA
Tan	158	*PTGES3*	159	*ARL13B*	287	*CDKL1*
Turquoise	1,069	*SLC35F5*	990	*ZFYVE28*	1,976	*ZDHHC17*
White	NA	NA	25	*TXLNA*	NA	*NA*
Yellow	422	*SLC39A14*	580	*ZHX3*	1,060	*SDC2*

NA, Non Applicable.

Table S 9. The number of genes and the hub gene in each module in the vascular smooth muscle cells dataset.

Module	**# of Genes (Combined)**	**Hub Gene (Combined)**	**# of Genes (HTN)**	**Hub Gene (HTN)**	**# of Genes (CTRL)**	**Hub Gene (CTRL)**
Black	63	*HDAC4*	37	*UBR4*	255	*PPFIBP2*
Blue	502	*MBTD1*	485	*STAT3*	1,181	*TYW1*
Brown	467	*AHCTF1*	333	*CNTNAP2*	622	*AGBL4*
Green	252	*YBX3*	50	*TCF25*	366	*RCAN2*
Greenyellow	NA	NA	20	*CNNM2*	NA	NA
Magenta	33	*NOTCH3*	35	*PTH1R*	NA	NA
Pink	42	*HDAC9*	37	*PTGES3*	149	*ANKIB1*
Purple	25	*DENND3*	31	*PRMT9*	NA	NA
Red	251	*KCMF1*	49	*DENND3*	279	*CAMK2D*
Turquoise	569	*BTBD9*	806	*BTBD9*	1,253	*HNRNPD*
Yellow	449	*CNTNAP2*	143	*KAT2B*	483	*ZNF592*

NA, Non Applicable.

Table S 10. Number of significant GWAS genes (p-value < 5 x 10^{-8}) for each trait-cell type combination.

Trait-Cell Type	Number of Significant GWAS genes
SBP_Astro	160
DBP_Astro	157
PP_Astro	133
DBP_Oligo	147
PP_Micro	134
SBP_EC	201
SBP_MC	164
DBP_EC	214
DBP_MC	150
PP_EC	157
PP_MC	161

Appendix B. Supplementary Figures

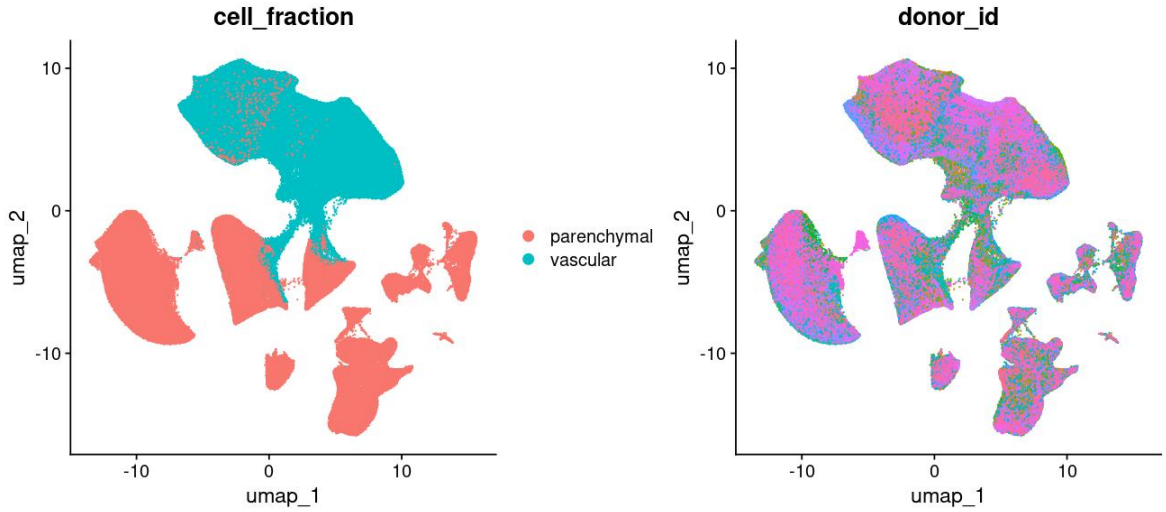

Figure S 1. UMAP plot labelled by cell fraction and donor.

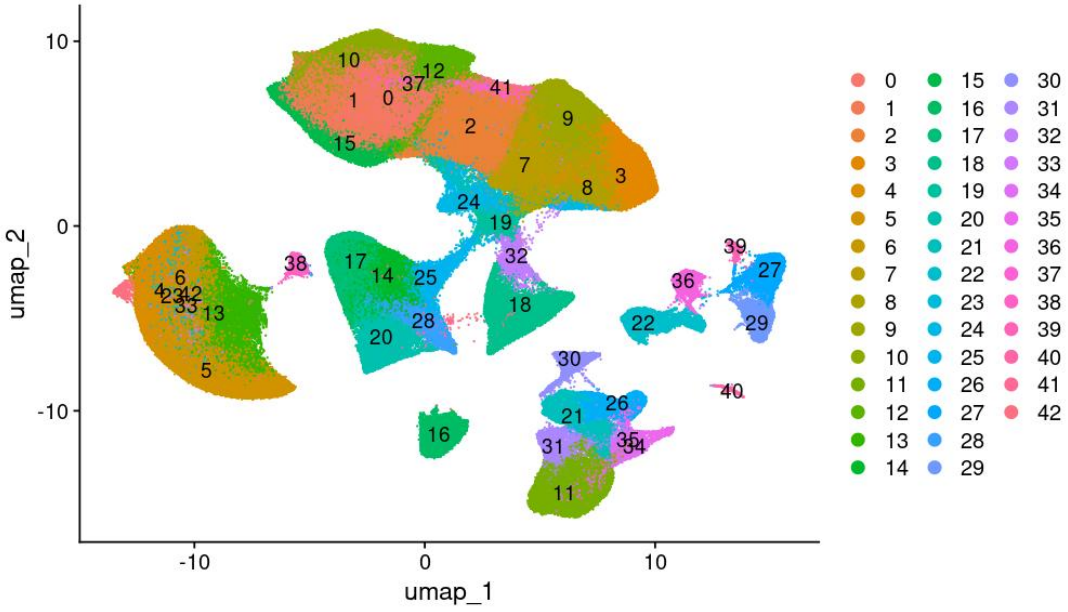

Figure S 2. UMAP of 43 clusters from the whole dataset for cell annotation.

Resolution: 1.0.

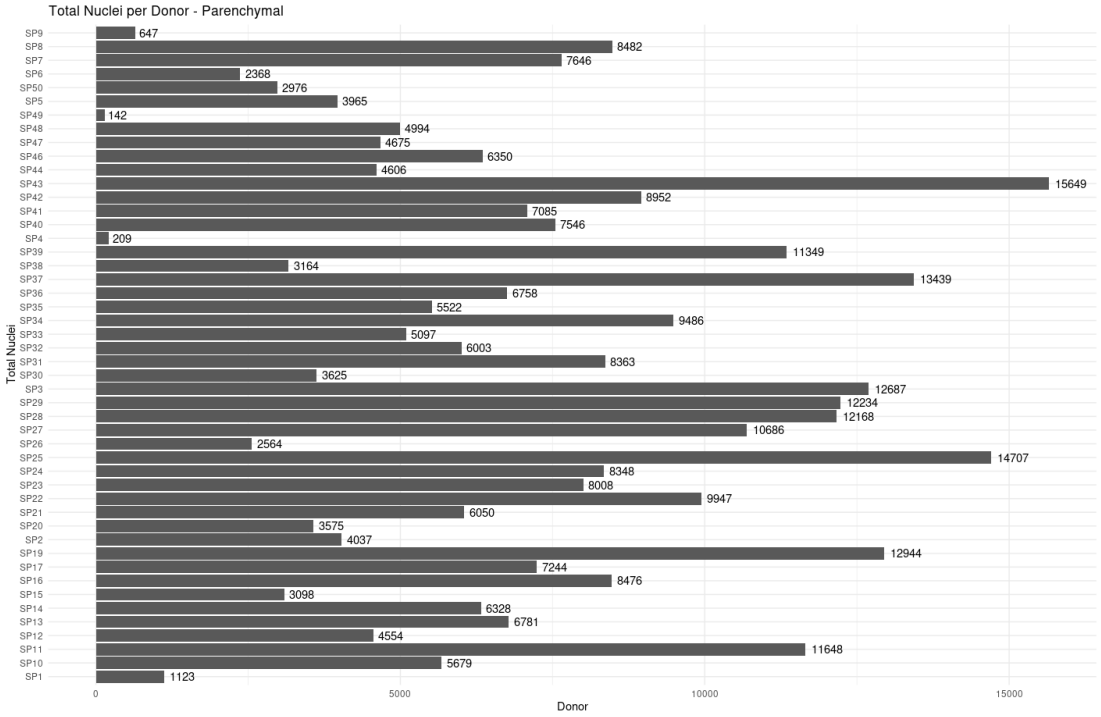

Figure S 3. The total number of nuclei in each donor parenchymal sample (n = 48).

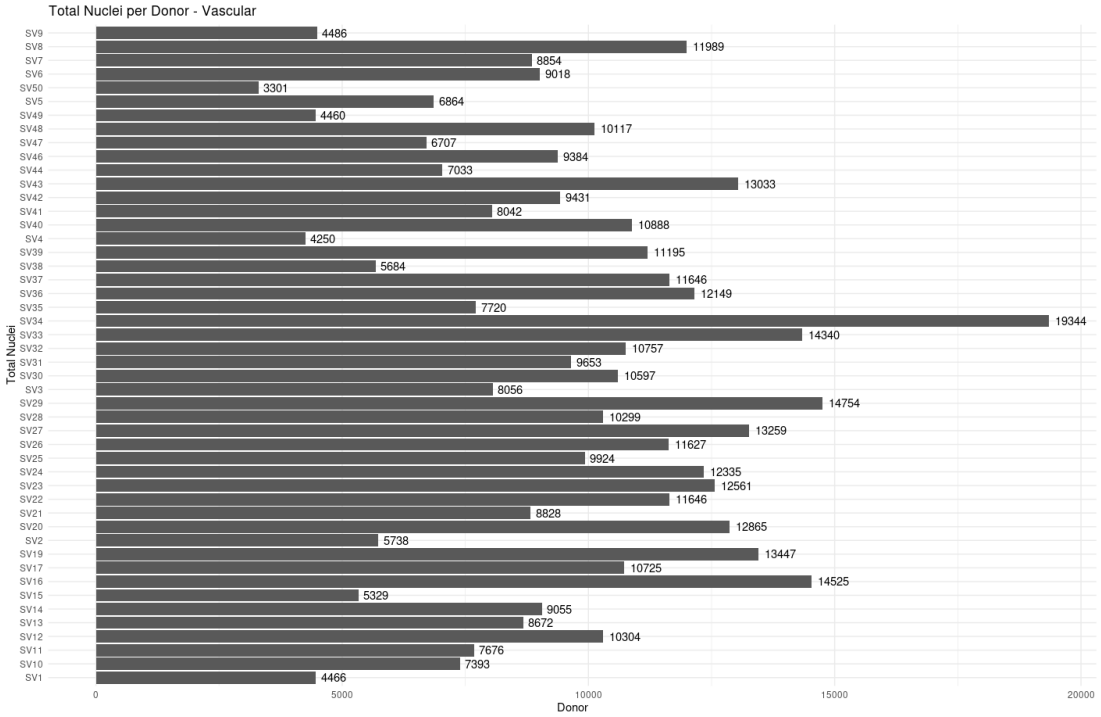

Figure S 4. The total number of nuclei in each donor vascular sample (n = 48).

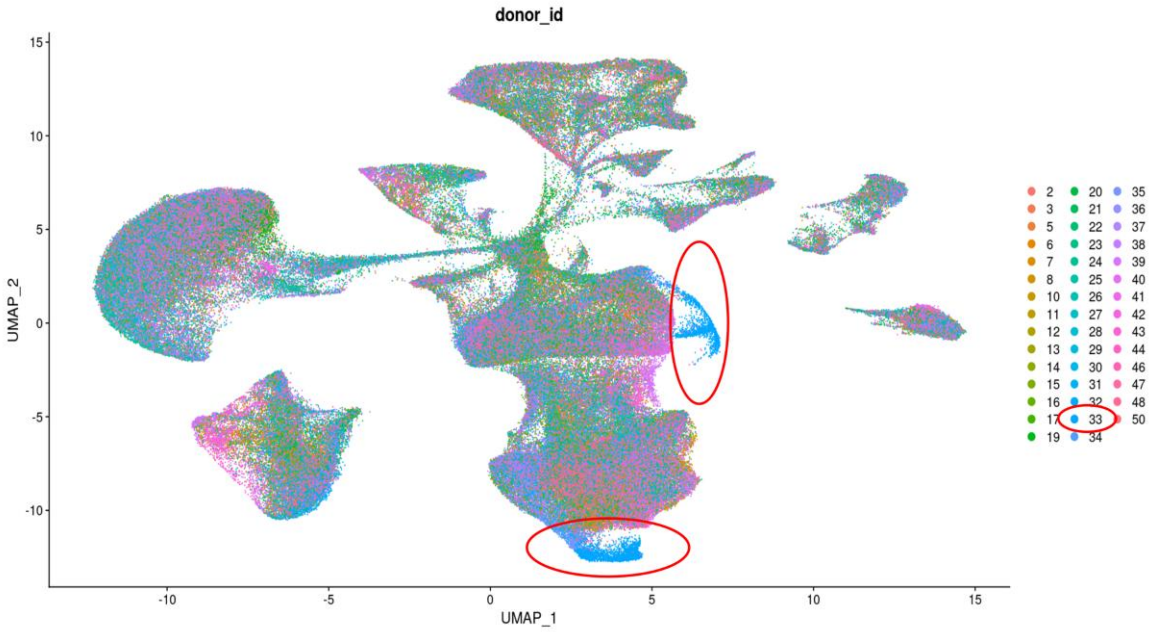

Figure S 5. Batch effects detected in Donor 33 (n = 44).

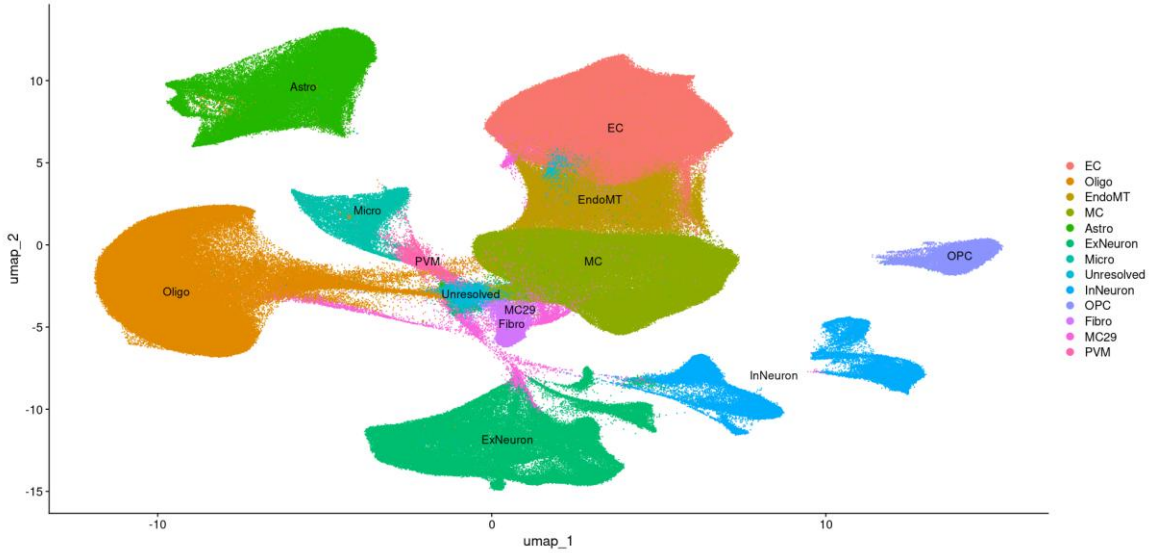

Figure S 6. Low-quality cluster 'MC29', which was highly expressing mitochondrial genes (n = 43)

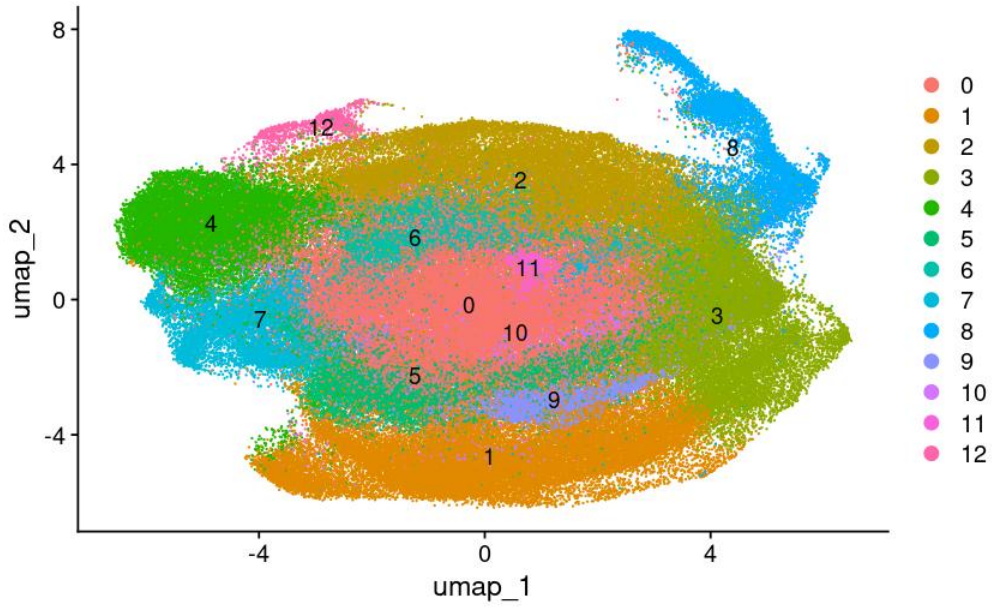

Figure S 7. UMAP of 13 clusters from the EC dataset for cell annotation.

Resolution: 0.3.

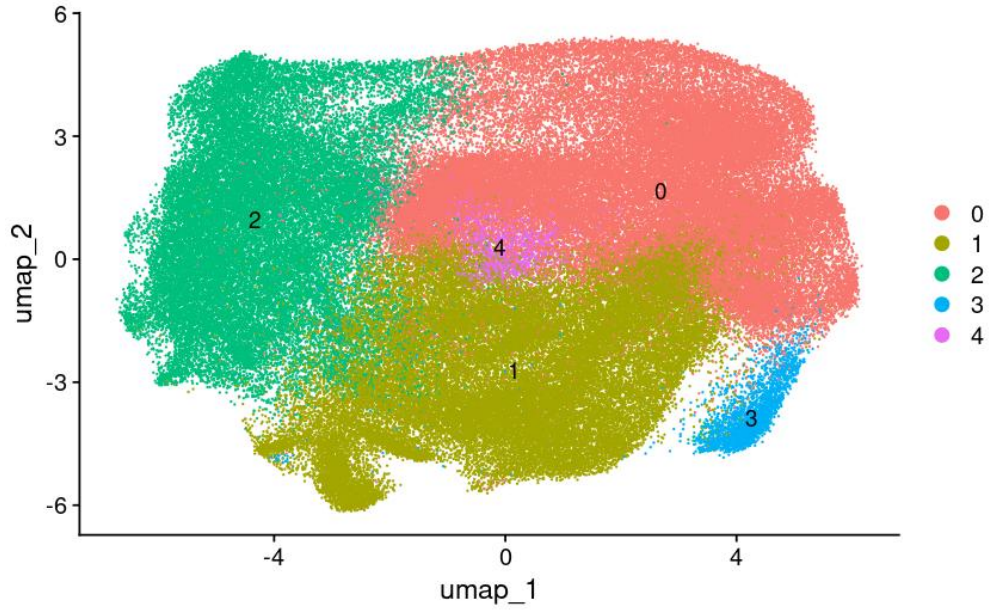

Figure S 8. UMAP of 5 clusters from the MC dataset for cell annotation.

Resolution: 0.1.

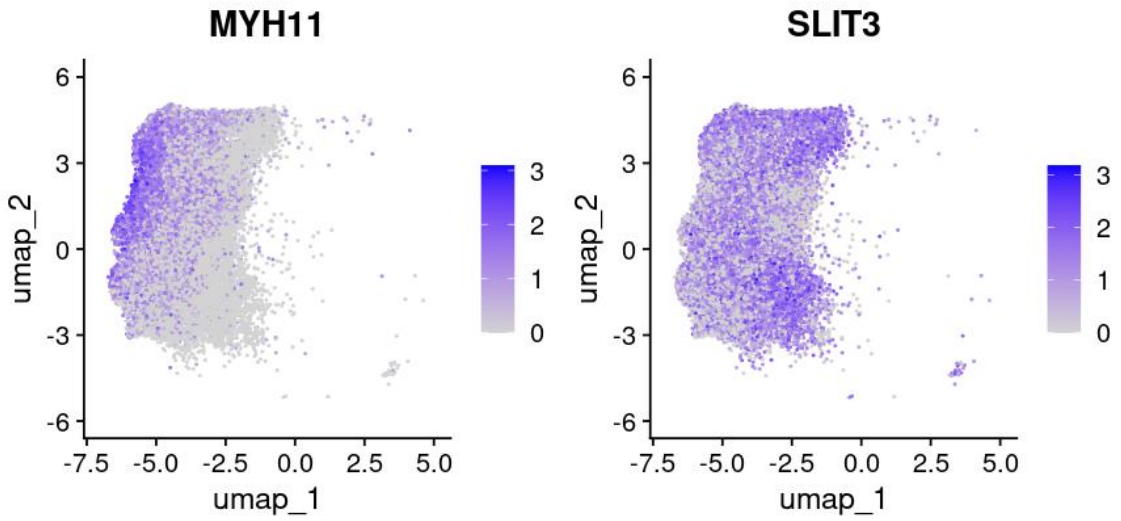

Figure S 9. Expression level of MYH11 (aSMC marker gene) and SLIT3 (aaSMC marker gene) in the smooth muscle cell (SMC) cluster.

aSMC, arterial smooth muscle cell; arteriolar smooth muscle cells aaSMC.

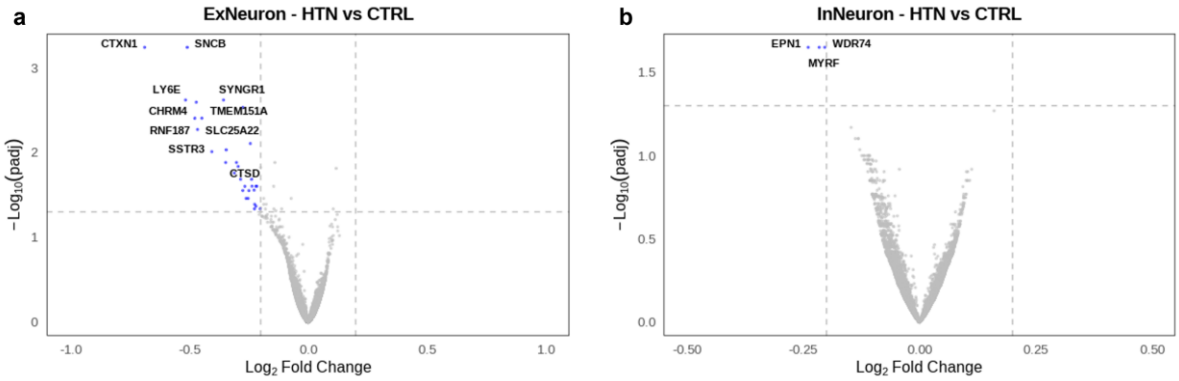

*Figure S 10. Volcano plots show DEGs in hypertensive donors (n = 27) compared to non-hypertensive donors (n = 16) in ExNeuron (**a**), and InNeuron (**b**).*

X-axis: Log_2FC (hypertensive relative to control); Y-axis: $-Log_{10}(padj)$-values. Horizontal dashed line represents a cutoff of adjusted p-values < 0.05, and vertical dashed lines represent Log_2FC cutoffs of > 0.2 or < -0.2. Genes meeting both cutoffs are represented by red circles (upregulated) and blue circles (downregulated). Top 10 up or downregulated DEGs (based on $|Log_2FC|$) were labelled.

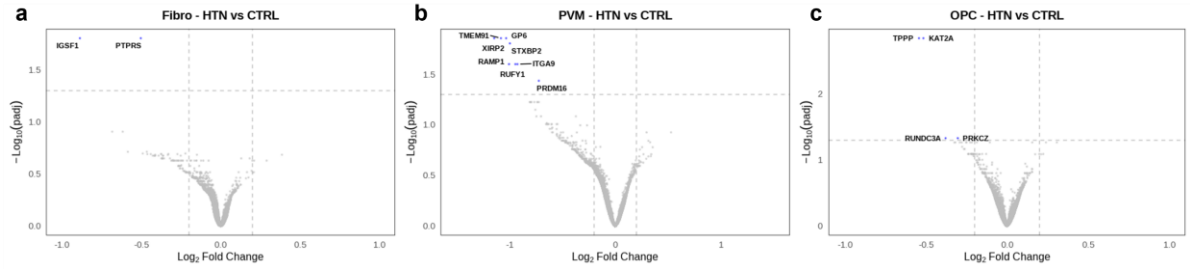

*Figure S 11. Volcano plots show DEGs in hypertensive donors (n = 27) compared to non-hypertensive donors (n = 16) in Fibro (**a**), PVM (**b**), and OPC (**c**).*

X-axis: Log_2FC (hypertensive relative to control); Y-axis: $-Log_{10}(padj)$-values. Horizontal dashed line represents a cutoff of adjusted p-values < 0.05, and vertical dashed lines represent Log_2FC cutoffs of > 0.2 or < -0.2. Genes meeting both cutoffs are represented by red circles (upregulated) and blue circles (downregulated). Top 10 up or downregulated DEGs (based on $|Log_2FC|$) were labelled.

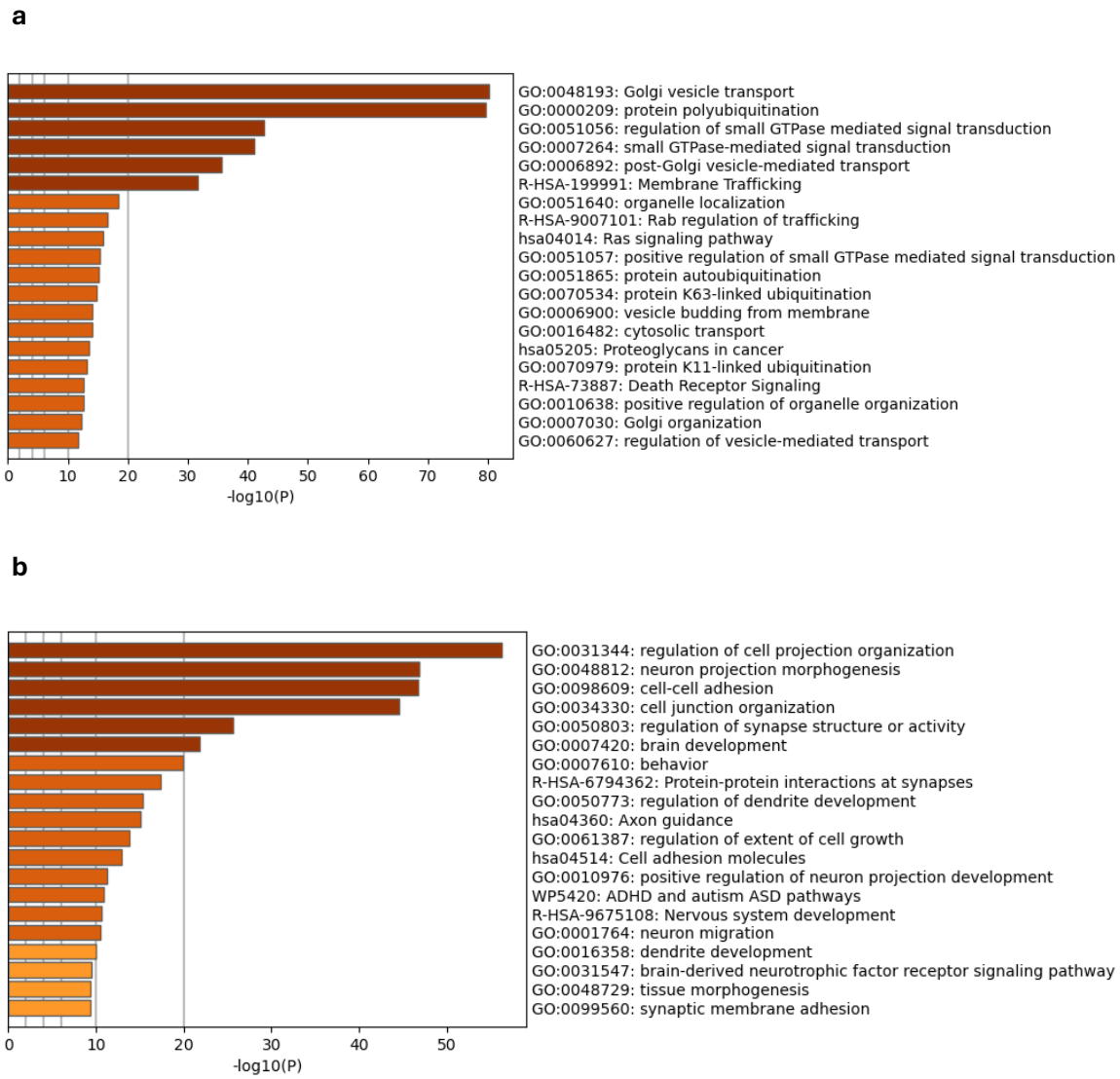

*Figure S 12. Top 20 enriched terms from dysregulated genes of common upregulated (**a**) and downregulated (**b**) pathways across EC, MC, and Astro in hypertension.*

Each bar represents an enriched term, ranked by statistical significance. Terms with a similarity score > 0.3 were grouped into clusters, and the most statistically significant term from each cluster was displayed among the top 20 clusters.

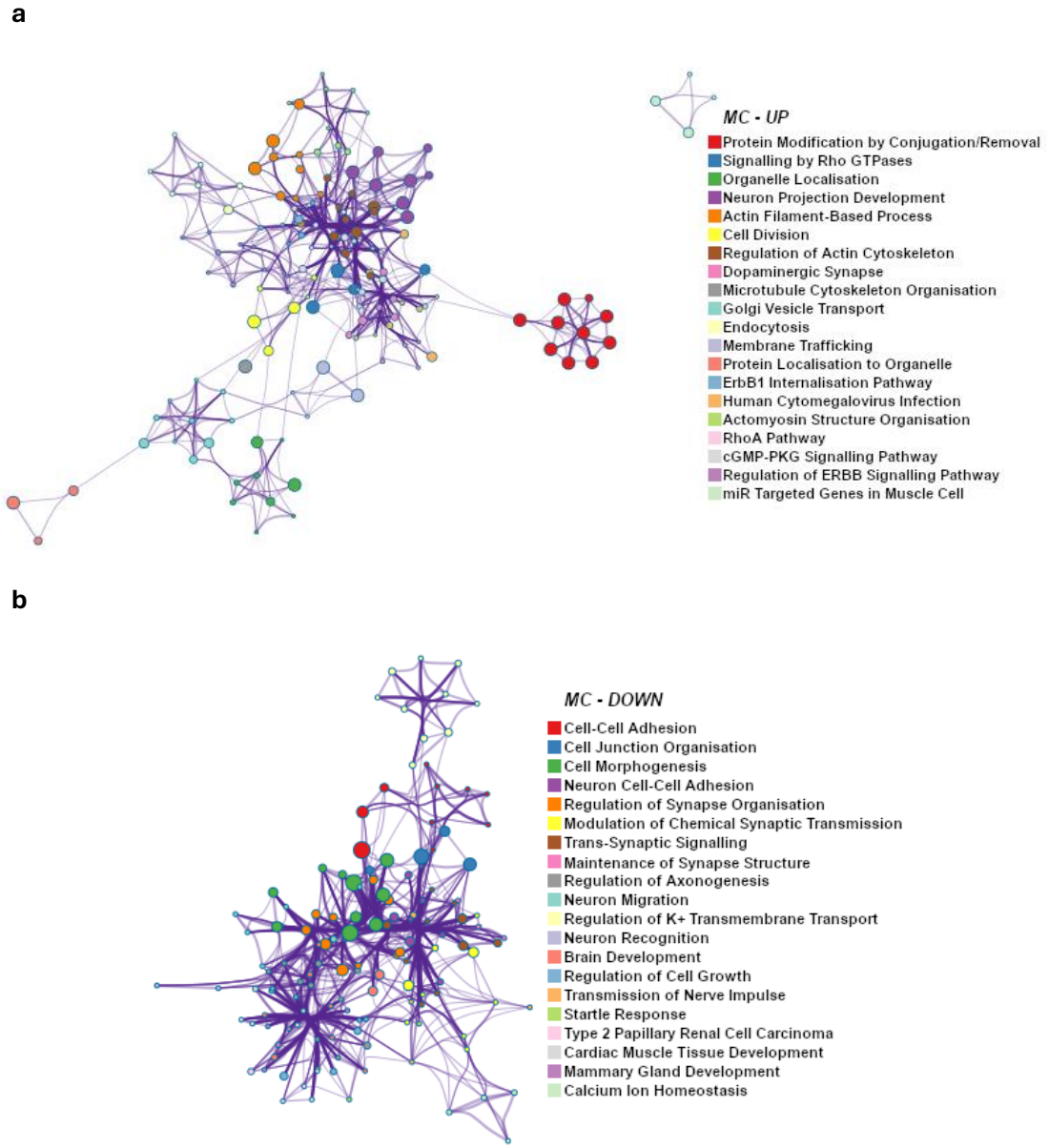

*Figure S 13. Network plot of enriched terms from MC upregulated (**a**) and downregulated (**b**) genes in hypertension.*

Each node represents an enriched term and terms with a similarity > 0.3 are connected by edges. Node size indicates the number of genes in the term overlapping with the input gene list. The most statistically significant term per cluster was labelled from the top 20 clusters.

The most significant enrichment from MC upregulated genes was *Protein Modification by Small Protein Conjugation or Removal (GO:0070647)* (34 genes) followed by *Signalling by Rho GTPases (R-HSA-194315)* (26 genes) and *Organelle Localisation (GO:0051640)* (24 genes) (Figure S 13a). The upregulated enriched terms in MC were mainly related to

signal transduction, organelle and cytoskeletal organisation, intracellular trafficking, and protein modification. The most significant enrichment from MC downregulated genes was *Cell-Cell Adhesion (GO:0098609)* (24 genes) followed by *Cell Junction Organisation (GO:0034330)* (18 genes) and *Cell Morphogenesis (GO:0000902)* (19 genes) (Figure S 13b). The downregulated enriched terms in MC were mainly related to neuronal function, synaptic signalling, ion transport, and cell adhesion.

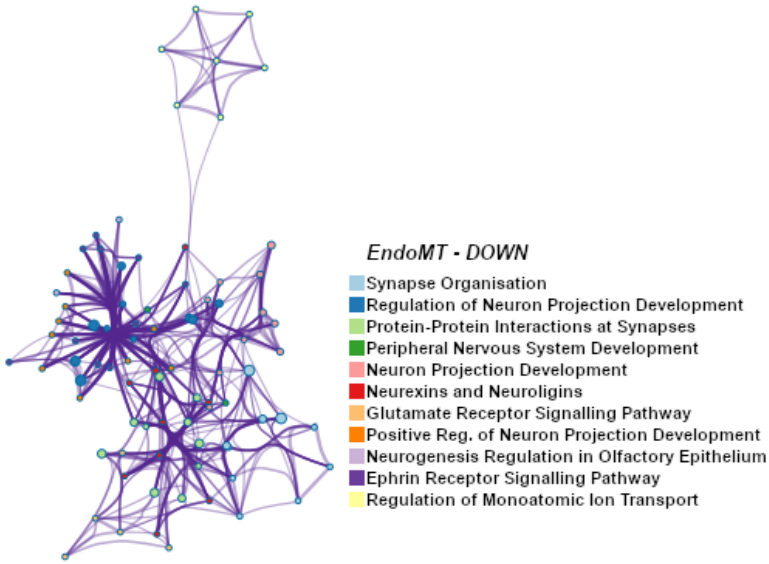

Figure S 14. Network plot of enriched terms from EndoMT downregulated genes in hypertension.

Each node represents an enriched term and terms with a similarity > 0.3 are connected by edges. Node size indicates the number of genes in the term overlapping with the input gene list. The most statistically significant term per cluster was labelled.

The most significant enrichment from EndoMT downregulated genes was *Synapse Organisation (GO:0050808)* (10 genes) followed by *Regulation of Neuron Projection Development (GO:0010975)* (9 genes) and *Protein-Protein Interactions at Synapses (R-HSA-6794362)* (5 genes) (Figure S 14). The downregulated enriched terms in EndoMT were mainly related to neuronal development, ion transport, synaptic organisation and signalling.

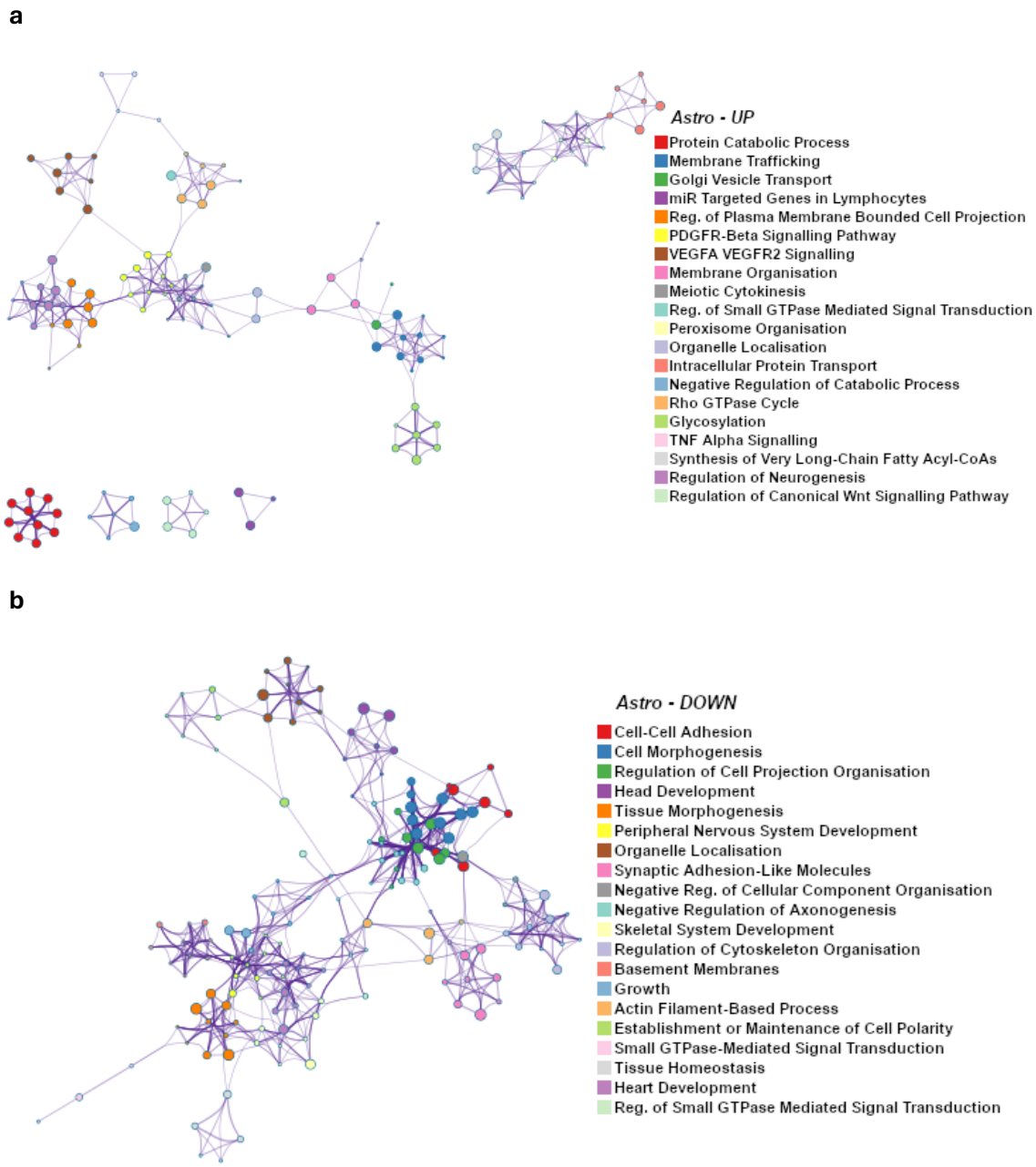

*Figure S 15. Network plot of enriched terms from Astro upregulated (**a**) and downregulated (**b**) genes in hypertension.*

Each node represents an enriched term and terms with a similarity > 0.3 are connected by edges. Node size indicates the number of genes in the term overlapping with the input gene list. The most statistically significant term per cluster was labelled from the top 20 clusters.

The most significant enrichment from Astro upregulated genes was *Protein Catabolic Process (GO:0030163)* (53 genes) followed by *Membrane Trafficking (R-HSA-199991)* (33 genes) and *Golgi Vesicle Transport (GO:0048193)* (23 genes) (Figure S 15a). The

upregulated enriched terms in Astro were mainly related to intracellular transport, signalling pathways, membrane and organelle organisation. The most significant enrichment from Astro downregulated genes was *Cell-Cell Adhesion (GO:0098609)* (29 genes) followed by *Cell Morphogenesis (GO:0000902)* (32 genes) and *Regulation of Cell Projection Organisation (GO:0031344)* (27 genes) (Figure S 15b). The downregulated enriched terms in Astro were mainly related to cytoskeleton organisation, tissue development, cell polarity and adhesion.

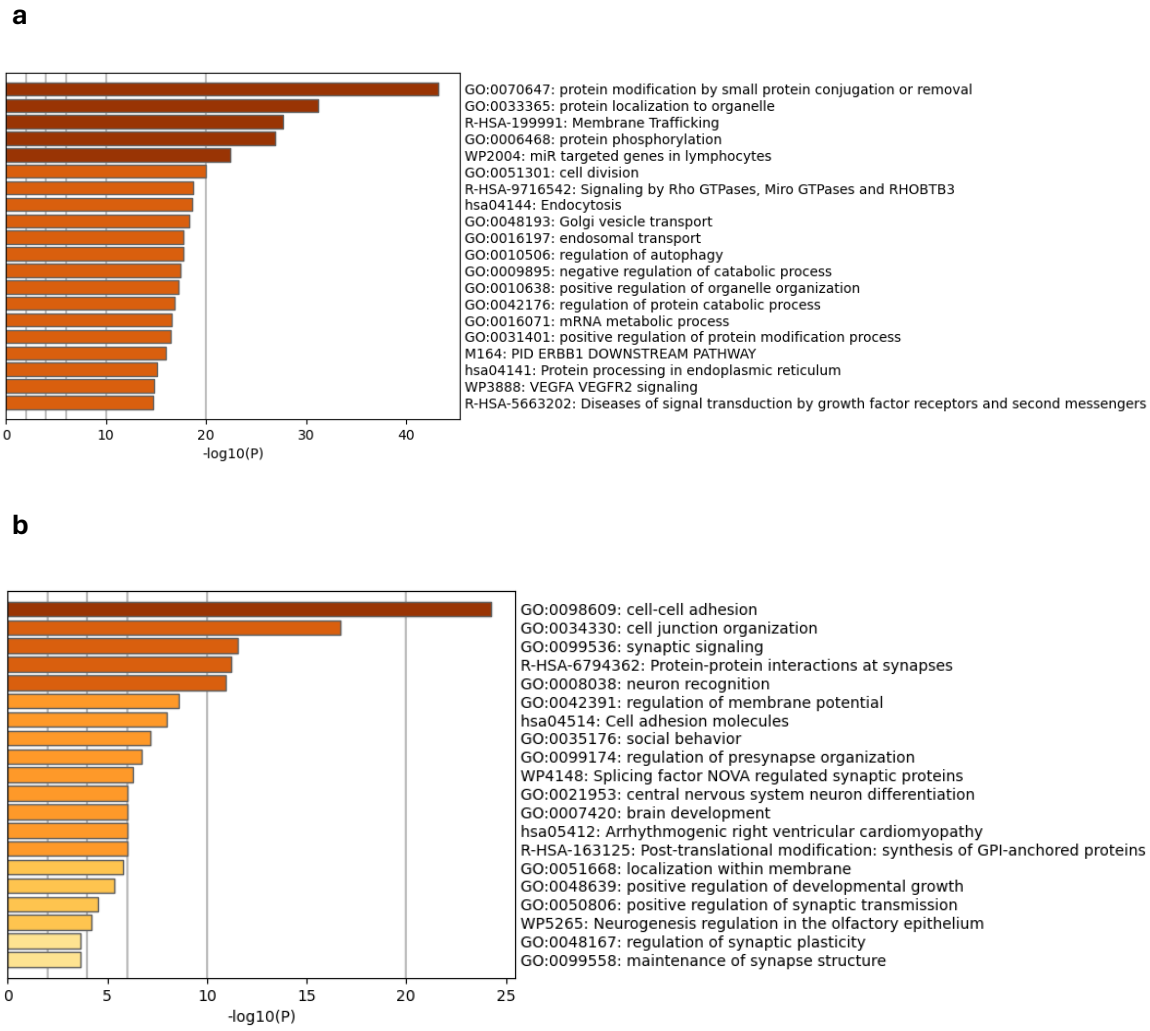

*Figure S 16. Top 20 enriched terms from EC upregulated (**a**) and downregulated (**b**) genes in hypertension.*

Each bar represents an enriched term, ranked by statistical significance. Terms with a similarity score > 0.3 were grouped into clusters, and the most statistically significant term from each cluster was displayed among the top 20 clusters.

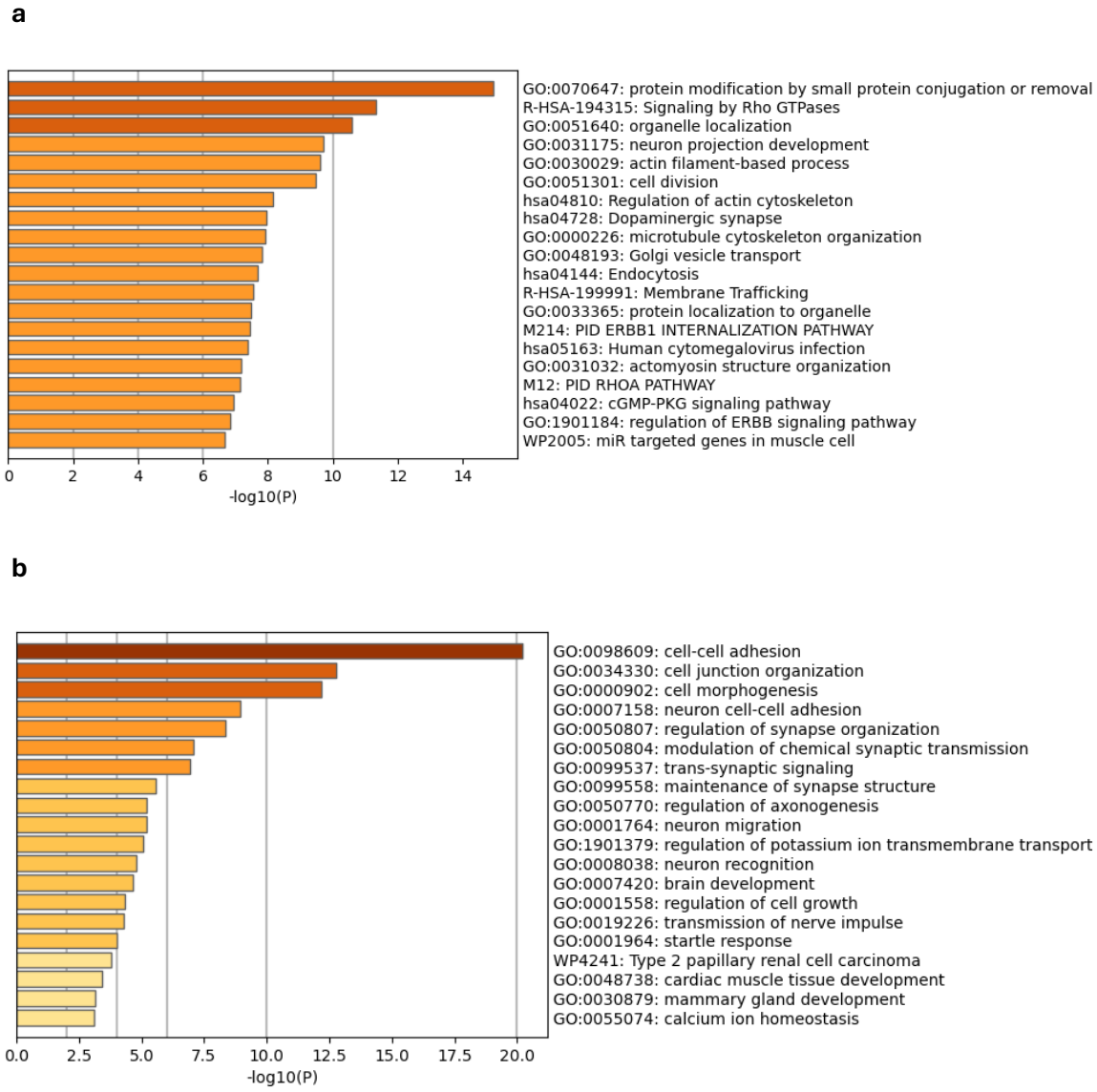

*Figure S 17. Top 20 enriched terms from MC upregulated (**a**) and downregulated (**b**) genes in hypertension.*

Each bar represents an enriched term, ranked by statistical significance. Terms with a similarity score > 0.3 were grouped into clusters, and the most statistically significant term from each cluster was displayed among the top 20 clusters.

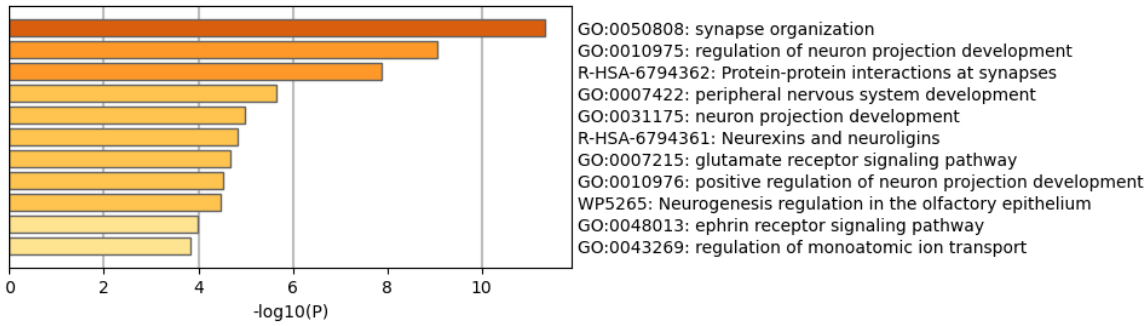

Figure S 18. Enriched terms from EndoMT downregulated genes in hypertension.

Each bar represents an enriched term, ranked by statistical significance. Terms with a similarity score > 0.3 were grouped into clusters, and the most statistically significant term from each cluster was displayed among the top clusters.

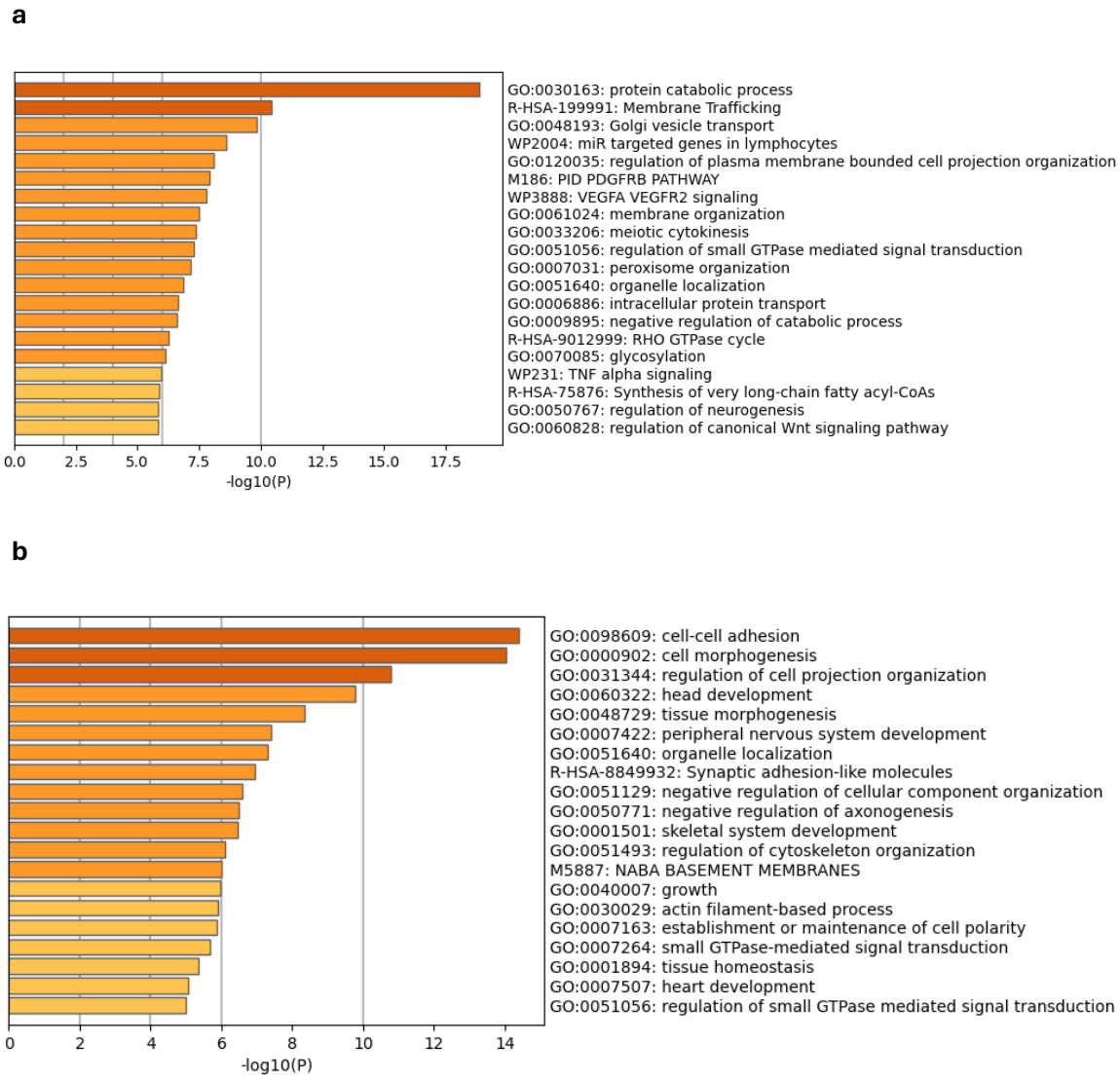

*Figure S 19. Top 20 enriched terms from Astro upregulated (**a**) and downregulated (**b**) genes in hypertension.*

Each bar represents an enriched term, ranked by statistical significance. Terms with a similarity score > 0.3 were grouped into clusters, and the most statistically significant term from each cluster was displayed among the top 20 clusters.

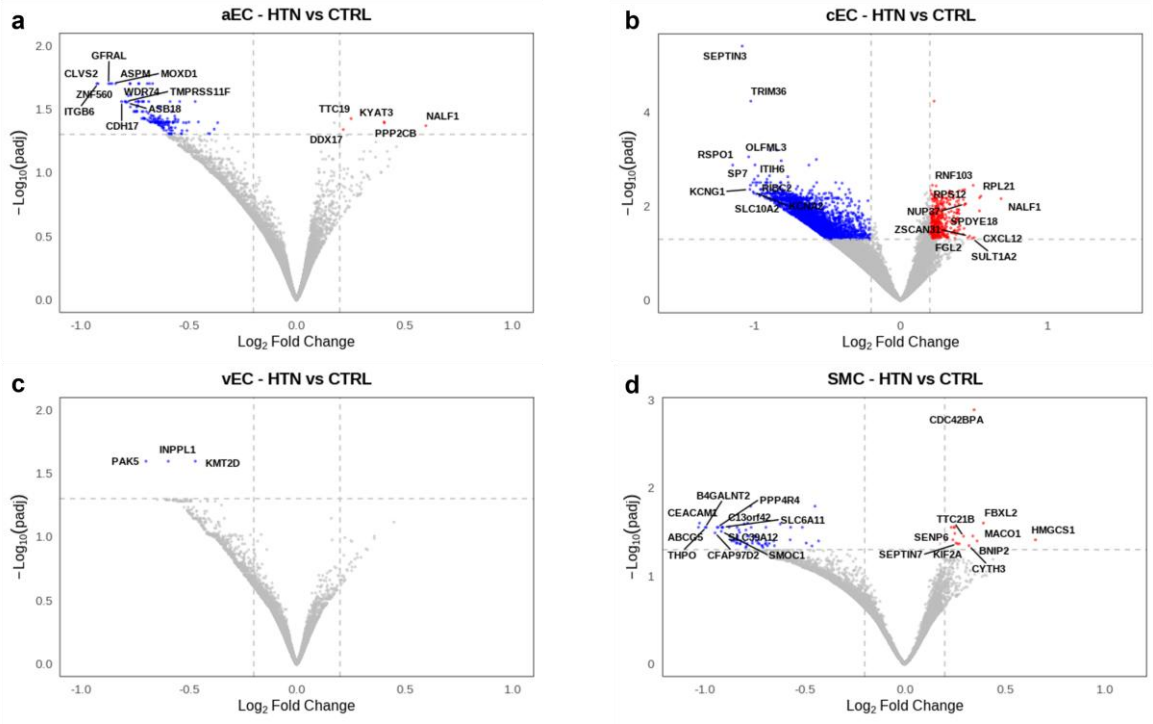

*Figure S 20. Volcano plots show DEGs in hypertensive donors (n = 27) compared to non-hypertensive donors (n = 16) in aEC (**a**), cEC (**b**), vEC (**c**), and SMC (**d**).*

X-axis: Log_2FC (hypertensive relative to control); Y-axis: $-Log_{10}$(padj)-values. Horizontal dashed line represents a cutoff of adjusted p-values < 0.05, and vertical dashed lines represent Log_2FC cutoffs of > 0.2 or < -0.2. Genes meeting both cutoffs are represented by red circles (upregulated) and blue circles (downregulated). Top 10 up or downregulated DEGs (based on $|Log_2FC|$) were labelled.

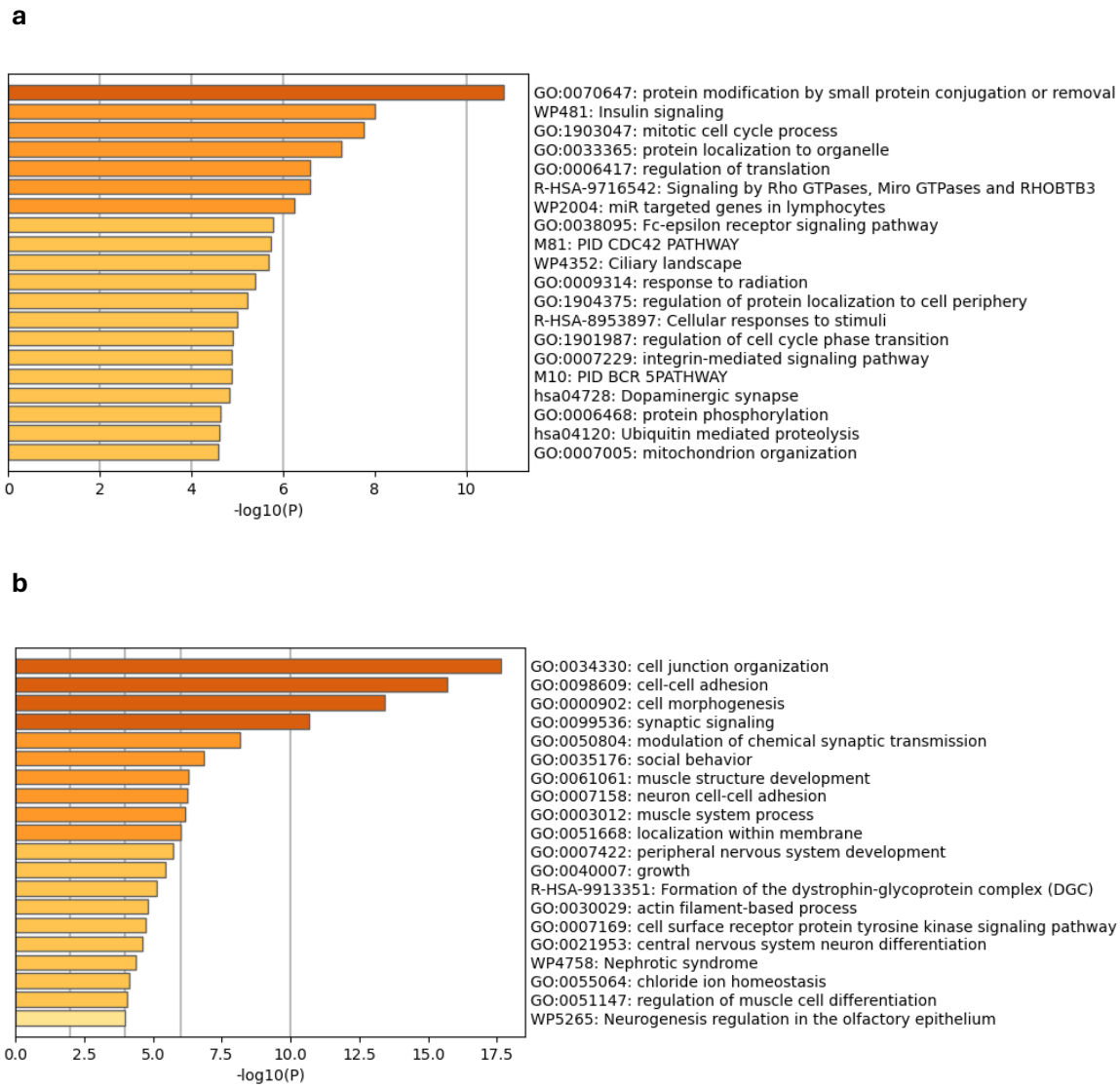

*Figure S 21. Top 20 enriched terms from cEC upregulated (**a**) and downregulated (**b**) genes in hypertension.*

Each bar represents an enriched term, ranked by statistical significance. Terms with a similarity score > 0.3 were grouped into clusters, and the most statistically significant term from each cluster was displayed among the top 20 clusters.

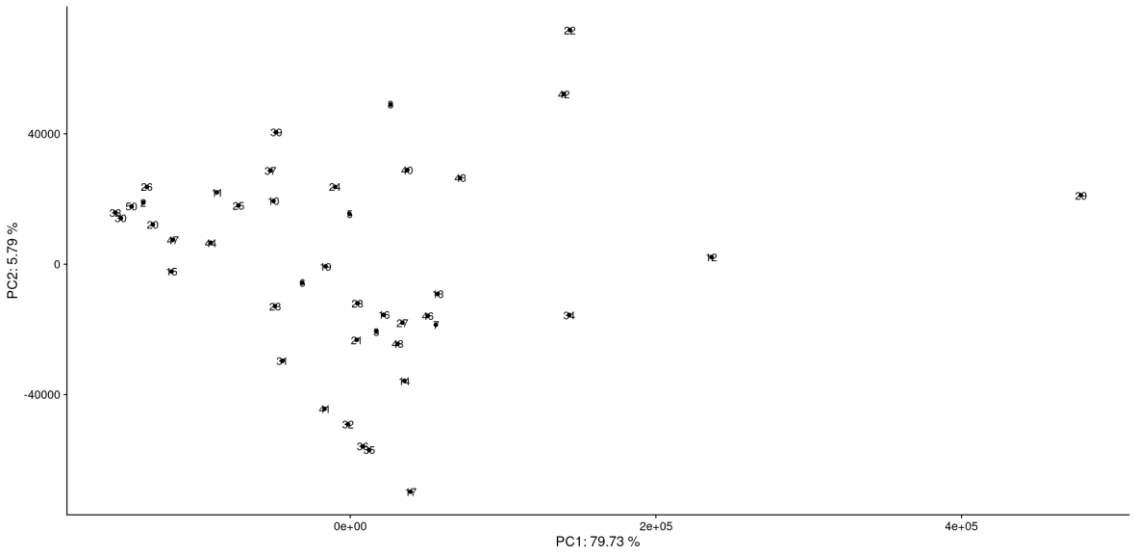

Figure S 22. PCA plot of donor samples of the EC dataset in WGCNA.

Each point represents a donor, with clustering based on the first two principal components (PC1 and PC2). Donor 29 was identified as the outlier donor, deviating substantially from the main cluster along PC1.

a

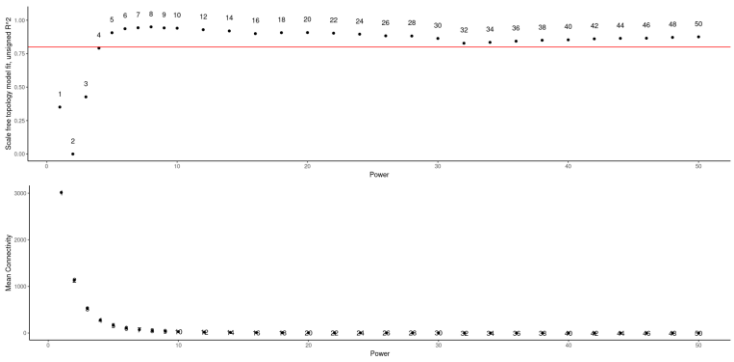

b

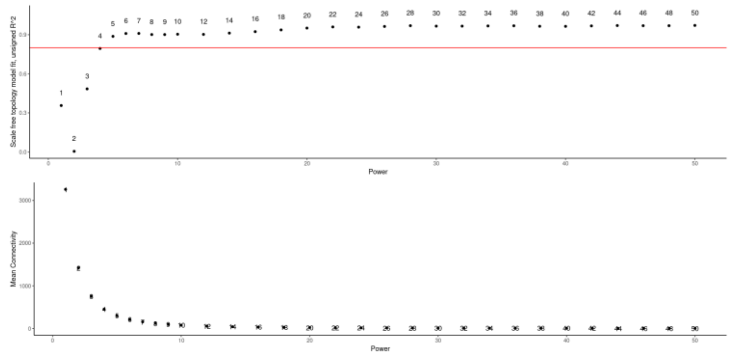

c

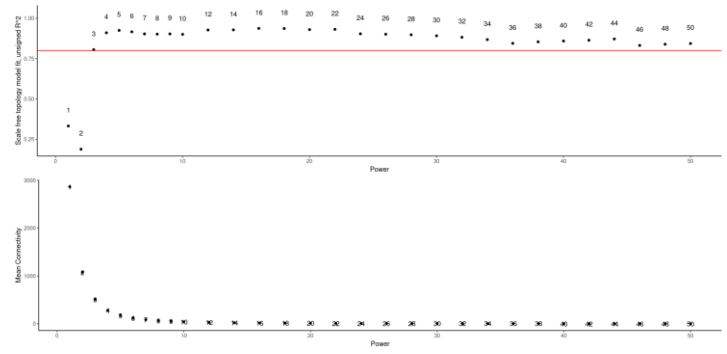

*Figure S 23. Selection of the soft-threshold power for WGCNA in HTN EC (**a**), CTRL EC (**b**), and combined EC (**c**) dataset.*

The scale-free topology model fit (R^2) as a function of soft-threshold power. The red horizontal line at $R^2 = 0.8$ indicates the commonly used threshold for approximate scale-free topology. The mean connectivity (k) as a function of soft-threshold power. Higher power values lead to lower mean connectivity, reducing noise while preserving the network structure.

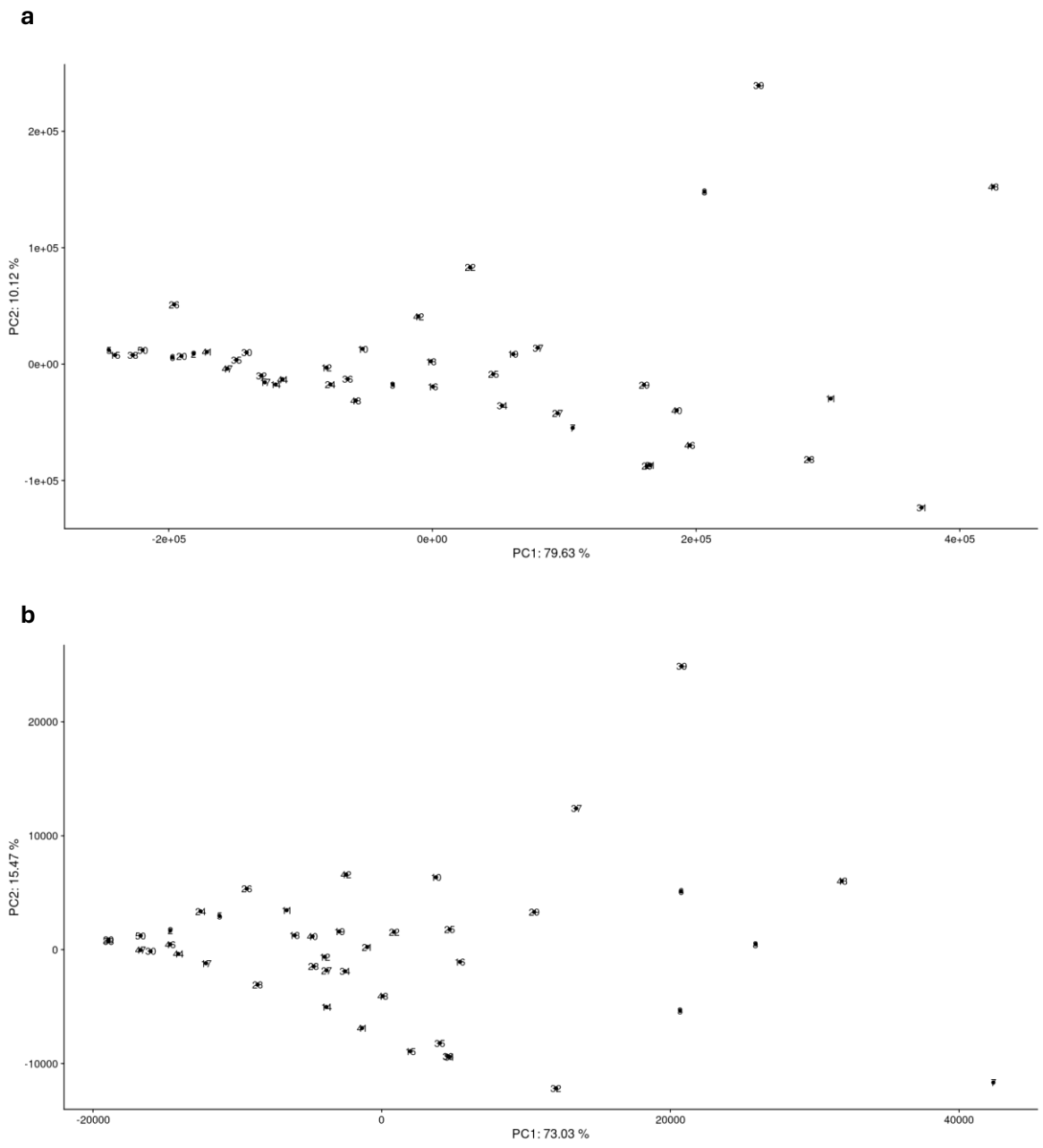

*Figure S 24. PCA plot of donor samples of the Astro (**a**) and the SMC (**b**) dataset in WGCNA.*

Each point represents a donor, with clustering based on the first two principal components (PC1 and PC2).

a

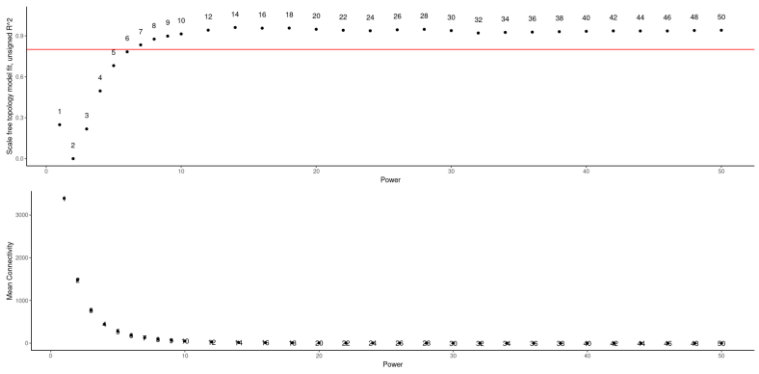

b

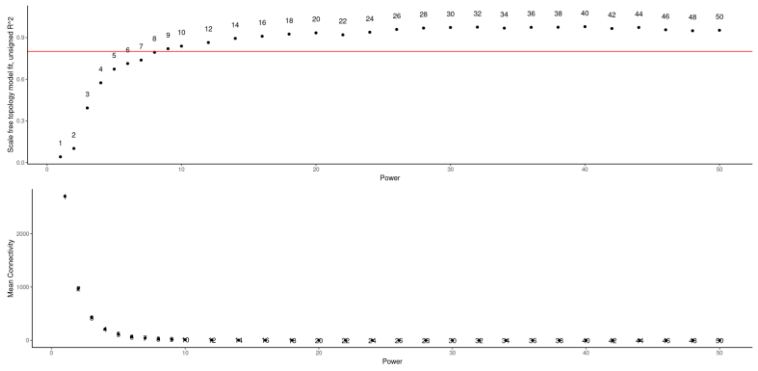

c

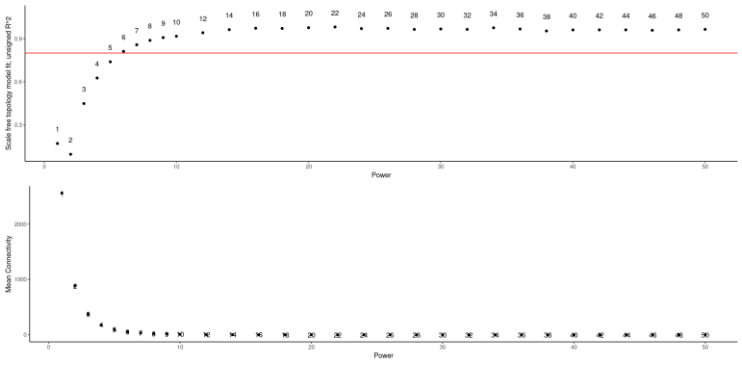

*Figure S 25. Selection of the soft-threshold power for WGCNA in HTN Astro (**a**), CTRL Astro (**b**), and combined Astro (**c**) dataset.*

The scale-free topology model fit (R^2) as a function of soft-threshold power. The red horizontal line at $R^2 = 0.8$ indicates the commonly used threshold for approximate scale-free topology. The mean connectivity (k) as a function of soft-threshold power. Higher power values lead to lower mean connectivity, reducing noise while preserving the network structure.

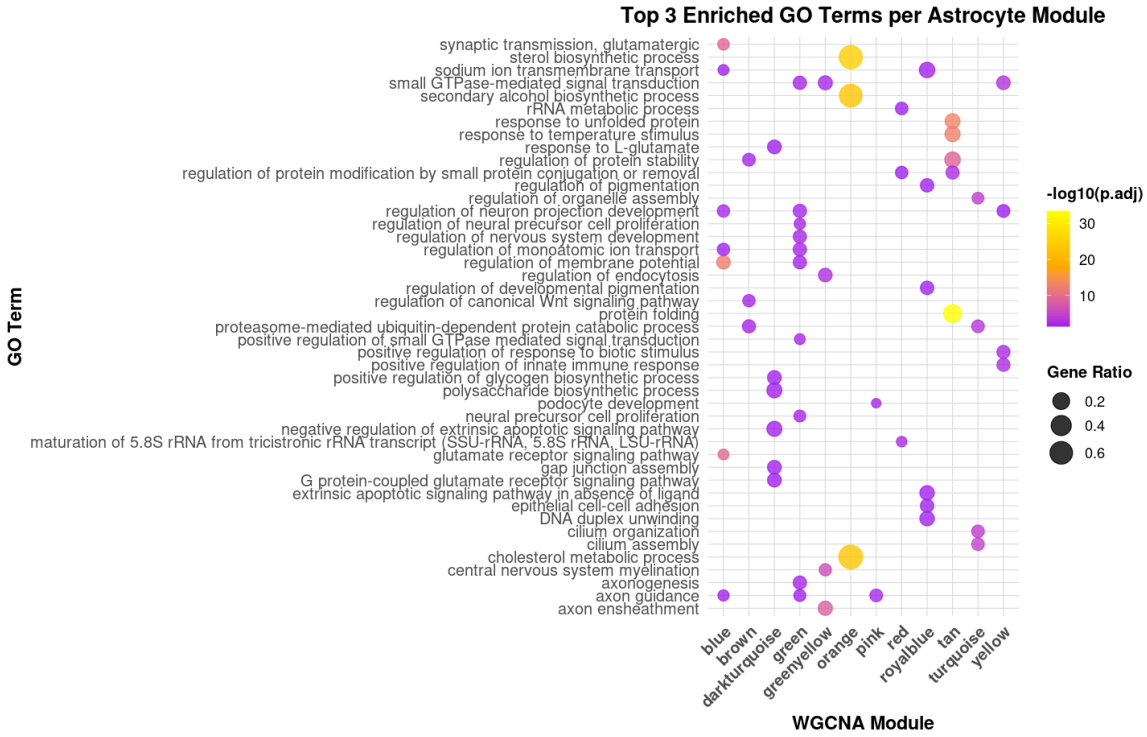

Figure S 26. Dot plot of functional profiles for genes in each module from WGCNA in the Astro combined dataset.

The dot size represents the gene ratio (proportion of module genes associated with each GO term), and the colour scale indicates -log10(adjusted p-value).

a

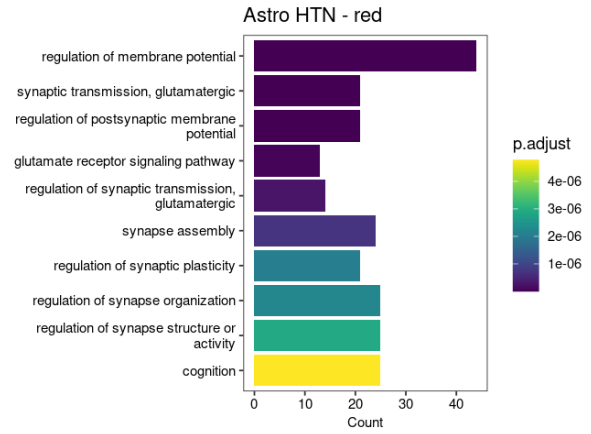

b

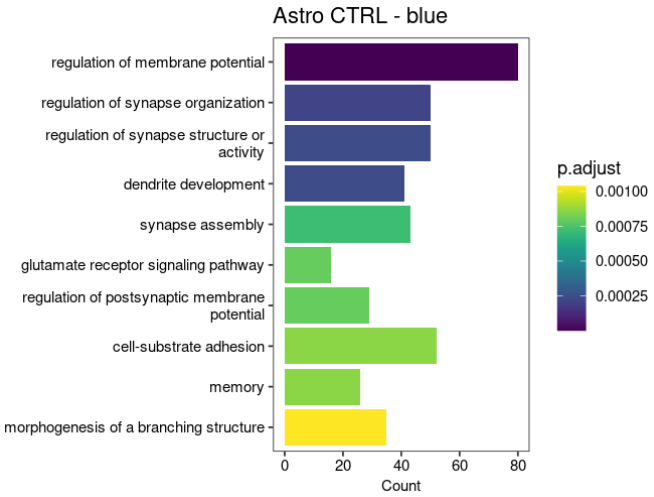

*Figure S 27. Top 10 enriched Biological Process (BP) GO terms for genes in the Astro HTN red module (**a**) and Astro CTRL blue module (**b**).*

The y-axis represents the GO terms, and the x-axis indicates the gene count associated with each term. The colour gradient corresponds to the adjusted p-value.

a

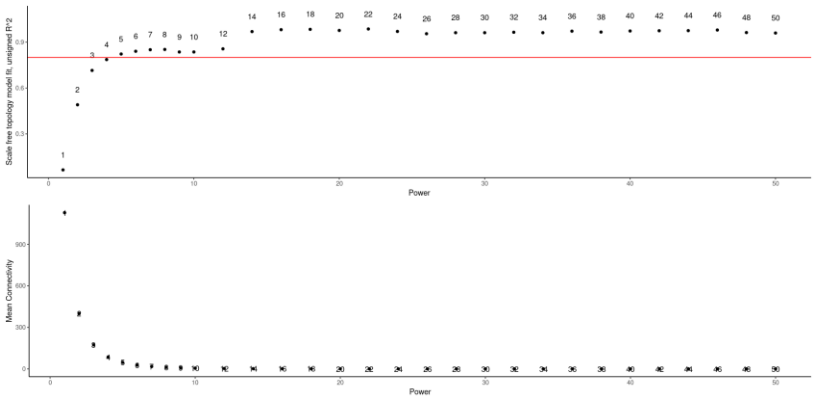

b

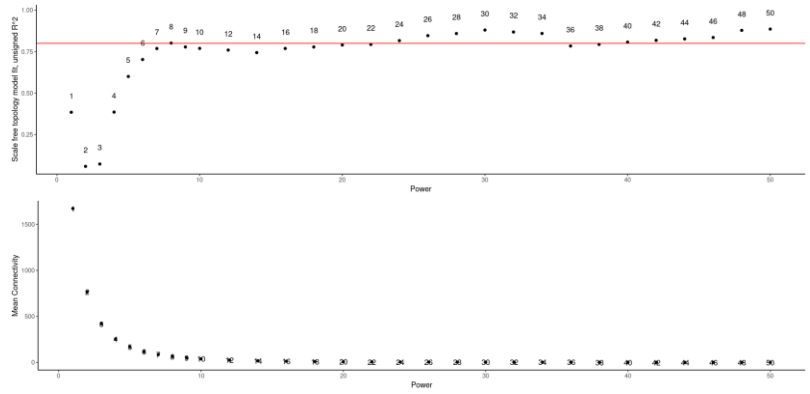

c

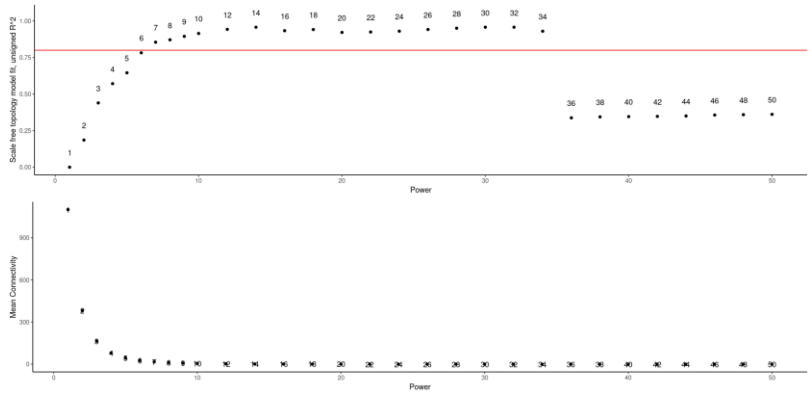

*Figure S 28. Selection of the soft-threshold power for WGCNA in HTN SMC (**a**), CTRL SMC (**b**), and combined SMC (**c**) dataset.*

The scale-free topology model fit (R^2) as a function of soft-threshold power. The red horizontal line at $R^2 = 0.8$ indicates the commonly used threshold for approximate scale-free topology. The mean connectivity (k) as a function of soft-threshold power. Higher power values lead to lower mean connectivity, reducing noise while preserving the network structure.

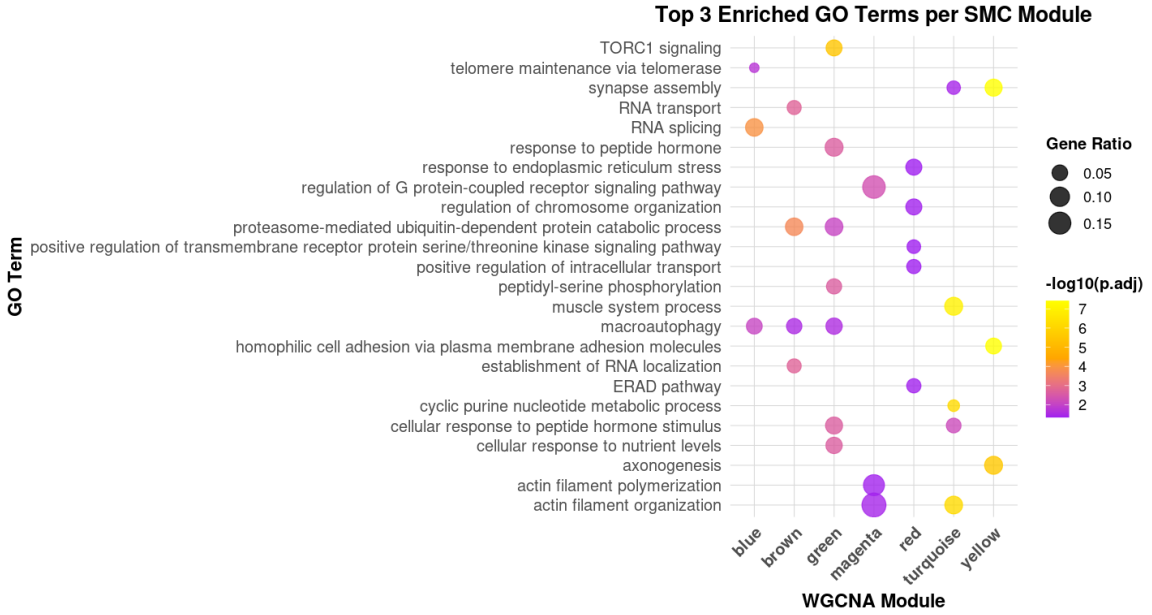

Figure S 29. Dot plot of functional profiles for genes in each module from WGCNA in the SMC combined dataset.

The dot size represents the gene ratio (proportion of module genes associated with each GO term), and the colour scale indicates -log10(adjusted p-value).

a

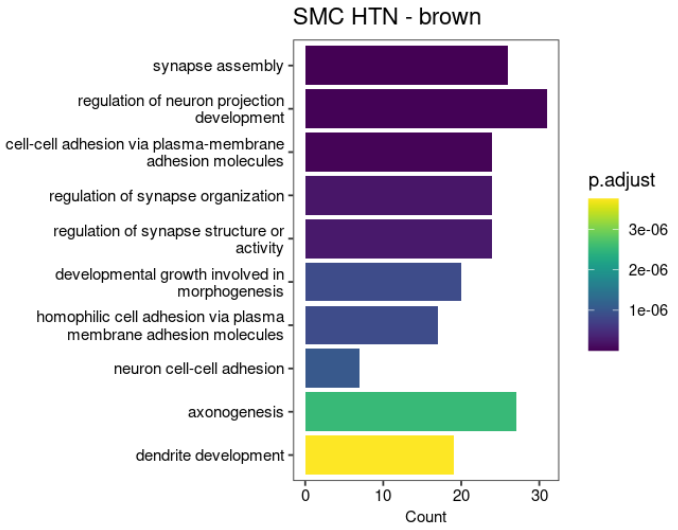

b

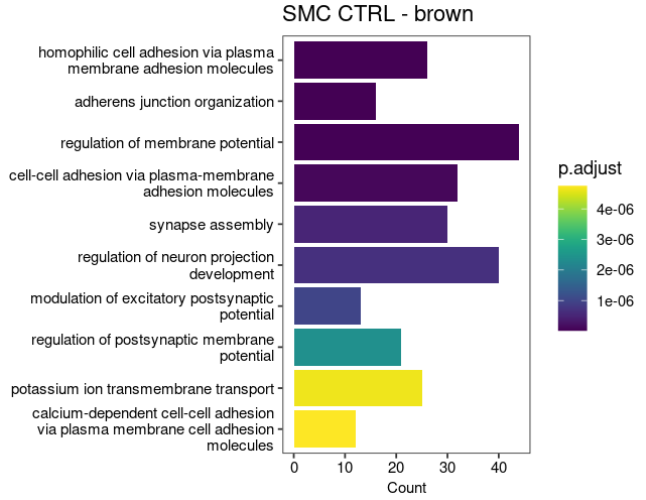

*Figure S 30. Top 10 enriched Biological Process (BP) GO terms for genes in the SMC HTN brown module (**a**) and SMC CTRL brown module (**b**).*

The y-axis represents the GO terms, and the x-axis indicates the gene count associated with each term. The colour gradient corresponds to the adjusted p-value.

a

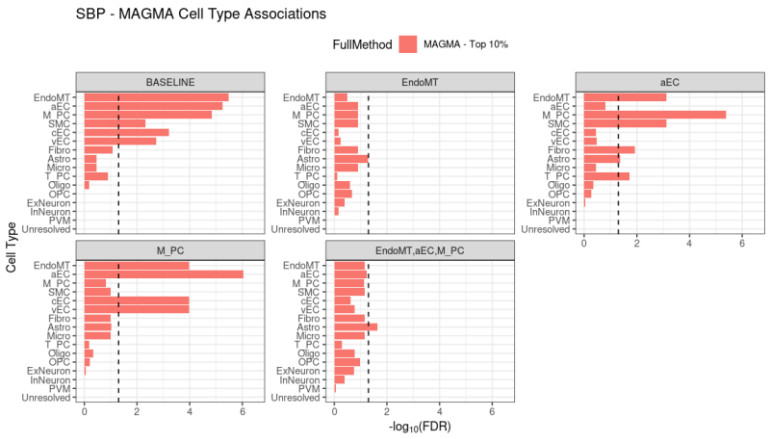

b

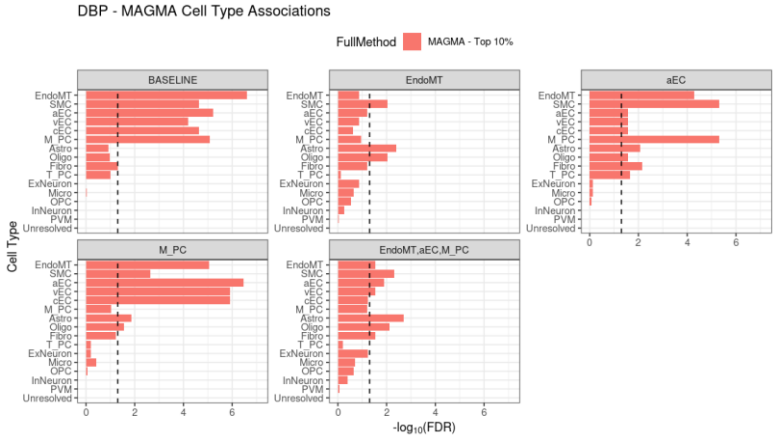

c

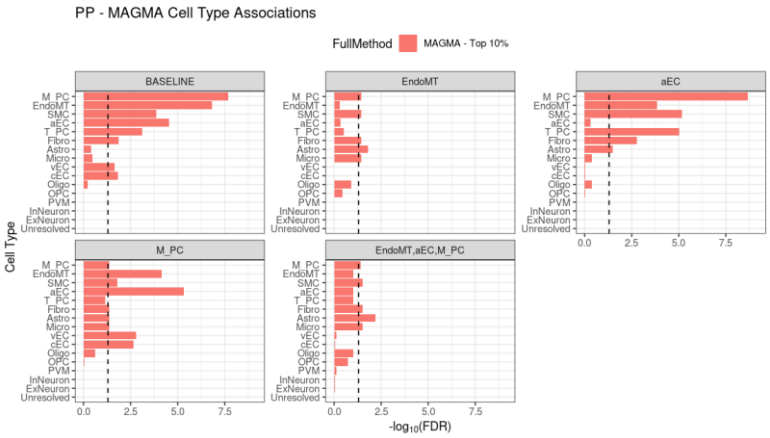

*Figure S 31. Conditional cell-subtype enrichment analysis of SBP (**a**), DBP (**b**), and PP (**c**).*

Bar plots show the -log$_{10}$(FDR) for cell subtype enrichment across different conditional models: baseline, individual conditions, and the combined model (aEC, EndoMT, M-PC). FDR correction was performed using the Benjamini-Hochberg (BH) method. The top 10% mode was used for enrichment tests. The vertical dashed line indicates the significance threshold (FDR = 0.05).

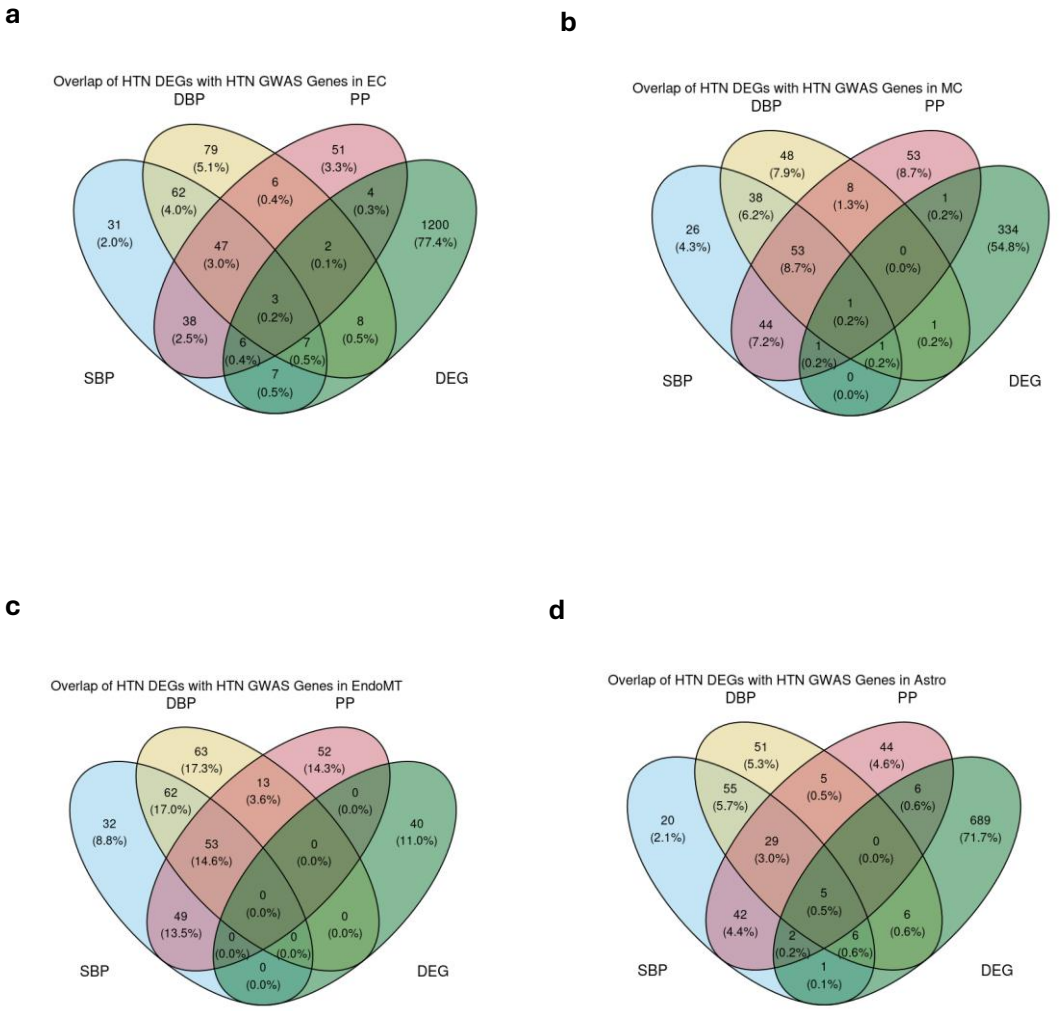

*Figure S 32. Venn diagram of the overlap of HTN DEGs with significant GWAS genes across hypertension traits (SBP, DBP, PP) in EC (**a**), MC (**b**), EndoMT (**c**), and Astro (**d**).*

Each circle represents the set of genes associated with the corresponding category. The percentages indicate the proportion of genes in each corresponding category relative to the total number of unique genes (N = 1,551 in EC, N = 609 in MC, N = 364 in EndoMT, and N = 961 in Astro).

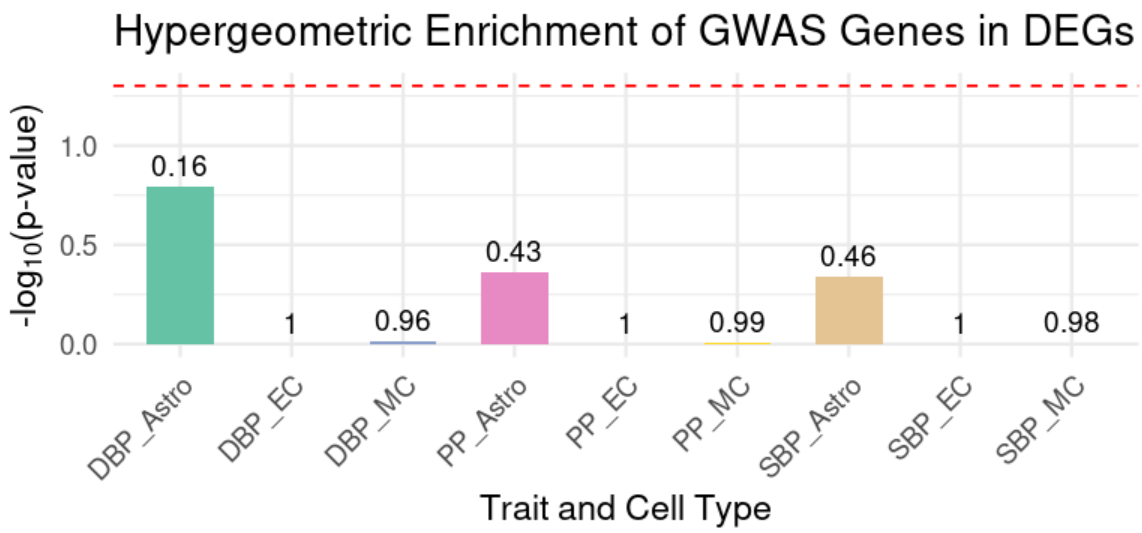

Figure S 33. Hypergeometric enrichment of HTN GWAS genes in DEGs.

Bar plot showing the hypergeometric enrichment of hypertension GWAS genes among differentially expressed genes in endothelial cells, mural cells, and astrocytes for three hypertension traits—SBP, DBP, PP. The y-axis represents the $-\log_{10}$(p-values) from one-sided hypergeometric tests. The red dashed line indicates the significance threshold at $p = 0.05$. The p-values were annotated.

a

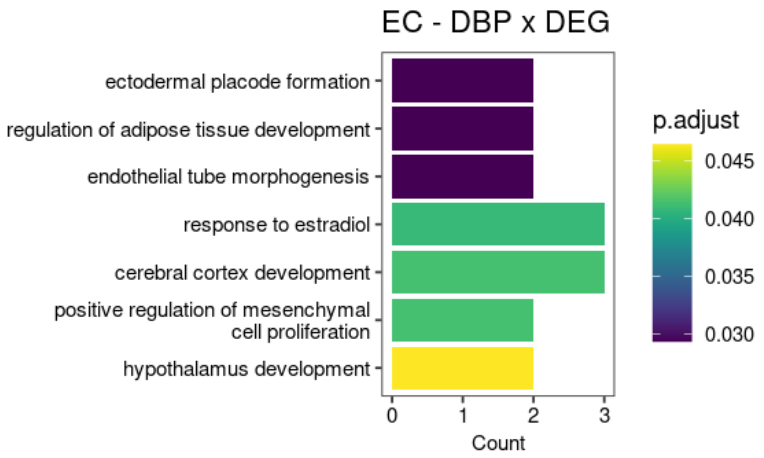

b

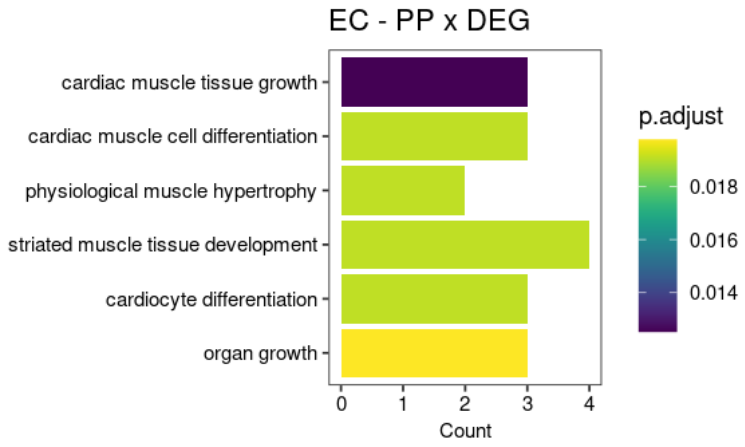

*Figure S 34. Enriched Biological Process (BP) GO terms for overlapping genes between DBP (**a**) and PP (**b**) associated significant GWAS genes and HTN DEGs in endothelial cells.*

The y-axis represents the GO terms, and the x-axis indicates the gene count associated with each term. The colour gradient corresponds to the adjusted p-value.

References

Abou Ziki, M. D., & Mani, A. (2017). Wnt signaling, a novel pathway regulating blood pressure? State of the art review. *Atherosclerosis*, *262*, 171-178. https://doi.org/10.1016/j.atherosclerosis.2017.05.001

Agrud, A., Subburaju, S., Goel, P., Ren, J., Kumar, A. S., Caldarone, B. J., Dai, W., Chavez, J., Fukumura, D., Jain, R. K., Kloner, R. A., & Vasudevan, A. (2022). Gabrb3 endothelial cell-specific knockout mice display abnormal blood flow, hypertension, and behavioral dysfunction. *Sci Rep*, *12*(1), 4922. https://doi.org/10.1038/s41598-022-08806-9

Alkayed, N. J., & Cipolla, M. J. (2023). The Ever-Evolving Concept of the Neurovascular Unit. *Stroke*, *54*(8), 2178-2180. https://doi.org/10.1161/STROKEAHA.123.042705

Alvandi, Z., & Bischoff, J. (2021). Endothelial-Mesenchymal Transition in Cardiovascular Disease. *Arterioscler Thromb Vasc Biol*, *41*(9), 2357-2369. https://doi.org/10.1161/ATVBAHA.121.313788

Andreone, B. J., Lacoste, B., & Gu, C. (2015). Neuronal and vascular interactions. *Annu Rev Neurosci*, *38*, 25-46. https://doi.org/10.1146/annurev-neuro-071714-033835

Antal, B., McMahon, L. P., Sultan, S. F., Lithen, A., Wexler, D. J., Dickerson, B., Ratai, E.-M., & Mujica-Parodi, L. R. (2022). Type 2 diabetes mellitus accelerates brain aging and cognitive decline: Complementary findings from UK Biobank and meta-analyses. *eLife*, *11*, e73138. https://doi.org/10.7554/eLife.73138

Antonioni, A., Raho, E. M., Lopriore, P., Pace, A. P., Latino, R. R., Assogna, M., Mancuso, M., Gragnaniello, D., Granieri, E., Pugliatti, M., Di Lorenzo, F., & Koch, G. (2023). Frontotemporal Dementia, Where Do We Stand? A Narrative Review. *Int J Mol Sci*, *24*(14). https://doi.org/10.3390/ijms241411732

Argaw, A. T., Asp, L., Zhang, J., Navrazhina, K., Pham, T., Mariani, J. N., Mahase, S., Dutta, D. J., Seto, J., Kramer, E. G., Ferrara, N., Sofroniew, M. V., & John, G. R.

(2012). Astrocyte-derived VEGF-A drives blood-brain barrier disruption in CNS inflammatory disease. *J Clin Invest*, *122*(7), 2454-2468. https://doi.org/10.1172/JCI60842

Attwell, D., Buchan, A. M., Charpak, S., Lauritzen, M., Macvicar, B. A., & Newman, E. A. (2010). Glial and neuronal control of brain blood flow. *Nature*, *468*(7321), 232-243. https://doi.org/10.1038/nature09613

Baggeroer, C. E., Cambronero, F. E., Savan, N. A., Jefferson, A. L., & Santisteban, M. M. (2024). Basic Mechanisms of Brain Injury and Cognitive Decline in Hypertension. *Hypertension*, *81*(1), 34-44. https://doi.org/10.1161/HYPERTENSIONAHA.123.19939

Barnett, S. N., Cujba, A. M., Yang, L., Maceiras, A. R., Li, S., Kedlian, V. R., Pett, J. P., Polanski, K., Miranda, A. M. A., Xu, C., Cranley, J., Kanemaru, K., Lee, M., Mach, L., Perera, S., Tudor, C., Joseph, P. D., Pritchard, S., Toscano-Rivalta, R., . . . Teichmann, S. A. (2024). An organotypic atlas of human vascular cells. *Nat Med*, *30*(12), 3468-3481. https://doi.org/10.1038/s41591-024-03376-x

Basu, R., Lee, J., Morton, J. S., Takawale, A., Fan, D., Kandalam, V., Wang, X., Davidge, S. T., & Kassiri, Z. (2013). TIMP3 is the primary TIMP to regulate agonist-induced vascular remodelling and hypertension. *Cardiovasc Res*, *98*(3), 360-371. https://doi.org/10.1093/cvr/cvt067

Beauchet, O., Celle, S., Roche, F., Bartha, R., Montero-Odasso, M., Allali, G., & Annweiler, C. (2013). Blood pressure levels and brain volume reduction: a systematic review and meta-analysis. *J Hypertens*, *31*(8), 1502-1516. https://doi.org/10.1097/HJH.0b013e32836184b5

Bellenguez, C., Kucukali, F., Jansen, I. E., Kleineidam, L., Moreno-Grau, S., Amin, N., Naj, A. C., Campos-Martin, R., Grenier-Boley, B., Andrade, V., Holmans, P. A., Boland, A., Damotte, V., van der Lee, S. J., Costa, M. R., Kuulasmaa, T., Yang, Q., de Rojas, I., Bis, J. C., . . . Lambert, J. C. (2022). New insights into the genetic

etiology of Alzheimer's disease and related dementias. *Nat Genet*, *54*(4), 412-436. https://doi.org/10.1038/s41588-022-01024-z

Beyer, K., Domingo-Sabat, M., Santos, C., Tolosa, E., Ferrer, I., & Ariza, A. (2010). The decrease of beta-synuclein in cortical brain areas defines a molecular subgroup of dementia with Lewy bodies. *Brain*, *133*(Pt 12), 3724-3733. https://doi.org/10.1093/brain/awq275

Binjawhar, D. N., Alhazmi, A. T., Bin Jawhar, W. N., MohammedSaeed, W., & Safi, S. Z. (2023). Hyperglycemia-induced oxidative stress and epigenetic regulation of ET-1 gene in endothelial cells. *Front Genet*, *14*, 1167773. https://doi.org/10.3389/fgene.2023.1167773

Bottos, A., Destro, E., Rissone, A., Graziano, S., Cordara, G., Assenzio, B., Cera, M. R., Mascia, L., Bussolino, F., & Arese, M. (2009). The synaptic proteins neurexins and neuroligins are widely expressed in the vascular system and contribute to its functions. *Proc Natl Acad Sci U S A*, *106*(49), 20782-20787. https://doi.org/10.1073/pnas.0809510106

Brandebura, A. N., Paumier, A., Onur, T. S., & Allen, N. J. (2023). Astrocyte contribution to dysfunction, risk and progression in neurodegenerative disorders. *Nat Rev Neurosci*, *24*(1), 23-39. https://doi.org/10.1038/s41583-022-00641-1

Browaeys, R., Saelens, W., & Saeys, Y. (2020). NicheNet: modeling intercellular communication by linking ligands to target genes. *Nat Methods*, *17*(2), 159-162. https://doi.org/10.1038/s41592-019-0667-5

Bryant, A., Li, Z., Jayakumar, R., Serrano-Pozo, A., Woost, B., Hu, M., Woodbury, M. E., Wachter, A., Lin, G., Kwon, T., Talanian, R. V., Biber, K., Karran, E. H., Hyman, B. T., Das, S., & Bennett, R. E. (2023). Endothelial Cells Are Heterogeneous in Different Brain Regions and Are Dramatically Altered in Alzheimer's Disease. *J Neurosci*, *43*(24), 4541-4557. https://doi.org/10.1523/JNEUROSCI.0237-23.2023

Burgmans, S., van Boxtel, M. P., Smeets, F., Vuurman, E. F., Gronenschild, E. H., Verhey, F. R., Uylings, H. B., & Jolles, J. (2009). Prefrontal cortex atrophy predicts

dementia over a six-year period. *Neurobiol Aging*, *30*(9), 1413-1419. https://doi.org/10.1016/j.neurobiolaging.2007.11.028

Bury, J. J., Chambers, A., Heath, P. R., Ince, P. G., Shaw, P. J., Matthews, F. E., Brayne, C., Simpson, J. E., Wharton, S. B., Cognitive, F., & Ageing, S. (2021). Type 2 diabetes mellitus-associated transcriptome alterations in cortical neurones and associated neurovascular unit cells in the ageing brain. *Acta Neuropathol Commun*, *9*(1), 5. https://doi.org/10.1186/s40478-020-01109-y

Busche, M. A., & Hyman, B. T. (2020). Synergy between amyloid-beta and tau in Alzheimer's disease. *Nat Neurosci*, *23*(10), 1183-1193. https://doi.org/10.1038/s41593-020-0687-6

Busik, J. V., Mohr, S., & Grant, M. B. (2008). Hyperglycemia-induced reactive oxygen species toxicity to endothelial cells is dependent on paracrine mediators. *Diabetes*, *57*(7), 1952-1965. https://doi.org/10.2337/db07-1520

Canavan, M., & O'Donnell, M. J. (2022). Hypertension and Cognitive Impairment: A Review of Mechanisms and Key Concepts. *Front Neurol*, *13*, 821135. https://doi.org/10.3389/fneur.2022.821135

Casalena, G. A., Yu, L., Gil, R., Rodriguez, S., Sosa, S., Janssen, W., Azeloglu, E. U., Leventhal, J. S., & Daehn, I. S. (2020). The diabetic microenvironment causes mitochondrial oxidative stress in glomerular endothelial cells and pathological crosstalk with podocytes. *Cell Commun Signal*, *18*(1), 105. https://doi.org/10.1186/s12964-020-00605-x

Castrillon, G., Epp, S., Bose, A., Fraticelli, L., Hechler, A., Belenya, R., Ranft, A., Yakushev, I., Utz, L., Sundar, L., Rauschecker, J. P., Preibisch, C., Kurcyus, K., & Riedl, V. (2023). An energy costly architecture of neuromodulators for human brain evolution and cognition. *Science Advances*, *9*(50), eadi7632. https://doi.org/doi:10.1126/sciadv.adi7632

Chatzinakos, C., Pernia, C. D., Morrison, F. G., Iatrou, A., McCullough, K. M., Schuler, H., Snijders, C., Bajaj, T., DiPietro, C. P., Soliva Estruch, M., Gassen, N. C.,

Anastasopoulos, C., Bharadwaj, R. A., Bowlby, B. C., Hartmann, J., Maihofer, A. X., Nievergelt, C. M., Ressler, N. M., Wolf, E. J., . . . Daskalakis, N. P. (2023). Single-Nucleus Transcriptome Profiling of Dorsolateral Prefrontal Cortex: Mechanistic Roles for Neuronal Gene Expression, Including the 17q21.31 Locus, in PTSD Stress Response. *Am J Psychiatry*, *180*(10), 739-754. https://doi.org/10.1176/appi.ajp.20220478

Chen, G. F., Xu, T. H., Yan, Y., Zhou, Y. R., Jiang, Y., Melcher, K., & Xu, H. E. (2017). Amyloid beta: structure, biology and structure-based therapeutic development. *Acta Pharmacol Sin*, *38*(9), 1205-1235. https://doi.org/10.1038/aps.2017.28

Chen, M. B., Yang, A. C., Yousef, H., Lee, D., Chen, W., Schaum, N., Lehallier, B., Quake, S. R., & Wyss-Coray, T. (2020). Brain Endothelial Cells Are Exquisite Sensors of Age-Related Circulatory Cues. *Cell Rep*, *30*(13), 4418-4432 e4414. https://doi.org/10.1016/j.celrep.2020.03.012

Chen, Y., He, Y., Han, J., Wei, W., & Chen, F. (2023). Blood-brain barrier dysfunction and Alzheimer's disease: associations, pathogenic mechanisms, and therapeutic potential. *Front Aging Neurosci*, *15*, 1258640. https://doi.org/10.3389/fnagi.2023.1258640

Cheng, C., Chen, W., Jin, H., & Chen, X. (2023). A Review of Single-Cell RNA-Seq Annotation, Integration, and Cell-Cell Communication. *Cells*, *12*(15). https://doi.org/10.3390/cells12151970

Chien, J. F., Liu, H., Wang, B. A., Luo, C., Bartlett, A., Castanon, R., Johnson, N. D., Nery, J. R., Osteen, J., Li, J., Altshul, J., Kenworthy, M., Valadon, C., Liem, M., Claffey, N., O'Connor, C., Seeker, L. A., Ecker, J. R., Behrens, M. M., & Mukamel, E. A. (2024). Cell-type-specific effects of age and sex on human cortical neurons. *Neuron*, *112*(15), 2524-2539 e2525. https://doi.org/10.1016/j.neuron.2024.05.013

Choi, S., Kim, K., Lee, J. K., Choi, J. Y., Shin, A., Park, S. K., Kang, D., & Park, S. M. (2019). Association between Change in Alcohol Consumption and Metabolic

Syndrome: Analysis from the Health Examinees Study. *Diabetes Metab J*, *43*(5), 615-626. https://doi.org/10.4093/dmj.2018.0128

Cicalese, S. M., da Silva, J. F., Priviero, F., Webb, R. C., Eguchi, S., & Tostes, R. C. (2021). Vascular Stress Signaling in Hypertension. *Circ Res*, *128*(7), 969-992. https://doi.org/10.1161/CIRCRESAHA.121.318053

Collaboration, N. C. D. R. F. (2021). Worldwide trends in hypertension prevalence and progress in treatment and control from 1990 to 2019: a pooled analysis of 1201 population-representative studies with 104 million participants. *Lancet*, *398*(10304), 957-980. https://doi.org/10.1016/S0140-6736(21)01330-1

Collaborators, G. B. D. D. (2023). Global, regional, and national burden of diabetes from 1990 to 2021, with projections of prevalence to 2050: a systematic analysis for the Global Burden of Disease Study 2021. *Lancet*, *402*(10397), 203-234. https://doi.org/10.1016/S0140-6736(23)01301-6

Collaborators, G. B. D. D. F. (2022). Estimation of the global prevalence of dementia in 2019 and forecasted prevalence in 2050: an analysis for the Global Burden of Disease Study 2019. *Lancet Public Health*, *7*(2), e105-e125. https://doi.org/10.1016/S2468-2667(21)00249-8

Colonna, M., & Butovsky, O. (2017). Microglia Function in the Central Nervous System During Health and Neurodegeneration. *Annu Rev Immunol*, *35*, 441-468. https://doi.org/10.1146/annurev-immunol-051116-052358

Conway, J. R., Lex, A., & Gehlenborg, N. (2017). UpSetR: an R package for the visualization of intersecting sets and their properties. *Bioinformatics*, *33*(18), 2938-2940. https://doi.org/10.1093/bioinformatics/btx364

Cortez, V. S., Cervantes-Barragan, L., Song, C., Gilfillan, S., McDonald, K. G., Tussiwand, R., Edelson, B. T., Murakami, Y., Murphy, K. M., Newberry, R. D., Sibley, L. D., & Colonna, M. (2014). CRTAM controls residency of gut CD4+CD8+ T cells in the steady state and maintenance of gut CD4+ Th17 during parasitic infection. *J Exp Med*, *211*(4), 623-633. https://doi.org/10.1084/jem.20130904

Cozza, M., Amadori, L., & Boccardi, V. (2023). Exploring cerebral amyloid angiopathy: Insights into pathogenesis, diagnosis, and treatment. *J Neurol Sci*, *454*, 120866. https://doi.org/10.1016/j.jns.2023.120866

Csaszar, E., Lenart, N., Cserep, C., Kornyei, Z., Fekete, R., Posfai, B., Balazsfi, D., Hangya, B., Schwarcz, A. D., Szabadits, E., Szollosi, D., Szigeti, K., Mathe, D., West, B. L., Sviatko, K., Bras, A. R., Mariani, J. C., Kliewer, A., Lenkei, Z., . . . Denes, A. (2022). Microglia modulate blood flow, neurovascular coupling, and hypoperfusion via purinergic actions. *J Exp Med*, *219*(3). https://doi.org/10.1084/jem.20211071

Dai, D. L., Li, M., & Lee, E. B. (2023). Human Alzheimer's disease reactive astrocytes exhibit a loss of homeostastic gene expression. *Acta Neuropathol Commun*, *11*(1), 127. https://doi.org/10.1186/s40478-023-01624-8

Dallinga, M. G., Boas, S. E. M., Klaassen, I., Merks, R. H. M., van Noorden, C. J. F., & Schlingemann, R. O. (2015). Tip Cells in Angiogenesis. In *Encyclopedia of Life Sciences* (pp. 1-10). https://doi.org/10.1002/9780470015902.a0025977

Daniele, A., Lucas, S. J. E., & Rendeiro, C. (2022). Detrimental effects of physical inactivity on peripheral and brain vasculature in humans: Insights into mechanisms, long-term health consequences and protective strategies. *Front Physiol*, *13*, 998380. https://doi.org/10.3389/fphys.2022.998380

Darden, J., Payne, L. B., Zhao, H., & Chappell, J. C. (2019). Excess vascular endothelial growth factor-A disrupts pericyte recruitment during blood vessel formation. *Angiogenesis*, *22*(1), 167-183. https://doi.org/10.1007/s10456-018-9648-z

Davidson, S. M., & Duchen, M. R. (2007). Endothelial mitochondria: contributing to vascular function and disease. *Circ Res*, *100*(8), 1128-1141. https://doi.org/10.1161/01.RES.0000261970.18328.1d

de la Monte, S. M., Tong, M., & Wands, J. R. (2018). The 20-Year Voyage Aboard the Journal of Alzheimer's Disease: Docking at 'Type 3 Diabetes', Environmental/Exposure Factors, Pathogenic Mechanisms, and Potential

Treatments. *J Alzheimers Dis*, *62*(3), 1381-1390. https://doi.org/10.3233/JAD-170829

de la Torre, J. (2018). The Vascular Hypothesis of Alzheimer's Disease: A Key to Preclinical Prediction of Dementia Using Neuroimaging. *J Alzheimers Dis*, *63*(1), 35-52. https://doi.org/10.3233/JAD-180004

de Montgolfier, O., Pouliot, P., Gillis, M. A., Ferland, G., Lesage, F., Thorin-Trescases, N., & Thorin, E. (2019). Systolic hypertension-induced neurovascular unit disruption magnifies vascular cognitive impairment in middle-age atherosclerotic LDLr(-/-):hApoB(+/+) mice. *Geroscience*, *41*(5), 511-532. https://doi.org/10.1007/s11357-019-00070-6

dela Paz, N. G., & D'Amore, P. A. (2009). Arterial versus venous endothelial cells. *Cell Tissue Res*, *335*(1), 5-16. https://doi.org/10.1007/s00441-008-0706-5

Devkota, P., & Wuchty, S. (2020). Controllability analysis of molecular pathways points to proteins that control the entire interaction network. *Sci Rep*, *10*(1), 2943. https://doi.org/10.1038/s41598-020-59717-6

Dikalov, S. I., & Ungvari, Z. (2013). Role of mitochondrial oxidative stress in hypertension. *Am J Physiol Heart Circ Physiol*, *305*(10), H1417-1427. https://doi.org/10.1152/ajpheart.00089.2013

Ding, R., Huang, L., Yan, K., Sun, Z., & Duan, J. (2024). New insight into air pollution-related cardiovascular disease: an adverse outcome pathway framework of PM2.5-associated vascular calcification. *Cardiovasc Res*, *120*(7), 699-707. https://doi.org/10.1093/cvr/cvae082

Do, D., Lee, T., Peasah, S., Inneh, A., Patel, U., & Good, C. (2025). Trends in first-line glucose-lowering medication use among US adults with type 2 diabetes from 2019 to 2023. *J Manag Care Spec Pharm*, *31*(5), 520-526. https://doi.org/10.18553/jmcp.2025.31.5.520

Dormanns, K., Brown, R. G., & David, T. (2016). The role of nitric oxide in neurovascular coupling. *J Theor Biol*, *394*, 1-17. https://doi.org/10.1016/j.jtbi.2016.01.009

Douet, V., Chang, L., Pritchett, A., Lee, K., Keating, B., Bartsch, H., Jernigan, T. L., Dale, A., Akshoomoff, N., Murray, S., Bloss, C., Kennedy, D. N., Amaral, D., Gruen, J., Kaufmann, W. E., Casey, B. J., Sowell, E., & Ernst, T. (2014). Schizophrenia-risk variant rs6994992 in the neuregulin-1 gene on brain developmental trajectories in typically developing children. *Transl Psychiatry*, *4*(5), e392. https://doi.org/10.1038/tp.2014.41

Dougherty, E. J., Chen, L. Y., Awad, K. S., Ferreyra, G. A., Demirkale, C. Y., Keshavarz, A., Gairhe, S., Johnston, K. A., Hicks, M. E., Sandler, A. B., Curran, C. S., Krack, J. M., Ding, Y., Suffredini, A. F., Solomon, M. A., Elinoff, J. M., & Danner, R. L. (2023). Inflammation and DKK1-induced AKT activation contribute to endothelial dysfunction following NR2F2 loss. *Am J Physiol Lung Cell Mol Physiol*, *324*(6), L783-L798. https://doi.org/10.1152/ajplung.00171.2022

Du, H., Xu, Y., & Zhu, L. (2022). Role of Semaphorins in Ischemic Stroke. *Front Mol Neurosci*, *15*, 848506. https://doi.org/10.3389/fnmol.2022.848506

Durinck, S., Moreau, Y., Kasprzyk, A., Davis, S., De Moor, B., Brazma, A., & Huber, W. (2005). BioMart and Bioconductor: a powerful link between biological databases and microarray data analysis. *Bioinformatics*, *21*(16), 3439-3440. https://doi.org/10.1093/bioinformatics/bti525

Durinck, S., Spellman, P. T., Birney, E., & Huber, W. (2009). Mapping identifiers for the integration of genomic datasets with the R/Bioconductor package biomaRt. *Nat Protoc*, *4*(8), 1184-1191. https://doi.org/10.1038/nprot.2009.97

Ferguson, H. J. M., Wragg, J. W., Ward, S., Heath, V. L., Ismail, T., & Bicknell, R. (2016). Glutamate dependent NMDA receptor 2D is a novel angiogenic tumour endothelial marker in colorectal cancer. *Oncotarget*, *7*(15). https://www.oncotarget.com/article/7812/text/

Filippov, I., Philip, C. S., Schauser, L., & Peterson, P. (2024). Comparative transcriptomic analyses of thymocytes using 10x Genomics and Parse scRNA-seq technologies. *BMC Genomics*, *25*(1). https://doi.org/10.1186/s12864-024-10976-x

Finak, G., McDavid, A., Yajima, M., Deng, J., Gersuk, V., Shalek, A. K., Slichter, C. K., Miller, H. W., McElrath, M. J., Prlic, M., Linsley, P. S., & Gottardo, R. (2015). MAST: a flexible statistical framework for assessing transcriptional changes and characterizing heterogeneity in single-cell RNA sequencing data. *Genome Biol*, *16*, 278. https://doi.org/10.1186/s13059-015-0844-5

Fisher, R. A., Miners, J. S., & Love, S. (2022). Pathological changes within the cerebral vasculature in Alzheimer's disease: New perspectives. *Brain Pathol*, *32*(6), e13061. https://doi.org/10.1111/bpa.13061

Fleegal-DeMotta, M. A., Doghu, S., & Banks, W. A. (2009). Angiotensin II modulates BBB permeability via activation of the AT(1) receptor in brain endothelial cells. *J Cereb Blood Flow Metab*, *29*(3), 640-647. https://doi.org/10.1038/jcbfm.2008.158

Flentje, A., Kalsi, R., & Monahan, T. S. (2019). Small GTPases and Their Role in Vascular Disease. *Int J Mol Sci*, *20*(4). https://doi.org/10.3390/ijms20040917

Foretz, M., Guigas, B., & Viollet, B. (2023). Metformin: update on mechanisms of action and repurposing potential. *Nat Rev Endocrinol*, *19*(8), 460-476. https://doi.org/10.1038/s41574-023-00833-4

Fournier, N. M., & Duman, R. S. (2012). Role of vascular endothelial growth factor in adult hippocampal neurogenesis: implications for the pathophysiology and treatment of depression. *Behav Brain Res*, *227*(2), 440-449. https://doi.org/10.1016/j.bbr.2011.04.022

Franzen, O., Gan, L. M., & Bjorkegren, J. L. M. (2019). PanglaoDB: a web server for exploration of mouse and human single-cell RNA sequencing data. *Database (Oxford)*, *2019*. https://doi.org/10.1093/database/baz046

Friedman, N. P., & Robbins, T. W. (2022). The role of prefrontal cortex in cognitive control and executive function. *Neuropsychopharmacology*, *47*(1), 72-89. https://doi.org/10.1038/s41386-021-01132-0

Gaengel, K., Genove, G., Armulik, A., & Betsholtz, C. (2009). Endothelial-mural cell signaling in vascular development and angiogenesis. *Arterioscler Thromb Vasc Biol*, *29*(5), 630-638. https://doi.org/10.1161/ATVBAHA.107.161521

Gal, Z., Torok, D., Gonda, X., Eszlari, N., Anderson, I. M., Deakin, B., Petschner, P., Juhasz, G., & Bagdy, G. (2024). New Evidence for the Role of the Blood-Brain Barrier and Inflammation in Stress-Associated Depression: A Gene-Environment Analysis Covering 19,296 Genes in 109,360 Humans. *Int J Mol Sci*, *25*(20). https://doi.org/10.3390/ijms252011332

Galicia-Garcia, U., Benito-Vicente, A., Jebari, S., Larrea-Sebal, A., Siddiqi, H., Uribe, K. B., Ostolaza, H., & Martin, C. (2020). Pathophysiology of Type 2 Diabetes Mellitus. *Int J Mol Sci*, *21*(17). https://doi.org/10.3390/ijms21176275

Gallo, G., Volpe, M., & Savoia, C. (2021). Endothelial Dysfunction in Hypertension: Current Concepts and Clinical Implications. *Front Med (Lausanne)*, *8*, 798958. https://doi.org/10.3389/fmed.2021.798958

Gao, S., Dai, Y., & Rehman, J. (2021). A Bayesian inference transcription factor activity model for the analysis of single-cell transcriptomes. *Genome Res*, *31*(7), 1296-1311. https://doi.org/10.1101/gr.265595.120

Garcia-Esparcia, P., Lopez-Gonzalez, I., Grau-Rivera, O., Garcia-Garrido, M. F., Konetti, A., Llorens, F., Zafar, S., Carmona, M., Del Rio, J. A., Zerr, I., Gelpi, E., & Ferrer, I. (2017). Dementia with Lewy Bodies: Molecular Pathology in the Frontal Cortex in Typical and Rapidly Progressive Forms. *Front Neurol*, *8*, 89. https://doi.org/10.3389/fneur.2017.00089

Garcia, F. J., Sun, N., Lee, H., Godlewski, B., Mathys, H., Galani, K., Zhou, B., Jiang, X., Ng, A. P., Mantero, J., Tsai, L. H., Bennett, D. A., Sahin, M., Kellis, M., & Heiman, M. (2022). Single-cell dissection of the human brain vasculature. *Nature*, *603*(7903), 893-899. https://doi.org/10.1038/s41586-022-04521-7

Gastfriend, B. D., Foreman, K. L., Katt, M. E., Palecek, S. P., & Shusta, E. V. (2021). Integrative analysis of the human brain mural cell transcriptome. *J Cereb Blood Flow Metab*, *41*(11), 3052-3068. https://doi.org/10.1177/0271678x211013700

Glodzik, L., & Santisteban, M. M. (2021). Blood-Brain Barrier Crossing Renin-Angiotensin System Drugs: Considerations for Dementia and Cognitive Decline. *Hypertension*, *78*(3), 644-646. https://doi.org/10.1161/HYPERTENSIONAHA.121.17595

Gonzalez, C. E., Pacheco, J., Beason-Held, L. L., & Resnick, S. M. (2015). Longitudinal changes in cortical thinning associated with hypertension. *J Hypertens*, *33*(6), 1242-1248. https://doi.org/10.1097/HJH.0000000000000531

Gorelova, A., Berman, M., & Al Ghouleh, I. (2021). Endothelial-to-Mesenchymal Transition in Pulmonary Arterial Hypertension. *Antioxid Redox Signal*, *34*(12), 891-914. https://doi.org/10.1089/ars.2020.8169

Grubb, S., Cai, C., Hald, B. O., Khennouf, L., Murmu, R. P., Jensen, A. G. K., Fordsmann, J., Zambach, S., & Lauritzen, M. (2020). Precapillary sphincters maintain perfusion in the cerebral cortex. *Nat Commun*, *11*(1), 395. https://doi.org/10.1038/s41467-020-14330-z

Gu, Z. (2022). Complex heatmap visualization. *Imeta*, *1*(3), e43. https://doi.org/10.1002/imt2.43

Guarino, A., Favieri, F., Boncompagni, I., Agostini, F., Cantone, M., & Casagrande, M. (2018). Executive Functions in Alzheimer Disease: A Systematic Review. *Front Aging Neurosci*, *10*, 437. https://doi.org/10.3389/fnagi.2018.00437

Guerit, S., Fidan, E., Macas, J., Czupalla, C. J., Figueiredo, R., Vijikumar, A., Yalcin, B. H., Thom, S., Winter, P., Gerhardt, H., Devraj, K., & Liebner, S. (2021). Astrocyte-derived Wnt growth factors are required for endothelial blood-brain barrier maintenance. *Prog Neurobiol*, *199*, 101937. https://doi.org/10.1016/j.pneurobio.2020.101937

Guy, R., Volkman, R., Wilczynski, E., Yagil, C., Yagil, Y., Findler, M., Auriel, E., Nevo, U., & Offen, D. (2022). A Novel Rodent Model of Hypertensive Cerebral Small Vessel

Disease with White Matter Hyperintensities and Peripheral Oxidative Stress. *Int J Mol Sci*, *23*(11). https://doi.org/10.3390/ijms23115915

Hafemeister, C., & Satija, R. (2019). Normalization and variance stabilization of single-cell RNA-seq data using regularized negative binomial regression. *Genome Biol*, *20*(1), 296. https://doi.org/10.1186/s13059-019-1874-1

Hamilton, H. L., Kinscherf, N. A., Balmer, G., Bresque, M., Salamat, S. M., Vargas, M. R., & Pehar, M. (2024). FABP7 drives an inflammatory response in human astrocytes and is upregulated in Alzheimer's disease. *Geroscience*, *46*(2), 1607-1625. https://doi.org/10.1007/s11357-023-00916-0

Hampel, H., Hardy, J., Blennow, K., Chen, C., Perry, G., Kim, S. H., Villemagne, V. L., Aisen, P., Vendruscolo, M., Iwatsubo, T., Masters, C. L., Cho, M., Lannfelt, L., Cummings, J. L., & Vergallo, A. (2021). The Amyloid-beta Pathway in Alzheimer's Disease. *Mol Psychiatry*, *26*(10), 5481-5503. https://doi.org/10.1038/s41380-021-01249-0

Harrison, D. G., Coffman, T. M., & Wilcox, C. S. (2021). Pathophysiology of Hypertension: The Mosaic Theory and Beyond. *Circ Res*, *128*(7), 847-863. https://doi.org/10.1161/CIRCRESAHA.121.318082

Hartmann, D. A., Berthiaume, A. A., Grant, R. I., Harrill, S. A., Koski, T., Tieu, T., McDowell, K. P., Faino, A. V., Kelly, A. L., & Shih, A. Y. (2021). Brain capillary pericytes exert a substantial but slow influence on blood flow. *Nat Neurosci*, *24*(5), 633-645. https://doi.org/10.1038/s41593-020-00793-2

Haruwaka, K., Ikegami, A., Tachibana, Y., Ohno, N., Konishi, H., Hashimoto, A., Matsumoto, M., Kato, D., Ono, R., Kiyama, H., Moorhouse, A. J., Nabekura, J., & Wake, H. (2019). Dual microglia effects on blood brain barrier permeability induced by systemic inflammation. *Nat Commun*, *10*(1), 5816. https://doi.org/10.1038/s41467-019-13812-z

Hellström, M., Kalén, M., Lindahl, P., Abramsson, A., & Betsholtz, C. (1999). Role of PDGF-B and PDGFR-β in recruitment of vascular smooth muscle cells and

pericytes during embryonic blood vessel formation in the mouse. *Development*, *126*(14), 3047-3055. https://doi.org/10.1242/dev.126.14.3047

Heneka, M. T., Morgan, D., & Jessen, F. (2024). Passive anti-amyloid beta immunotherapy in Alzheimer's disease-opportunities and challenges. *Lancet*, *404*(10468), 2198-2208. https://doi.org/10.1016/S0140-6736(24)01883-X

Higashi, Y., Kihara, Y., & Noma, K. (2012). Endothelial dysfunction and hypertension in aging. *Hypertens Res*, *35*(11), 1039-1047. https://doi.org/10.1038/hr.2012.138

Hosoki, S., Hansra, G. K., Jayasena, T., Poljak, A., Mather, K. A., Catts, V. S., Rust, R., Sagare, A., Kovacic, J. C., Brodtmann, A., Wallin, A., Zlokovic, B. V., Ihara, M., & Sachdev, P. S. (2023). Molecular biomarkers for vascular cognitive impairment and dementia. *Nat Rev Neurol*, *19*(12), 737-753. https://doi.org/10.1038/s41582-023-00884-1

Hsu, I. S., & Moses, A. M. (2022). Stochastic models for single-cell data: Current challenges and the way forward. *FEBS J*, *289*(3), 647-658. https://doi.org/10.1111/febs.15760

Hughes, D., Judge, C., Murphy, R., Loughlin, E., Costello, M., Whiteley, W., Bosch, J., O'Donnell, M. J., & Canavan, M. (2020). Association of Blood Pressure Lowering With Incident Dementia or Cognitive Impairment: A Systematic Review and Meta-analysis. *JAMA*, *323*(19), 1934-1944. https://doi.org/10.1001/jama.2020.4249

Hung, T. H., Chen, V. C., Chuang, Y. C., Hsu, Y. H., Wu, W. C., Tsai, Y. H., McIntyre, R. S., & Weng, J. C. (2024). Investigating the effect of hypertension on vascular cognitive impairment by using the resting-state functional connectome. *Sci Rep*, *14*(1), 4580. https://doi.org/10.1038/s41598-024-54996-9

Huuki-Myers, L. A., Spangler, A., Eagles, N. J., Montgomery, K. D., Kwon, S. H., Guo, B., Grant-Peters, M., Divecha, H. R., Tippani, M., Sriworarat, C., Nguyen, A. B., Ravichandran, P., Tran, M. N., Seyedian, A., Psych, E. C., Hyde, T. M., Kleinman, J. E., Battle, A., Page, S. C., . . . Psych, E. C. (2024). A data-driven single-cell and

spatial transcriptomic map of the human prefrontal cortex. *Science*, *384*(6698), eadh1938. https://doi.org/10.1126/science.adh1938

Iadecola, C., & Nedergaard, M. (2007). Glial regulation of the cerebral microvasculature. *Nat Neurosci*, *10*(11), 1369-1376. https://doi.org/10.1038/nn2003

Ibrahim, A. R. N., & Orayj, K. M. (2024). Impact of ADA Guidelines and Medication Shortage on GLP-1 Receptor Agonists Prescribing Trends in the UK: A Time-Series Analysis with Country-Specific Insights. *J Clin Med*, *13*(20). https://doi.org/10.3390/jcm13206256

Iragavarapu-Charyulu, V., Wojcikiewicz, E., & Urdaneta, A. (2020). Semaphorins in Angiogenesis and Autoimmune Diseases: Therapeutic Targets? *Front Immunol*, *11*, 346. https://doi.org/10.3389/fimmu.2020.00346

Is, O., Wang, X., Reddy, J. S., Min, Y., Yilmaz, E., Bhattarai, P., Patel, T., Bergman, J., Quicksall, Z., Heckman, M. G., Tutor-New, F. Q., Can Demirdogen, B., White, L., Koga, S., Krause, V., Inoue, Y., Kanekiyo, T., Cosacak, M. I., Nelson, N., . . . Ertekin-Taner, N. (2024). Gliovascular transcriptional perturbations in Alzheimer's disease reveal molecular mechanisms of blood brain barrier dysfunction. *Nat Commun*, *15*(1), 4758. https://doi.org/10.1038/s41467-024-48926-6

Islam, S., Bostrom, K. I., Di Carlo, D., Simmons, C. A., Tintut, Y., Yao, Y., & Hsu, J. J. (2021). The Mechanobiology of Endothelial-to-Mesenchymal Transition in Cardiovascular Disease. *Front Physiol*, *12*, 734215. https://doi.org/10.3389/fphys.2021.734215

Jiang, Z. M., Wu, X. J., Liu, Y., Du, X. H., Shen, S. J., Xu, L. Y., & Sun, W. X. (2013). Changes of gene expression profiles across different phases of vascular calcification in rats. *Genet Mol Res*, *12*(4), 5945-5957. https://doi.org/10.4238/2013.November.26.4

Jin, S., Guerrero-Juarez, C. F., Zhang, L., Chang, I., Ramos, R., Kuan, C.-H., Myung, P., Plikus, M. V., & Nie, Q. (2021). Inference and analysis of cell-cell communication

using CellChat. *Nature Communications*, *12*(1). https://doi.org/10.1038/s41467-021-21246-9

Jin, S., Plikus, M. V., & Nie, Q. (2024). CellChat for systematic analysis of cell-cell communication from single-cell transcriptomics. *Nat Protoc*. https://doi.org/10.1038/s41596-024-01045-4

Kaiser, D., Weise, G., Möller, K., Scheibe, J., Pösel, C., Baasch, S., Gawlitza, M., Lobsien, D., Diederich, K., Minnerup, J., Kranz, A., Boltze, J., & Wagner, D.-C. (2014). Spontaneous white matter damage, cognitive decline and neuroinflammation in middle-aged hypertensive rats: an animal model of early-stage cerebral small vessel disease. *Acta Neuropathologica Communications*, *2*(1), 169. https://doi.org/10.1186/s40478-014-0169-8

Kalucka, J., de Rooij, L. P. M. H., Goveia, J., Rohlenova, K., Dumas, S. J., Meta, E., Conchinha, N. V., Taverna, F., Teuwen, L.-A., Veys, K., García-Caballero, M., Khan, S., Geldhof, V., Sokol, L., Chen, R., Treps, L., Borri, M., de Zeeuw, P., Dubois, C., . . . Carmeliet, P. (2020). Single-Cell Transcriptome Atlas of Murine Endothelial Cells. *Cell*, *180*(4), 764-779.e720. https://doi.org/https://doi.org/10.1016/j.cell.2020.01.015

Keaton, J. M., Kamali, Z., Xie, T., Vaez, A., Williams, A., Goleva, S. B., Ani, A., Evangelou, E., Hellwege, J. N., Yengo, L., Young, W. J., Traylor, M., Giri, A., Zheng, Z., Zeng, J., Chasman, D. I., Morris, A. P., Caulfield, M. J., Hwang, S. J., . . . Warren, H. R. (2024). Genome-wide analysis in over 1 million individuals of European ancestry yields improved polygenic risk scores for blood pressure traits. *Nat Genet*, *56*(5), 778-791. https://doi.org/10.1038/s41588-024-01714-w

Killoy, K. M., Harlan, B. A., Pehar, M., & Vargas, M. R. (2020). FABP7 upregulation induces a neurotoxic phenotype in astrocytes. *Glia*, *68*(12), 2693-2704. https://doi.org/10.1002/glia.23879

Kim, H. G., Kim, H. T., Leach, N. T., Lan, F., Ullmann, R., Silahtaroglu, A., Kurth, I., Nowka, A., Seong, I. S., Shen, Y., Talkowski, M. E., Ruderfer, D., Lee, J. H.,

Glotzbach, C., Ha, K., Kjaergaard, S., Levin, A. V., Romeike, B. F., Kleefstra, T., . . . Gusella, J. F. (2012). Translocations disrupting PHF21A in the Potocki-Shaffer-syndrome region are associated with intellectual disability and craniofacial anomalies. *Am J Hum Genet*, *91*(1), 56-72. https://doi.org/10.1016/j.ajhg.2012.05.005

Kisanuki, Y. Y., Emoto, N., Ohuchi, T., Widyantoro, B., Yagi, K., Nakayama, K., Kedzierski, R. M., Hammer, R. E., Yanagisawa, H., Williams, S. C., Richardson, J. A., Suzuki, T., & Yanagisawa, M. (2010). Low blood pressure in endothelial cell-specific endothelin 1 knockout mice. *Hypertension*, *56*(1), 121-128. https://doi.org/10.1161/HYPERTENSIONAHA.109.138701

Koenen, M., Hill, M. A., Cohen, P., & Sowers, J. R. (2021). Obesity, Adipose Tissue and Vascular Dysfunction. *Circ Res*, *128*(7), 951-968. https://doi.org/10.1161/CIRCRESAHA.121.318093

Kolde, R. (2018). *pheatmap: Pretty Heatmaps*. In R package. https://github.com/raivokolde/pheatmap

Kolk, S. M., & Rakic, P. (2022). Development of prefrontal cortex. *Neuropsychopharmacology*, *47*(1), 41-57. https://doi.org/10.1038/s41386-021-01137-9

Komnig, D., Schulz, J. B., Reich, A., & Falkenburger, B. H. (2016). Mice lacking Faim2 show increased cell death in the MPTP mouse model of Parkinson disease. *J Neurochem*, *139*(5), 848-857. https://doi.org/10.1111/jnc.13847

Krumbiegel, M., Pasutto, F., Schlotzer-Schrehardt, U., Uebe, S., Zenkel, M., Mardin, C. Y., Weisschuh, N., Paoli, D., Gramer, E., Becker, C., Ekici, A. B., Weber, B. H., Nurnberg, P., Kruse, F. E., & Reis, A. (2011). Genome-wide association study with DNA pooling identifies variants at CNTNAP2 associated with pseudoexfoliation syndrome. *Eur J Hum Genet*, *19*(2), 186-193. https://doi.org/10.1038/ejhg.2010.144

Lambert, S. A., Jolma, A., Campitelli, L. F., Das, P. K., Yin, Y., Albu, M., Chen, X., Taipale, J., Hughes, T. R., & Weirauch, M. T. (2018). The Human Transcription Factors. *Cell*, *172*(4), 650-665. https://doi.org/10.1016/j.cell.2018.01.029

Langfelder, P., & Horvath, S. (2008). WGCNA: an R package for weighted correlation network analysis. *BMC Bioinformatics*, *9*, 559. https://doi.org/10.1186/1471-2105-9-559

Laporte, J. P., Faulkner, M. E., Gong, Z., Akhonda, M., Ferrucci, L., Egan, J. M., & Bouhrara, M. (2023). Hypertensive Adults Exhibit Lower Myelin Content: A Multicomponent Relaxometry and Diffusion Magnetic Resonance Imaging Study. *Hypertension*, *80*(8), 1728-1738. https://doi.org/10.1161/HYPERTENSIONAHA.123.21012

Lee, H. W., Xu, Y., He, L., Choi, W., Gonzalez, D., Jin, S. W., & Simons, M. (2021). Role of Venous Endothelial Cells in Developmental and Pathologic Angiogenesis. *Circulation*, *144*(16), 1308-1322. https://doi.org/10.1161/CIRCULATIONAHA.121.054071

Lee, M. L., Martinez-Lozada, Z., Krizman, E. N., & Robinson, M. B. (2017). Brain endothelial cells induce astrocytic expression of the glutamate transporter GLT-1 by a Notch-dependent mechanism. *J Neurochem*, *143*(5), 489-506. https://doi.org/10.1111/jnc.14135

Leger, C., Dupre, N., Aligny, C., Benard, M., Lebon, A., Henry, V., Hauchecorne, M., Galas, L., Frebourg, T., Leroux, P., Vivien, D., Lecointre, M., Marret, S., & Gonzalez, B. J. (2020). Glutamate controls vessel-associated migration of GABA interneurons from the pial migratory route via NMDA receptors and endothelial protease activation. *Cell Mol Life Sci*, *77*(10), 1959-1986. https://doi.org/10.1007/s00018-019-03248-5

Levy, R. (2024). The prefrontal cortex: from monkey to man. *Brain*, *147*(3), 794-815. https://doi.org/10.1093/brain/awad389

Li, S., Kumar, T. P., Joshee, S., Kirschstein, T., Subburaju, S., Khalili, J. S., Kloepper, J., Du, C., Elkhal, A., Szabo, G., Jain, R. K., Kohling, R., & Vasudevan, A. (2018). Endothelial cell-derived GABA signaling modulates neuronal migration and postnatal behavior. *Cell Res*, *28*(2), 221-248. https://doi.org/10.1038/cr.2017.135

Li, X., Song, D., & Leng, S. X. (2015). Link between type 2 diabetes and Alzheimer's disease: from epidemiology to mechanism and treatment. *Clin Interv Aging*, *10*, 549-560. https://doi.org/10.2147/CIA.S74042

Li, X., Yu, L., Liu, X., Shi, T., Zhang, Y., Xiao, Y., Wang, C., Song, L., Li, N., Liu, X., Chen, Y., Petersen, R. B., Cheng, X., Xue, W., Yu, Y. V., Xu, L., Zheng, L., Chen, H., & Huang, K. (2024). beta-synuclein regulates the phase transitions and amyloid conversion of alpha-synuclein. *Nat Commun*, *15*(1), 8748. https://doi.org/10.1038/s41467-024-53086-8

Li, Y., Liu, Y., Liu, S., Gao, M., Wang, W., Chen, K., Huang, L., & Liu, Y. (2023). Diabetic vascular diseases: molecular mechanisms and therapeutic strategies. *Signal Transduct Target Ther*, *8*(1), 152. https://doi.org/10.1038/s41392-023-01400-z

Li, Z., Kong, X., Zhang, Y., Zhang, Y., Yu, L., Guo, J., & Xu, Y. (2020). Dual roles of chromatin remodeling protein BRG1 in angiotensin II-induced endothelial-mesenchymal transition. *Cell Death Dis*, *11*(7), 549. https://doi.org/10.1038/s41419-020-02744-y

Liang, C. S., Li, D. J., Yang, F. C., Tseng, P. T., Carvalho, A. F., Stubbs, B., Thompson, T., Mueller, C., Shin, J. I., Radua, J., Stewart, R., Rajji, T. K., Tu, Y. K., Chen, T. Y., Yeh, T. C., Tsai, C. K., Yu, C. L., Pan, C. C., & Chu, C. S. (2021). Mortality rates in Alzheimer's disease and non-Alzheimer's dementias: a systematic review and meta-analysis. *Lancet Healthy Longev*, *2*(8), e479-e488. https://doi.org/10.1016/S2666-7568(21)00140-9

Liang, X., Wu, H., Colt, M., Guo, X., Pluimer, B., Zeng, J., Dong, S., & Zhao, Z. (2021). Microglia and its Genetics in Alzheimer's Disease. *Curr Alzheimer Res*, *18*(9), 676-688. https://doi.org/10.2174/1567205018666211105140732

Lisek, M., Przybyszewski, O., Zylinska, L., Guo, F., & Boczek, T. (2023). The Role of MEF2 Transcription Factor Family in Neuronal Survival and Degeneration. *Int J Mol Sci*, *24*(4). https://doi.org/10.3390/ijms24043120

Liu, M., Solomon, W., Cespedes, J. C., Wilson, N. O., Ford, B., & Stiles, J. K. (2018). Neuregulin-1 attenuates experimental cerebral malaria (ECM) pathogenesis by regulating ErbB4/AKT/STAT3 signaling. *J Neuroinflammation*, *15*(1), 104. https://doi.org/10.1186/s12974-018-1147-z

Liu, Y., Huang, J., Pandey, R., Liu, P., Therani, B., Qiu, Q., Rao, S., Geurts, A. M., Cowley, A. W., Jr., Greene, A. S., & Liang, M. (2023). Robustness of single-cell RNA-seq for identifying differentially expressed genes. *BMC Genomics*, *24*(1), 371. https://doi.org/10.1186/s12864-023-09487-y

Livingston, G., Huntley, J., Liu, K. Y., Costafreda, S. G., Selbaek, G., Alladi, S., Ames, D., Banerjee, S., Burns, A., Brayne, C., Fox, N. C., Ferri, C. P., Gitlin, L. N., Howard, R., Kales, H. C., Kivimaki, M., Larson, E. B., Nakasujja, N., Rockwood, K., . . . Mukadam, N. (2024). Dementia prevention, intervention, and care: 2024 report of the Lancet standing Commission. *Lancet*, *404*(10452), 572-628. https://doi.org/10.1016/S0140-6736(24)01296-0

Lok, J., Sardi, S. P., Guo, S., Besancon, E., Ha, D. M., Rosell, A., Kim, W. J., Corfas, G., & Lo, E. H. (2009). Neuregulin-1 signaling in brain endothelial cells. *J Cereb Blood Flow Metab*, *29*(1), 39-43. https://doi.org/10.1038/jcbfm.2008.94

Lok, J., Zhao, S., Leung, W., Seo, J. H., Navaratna, D., Wang, X., Whalen, M. J., & Lo, E. H. (2012). Neuregulin-1 effects on endothelial and blood-brain-barrier permeability after experimental injury. *Transl Stroke Res*, *3 Suppl 1*(S1), S119-124. https://doi.org/10.1007/s12975-012-0157-x

Longden, T. A., Mughal, A., Hennig, G. W., Harraz, O. F., Shui, B., Lee, F. K., Lee, J. C., Reining, S., Kotlikoff, M. I., König, G. M., Kostenis, E., Hill-Eubanks, D., & Nelson, M. T. (2021). Local IP₃ receptor–mediated

Ca²⁺ signals compound to direct blood flow in brain capillaries. *Science Advances*, *7*(30), eabh0101. https://doi.org/doi:10.1126/sciadv.abh0101

Love, M. I., Huber, W., & Anders, S. (2014). Moderated estimation of fold change and dispersion for RNA-seq data with DESeq2. *Genome Biol*, *15*(12), 550. https://doi.org/10.1186/s13059-014-0550-8

Lu, X., Gong, J., Dennery, P. A., & Yao, H. (2019). Endothelial-to-mesenchymal transition: Pathogenesis and therapeutic targets for chronic pulmonary and vascular diseases. *Biochem Pharmacol*, *168*, 100-107. https://doi.org/10.1016/j.bcp.2019.06.021

Ma, Q., Gu, W., Li, T., Zhang, K., Cui, Y., Qu, K., Wang, N., Humphry, R., Durkan, C., Qiu, J., & Wang, G. (2020). SRGN, a new identified shear-stress-responsive gene in endothelial cells. *Mol Cell Biochem*, *474*(1-2), 15-26. https://doi.org/10.1007/s11010-020-03830-7

Magaki, S., Tang, Z., Tung, S., Williams, C. K., Lo, D., Yong, W. H., Khanlou, N., & Vinters, H. V. (2018). The effects of cerebral amyloid angiopathy on integrity of the blood-brain barrier. *Neurobiol Aging*, *70*, 70-77. https://doi.org/10.1016/j.neurobiolaging.2018.06.004

Malik, R., Chauhan, G., Traylor, M., Sargurupremraj, M., Okada, Y., Mishra, A., Rutten-Jacobs, L., Giese, A. K., van der Laan, S. W., Gretarsdottir, S., Anderson, C. D., Chong, M., Adams, H. H. H., Ago, T., Almgren, P., Amouyel, P., Ay, H., Bartz, T. M., Benavente, O. R., . . . Dichgans, M. (2018). Multiancestry genome-wide association study of 520,000 subjects identifies 32 loci associated with stroke and stroke subtypes. *Nat Genet*, *50*(4), 524-537. https://doi.org/10.1038/s41588-018-0058-3

Mani, A. (2024). Update in genetic and epigenetic causes of hypertension. *Cell Mol Life Sci*, *81*(1), 201. https://doi.org/10.1007/s00018-024-05220-4

Manu, D. R., Slevin, M., Barcutean, L., Forro, T., Boghitoiu, T., & Balasa, R. (2023). Astrocyte Involvement in Blood-Brain Barrier Function: A Critical Update

Highlighting Novel, Complex, Neurovascular Interactions. *Int J Mol Sci*, *24*(24). https://doi.org/10.3390/ijms242417146

Mao, Y., Chen, Y., & Zhang, Z. (2023). Molecular function of Kruppel-like factor 7 in biology. *Acta Biochim Biophys Sin (Shanghai)*, *55*(5), 713-725. https://doi.org/10.3724/abbs.2023061

Marek-Trzonkowska, N., Kwieczynska, A., Reiwer-Gostomska, M., Kolinski, T., Molisz, A., & Siebert, J. (2015). Arterial Hypertension Is Characterized by Imbalance of Pro-Angiogenic versus Anti-Angiogenic Factors. *PLoS One*, *10*(5), e0126190. https://doi.org/10.1371/journal.pone.0126190

Marina, N., Christie, I. N., Korsak, A., Doronin, M., Brazhe, A., Hosford, P. S., Wells, J. A., Sheikhbahaei, S., Humoud, I., Paton, J. F. R., Lythgoe, M. F., Semyanov, A., Kasparov, S., & Gourine, A. V. (2020). Astrocytes monitor cerebral perfusion and control systemic circulation to maintain brain blood flow. *Nat Commun*, *11*(1), 131. https://doi.org/10.1038/s41467-019-13956-y

Maruhashi, T., & Higashi, Y. (2024). Current topic of vascular function in hypertension in 2023-2024. *Hypertens Res*, *47*(12), 3310-3317. https://doi.org/10.1038/s41440-024-01885-3

Mauricio, D., Gratacos, M., & Franch-Nadal, J. (2023). Diabetic microvascular disease in non-classical beds: the hidden impact beyond the retina, the kidney, and the peripheral nerves. *Cardiovasc Diabetol*, *22*(1), 314. https://doi.org/10.1186/s12933-023-02056-3

McCalla, S. G., Fotuhi Siahpirani, A., Li, J., Pyne, S., Stone, M., Periyasamy, V., Shin, J., & Roy, S. (2023). Identifying strengths and weaknesses of methods for computational network inference from single-cell RNA-seq data. *G3 Genes|Genomes|Genetics*, *13*(3). https://doi.org/10.1093/g3journal/jkad004

McCarron, J. G., Lee, M. D., & Wilson, C. (2017). The Endothelium Solves Problems That Endothelial Cells Do Not Know Exist. *Trends Pharmacol Sci*, *38*(4), 322-338. https://doi.org/10.1016/j.tips.2017.01.008

McCaslin, A. F., Chen, B. R., Radosevich, A. J., Cauli, B., & Hillman, E. M. (2011). In vivo 3D morphology of astrocyte-vasculature interactions in the somatosensory cortex: implications for neurovascular coupling. *J Cereb Blood Flow Metab*, *31*(3), 795-806. https://doi.org/10.1038/jcbfm.2010.204

McConnell, H. L., & Mishra, A. (2022). Cells of the Blood-Brain Barrier: An Overview of the Neurovascular Unit in Health and Disease. *Methods Mol Biol*, *2492*, 3-24. https://doi.org/10.1007/978-1-0716-2289-6_1

McGrath, E. R., Beiser, A. S., DeCarli, C., Plourde, K. L., Vasan, R. S., Greenberg, S. M., & Seshadri, S. (2017). Blood pressure from mid- to late life and risk of incident dementia. *Neurology*, *89*(24), 2447-2454. https://doi.org/10.1212/wnl.0000000000004741

McKean, D. M., Zhang, Q., Narayan, P., Morton, S. U., Strohmenger, V., Tang, V. T., McAllister, S., Sharma, A., Quiat, D., Reichart, D., DeLaughter, D. M., Wakimoto, H., Gorham, J. M., Brown, K., McDonough, B., Willcox, J. A., Jang, M. Y., DePalma, S. R., Ward, T., . . . Seidman, C. E. (2024). Increased endothelial sclerostin caused by elevated DSCAM mediates multiple trisomy 21 phenotypes. *J Clin Invest*, *134*(11). https://doi.org/10.1172/JCI167811

Memis, I., Mittal, R., Furar, E., White, I., Eshraghi, R. S., Mittal, J., & Eshraghi, A. A. (2022). Altered Blood Brain Barrier Permeability and Oxidative Stress in Cntnap2 Knockout Rat Model. *J Clin Med*, *11*(10). https://doi.org/10.3390/jcm11102725

Meyers, T. J., Yin, J., Herrera, V. A., Pressman, A. R., Hoffmann, T. J., Schaefer, C., Avins, A. L., & Choquet, H. (2023). Transcriptome-wide association study identifies novel candidate susceptibility genes for migraine. *HGG Adv*, *4*(3), 100211. https://doi.org/10.1016/j.xhgg.2023.100211

Michailidis, M., Tata, D. A., Moraitou, D., Kavvadas, D., Karachrysafi, S., Papamitsou, T., Vareltzis, P., & Papaliagkas, V. (2022). Antidiabetic Drugs in the Treatment of Alzheimer's Disease. *Int J Mol Sci*, *23*(9). https://doi.org/10.3390/ijms23094641

Mishra, A. (2017). Binaural blood flow control by astrocytes: listening to synapses and the vasculature. *J Physiol*, *595*(6), 1885-1902. https://doi.org/10.1113/JP270979

Mishra, A., Reynolds, J. P., Chen, Y., Gourine, A. V., Rusakov, D. A., & Attwell, D. (2016). Astrocytes mediate neurovascular signaling to capillary pericytes but not to arterioles. *Nat Neurosci*, *19*(12), 1619-1627. https://doi.org/10.1038/nn.4428

Moccia, F., Brunetti, V., Soda, T., Berra-Romani, R., & Scarpellino, G. (2023). Cracking the Endothelial Calcium (Ca2+) Code: A Matter of Timing and Spacing. *International Journal of Molecular Sciences*, *24*(23). https://doi.org/10.3390/ijms242316765

Mok, V. C. T., Cai, Y., & Markus, H. S. (2024). Vascular cognitive impairment and dementia: Mechanisms, treatment, and future directions. *Int J Stroke*, *19*(8), 838-856. https://doi.org/10.1177/17474930241279888

Mollah, S. A., Nayak, A., Barhai, S., & Maity, U. (2024). A comprehensive review on frontotemporal dementia: its impact on language, speech and behavior. *Dement Neuropsychol*, *18*, e20230072. https://doi.org/10.1590/1980-5764-DN-2023-0072

Montagne, A., Nation, D. A., Sagare, A. P., Barisano, G., Sweeney, M. D., Chakhoyan, A., Pachicano, M., Joe, E., Nelson, A. R., D'Orazio, L. M., Buennagel, D. P., Harrington, M. G., Benzinger, T. L. S., Fagan, A. M., Ringman, J. M., Schneider, L. S., Morris, J. C., Reiman, E. M., Caselli, R. J., . . . Zlokovic, B. V. (2020). APOE4 leads to blood-brain barrier dysfunction predicting cognitive decline. *Nature*, *581*(7806), 71-76. https://doi.org/10.1038/s41586-020-2247-3

Monteiro, J. P., Rodor, J., Caudrillier, A., Scanlon, J. P., Spiroski, A. M., Dudnakova, T., Pfluger-Muller, B., Shmakova, A., von Kriegsheim, A., Deng, L., Taylor, R. S., Wilson-Kanamori, J. R., Chen, S. H., Stewart, K., Thomson, A., Mitic, T., McClure, J. D., Iynikkel, J., Hadoke, P. W. F., . . . Baker, A. H. (2021). MIR503HG Loss Promotes Endothelial-to-Mesenchymal Transition in Vascular Disease. *Circ Res*, *128*(8), 1173-1190. https://doi.org/10.1161/CIRCRESAHA.120.318124

Moran, C., Phan, T. G., Chen, J., Blizzard, L., Beare, R., Venn, A., Munch, G., Wood, A. G., Forbes, J., Greenaway, T. M., Pearson, S., & Srikanth, V. (2013). Brain atrophy in type 2 diabetes: regional distribution and influence on cognition. *Diabetes Care*, *36*(12), 4036-4042. https://doi.org/10.2337/dc13-0143

Mortensen, M. B., Dzaye, O., Botker, H. E., Jensen, J. M., Maeng, M., Bentzon, J. F., Kanstrup, H., Sorensen, H. T., Leipsic, J., Blankstein, R., Nasir, K., Blaha, M. J., & Norgaard, B. L. (2023). Low-Density Lipoprotein Cholesterol Is Predominantly Associated With Atherosclerotic Cardiovascular Disease Events in Patients With Evidence of Coronary Atherosclerosis: The Western Denmark Heart Registry. *Circulation*, *147*(14), 1053-1063. https://doi.org/10.1161/CIRCULATIONAHA.122.061010

Motaghi, M., Potvin, O., & Duchesne, S. (2024). A systematic review of the impact of type 2 diabetes on brain cortical thickness. *Front Dement*, *3*, 1418037. https://doi.org/10.3389/frdem.2024.1418037

Murphy, A. E., Schilder, B. M., & Skene, N. G. (2021). MungeSumstats: a Bioconductor package for the standardization and quality control of many GWAS summary statistics. *Bioinformatics*, *37*(23), 4593-4596. https://doi.org/10.1093/bioinformatics/btab665

Murphy, A. E., & Skene, N. G. (2022). A balanced measure shows superior performance of pseudobulk methods in single-cell RNA-sequencing analysis. *Nat Commun*, *13*(1), 7851. https://doi.org/10.1038/s41467-022-35519-4

Nagai, M., Dote, K., & Forster, C. Y. (2022). Is unrecognized cognitive impairment in hypertension unmasked by diabetes mellitus? *Hypertens Res*, *45*(6), 1082-1084. https://doi.org/10.1038/s41440-022-00906-3

Nakao, K., Kuwahara, K., Nishikimi, T., Nakagawa, Y., Kinoshita, H., Minami, T., Kuwabara, Y., Yamada, C., Yamada, Y., Tokudome, T., Nagai-Okatani, C., Minamino, N., Nakao, Y. M., Yasuno, S., Ueshima, K., Sone, M., Kimura, T., Kangawa, K., & Nakao, K. (2017). Endothelium-Derived C-Type Natriuretic

Peptide Contributes to Blood Pressure Regulation by Maintaining Endothelial Integrity. *Hypertension*, *69*(2), 286-296. https://doi.org/10.1161/HYPERTENSIONAHA.116.08219

Nation, D. A., Sweeney, M. D., Montagne, A., Sagare, A. P., D'Orazio, L. M., Pachicano, M., Sepehrband, F., Nelson, A. R., Buennagel, D. P., Harrington, M. G., Benzinger, T. L. S., Fagan, A. M., Ringman, J. M., Schneider, L. S., Morris, J. C., Chui, H. C., Law, M., Toga, A. W., & Zlokovic, B. V. (2019). Blood-brain barrier breakdown is an early biomarker of human cognitive dysfunction. *Nat Med*, *25*(2), 270-276. https://doi.org/10.1038/s41591-018-0297-y

National Institute for Health and Care Excellence, N. (2024). *Dementia*. https://cks.nice.org.uk/topics/dementia/#!backgroundsub:1

Nelson, A. R., Sagare, M. A., Wang, Y., Kisler, K., Zhao, Z., & Zlokovic, B. V. (2020). Channelrhodopsin Excitation Contracts Brain Pericytes and Reduces Blood Flow in the Aging Mouse Brain in vivo. *Front Aging Neurosci*, *12*, 108. https://doi.org/10.3389/fnagi.2020.00108

Nguyen, A., & Cai, H. (2006). Netrin-1 induces angiogenesis via a DCC-dependent ERK1/2-eNOS feed-forward mechanism. *Proc Natl Acad Sci U S A*, *103*(17), 6530-6535. https://doi.org/10.1073/pnas.0511011103

Niswender, C. M., & Conn, P. J. (2010). Metabotropic glutamate receptors: physiology, pharmacology, and disease. *Annu Rev Pharmacol Toxicol*, *50*, 295-322. https://doi.org/10.1146/annurev.pharmtox.011008.145533

Nott, A., & Holtman, I. R. (2023). Genetic insights into immune mechanisms of Alzheimer's and Parkinson's disease. *Front Immunol*, *14*, 1168539. https://doi.org/10.3389/fimmu.2023.1168539

Oguro-Ando, A., Bamford, R. A., Sital, W., Sprengers, J. J., Zuko, A., Matser, J. M., Oppelaar, H., Sarabdjitsingh, A., Joels, M., Burbach, J. P. H., & Kas, M. J. (2021). Cntn4, a risk gene for neuropsychiatric disorders, modulates hippocampal

synaptic plasticity and behavior. *Transl Psychiatry*, *11*(1), 106. https://doi.org/10.1038/s41398-021-01223-y

Paczkowska-Walendowska, M., Sip, S., Staszewski, R., & Cielecka-Piontek, J. (2022). Single-Pill Combination to Improve Hypertension Treatment: Pharmaceutical Industry Development. *Int J Environ Res Public Health*, *19*(7). https://doi.org/10.3390/ijerph19074156

Parhizkar, S., & Holtzman, D. M. (2022). APOE mediated neuroinflammation and neurodegeneration in Alzheimer's disease. *Semin Immunol*, *59*, 101594. https://doi.org/10.1016/j.smim.2022.101594

Phipson, B., Sim, C. B., Porrello, E. R., Hewitt, A. W., Powell, J., & Oshlack, A. (2022). propeller: testing for differences in cell type proportions in single cell data. *Bioinformatics*, *38*(20), 4720-4726. https://doi.org/10.1093/bioinformatics/btac582

Piano, M. R. (2017). Alcohol's Effects on the Cardiovascular System. *Alcohol Res*, *38*(2), 219-241.

Pokhilko, A., Handel, A. E., Curion, F., Volpato, V., Whiteley, E. S., Bostrand, S., Newey, S. E., Akerman, C. J., Webber, C., Clark, M. B., Bowden, R., & Cader, M. Z. (2021). Targeted single-cell RNA sequencing of transcription factors enhances the identification of cell types and trajectories. *Genome Res*, *31*(6), 1069-1081. https://doi.org/10.1101/gr.273961.120

Prasad, S., Katta, M. R., Abhishek, S., Sridhar, R., Valisekka, S. S., Hameed, M., Kaur, J., & Walia, N. (2023). Recent advances in Lewy body dementia: A comprehensive review. *Dis Mon*, *69*(5), 101441. https://doi.org/10.1016/j.disamonth.2022.101441

Presa, J. L., Saravia, F., Bagi, Z., & Filosa, J. A. (2020). Vasculo-Neuronal Coupling and Neurovascular Coupling at the Neurovascular Unit: Impact of Hypertension. *Front Physiol*, *11*, 584135. https://doi.org/10.3389/fphys.2020.584135

Qi, X., Zhu, Z., Luo, H., Schwartz, M. D., & Wu, B. (2024). Age at diagnosis of diabetes, obesity, and the risk of dementia among adult patients with type 2 diabetes. *PLoS One*, *19*(11), e0310964. https://doi.org/10.1371/journal.pone.0310964

Rama, N., Dubrac, A., Mathivet, T., Ni Charthaigh, R. A., Genet, G., Cristofaro, B., Pibouin-Fragner, L., Ma, L., Eichmann, A., & Chedotal, A. (2015). Slit2 signaling through Robo1 and Robo2 is required for retinal neovascularization. *Nat Med*, *21*(5), 483-491. https://doi.org/10.1038/nm.3849

Rao, Y. L., Ganaraja, B., Murlimanju, B. V., Joy, T., Krishnamurthy, A., & Agrawal, A. (2022). Hippocampus and its involvement in Alzheimer's disease: a review. *3 Biotech*, *12*(2), 55. https://doi.org/10.1007/s13205-022-03123-4

Ratti, E., Domoto-Reilly, K., Caso, C., Murphy, A., Brickhouse, M., Hochberg, D., Makris, N., Cudkowicz, M. E., & Dickerson, B. C. (2021). Regional prefrontal cortical atrophy predicts specific cognitive-behavioral symptoms in ALS-FTD. *Brain Imaging Behav*, *15*(5), 2540-2551. https://doi.org/10.1007/s11682-021-00456-1

Rawlings, A. M., Sharrett, A. R., Schneider, A. L., Coresh, J., Albert, M., Couper, D., Griswold, M., Gottesman, R. F., Wagenknecht, L. E., Windham, B. G., & Selvin, E. (2014). Diabetes in midlife and cognitive change over 20 years: a cohort study. *Ann Intern Med*, *161*(11), 785-793. https://doi.org/10.7326/M14-0737

Redon, J., & Carmena, R. (2024). Present and future of drug therapy in hypertension: an overview. *Blood Press*, *33*(1), 2320401. https://doi.org/10.1080/08037051.2024.2320401

Reich, A., Spering, C., Gertz, K., Harms, C., Gerhardt, E., Kronenberg, G., Nave, K. A., Schwab, M., Tauber, S. C., Drinkut, A., Harms, K., Beier, C. P., Voigt, A., Gobbels, S., Endres, M., & Schulz, J. B. (2011). Fas/CD95 regulatory protein Faim2 is neuroprotective after transient brain ischemia. *J Neurosci*, *31*(1), 225-233. https://doi.org/10.1523/JNEUROSCI.2188-10.2011

Reuben, D. B., Kremen, S., & Maust, D. T. (2024). Dementia Prevention and Treatment: A Narrative Review. *JAMA Intern Med*, *184*(5), 563-572. https://doi.org/10.1001/jamainternmed.2023.8522

Ribatti, D., & Guidolin, D. (2022). Morphogenesis of vascular and neuronal networks and the relationships between their remodeling processes. *Brain Res Bull*, *186*, 62-69. https://doi.org/10.1016/j.brainresbull.2022.05.015

Robinson, B. G., Oster, B. A., Robertson, K., & Kaltschmidt, J. A. (2023). Loss of ASD-related molecule Cntnap2 affects colonic motility in mice. *Front Neurosci*, *17*, 1287057. https://doi.org/10.3389/fnins.2023.1287057

Rosenberg, A. B., Roco, C. M., Muscat, R. A., Kuchina, A., Sample, P., Yao, Z., Graybuck, L. T., Peeler, D. J., Mukherjee, S., Chen, W., Pun, S. H., Sellers, D. L., Tasic, B., & Seelig, G. (2018). Single-cell profiling of the developing mouse brain and spinal cord with split-pool barcoding. *Science*, *360*(6385), 176-182. https://doi.org/10.1126/science.aam8999

Rouch, L., Cestac, P., Hanon, O., Cool, C., Helmer, C., Bouhanick, B., Chamontin, B., Dartigues, J. F., Vellas, B., & Andrieu, S. (2015). Antihypertensive drugs, prevention of cognitive decline and dementia: a systematic review of observational studies, randomized controlled trials and meta-analyses, with discussion of potential mechanisms. *CNS Drugs*, *29*(2), 113-130. https://doi.org/10.1007/s40263-015-0230-6

Sane, D., Anton, L., & Brosnihan, K. (2004). Angiogenic growth factors and hypertension. *Angiogenesis*, *7*, 193-201. https://doi.org/10.1007/s10456-004-2699-3

Sang-Aram, C., Browaeys, R., Seurinck, R., & Saeys, Y. (2025). Unraveling cell-cell communication with NicheNet by inferring active ligands from transcriptomics data. *Nat Protoc*. https://doi.org/10.1038/s41596-024-01121-9

Santarelli, D. M., Carroll, A. P., Cairns, H. M., Tooney, P. A., & Cairns, M. J. (2019). Schizophrenia-associated MicroRNA-Gene Interactions in the Dorsolateral Prefrontal Cortex. *Genomics Proteomics Bioinformatics*, *17*(6), 623-634. https://doi.org/10.1016/j.gpb.2019.10.003

Satija, R., Farrell, J. A., Gennert, D., Schier, A. F., & Regev, A. (2015). Spatial reconstruction of single-cell gene expression data. *Nat Biotechnol*, *33*(5), 495-502. https://doi.org/10.1038/nbt.3192

Scheffer, S., Hermkens, D. M. A., van der Weerd, L., de Vries, H. E., & Daemen, M. (2021). Vascular Hypothesis of Alzheimer Disease: Topical Review of Mouse Models. *Arterioscler Thromb Vasc Biol*, *41*(4), 1265-1283. https://doi.org/10.1161/ATVBAHA.120.311911

Shah, N. S., Vidal, J. S., Masaki, K., Petrovitch, H., Ross, G. W., Tilley, C., DeMattos, R. B., Tracy, R. P., White, L. R., & Launer, L. J. (2012). Midlife blood pressure, plasma beta-amyloid, and the risk for Alzheimer disease: the Honolulu Asia Aging Study. *Hypertension*, *59*(4), 780-786. https://doi.org/10.1161/HYPERTENSIONAHA.111.178962

Shannon, P., Markiel, A., Ozier, O., Baliga, N. S., Wang, J. T., Ramage, D., Amin, N., Schwikowski, B., & Ideker, T. (2003). Cytoscape: a software environment for integrated models of biomolecular interaction networks. *Genome Res*, *13*(11), 2498-2504. https://doi.org/10.1101/gr.1239303

Shehadeh, L. A., Webster, K. A., Hare, J. M., & Vazquez-Padron, R. I. (2011). Dynamic regulation of vascular myosin light chain (MYL9) with injury and aging. *PLoS One*, *6*(10), e25855. https://doi.org/10.1371/journal.pone.0025855

Shen, X. Z., Li, Y., Li, L., Shah, K. H., Bernstein, K. E., Lyden, P., & Shi, P. (2015). Microglia participate in neurogenic regulation of hypertension. *Hypertension*, *66*(2), 309-316. https://doi.org/10.1161/HYPERTENSIONAHA.115.05333

Siekmann, A. F. (2023). Biology of vascular mural cells. *Development*, *150*(16). https://doi.org/10.1242/dev.200271

Skene, N. G., Bryois, J., Bakken, T. E., Breen, G., Crowley, J. J., Gaspar, H. A., Giusti-Rodriguez, P., Hodge, R. D., Miller, J. A., Munoz-Manchado, A. B., O'Donovan, M. C., Owen, M. J., Pardinas, A. F., Ryge, J., Walters, J. T. R., Linnarsson, S., Lein, E. S., Major Depressive Disorder Working Group of the Psychiatric Genomics, C.,

Sullivan, P. F., & Hjerling-Leffler, J. (2018). Genetic identification of brain cell types underlying schizophrenia. *Nat Genet*, *50*(6), 825-833. https://doi.org/10.1038/s41588-018-0129-5

Skene, N. G., & Grant, S. G. (2016). Identification of Vulnerable Cell Types in Major Brain Disorders Using Single Cell Transcriptomes and Expression Weighted Cell Type Enrichment. *Front Neurosci*, *10*, 16. https://doi.org/10.3389/fnins.2016.00016

Slouha, E., Ibrahim, F., Rezazadah, A., Esposito, S., Clunes, L. A., & Kollias, T. F. (2023). Anti-diabetics and the Prevention of Dementia: A Systematic Review. *Cureus*, *15*(11), e49515. https://doi.org/10.7759/cureus.49515

Sofroniew, M. V., & Vinters, H. V. (2010). Astrocytes: biology and pathology. *Acta Neuropathol*, *119*(1), 7-35. https://doi.org/10.1007/s00401-009-0619-8

Speyer, C. L., Hachem, A. H., Assi, A. A., Johnson, J. S., DeVries, J. A., & Gorski, D. H. (2014). Metabotropic glutamate receptor-1 as a novel target for the antiangiogenic treatment of breast cancer. *PLoS One*, *9*(3), e88830. https://doi.org/10.1371/journal.pone.0088830

Squair, J. W., Gautier, M., Kathe, C., Anderson, M. A., James, N. D., Hutson, T. H., Hudelle, R., Qaiser, T., Matson, K. J. E., Barraud, Q., Levine, A. J., La Manno, G., Skinnider, M. A., & Courtine, G. (2021). Confronting false discoveries in single-cell differential expression. *Nat Commun*, *12*(1), 5692. https://doi.org/10.1038/s41467-021-25960-2

Stephens, M. (2017). False discovery rates: a new deal. *Biostatistics*, *18*(2), 275-294. https://doi.org/10.1093/biostatistics/kxw041

Stern, J. E., Son, S., Biancardi, V. C., Zheng, H., Sharma, N., & Patel, K. P. (2016). Astrocytes Contribute to Angiotensin II Stimulation of Hypothalamic Neuronal Activity and Sympathetic Outflow. *Hypertension*, *68*(6), 1483-1493. https://doi.org/10.1161/HYPERTENSIONAHA.116.07747

Su, J., Song, Y., Zhu, Z., Huang, X., Fan, J., Qiao, J., & Mao, F. (2024). Cell-cell communication: new insights and clinical implications. *Signal Transduct Target Ther*, *9*(1), 196. https://doi.org/10.1038/s41392-024-01888-z

Sun, N., Akay, L. A., Murdock, M. H., Park, Y., Galiana-Melendez, F., Bubnys, A., Galani, K., Mathys, H., Jiang, X., Ng, A. P., Bennett, D. A., Tsai, L. H., & Kellis, M. (2023). Single-nucleus multiregion transcriptomic analysis of brain vasculature in Alzheimer's disease. *Nat Neurosci*, *26*(6), 970-982. https://doi.org/10.1038/s41593-023-01334-3

Sun, Z., Zhang, X., So, K. F., Jiang, W., & Chiu, K. (2024). Targeting Microglia in Alzheimer's Disease: Pathogenesis and Potential Therapeutic Strategies. *Biomolecules*, *14*(7). https://doi.org/10.3390/biom14070833

Suzuki, K., Hatzikotoulas, K., Southam, L., Taylor, H. J., Yin, X., Lorenz, K. M., Mandla, R., Huerta-Chagoya, A., Melloni, G. E. M., Kanoni, S., Rayner, N. W., Bocher, O., Arruda, A. L., Sonehara, K., Namba, S., Lee, S. S. K., Preuss, M. H., Petty, L. E., Schroeder, P., . . . Zeggini, E. (2024). Genetic drivers of heterogeneity in type 2 diabetes pathophysiology. *Nature*, *627*(8003), 347-357. https://doi.org/10.1038/s41586-024-07019-6

Takeda, S., Rakugi, H., & Morishita, R. (2020). Roles of vascular risk factors in the pathogenesis of dementia. *Hypertens Res*, *43*(3), 162-167. https://doi.org/10.1038/s41440-019-0357-9

Tang, H., de Leeuw, C. A., Mooij, J. M., Heskes, T., & Posthuma, D. (2015). MAGMA: Generalized Gene-Set Analysis of GWAS Data. *PLOS Computational Biology*, *11*(4). https://doi.org/10.1371/journal.pcbi.1004219

Tegegne, B. A., Adugna, A., Yenet, A., Yihunie Belay, W., Yibeltal, Y., Dagne, A., Hibstu Teffera, Z., Amare, G. A., Abebaw, D., Tewabe, H., Abebe, R. B., & Zeleke, T. K. (2024). A critical review on diabetes mellitus type 1 and type 2 management approaches: from lifestyle modification to current and novel targets and

therapeutic agents. *Front Endocrinol (Lausanne)*, *15*, 1440456. https://doi.org/10.3389/fendo.2024.1440456

Tessarin, G. W. L., Michalec, O. M., Torres-da-Silva, K. R., Da Silva, A. V., Cruz-Rizzolo, R. J., Goncalves, A., Gasparini, D. C., Horta-Junior, J. A. C., Ervolino, E., Bittencourt, J. C., Lovejoy, D. A., & Casatti, C. A. (2019). A Putative Role of Teneurin-2 and Its Related Proteins in Astrocytes. *Front Neurosci*, *13*, 655. https://doi.org/10.3389/fnins.2019.00655

Touyz, R. M., Alves-Lopes, R., Rios, F. J., Camargo, L. L., Anagnostopoulou, A., Arner, A., & Montezano, A. C. (2018). Vascular smooth muscle contraction in hypertension. *Cardiovasc Res*, *114*(4), 529-539. https://doi.org/10.1093/cvr/cvy023

Traylor, M., Tozer, D. J., Croall, I. D., Lisiecka-Ford, D. M., Olorunda, A. O., Boncoraglio, G., Dichgans, M., Lemmens, R., Rosand, J., Rost, N. S., Rothwell, P. M., Sudlow, C. L. M., Thijs, V., Rutten-Jacobs, L., Markus, H. S., & International Stroke Genetics, C. (2019). Genetic variation in PLEKHG1 is associated with white matter hyperintensities (n = 11,226). *Neurology*, *92*(8), e749-e757. https://doi.org/10.1212/WNL.0000000000006952

Trimm, E., & Red-Horse, K. (2023). Vascular endothelial cell development and diversity. *Nat Rev Cardiol*, *20*(3), 197-210. https://doi.org/10.1038/s41569-022-00770-1

Trubetskoy, V., Pardinas, A. F., Qi, T., Panagiotaropoulou, G., Awasthi, S., Bigdeli, T. B., Bryois, J., Chen, C. Y., Dennison, C. A., Hall, L. S., Lam, M., Watanabe, K., Frei, O., Ge, T., Harwood, J. C., Koopmans, F., Magnusson, S., Richards, A. L., Sidorenko, J., . . . Schizophrenia Working Group of the Psychiatric Genomics, C. (2022). Mapping genomic loci implicates genes and synaptic biology in schizophrenia. *Nature*, *604*(7906), 502-508. https://doi.org/10.1038/s41586-022-04434-5

Tsartsalis, S., Sleven, H., Fancy, N., Wessely, F., Smith, A. M., Willumsen, N., Cheung, T. K. D., Rokicki, M. J., Chau, V., Ifie, E., Khozoie, C., Ansorge, O., Yang, X., Jenkyns, M. H., Davey, K., McGarry, A., Muirhead, R. C. J., Debette, S., Jackson,

J. S., . . . Matthews, P. M. (2024). A single nuclear transcriptomic characterisation of mechanisms responsible for impaired angiogenesis and blood-brain barrier function in Alzheimer's disease. *Nat Commun*, *15*(1), 2243. https://doi.org/10.1038/s41467-024-46630-z

Uchewa, O. O., Ibegbu, A. O., Okafor, S. O., Nwafor, J. A., & Egwu, O. A. (2025). Regulatory roles of eugenol in paraquat-altered SNCA/LZTS3/MAPT in the cerebellum of Wistar rats. *Lab Anim Res*, *41*(1), 2. https://doi.org/10.1186/s42826-025-00236-8

Valero-Mora, P. M. (2010). ggplot2: Elegant Graphics for Data Analysis. *Journal of Statistical Software, Book Reviews*, *35*(1), 1 - 3. https://doi.org/10.18637/jss.v035.b01

Vallee, A., Vallee, J. N., & Lecarpentier, Y. (2022). WNT/beta-catenin Pathway: a Possible Link Between Hypertension and Alzheimer's Disease. *Curr Hypertens Rep*, *24*(10), 465-475. https://doi.org/10.1007/s11906-022-01209-1

Vanlandewijck, M., He, L., Mäe, M. A., Andrae, J., Ando, K., Del Gaudio, F., Nahar, K., Lebouvier, T., Laviña, B., Gouveia, L., Sun, Y., Raschperger, E., Räsänen, M., Zarb, Y., Mochizuki, N., Keller, A., Lendahl, U., & Betsholtz, C. (2018). A molecular atlas of cell types and zonation in the brain vasculature. *Nature*, *554*(7693), 475-480. https://doi.org/10.1038/nature25739

Veldsman, M., Tai, X. Y., Nichols, T., Smith, S., Peixoto, J., Manohar, S., & Husain, M. (2020). Cerebrovascular risk factors impact frontoparietal network integrity and executive function in healthy ageing. *Nat Commun*, *11*(1), 4340. https://doi.org/10.1038/s41467-020-18201-5

Verma, R., Kubendran, S., Das, S. K., Jain, S., & Brahmachari, S. K. (2005). SYNGR1 is associated with schizophrenia and bipolar disorder in southern India. *J Hum Genet*, *50*(12), 635-640. https://doi.org/10.1007/s10038-005-0307-z

Vogel, J. W., Iturria-Medina, Y., Strandberg, O. T., Smith, R., Levitis, E., Evans, A. C., Hansson, O., Alzheimer's Disease Neuroimaging, I., & Swedish BioFinder, S.

(2020). Spread of pathological tau proteins through communicating neurons in human Alzheimer's disease. *Nat Commun*, *11*(1), 2612. https://doi.org/10.1038/s41467-020-15701-2

Wälchli, T., Ghobrial, M., Schwab, M., Takada, S., Zhong, H., Suntharalingham, S., Vetiska, S., Gonzalez, D. R., Wu, R., Rehrauer, H., Dinesh, A., Yu, K., Chen, E. L. Y., Bisschop, J., Farnhammer, F., Mansur, A., Kalucka, J., Tirosh, I., Regli, L., . . . Radovanovic, I. (2024). Single-cell atlas of the human brain vasculature across development, adulthood and disease. *Nature*. https://doi.org/10.1038/s41586-024-07493-y

Walker, K. A., Sharrett, A. R., Wu, A., Schneider, A. L. C., Albert, M., Lutsey, P. L., Bandeen-Roche, K., Coresh, J., Gross, A. L., Windham, B. G., Knopman, D. S., Power, M. C., Rawlings, A. M., Mosley, T. H., & Gottesman, R. F. (2019). Association of Midlife to Late-Life Blood Pressure Patterns With Incident Dementia. *JAMA*, *322*(6), 535-545. https://doi.org/10.1001/jama.2019.10575

Walker, Z., Possin, K. L., Boeve, B. F., & Aarsland, D. (2015). Lewy body dementias. *Lancet*, *386*(10004), 1683-1697. https://doi.org/10.1016/S0140-6736(15)00462-6

Wardlaw, J. M., Smith, C., & Dichgans, M. (2019). Small vessel disease: mechanisms and clinical implications. *Lancet Neurol*, *18*(7), 684-696. https://doi.org/10.1016/S1474-4422(19)30079-1

Watson, E. C., Whitehead, L., Adams, R. H., Dewson, G., & Coultas, L. (2016). Endothelial cell survival during angiogenesis requires the pro-survival protein MCL1. *Cell Death Differ*, *23*(8), 1371-1379. https://doi.org/10.1038/cdd.2016.20

Whitehead, A. K., Erwin, A. P., & Yue, X. (2021). Nicotine and vascular dysfunction. *Acta Physiol (Oxf)*, *231*(4), e13631. https://doi.org/10.1111/apha.13631

Winkler, E. A., Kim, C. N., Ross, J. M., Garcia, J. H., Gil, E., Oh, I., Chen, L. Q., Wu, D., Catapano, J. S., Raygor, K., Narsinh, K., Kim, H., Weinsheimer, S., Cooke, D. L., Walcott, B. P., Lawton, M. T., Gupta, N., Zlokovic, B. V., Chang, E. F., . . . Nowakowski, T. J. (2022). A single-cell atlas of the normal and malformed human

brain vasculature. *Science*, *375*(6584), eabi7377. https://doi.org/10.1126/science.abi7377

Wu, K., Bu, F., Wu, Y., Zhang, G., Wang, X., He, S., Liu, M. F., Chen, R., & Yuan, H. (2024). Exploring noncoding variants in genetic diseases: from detection to functional insights. *J Genet Genomics*, *51*(2), 111-132. https://doi.org/10.1016/j.jgg.2024.01.001

Wu, T., Hu, E., Xu, S., Chen, M., Guo, P., Dai, Z., Feng, T., Zhou, L., Tang, W., Zhan, L., Fu, X., Liu, S., Bo, X., & Yu, G. (2021). clusterProfiler 4.0: A universal enrichment tool for interpreting omics data. *Innovation (Camb)*, *2*(3), 100141. https://doi.org/10.1016/j.xinn.2021.100141

Wu, Y., Jin, F., Huang, H., & Wang, S. (2022). Suppression of KLF7 gene expression inhibits proliferation and induces apoptosis of hemangioma cells via NF-κB signaling pathway. *Tropical Journal of Pharmaceutical Research*, *20*(7), 1351-1356. https://doi.org/10.4314/tjpr.v20i7.5

Xie, Y., Chen, H., Chellamuthu, V. R., Lajam, A. B. M., Albani, S., Low, A. H. L., Petretto, E., & Behmoaras, J. (2024). Comparative Analysis of Single-Cell RNA Sequencing Methods with and without Sample Multiplexing. *Int J Mol Sci*, *25*(7). https://doi.org/10.3390/ijms25073828

Xu, H., Garcia-Ptacek, S., Jonsson, L., Wimo, A., Nordstrom, P., & Eriksdotter, M. (2021). Long-term Effects of Cholinesterase Inhibitors on Cognitive Decline and Mortality. *Neurology*, *96*(17), e2220-e2230. https://doi.org/10.1212/WNL.0000000000011832

Xue, L., Wu, Y., & Lin, Y. (2023). Dissecting and improving gene regulatory network inference using single-cell transcriptome data. *Genome Res*, *33*(9), 1609-1621. https://doi.org/10.1101/gr.277488.122

Yaghmaei, E., Lu, H., Ehwerhemuepha, L., Zheng, J., Danioko, S., Rezaie, A., Sajjadi, S. A., & Rakovski, C. (2024). Combined use of Donepezil and Memantine increases the probability of five-year survival of Alzheimer's disease patients. *Commun Med (Lond)*, *4*(1), 99. https://doi.org/10.1038/s43856-024-00527-6

Yang, A. C., Vest, R. T., Kern, F., Lee, D. P., Agam, M., Maat, C. A., Losada, P. M., Chen, M. B., Schaum, N., Khoury, N., Toland, A., Calcuttawala, K., Shin, H., Palovics, R., Shin, A., Wang, E. Y., Luo, J., Gate, D., Schulz-Schaeffer, W. J., . . . Wyss-Coray, T. (2022). A human brain vascular atlas reveals diverse mediators of Alzheimer's risk. *Nature*, *603*(7903), 885-892. https://doi.org/10.1038/s41586-021-04369-3

Yao, L., Romero, M. J., Toque, H. A., Yang, G., Caldwell, R. B., & Caldwell, R. W. (2010). The role of RhoA/Rho kinase pathway in endothelial dysfunction. *J Cardiovasc Dis Res*, *1*(4), 165-170. https://doi.org/10.4103/0975-3583.74258

Yao, L. L., Hu, J. X., Li, Q., Lee, D., Ren, X., Zhang, J. S., Sun, D., Zhang, H. S., Wang, Y. G., Mei, L., & Xiong, W. C. (2020). Astrocytic neogenin/netrin-1 pathway promotes blood vessel homeostasis and function in mouse cortex. *J Clin Invest*, *130*(12), 6490-6509. https://doi.org/10.1172/JCI132372

Yao, Y., Chen, Z. L., Norris, E. H., & Strickland, S. (2014). Astrocytic laminin regulates pericyte differentiation and maintains blood brain barrier integrity. *Nat Commun*, *5*, 3413. https://doi.org/10.1038/ncomms4413

Yevshin, I., Sharipov, R., Kolmykov, S., Kondrakhin, Y., & Kolpakov, F. (2019). GTRD: a database on gene transcription regulation-2019 update. *Nucleic Acids Res*, *47*(D1), D100-D105. https://doi.org/10.1093/nar/gky1128

Yu, G., Wang, L., Han, Y., & He, Q. (2012). clusterProfiler: an R package for comparing biological themes among gene clusters. *OMICS: A Journal of Integrative Biology*, *16*(5), 284-287. https://doi.org/10.1089/omi.2011.0118

Yu, L., Ma, W., Song, B., Wang, S., Li, X., & Wang, Z. (2022). Hsa_circ_0030042 Ameliorates Oxidized Low-Density Lipoprotein-Induced Endothelial Cell Injury via the MiR-616-3p/RFX7 Axis. *Int Heart J*, *63*(4), 763-772. https://doi.org/10.1536/ihj.22-065

Zarb, Y., Weber-Stadlbauer, U., Kirschenbaum, D., Kindler, D. R., Richetto, J., Keller, D., Rademakers, R., Dickson, D. W., Pasch, A., Byzova, T., Nahar, K., Voigt, F. F., Helmchen, F., Boss, A., Aguzzi, A., Klohs, J., & Keller, A. (2019). Ossified blood

vessels in primary familial brain calcification elicit a neurotoxic astrocyte response. *Brain*, *142*(4), 885-902. https://doi.org/10.1093/brain/awz032

Zhang, J. (2021). The Bidirectional Relationship between Body Weight and Depression across Gender: A Simultaneous Equation Approach. *Int J Environ Res Public Health*, *18*(14). https://doi.org/10.3390/ijerph18147673

Zhao, L., Li, Z., Vong, J. S. L., Chen, X., Lai, H. M., Yan, L. Y. C., Huang, J., Sy, S. K. H., Tian, X., Huang, Y., Chan, H. Y. E., So, H. C., Ng, W. L., Tang, Y., Lin, W. J., Mok, V. C. T., & Ko, H. (2020). Pharmacologically reversible zonation-dependent endothelial cell transcriptomic changes with neurodegenerative disease associations in the aged brain. *Nat Commun*, *11*(1), 4413. https://doi.org/10.1038/s41467-020-18249-3

Zhao, S., Zhu, L., & Yang, J. (2023). Association between depression and macrovascular disease: a mini review. *Front Psychiatry*, *14*, 1215173. https://doi.org/10.3389/fpsyt.2023.1215173

Zhao, Z. A., Yan, L., Wen, J., Satyanarayanan, S. K., Yu, F., Lu, J., Liu, Y. U., & Su, H. (2023). Cellular and molecular mechanisms in vascular repair after traumatic brain injury: a narrative review. *Burns Trauma*, *11*, tkad033. https://doi.org/10.1093/burnst/tkad033

Zhou, Y., Zhou, B., Pache, L., Chang, M., Khodabakhshi, A. H., Tanaseichuk, O., Benner, C., & Chanda, S. K. (2019). Metascape provides a biologist-oriented resource for the analysis of systems-level datasets. *Nat Commun*, *10*(1), 1523. https://doi.org/10.1038/s41467-019-09234-6

Zhou, Z., Zhu, Y., Liu, Y., & Yin, Y. (2019). Comprehensive transcriptomic analysis indicates brain regional specific alterations in type 2 diabetes. *Aging (Albany NY)*, *11*(16), 6398-6421. https://doi.org/10.18632/aging.102196

Zhu, K., Wang, H., Ye, K., Chen, G., & Zhang, Z. (2025). Netrin-1 signaling pathway mechanisms in neurodegenerative diseases. *Neural Regen Res*, *20*(4), 960-972. https://doi.org/10.4103/NRR.NRR-D-23-01573